



IAHR
2017

37th IAHR
WORLD CONGRESS
13-18 August, 2017
Kuala Lumpur, Malaysia

STORMWATER MANAGEMENT

A FRAMEWORK FOR RISK ASSESSMENT OF STORM WATER DRAINAGE SYSTEMS UNDER UNCERTAINTIES

ABBAS ROOZBAHANI⁽¹⁾ & REYHANEH SHARIAT⁽²⁾

^(1,2) Assistant Professor, College of Aburairhan, University of Tehran, Tehran, Iran
roozbahany@ut.ac.ir; shariat.r92@ut.ac.ir

ABSTRACT

Urban flood management is one of the most important issues that the governments and managers face today. In recent years, due to climate change, old storm water drainage systems as well as the mismanagement of these infrastructures, considerable damages have occurred in major cities around the world, especially in Iran. One of the most practical methods to manage these complex urban systems is using risk assessment techniques to be able to take the uncertainties in design and operation into account. In this paper, a framework for comprehensive risk assessment of storm water drainage systems is presented. This framework consists of three main parts: Determination of the probability of flooding using the hydraulic and hydrologic modeling, calculation of consequences as a function of vulnerability and damage caused by flooding and finally risk estimation regarding the probability and consequence parameters. For the first stage, Autodesk SSA model was used to simulate the existing drainage system and the critical points and channels are identified by considering the different hydrological return periods. In the second stage, by using the capabilities of GIS and definition of economic, social and technical criteria, consequence parameter is estimated based on spatial decision making approach. Finally, the risk of flooding is calculated using fuzzy weighted approach to consider the uncertainties. Efficiency of a part of the proposed methodology is examined in one of the strategic and overcrowded regions in Tehran City. The proposed approach is able to reduce the flooding risk of the mentioned region and other similar cases.

Keywords: Risk assessment; storm water drainage; autodesk SSA; fuzzy; GIS.

1 INTRODUCTION

With the advent of urbanism, humans understood that they have to manage the rain water and protect the structures from flood. Since 3000 B.C. until now, during different time periods and in different locations, urban drainage systems and rain water have been considered in various aspects. For instance, ancient Persians collected this natural source in cisterns and used it for daily purposes (Burian and Edwards, 2002). Since then, together with the advancement and development of urbanism, increasing social and individual properties in cities and climate change, city conserving has turned out to be one of the main apprehensions of managers of city affairs. According to the report of Tehran Disaster Mitigation and Management Organization, 70 percent of the annual resources of this organization in Tehran were spent on covering the expenses of damages caused by flood. Regarding the reasons for the occurrence and intensity of floods in urban areas, the following can be noted:

- The city development and dramatic increase in urban population.
For the effects of this issue, we can refer to the permanent decrease in penetrable surfaces, the increase of water speed in channels, increase in flood peak and imposing overburden on transferring flood channels.
- Uncertain nature of flood event.
It is not easy to protect urban storm water drainage systems from the phenomenon that has wide range of uncertain domain (Tahmasebi and Yazdandoost, 2016). Therefore, researchers and managers have tried much to predict the future conditions, vulnerability reduction and damage reduction.
- Uncertainty of the design parameters of urban flood drainage systems.
These systems are designed according to parameters such as rain rate, land use, the percentage of influential surfaces, runoff curve number and the Manning's roughness coefficient, and parameters like these which because of reasons like climate changes and increase of extreme events, each of these parameters have wide range of uncertainty due to reasons such as climate change and increase of extreme events.
- The connection of different components of urban drainage system and unavailability of some parts of the system.

Disorder in the operation of other parts of the system in the case of malfunctioning in one or a group of components and non-discerning of the incorrect parts of the system because of being buried are other problems.

The factor that gives importance to the flood phenomenon in urban areas is the relation between social and personal properties and urban textures, so far that in the case of malfunctioning, not only each of these parts, other parts of the system are damaged, but this event will also cause a great loss in city proportion. The loss can be investigated from various aspects, such as social and financial losses, general health loss, environmental damage and causing public dissatisfaction. Therefore, its domain is wide and it varies according to time, place, intensity, and duration of flood.

Some researchers are trying to consider this natural incident with variety of tools where some of them are mentioned in this section. Buchele et al. (2006) have focused in the estimation of extreme flood events and estimated the risk of flood hazard using GIS tools capabilities. They showed that studying flood risk assessment needs to consider the various uncertainty sources. Zhou et al. (2011) presented a method to calculate the urban flooding risk assessment in a GIS domain as a function of assets' vulnerabilities, flood probability and intensity. Araqhinejad and Radmehr (2015), by dividing Tehran into 4 regions and considering land use and topographic criteria, these subdivisions were ranked based on vulnerability against flooding using method called spatial MCDM in a GIS environment. The results of this research showed that the central subdivision of Tehran is the most vulnerable part and they emphasized on methods for flood control in smaller scales.

In this paper, a framework for comprehensive risk assessment of storm water drainage systems in urban areas was presented. In this method, hydrologic, hydraulic, social, political, economic and environment aspects were considered. In fact, by using the capabilities of GIS and definition of different criteria, consequence parameter was estimated based on spatial decision making approach. Finally, the risk of flooding was calculated using fuzzy weighted approach to consider the uncertainties. Efficiency of the proposed methodology was examined in one of the strategic and overcrowded regions in Tehran City by prioritizing the channels in terms of the flood risk values.

2 METHODOLOGY

Risk Management includes the processes that are concerned with conducting risk management planning, identification, analysis, responses, monitoring and control on a project. The objectives of Risk Management are to increase the probability and impact of positive events, and decrease the probability and impact of events adverse to the project (PMBOK, 2004).

Therefore, the first step in risk management is defining the flood risk. In the present study, flood risk is defined as a function of the extent to which the flood is deemed probable to take place and the flood consequences intensities are also taken into consideration. The intensity of flood consequences is also defined as a function of the system's vulnerability and damage incurred thereon. The general risk relation was presented as Eq. [1]:

$$Risk = f(P, C, V) \quad [1]$$

where P, C and V are probability of hazards, consequences of hazards, and vulnerabilities of the facilities against these hazards respectively, which can be evaluated through risk assessment approaches (Roozbahani et al., 2013). The proposed factors that influence the urban flood risks, as pointed out in the current article, as well as the overall stages of risk assessment are illustrated in Figure 1.

In the present study, firstly, we addressed the issue of providing a definition and determination of the flood incidence probability as a function of probabilistic hydrologic and hydraulic conditions of the channels as well as the region under study, in the next step, the flood intensity of consequences is determined as a function of the time and place of flood occurrence and, in the final step, flood risk is calculated via the above data pooling in a spatial manner and in GIS environment. It is worth mentioning that fuzzy theory has been used for the purpose of analyzing the uncertainties of the parameters.

2.1 Uncertainty Analysis and Fuzzy Theory

2.1.1 Uncertainty analysis

A parameter's uncertainty is, in fact, defined as the existence of some sort of ambiguity regarding the value of such a parameter; such an uncertainty is predominantly a result of the lack of sufficient information, the low accuracy of the extant information, data deficits, the existence of discrepancies between the existing data, various notions opined by different specialists and so forth. In the case where the source of the uncertainty is the data being found with deficits or having low knowledge of the value of a parameter, an extensive part of it can be resolved via converting the probable discrete value to a fuzzy number and by doing so and taking such an uncertainty into consideration in the calculations, a considerable increase can be seen in the accuracy of the output parameters.

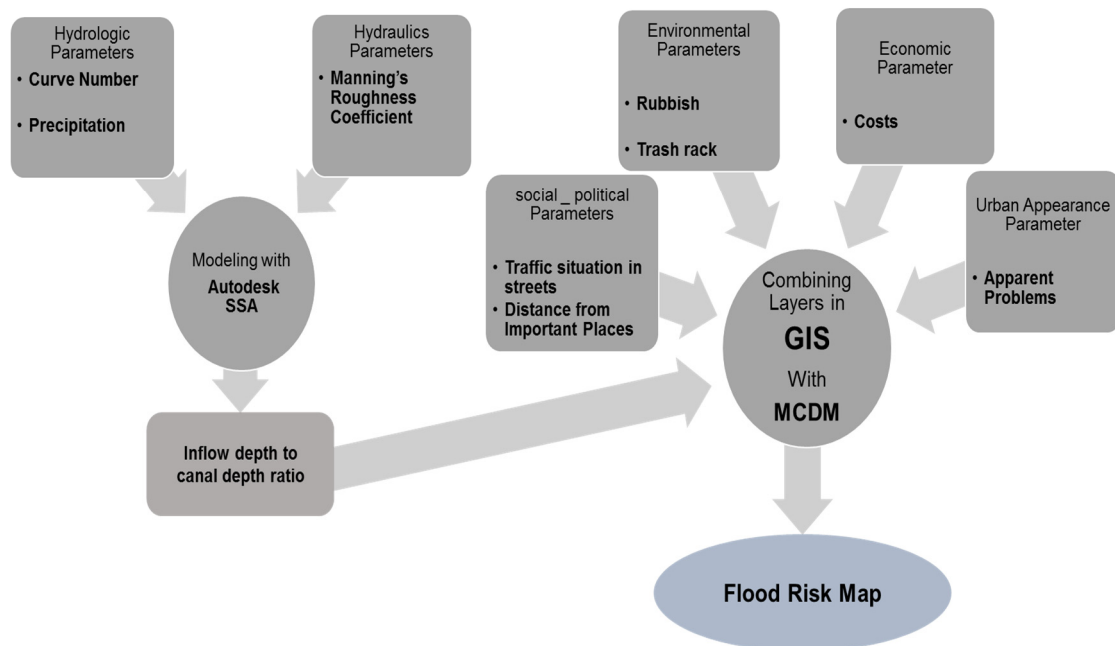


Figure 1. The stages of risk assessment method in this paper.

2.1.2 Fuzzy theory

Fuzzy collections theory and fuzzy logic, as mathematical theories, are efficient and useful instruments for mathematical modeling and configuring the uncertainty and inaccuracy present in the human cognitive processes (Lootsma, 2005). This theory, proposed for the first time by (Lotfizadeh, 1965), influenced many areas in various sciences, especially the urban water planning.

In fuzzy theory, each probable value pertaining to a parameter is expressed in the form of a membership degree related to that value. For example, triangular fuzzy value $X(a,b,c)$ is assumed for expressing parameter X in a probabilistic manner:

- X parameter value, equal to a , is given a membership degree of zero.
- X parameter value, equal to b , is given a membership degree of one.
- X parameter value, equal to c , is given a membership degree of zero.
- And, any other probable value in the interval (a,b) and (b,c) for parameter X will be having a membership degree in an interval $(0, 1)$.

The fuzzy numbers and fuzzy multi-criteria decision making (FMCDM) were, respectively, used in the present study to take the uncertainty of each of the factors effective on the flood risk into consideration and also for considering the uncertainty regarding the amounts of each of the scales (the amounts proposed for pooling of the scales and creating risk zoning map).

2.2 Flood occurrence probability calculation

Flood occurrence probability was defined as a function of hydrologic and hydraulic conditions of urban drainage systems in the present research. To do so, drainage system modeling were done in state-of-the-art, strong and novel of Autodesk SSA software. Precipitation hydrologic parameters uncertainties and the basin's runoff curve number as well as the channel-related Manning's roughness coefficient of the hydraulic parameters were simultaneously applied in the modeling process.

2.2.1 Modeling by means of autodesk SSA

Autodesk Storm and Sanitary Analysis is an advanced, powerful, and comprehensive modeling package for analyzing and designing urban drainage systems, storm-water sewers, and sanitary sewers. The software has been used in thousands of sewer and storm-water studies throughout the world and it has the capability to simultaneously model the hydrologic, hydraulic and water quality parameters. The channels' hydraulic capacity is entered to the risk function in the form of a fuzzy number for each of the channels as the output acquired from the region's model. This in-filling percentage can be computed via taking the precipitation, sub-basin hydrologic curve number and Manning's roughness coefficient of channel into consideration in a fuzzy manner.

2.2.2 Hydrologic and Hydraulic parameters scales

- Precipitation

As the most genuine input variable, precipitation determines the total volume of runoffs. It has been underlined in various studies on the necessity to exercise sufficient precision in measuring this parameter; additionally, the uncertainty intrinsic in measuring and predicting this parameter is considered as the most important source of uncertainty in urban flood measurement (Schellart et al., 2014; Schilling, 1991; Schilling and Fuchs, 1986). Among the precipitation features including intensity, duration, temporal distribution, spatial distribution and precipitation depth, the precipitation depth is considered as an uncertain parameter. According to the fact that the present study aims at offering a method for the calculation of the flood risk in channels which are maximally associated with the cities' social and individual assets, the modeling and management of secondary channels (channels with height less than 90 cm and width less than 80 cm) have been taken into consideration in such a pattern. Designing such channels is mostly for the purpose of getting the flood passed, considering a return period of 5 and/or 10 years.

- Basin Curve Number

The curve number of the basins, as one of the main parameters, plays a significant role in modeling as well as in transforming precipitation to runoff. The amount of the effective runoff which is the total volume of rainfall minus the overland flow retention can be calculated by the use of the US soil conservation standards (SCS) and the soil type of the basins (based on their soil zoning map). Based on this, the total CN of every sub-basin is computed according to the area covered by each land used in a weighted manner. According to the urban constant developments and the continuous variations taking place in the land, a range of uncertainty should be considered for this parameter.

- Manning's roughness coefficient

Manning equation is the simplest and, in the meantime, the most common equation for the calculation of the velocity of the flow; in addition, it is widely used in designing the surface water drainage network. The important point in taking advantage of this equation is the correct estimation of Manning's coefficient of roughness. Although the coefficient changes with the flow depth, but, in practical use, it is extracted from the empirical tables according to the channel type, area cross-section irregularities, the type and the density of the vegetative cover, the flow path shape and the existence of barriers along the path in the form of a constant number. In these tables, a range of n numbers has been defined for each type of channels or the water transferring ditches. The drainage system's age and the engineering judgment are the determiners of the final amount of n according to a suggested range proposed in such tables. Besides the uncertainties intrinsic in the determination of this parameter which lead to ambiguities in its value, sedimentation in the channels, sandstone being exposed or the channel bedding destruction and subsequently the changes in the roughness coefficient are among the problems possible and probable in the entire urban drainage systems. Considering all of the aforementioned cases in modeling, an uncertainty interval can be accepted for Manning's coefficient of roughness.

2.3 Flood Occurrence Consequences Intensity Calculation

The intensity of the consequences resulting from the gullies' inundation is determined according to the position of the inundated area as well as the flood volume in the present study. In the following section, we deal with the explanation and interpretation of each of the parameters which play a determinant role in calculation of the inundation consequences intensity.

2.3.1 Social-Political Scale:

- Traffic

Secondary channels in urban flood collection systems serve the duty of gathering the floods from the alleys and the streets and transferring them to the main channels. Due to the same reason, the inundations in the secondary channels lead to the congestion in the adjacent routes and disrupt the smooth flow of the traffic. Now, if such an indentation occurs in the channels in the vicinity of the crowded and highly congested traffic routes, the results will be higher disruptions and confusions which may sometimes cause the clogging of the streets or the vehicles complete inability to advance on the main and important streets of the city. Therefore, the traffic situation of the routes in adjacency to the channels can be discussed as an index for rating the channels with a score. Since during various hours of a day as well as during various days of the week, the traffic situation differs at different streets under the circumstances which the normal traffic situation of the streets can be investigated by means of Google Earth during all days of the week and during four different time spans, namely 8 A.M., 12 at noon, 4 P.M. and 8 at night). Then, a triangular fuzzy number can be finally assigned to the traffic situation of every channel.

- Distance from the sensitive centers

Inundation in important political (such as in embassies), educational (such as schools), cultural (such as theaters and cinemas), military (such as police stations) centers, crowded spaces and important business localities (such as the centers for distributing and dispatching of the goods and in markets) can lead to greater damages to the public properties in comparison to the inundation in less crowded places and on less congested routes as a result of the higher rate of the crowd going back and forth in such centers. As a result, a greater number of individuals will be influenced and greater discontents may arise. Therefore, the importance of every land use determines the vulnerability rate and the distance between each of the channels from the land use determines the damage rate, in case an inundation occurs.

To determine the distance between the channel to the vulnerable centers, GIS qualities can be taken advantage of. First of all, the smallest distance between each channel to each of the land uses is computed and each of the land uses are rated through taking advantage of the experts' ideas and by making use of multi criteria decision making technique, FAHP, capabilities. Finally, each of the channels is assigned with a fuzzy value in terms of its distance to the important and sensitive centers.

- Fuzzy Analytic Hierarchy Process (FAHP):

FAHP is a fuzzy extension of the well-known AHP method developed by Saaty (1980). AHP is based on the way a human thinks logically and furnishes a hierarchical structure to analyze complex decision-making problems. It adopts the pair-wise comparisons method in order to elicit the weights of criteria and alternatives. The fuzzy extension of AHP has been developed by different researchers. For the purpose of this paper, the FAHP method proposed by Buckley (1985) was selected (Motevallian et al., 2014).

2.3.2 Bioenvironmental Scale

- Physical Barriers to Channels' inflows

One of the main problems of the open channels in urban drainage system is the inflow of the extraneous objects to these channels which leads to the reduction in the channel capacity; furthermore, these inflows may result in complete inundation and disruption of the drainage system performance in certain places like the channels intersections or in places where the channels are narrowed down. To rate the channels in terms of the amount of the garbage or the physical barriers entering therein, the information from the urban services department and municipality organization, which is responsible for removing such barriers were used. This organization's description of the status pertaining to each of the districts within the area under study was turned into a fuzzy number by taking advantage of table 1 and the channels existing in those sub-basins was given a negative score. The channels with higher rates of inflowing objects of extraneous material as a result of their being in the vicinity of streets and highly crowded business centers are assigned with higher negative scores.

Table 1. Discrete and fuzzy values used to describe the districts' bioenvironmental status.

Linguistic values for the parameters with negative nature	contrastive fuzzy values	Linguistic values for the parameters with positive nature
Very Good	(0,1,3)	Very Bad
Good	(1,3,5)	Bad
Medium	(3,5,7)	Medium
Bad	(5,7,9)	Good
Very Bad	(7,9,10)	Very Good

- Trash racks:

The existence of some installations such as trash rack and/or the sediment boxes on the path of the flow leads to the reduction in the sediment load and the objects inflowing to the channels and facilitates the removal of such objects from the channels. Therefore, equipping the channels with such installations is considered as a positive point for the channels in terms of bioenvironmental considerations. Each of the channels equipped with such installations are given a positive score in terms of bioenvironmental concerns according to the number of such installations in every channel's entrance, the way they act and the amount of the current installations' effects. The scores are again extracted from Table 1.

2.3.3 Economical Scale

- Costs:

The cost of repairing the channels for the purpose of reducing the flooding likelihood is one of the determinant factors in flood risk management in the region. Correcting the channel according to the flood discharge rate, apparent issues such as the fractures in the channel walls and/or the channel floor's destruction and channel position can incorporate structural modification. For instance, increasing the channel dimensions, and/or nonstructural modifications and the use of novel technologies such as Low Impact Development (LID) or Best Management Practices (BMP). Based on the above-mentioned issues and according to the indecisive nature of the parameters that influence the costs, risk reduction expenditures in each of the channels is calculated in a fuzzy and nondeterministic manner. (For example, if the cost of a channel's modification is solely calculated based on the flood discharge rate, the latter will be assigned a fuzzy amount according to the channel filling-in percentage which is also a fuzzy number and the cost will be reported in a fuzzy form within an uncertainty domain).

2.3.4 Urban Appearance Scale

- Apparent Problems:

The channel walls fracture, channel floor's erosion, the channels not being on the same level as one another in the intersection point, and other problems alike, will not only be followed with hydraulic problems but these will also cause disorders in the appearance of the city. In case there are any of the aforesaid problems present in channels, the respective channel will be given negative points according to the values presented in Table 1.

2.4 Risk Zoning Map Preparation

The multi criteria spatial decision-making techniques was used to combine the information layers in GIS and for preparing a flood risk zoning map. According to the fact that each of the aforesaid scales will be indicative of different values under various conditions and making decisions decisively regarding the superiority of each of the scales over the other is a difficult task, the specialists were asked to describe the superiority rate of each of the scales in respect to the other via verbal variables. Next, Buckley's proposed FAHP method (explained in the section 2.3.1) was used to calculate each of the layer's weight and the resulting fuzzy layers were combined with the fuzzy values by the use of Fuzzy SAW technique. The general formulation of the method is as stated in the Eq. [2]:

$$FinalRisk = (\tilde{W}_1 \times \tilde{L}_1) + (\tilde{W}_2 \times \tilde{L}_2) + \dots \quad [2]$$

where W and L are the relative fuzzy weight and rate of each parameter, respectively. The ultimate goal of such a paradigm is to generate a comprehensive flood risk zoning map. The map produced in this way can provide us with an accurate insight of the prioritized modifications and it can be applied as an efficient tool serving the managers' decision making.

3 CASE STUDY AND RESULTS

In this section, the efficiency of the above-mentioned framework is tested on a crowded and strategic region in the city of Tehran.

3.1 Study region

Tehran, capital city of Iran, with an area of over 68000 Ha is situated in such a manner that it is exposed to flood originating from the outer city basins from the north and east besides runoffs resulting from the precipitations in various levels of the city. The important intra-city basins can be divided into eastern, northern and central basins the three of which are located at the eastern brink of Kan River as well as Chitgar basin which is located along the western border of the Kan River. The study region investigated in the present research is the district 11 of Tehran Municipality. The region is extended over an area of 12.06 km² accounting for 8.1% of the total area of the city of Tehran. The approximate population of the region reaches to 289 thousand people and the substantial part of its land use is for residential purposes. The study region and its position are illustrated in figure 2. The presence of important historical and political centers has made the region to be continuously hosting external guests and their travelling to and from the region all of which have caused the region to become a strategic position. Besides, the presence of important economical centers, specialized markets, important university and academic centers, and important educational centers of the country has featured the region with a specific centrality.

Based on the aforementioned classifications, the district 11 is situated in the central catchment basin. Although the duty of transferring the flood away from this region is to be shouldered by the main drainage systems, special attention has been paid to the secondary channels in the present study, both of which are responsible for collecting the flood from the region and transferring it to the main drainage system and numerous cases of inundation have been observed during the

recent years in the region. Generally, District 11 is networked with 1193 secondary channels with a total length of 176.68 Kilometers.

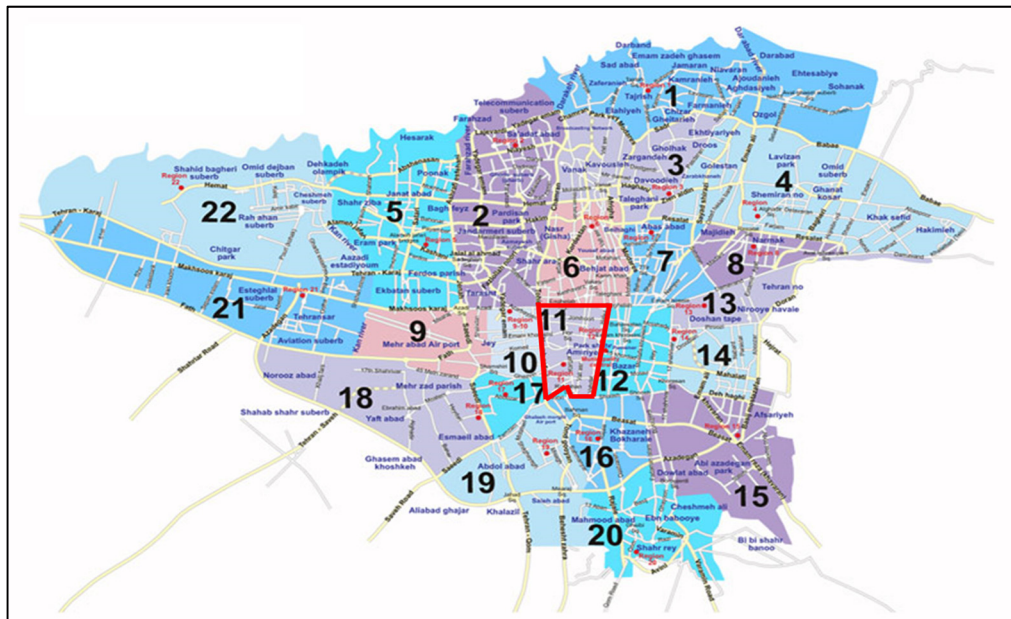


Figure 2. District 11 of Tehran municipality and its location in the city

3.2 Risk zoning in district 11 of Tehran

Among the fuzzy scales and parameters introduced for flood risk zoning, the ones presented in figure 3 were applied for study area risk zoning and illustration of the results.

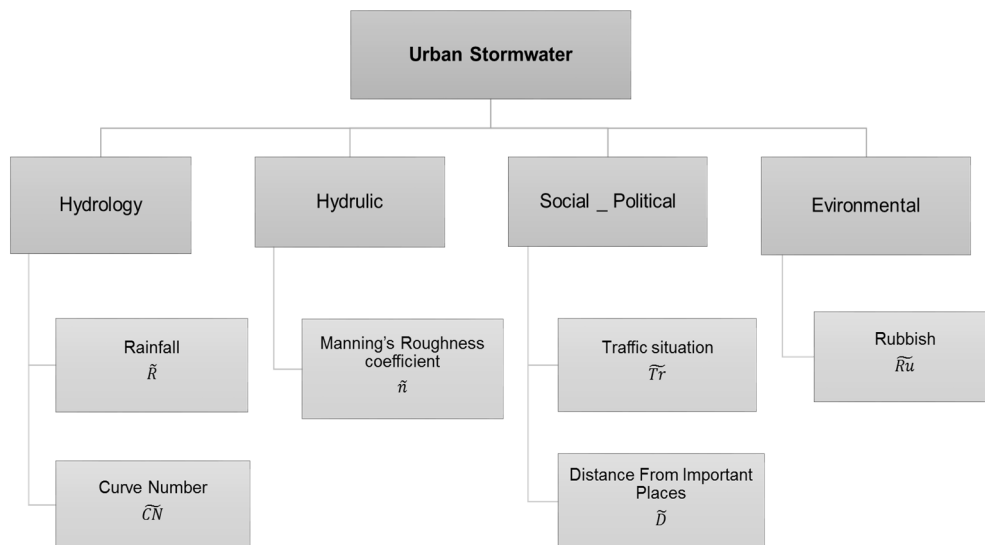


Figure 3. Scales used in risk zoning regarding the study area.

3.2.1 Calculating the flood occurrence probability.

The zoning of Tehran Municipality District 11 modeling was carried out in Autodesk SSA software domain. The three parameters of precipitation, sub-basins curve number and Manning's coefficient of roughness of the channel are the uncertain hydrologic and hydraulic parameters which were entered to the region's model in the form of fuzzy numbers. By combining the model's uncertain outputs, the flow depth to channel depth ratio for each of the channels was calculated in a nondeterministic manner and results were inserted to GIS. The study area model in Autodesk SSA environment and a schematic view of the outputs is displayed in Figure 4.

Since an 85% threshold has been set for the flow depth to channel depth ratio criterion for the model, the blue lines and points illustrated in the model output indicate the nodes and the channels with a ratio above 85%.

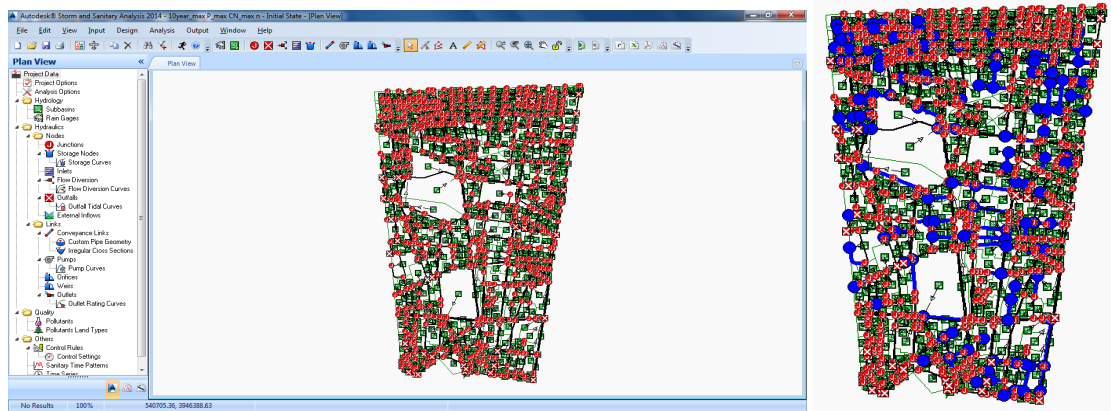


Figure 4. Study area model in Autodesk SSA and schematic view of the model output.

3.2.2 Calculating the Intensity of flood consequences

To calculate the flood consequences intensity, in the first step, the information layer pertaining to each of the parameters related to the distance from the sensitive centers, traffic situation, channels status in terms of the amount of the inflowing rubbish and the flow depth to channel depth ratio were prepared corresponding to what has been described so far. Next, these layers were combined by making use of MCDM, Fuzzy AHP. A schematic view of the information layers for each of the mentioned parameters is demonstrated in Figure 5.

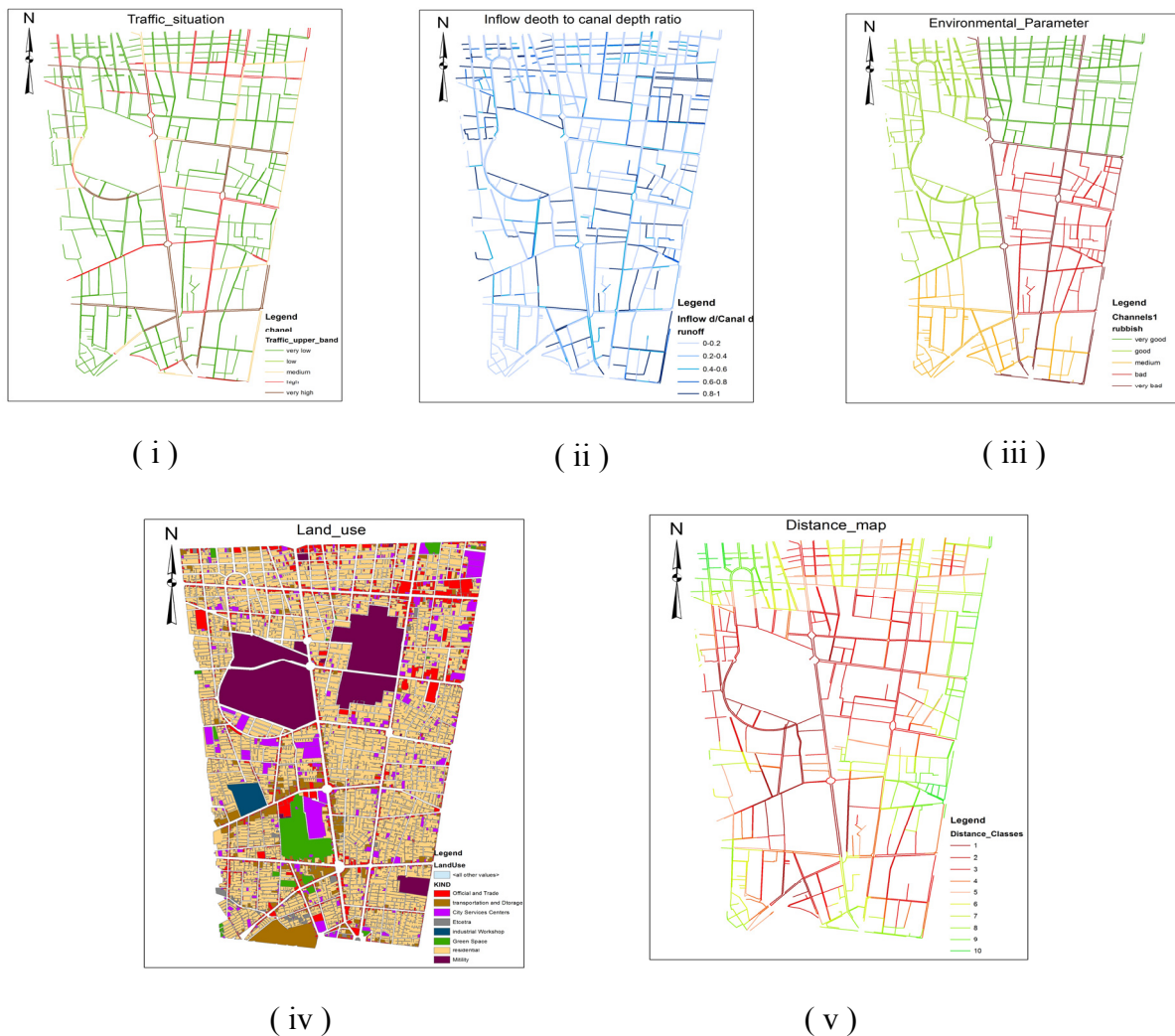


Figure 5. (i) the region's traffic situation; (ii) the flow depth to channel depth ratio; (iii) the study area situation in terms of the amount of channel's inflowing rubbish; (iv) the study area land use; (v) the distance map obtained from pooling the land use information.

3.2.3 Final risk zoning map extraction

The risk intensity final map obtained from combining the information layers of flood incidence probability and the intensity of its consequences are illustrated in figure 6. As it is evident from the figure, flood risk was categorized into five classes and each channel was assigned with a certain risk value. The number of the channels having any certain risk class is provided in table 2. It is noteworthy that because the channels have been classified during the modeling operation (for better modeling of the connections), the 1193 channels, in the study area, were transformed into 1323 channel sections.

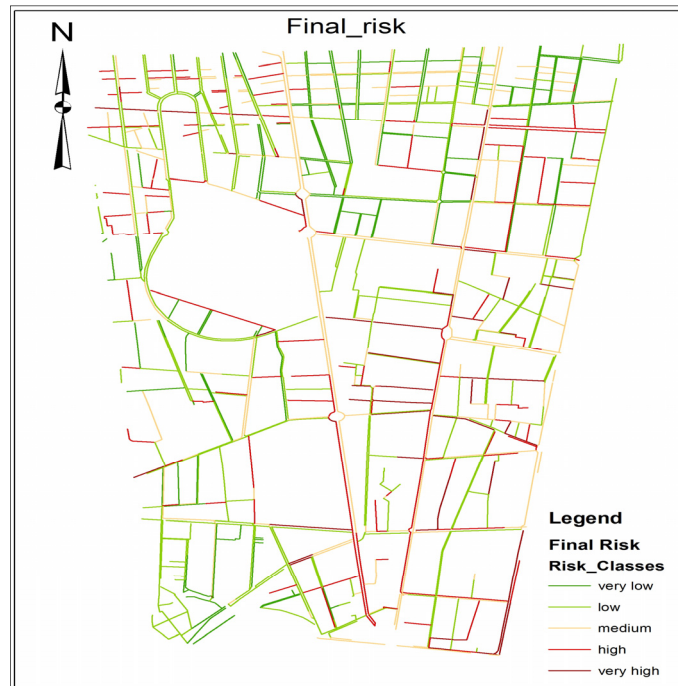


Figure 6. Flood risk zoning final map in channels.

Among the issues worthy to be attended to in the study results are the places where the channels with modification priority have been situated. From the specialists' point of view, the first priority belongs to the hydrologic and hydraulic scales, the second priority goes to the political-social scale and the third priority is given to the bio-environmental scale. According to the same issue and based on the map displaying the channels' flow depth to channel depth ratio, the similarity of the risk final map to this map is tangible. This is suggestive of the specialists' ideas effect on the study results. Taking the aforementioned scales' uncertainty as well as the ambiguities in the specialists' ideas and decisions into consideration, a comprehensive final risk map of the study area can be generated. The results obtained can explicitly be adopted by the managers and decision makers to serve them as a guide in dealing with the urban issues for the purpose of modification interventions' prioritization regarding the urban drainage systems.

Table 2. Linguistic variables describing the risk value and the number of channels with every risk class.

LINGUISTIC VARIABLE DESCRIBING THE RISK VALUE	NUMBER OF CHANNELS
Very Low	228
Low	538
Medium	292
High	188
Very High	77

4 CONCLUSIONS

Due to the uncertain nature of the floods and their dependence on various parameters, deterministic protection of the cities against them, is practically an impossible issue. Therefore, the managers and the urban affairs authorities mostly concentrate on mitigating the unfavorable effects of such natural phenomena. Flood risk analysis is an efficient method in line with flood risk assessment method. In the present article, an urban

flood risk management has been presented with an emphasis on the hydrologic and hydraulic, social-political, economic, bio-environmental and city appearance issues. To do so, flood risk was defined as a function of its occurrence probability and the intensity of the relative consequences. Implementing of the proposed framework for an urban storm water drainage system consists of three general stages. The first step is the calculation of flood occurrence probability as a function of the uncertain hydrologic and hydraulic parameters and through modeling the system via Autodesk SSA software. The model outputs in a fuzzy environment are indicative of the channel's hydraulic capacity under various conditions, which is served as an input to the final stage, which is the risk calculation. The second step includes the calculation of the intensity of the consequences resulting from a flood as a function of the sociopolitical, economical, bio-environmental and city appearance scales. The parameters pertaining to each of the aforementioned scales are defined in the form of an isolate layer in GIS. Finally, the last step is the calculation of flood risk in the drainage network. In this stage, the layers' weights are specified and combined by the use of fuzzy spatial multi-criteria decision making method. The output of this framework is expressive of the risk value in each of the channels from the study area and a summary report of the urban storm water drainage system status can be attained through transforming risk fuzzy values for each of the channels to linguistic variables. In fact, the entire possible modes that may come along in future are covered by an investigation of the urban drainage system performance as proposed in the present study along with the comprehensive evaluation of the system.

The efficiency of the framework proposed in the present study has been assessed in investigating the urban storm water drainage system performance in one of the important, highly crowded and strategic regions in the city of Tehran in Iran. The final results are indicative of very high and high risks in 265 channel sections which has to be considered in the short term and long term rehabilitation plans. This approach is able to prioritize the flooding risk in other similar cities.

REFERENCES

- Buchele, B., Kreibich, H., Kron A., Thielen, A., Ihringer, J., Oberle, P., Merz, B. & Nestmann F. (2006). Flood-Risk Mapping: Contributions towards an Enhanced Assessment of Extreme Events and Associated Risks. *Natural Hazard and Earth System Sciences*, 6, 485-503.
- Buckley, J.J. (1985). Fuzzy Hierarchical Analysis. *Fuzzy Sets and Systems*, 17(3), 223–247.
- Burian, S.J. & Edwards, F.G. (2002). Historical Perspectives of Urban Drainage. *Ninth International Conference on Urban drainage (9ICUD)*.
- Lootsma, F.A. (2005). *Fuzzy Logic or Planning and Decision Making*. Dordrecht, Kluwer Academic Publisher.
- Motevallian, S.S., Tabesh, M. & Roozbahani, A. (2014). Sustainability Assessment of Urban Water Systems: A Case Study. *Engineering Sustainability*, 167, 157-169.
- Radmehr, A. & Araghinejad, Sh. (2015), Flood Vulnerability Analysis by Fuzzy Spatial Multi Criteria Decision Making. *Water Resource Management*, 29, 4427-4445.
- Roozbahani, A., Zahraie, B. & Tabesh M. (2013). Integrated Risk Assessment of Urban Water Supply Systems from Source to Tap. *Stochastic Environmental Research and Risk Assessment*, 27, 923-944.
- S.C. PMI (2004). *A Guide to the Project Management Body of Knowledge (PMBOK) (2004ed.)*, Project Management Institute, Newton Square, PA, USA.
- Saaty, T.L. (1980). *The Analytic Hierarchy Process*. McGraw Hill International. New York, USA.
- Schellart, A., Linguori, S., Kramer, S., Saul, A. & Rico-Ramirez M.A. (2014). Comparing Quantitative Precipitation Forecast Methods for Prediction of Sewer Flows in Small Urban Area. *Hydrological Science Journal*, 59(7), 1418-1436.
- Schilling, W. (1991). Rainfall Data for Urban Hydrology: What Do We Need? *Atmospheric Research*, 27(1-3), 5-21.
- Schilling, W. & Fuchs, L. (1986). Errors in Storm Water Modeling-a Quantitative Assessment. *Hydraulic Engineering*, 112(2), 111-123.
- TahmasebiBirgani, Y. & Yazdandoost, F. (2016). Resilience in Urban Drainage Risk Management Systems. *Water Management*, 169(1), 3-16.
- Zadeh, L.A. (1965). Fuzzy Sets. *Information and control*, 8, 338-353.
- Zhou, Q., Mikkelsen, P.S., Halsnaes, K. & Arnbjerg-Nielsen, K. (2012). Framework for Economic Pluvial Flood Risk Assessment Considering Climate Change Effects and Adaptation Benefits. *Journal of Hydrology*, 414-415, 539-549.

HYDRAULIC RESPONSES ON STORMWATER TREATMENT FOR VARIATION OF FILTER MEDIA DEPTHS

HUSNA TAKAIJUDIN⁽¹⁾, AMINUDDIN AB. GHANI⁽²⁾, NOR AZAZI ZAKARIA⁽³⁾ & TZE LAU LIANG⁽⁴⁾

⁽¹⁾ Civil and Environmental Engineering Department, Faculty of Engineering, Universiti Teknologi PETRONAS, Perak, Malaysia, husna_takaijudin@utp.edu.my

^(1,2,3) River Engineering and Urban Drainage Research Centre (REDAC), Universiti Sains Malaysia, Engineering School of Civil Engineering, Universiti Sains Malaysia, Penang, Malaysia,

⁽⁴⁾ School of Civil Engineering, Universiti Sains Malaysia, Engineering Campus, Penang, Malaysia

ABSTRACT

Media depth is the main design element in bioretention system. However, the range of depth which used in this approach are still questionable when dealing with the hydraulic and treatment performance. Hence, this paper investigates the relationship between hydraulic and stormwater treatment performance in predicting long-term performance of bioretention by variation of filter media depths. A preliminary study focused on three small-scale columns, namely C1, C2 and C3 with 74mm in diameter and 700mm in height. Column C1, C2 and C3 comprise 300mm, 400mm, 500mm deep engineered soil media, respectively. Soil composition of engineered soil media consists of 50% medium sand, 30% topsoil, and 20% organic leaf compost. Approximately 3.3 L of collected raw stormwater samples were poured into each column in four (4) repetition cycles. Both influent and effluent were collected and tested. Declination trends was observed in hydraulic conductivity (K_{sat}) as the sedimentation start to develop and clogged on top of surface layer. The results revealed that deeper media depth effectively removed the wastes with the mean±standard deviation (SD) for removal is at 93.4±5.2, 69.5±17.0, 40.0±13.7% for TSS, TN and TP, respectively. The responses between hydraulic and treatment performance are established using regression method. The relative K, TSS and TP removal had good agreement because R^2 is within 0.72 to 0.91. Hence, the prediction of infiltration parameters can be relied on the contaminant removal through sedimentation and filtration process.

Keywords: Bioretention; soil column studies; filter media depth; hydraulic conductivity (K_{sat}); stormwater treatment.

1 INTRODUCTION

Bioretention is a typical Low Impact Development (LID) tool which offers multiple solution by applying more natural hydrological processes and contaminant removal mechanisms in dealing with stormwater runoff (Brown and Hunt, 2011). This is a flexible approach where it is applicable to be installed as individual or regional system and can be designed from single to larger development project area (Davis and Mc Cuen, 2005).

Filter zone consists of multilayer of soil, sand, and silt with the minimum of clay content in order to prevent low infiltration rate. Media depth is the major factor in controlling hydrologic performance in bioretention (Li et al., 2009; Brown and Hunt, 2009). Table 1 lists some of the recommended filter media depths from previous studies. Based on their findings, the deeper depth provides better performance which promotes more storage volume (Brown and Hunt, 2011). Besides that, the deeper filter media allow higher amounts of runoff volume to be treated. However, deeper media might increase excavation cost and also disturb the groundwater level that resulted in the failure of bioretention system (Li et al., 2009; Brown, 2011).

Besides, filter media depth is one of the main design criteria of bioretention system. However, there was large difference of design criteria, mainly infiltration rate from available guidelines (e.g. 13mm/hr is recommended for greater than 100mm topsoil while 13-130mm/hr for the depth of topsoil greater than 45mm in are proposed by Californian systems (Good et al., 2012). Brown and Hunt (2011) also added that bioretention is still required specifically for fill media design criteria (e.g. depth of the media) that kept changing depending on the condition of drainage area criterion, drainage design, and suitability of soil on the site. Guo et al. (2014) highlighted that porous filter media is the crucial component to capture contaminants from waterways. The filter media used to provide sufficient infiltration capability, but yet simultaneously it must provide sufficient retention time to support vegetation growth. Hence, the characteristics of filter media mainly depth and types of materials required further investigation on this aspect.

Thus, the summary of the design criterion of selected technical guidelines, mainly design flow or water quality volume, range of K_{sat} and targeted pollutant removal are tabulated in Table 2. Typically, the design of storm for bioretention system can be classified into minor and major storm where it is designed for 1 to 5 years. ARI storm event for minor storm and 100 years ARI for major storm.

Table 1. Proposed filter media depths across literature.

Author (year)	Recommended filter media depths
Davis and Mc Cuen (2005)	The recommended depth of filter media ranged 150– 200mm
Hunt et al. (2006)	They proposed 1200mm depth which was deeper filter depth that allows more water seep through into the system.
Clar et al. (2007)	They proposed the depth of 760-1220cm (30-48 inches) suitable for plant to grow.
Brown and Hunt (2009)	They expressed that the deeper media depths fulfilled the LID requirement in eliminating runoff volume regularly.
Li et al. (2009)	They suggested that the media depth varied from 500mm to 120mm.
Brown and Hunt (2011)	The study continued at field with 600 and 900mm to cater runoff from parking lot.

However, the recommendation for design for this is slightly different which was designed for 40mm rainfall depth or 3 month ARI design of rainfall due to Malaysia receiving heavy rainfall throughout the year compared to other country (DID, 2012). According to the table, there are proposed ranges of K_{sat} values for bioretention design. Nevertheless, the accuracy of the K_{sat} values on the bioretention site is challenging because it was exposed to a number of external factors such as natural compaction, unpredictable weather, and growth of unwanted vegetation which caused high variation of K_{sat} data that exceeded the recommended values which affected the performance in long term duration. According to Table 2, TSS removal is the highest targeted removal compared to TN and TP which showed that physical contaminant can be removed excellently in bioretention system. It has been proved by previous researches where more than 80% of TSS was captured in the system (Blecken et al., 2007; Brown and Hunt, 2011; Sidek et al., 2016). Furthermore, it also had shown impressive pollutant removal through laboratory studies in the reduction in concentration of TP (70 to 85%) and NH_4^+ (60 to 80%) (Davis et al., 2006). In 2007, the researchers set up column studies to observe the performance of nutrient removal (Blecken et al., 2007). They assessed fifteen (15) biofilter columns in treating synthetic runoff at low temperatures and found that biofilters performed well in eliminating TP. Dissolved P was also removed well by biofilters from 69 to 77% for high and low temperatures, respectively. Mechanical removal was the main factor in dissolved P removal. Conversely, the results showed that poor performance occurred in removing TN due to high leaching and lacking of denitrification process. However, due to variability of construction of sand and planting soil occurs due to local guidelines (DID, 2012) which specified the TSS, TP and TN removal (Guo et al., 2014). Thus, this study is carried out in order to examine the level of soil capabilities in treating this kind of pollutants. Researches using both soil column laboratory and field studies have evaluated the bioretention performance emphasizing on the interaction between hydrologic and treatment performance (Heasom, 2006; Mangangka et al., 2015). Past researches have typically assessed long term performance of bioretention which split the response between these two aspects *i.e.* hydrologic and pollutant removal (Mangangka et al., 2015). Hence, this paper is to establish the relationship between infiltration parameter (which one of hydrologic elements) and treatment performance for primary pollutants TSS, TN and TP with respect to different filter media depth.

2 MATERIAL AND METHODS

2.1 Column setup and configuration

Three (3) small-scale columns namely C1, C2 and C3 consisting of 300mm, 400mm and 500mm of soil media depth are readied. These soil column preliminary works were setup in in the Physical Modeling Laboratory, River Engineering and Urban Drainage Research Centre (REDAC), Universiti Sains Malaysia, Penang, Malaysia. The columns were scaled to the ratio 1:20 from actual catchment area as reported by Takaijudin et al. (2015). Typically engineered soil composition was used in these columns with 50% of medium sand (size range 0.2-0.6mm), 30% topsoil (medium loam) and 20% organic compost (Carpenter and Hallam, 2010). The net was placed between underdrain and soil layer as a separator to prevent soil accumulation into the drainage layer which reduces the volume of soil media. The engineered soil media were compacted softly using a rod at every 50mm depth to minimize compaction influence on K_{sat} .

Approximately 27 blows were applied for each layer as referred to Proctor test procedure (BSI, 1992) to ensure the soil sampled were well-compacted. 30mm gravel as underdrain layer was placed at the bottom to prevent movement of filter media layer. (Kandra et al., 2014). The engineered soil media were filled on top of the gravel layer with the different depth for each column ranged from 30cm to 50cm. Figure 1 illustrates the soil column laboratory setup.

Table 2. Recommendation of design criterion of several technical guidelines.

Guidelines	Country	Recommended filter media depths	Water quality volume / Design flow	Recommended K_{sat}	Recommended Pollutant Removal (%)		
					TSS	TN	TP
LID: Urban Design Tools (LID, 2007)	Maryland, USA	<ol style="list-style-type: none"> recommended minimum depth of 600mm to 760mm without large tree plantings if shallow rooted plants are used, soil depth may be reduced to 460mm recommended depth of 1200mm to 1400mm with large trees 	10 years ARI storm event	-	86	60 (TKN) 70 - 80 (NH ₃ -N)	80
North Shore City Bioretention Guidelines (North Shore City, 2008)	New Zealand	500 -1000mm depth (minimum 300mm for shrub and grass and maximum 1000mm for trees)	1/3 of 2 year ARI for minor storm	100-300mm/hr			
WSUD Engineering Procedures (Melbourne Water, 2005)	Australia	<ol style="list-style-type: none"> Lined biofiltration system with submerged zone 300 -500mm Standard lined biofiltration system 400 – 700mm 	Minor storm: 5 years ARI for temperate climate, 2 years ARI for tropical climate. Major storm: 100 years ARI for temperate climate, 50 years ARI for tropical climate.	100-300mm/hr	80	45	45
Bioretention Manual (The Prince George County, 2009)	North Carolina, USA	<ol style="list-style-type: none"> Min 18" (458mm) 	25.4mm (1") rainfall depth or 1 year ARI storm event.	K_{sat} is based on soil classifications from loam to sandy loam with 13.2 to 61.2mm/hr (0.52 – 2.41in./hr)	97	33 - 66	35 - 65
Engineering procedures for ABC Waters Design Features (PUB, 2011)	Singapore	<ol style="list-style-type: none"> Similar standard as recommended by FAWB (2009) 	Minor storm: 5 years ARI Major storm: 100 years ARI	50-200mm/hr but not exceed 500mm/hr	80	45	45
Stormwater Management Manual for Malaysia (MSMA) (DID, 2012)	Malaysia	<ol style="list-style-type: none"> 450 -1000mm for both permeable and impermeable bioretention systems 	40mm rainfall depth or 3 month ARI	Based on soil classification with ranges of 13-200mm/hr	80	50	60

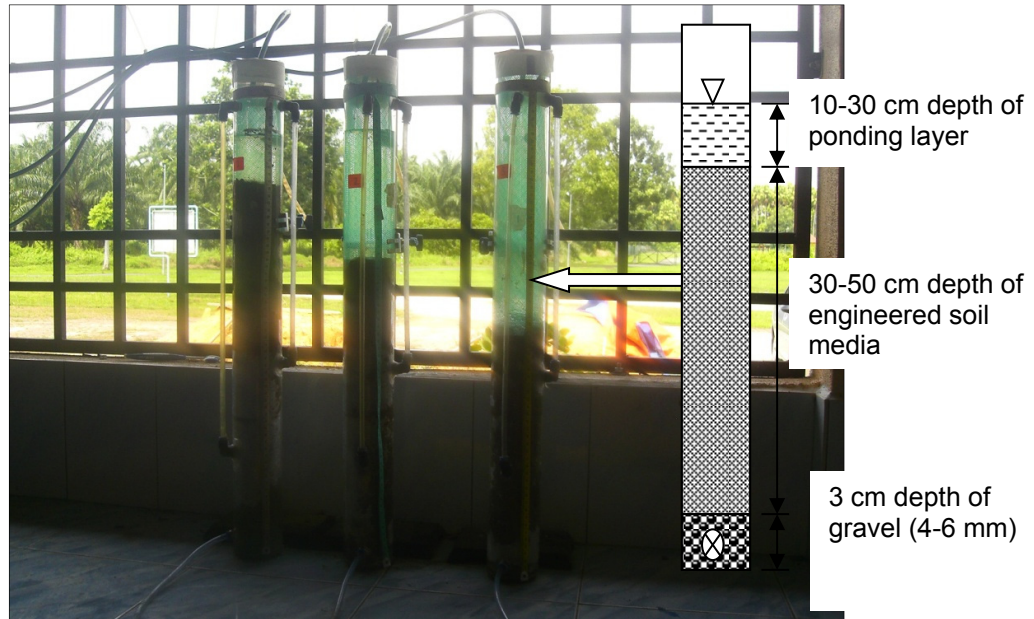


Figure 1. Soil-column setup for different filter media depths.

2.2 Constant head test

Constant head conceptual was implemented for these column studies. It was modified by the derivation of Darcy's Law (Good et al., 2012). Tap water was used as the main source of water. Then, it is discharged to the cylindrical column through 6mm tubes in parallel condition. The inflow rate was adjusted using valves to obtain constant 100mm ponding layers at the top of engineered soil media. Once ponding became steady (meeting saturated condition) within 24 hours, initial outflow rate was measured using stopwatch and 100ml of beaker ($n = 5$ measurement for each column). The measurement was conducted concurrently with treated stormwater sampling.

2.3 Stormwater quality sampling and testing

After completing initial hydraulic conductivity, the columns were flushed again with natural stormwater runoff. For the treatment of storm water runoff, TSS, TN and TP tests were conducted for this preliminary study due to many findings related to these pollutants were treated well in bioretention systems across the literature (Blecken et al., 2007; Erickson et al., 2007; Lucas, 2008). Then, initial K_{sat} (K_{ini}) was recorded. It was then flushed with natural stormwater runoff. One (1) L influent of stormwater sample was collected from the source tank. Approximately 3.4 L of natural stormwater sample (assuming bioretention size to 5% of the impervious catchment area) was discharged into each cell. Stormwater sample was conveyed into bioretention for six (6) hours measurement. Then, about one (1) L of treated stormwater sample was collected in outlet tubes for every two (2) hours. K_{sat} was also measured during the sampling time for every two (2) hours. The performance was assessed based on event in order to mimic the actual performance on site (Hatt et al., 2009; Mangangka et al., 2015). Four (4) repetitions represented four (4) storm events that occurred once a week. Each event lasted in six (6) hours duration with total stormwater samples, $N = 48$. TSS was analyzed by the gravimetric method and filtered using Whatman 47mm diameter glass fiber filter papers (Guo et al., 2014). The nitrogen concentration was tested using the Persulfate Digestion Method according to Standard Method 4500-NC (APHA, 2005) where the unit is in mg/L N. Phosphorus concentration was tested using the USEPA PhosVer®3 with Acid Persulfate Digestion Method based on Standard Method 4500-P (APHA, 2005) where the unit is in mg/L PO_4^{3-} . The treatment efficiency was computed as in Equation 1.

$$Removal\ Efficiency = \frac{C_{inf} - C_{eff}}{C_{inf}} \times 100\% \quad [1]$$

where; C_{inf} = Influent concentration (mg/L); C_{eff} = Effluent Concentration (mg/L).

2.4 Data analysis

Firstly, a preliminary analysis was attempted for determining the effects of filter media depth on infiltration parameters and water quality performance by having comparison for each treatment condition using Pearson product moment correlation. This method was applied to measure the correlation between tested variables. Additionally, regression model was used to investigate the relationship between treatment performance and infiltration parameters *i.e.* hydraulic conductivity.

3 RESULTS AND DISCUSSIONS

3.1 Hydraulic conductivity and water quality performance

Table 3 shows the summary of mean hydraulic conductivity and pollutant performance for each soil media depth treatment conditions. It was found that the trends of hydraulic conductivity and pollutant concentration were reduced across the columns. This was explained by deeper soil depth lead to decelerate the flow velocity in the system which at the same time enhance treatment performance. Longer flow paths is created in C3 compared to C1 and C2 where it tends to have longer hydraulic retention time. This is good for treatment processes where more reaction between soil microbes and pollutants occurred in the soil system. Besides, this was supported by Hou et al. (2014) where longer degradation process occurred in deeper soil system. The soil with more than 400mm achieved the targeted TSS removal more than 80% (DID, 2012). For TP removal, all soil columns have exceeded recommended removal more than 60%. Conversely, TN showed poor performance where all column have failed to reach the targeted values. The results were compared with previous studies as listed in Table 3. It was found that the results were consistent with previous studies for TSS and TN but TP performed slightly lower as compared to O'Neill et al. (2012). Many factors have influenced the variation, mainly column sizing (filter media and bioretention area) and also the soil characteristics (soil mixtures, grain sizes).

Table 3. Saturated hydraulic conductivity and water quality treatment performance from all experimental work at different soil media depth. Data is presented in average±standard deviation (SD).

Parameters	Inflow	Outflow			Previous studies	
		C1 (300mm)	C2 (400mm)	C3 (500mm)	Inflow	Outflow
Saturated Hydraulic Conductivity (mm/hr)						
Initial	NA	534±36	260±22	222±30		
Final	NA	244±9	154±8	177±17		
TSS concentration (mg/L)	48±7	10±3	7±3	3±2	2.1 to 43.2 ^a	5.3 to 7.6 ^a
% removal		78.5±8.5	84.4±7.3	93.4±5.2		93.4 ^a
TN concentration (mg/L)	17.1±1.8	11.3±2.2	10.8±2.3	10.2±2.4	2.3±1.2 ^b	1.4±0.7 ^b
% removal		33.5±13.7	36.9±13.5	40.0±13.7		37.3±18.3 ^b
TP concentration (mg/L)	5.32±0.18	1.81±0.93	1.66±0.97	1.62±0.92	0.14±0.08 ^b	0.02±0.01 ^b
% removal		66.0±17.4	69.4±18.4	69.5±17.0		87.2±5.8 ^b

^a Guo et al. (2014); ^b O'Neill et al. (2012).

The Pearson correlation matrix (Table 4) showed that TSS and TP was very close correlation with hydraulic conductivity as the coefficients are 0.737 and 0.536 ($p < 0.01$), respectively. This essentially confirms that the both water quality parameters were influenced by physical treatment mechanisms mainly infiltration parameter which has been expressed by hydraulic conductivity. Considering good correlation, hydraulic conductivity, TSS and TP treatment performance were selected for further analysis. Poor and negative correlation is indicated between TN and other parameters. It was explained that TN has different treatment mechanisms which included more complex process like nitrification and denitrification in the soil system. This may be assisted by the presence of vegetation where nutrient can be uptake by plant for its growth as recommended by Glaister et al. (2014).

Table 4. Pearson correlation matrix (number of water sampling, $n=36$).

	TSS	TN	TP
Hydraulic Conductivity	0.737	-0.192	0.536
TP	0.692	-0.538	
TN	-0.241		

3.2 Relationship between treatment performance and hydraulic conductivity

Based on correlation in Table 4, it is indicated that only TP and TSS had good correlation with hydraulic conductivity. Hence, these variables were used for regression analysis. The basic model was established to predict the hydraulic function of a bioretention system based upon the related treatment performance. Both single linear regression (SLR) and multiple linear regression (MLR) models were developed to examine the interaction or response between water quality and hydraulic performance as shown in Table 5. Relative hydraulic conductivity (K_{rel}) is defined as the ratio of final hydraulic conductivity when applying synthetic runoff on soil column to the initial hydraulic conductivity during the application of clean water (Bozorg et al., 2015). Pollutant removal is indicated by Total Phosphorus removal (TP_r) and Total Suspended Solids removal (TSS_r). Based on the results in Table 5, there is a strong relationship between hydraulic conductivity and TP_r with adjusted R^2 is more than 0.75 across any soil depths as expressed in Equation 1a, 2a and 3a. However, TSS_r had poor relationship for narrower depth (300mm) (Equation 1b) but good relationship with the depth more

than 400mm (adjusted $R^2 > 0.7$) (See Equation 2b and 3b). It shows that by having greater depth of soil media, more physical sediments are captured in the first place *i.e.* at the soil surface. Hence, the combination of these pollutant removals had greater influenced on hydraulic conductivity with respect to the depth. This was explained by the deeper depth, more pollutants were trapped in the system which allow the sufficient time for soil microbes to react with phosphorus-bound particulates through deposition as well as adsorption impressively as highlighted by previous researchers (Davis et al., 2006; Hunt et al., 2006; Bratieres et al., 2008; Passeport et al., 2009).

Table 5. SLR and MLR equations for soil media depths condition.

Soil Configurations	Regression model	Adjusted R ²
300 mm		
Equation 1a	$K_{rel} = 0.743 - 0.00365 TP_r$	0.78
Equation 1b	$K_{rel} = 0.948 - 0.00568 TSS_r$	0.41
Equation 1c	$K_{rel} = 0.748 - 0.00362 TP_r - 0.00009 TSS_r$	0.76
400 mm		
Equation 2a	$K_{rel} = 0.970 - 0.00416 TP_r$	0.75
Equation 2b	$K_{rel} = 1.62 - 0.0111 TSS_r$	0.85
Equation 2c	$K_{rel} = 1.44 - 0.00185 TP_r - 0.00744 TSS_r$	0.91
500 mm		
Equation 3a	$K_{rel} = 1.04 - 0.00181 TP_r$	0.82
Equation 3b	$K_{rel} = 1.34 - 0.00446 TSS_r$	0.72
Equation 3c	$K_{rel} = 0.747 - 0.00301 TP_r + 0.00406 TSS_r$	0.85

Comparing the observed K_{rel} for all tested condition *i.e.* variation media depths to establish regression model of TSS_r and TP_r , it is evident that each single equation is a fit for the observed data (Figure 2). There were outliers for the soil column with 500mm depth due to leaking at the wall column during the final measurement. Hence, the water flow through the outlet tube was less which leads to having extremely low hydraulic conductivity. However, it has not influenced the TP and TSS treatment performance.

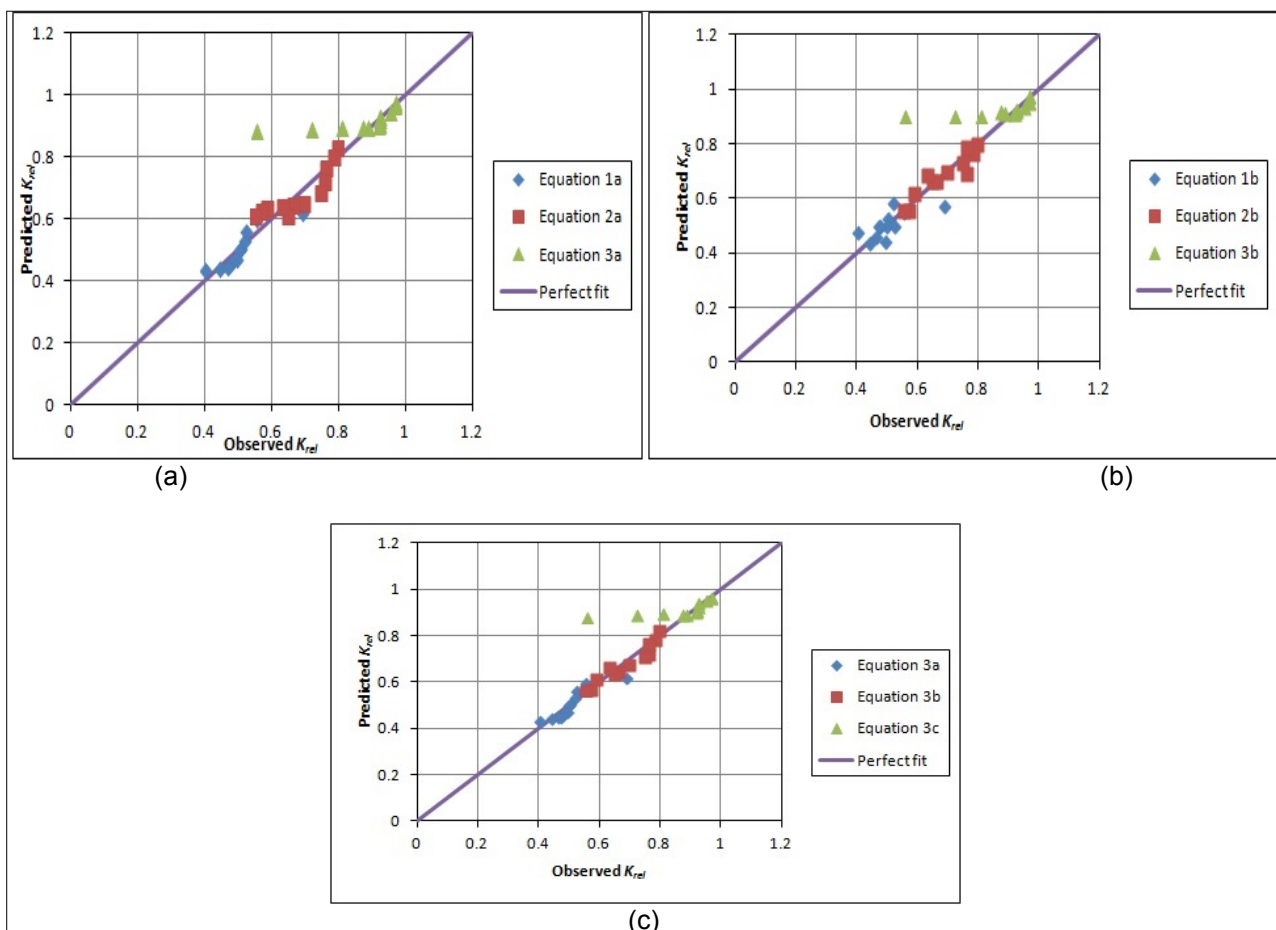


Figure 2. Relationship between predicted K_{rel} and measured K_{rel} for variation soil media depths. (a) SLR model of K_{rel} and TP_r ; (b) SLR model of K_{rel} and TSS_r (c) MLR model of K_{rel} , TP_r and TSS_r .

4 CONCLUSIONS

Results found TSS and TP were treated well without the presence of vegetation since it can be treated through filtration and adsorption as stated in literature. K_{sat} values significantly declined with the increasing of TSS and TP removal with respect to the depth. Deeper depth promotes lower hydraulic conductivity which leads to provide more retention time for soil microbes to react with pollutants where absorption and sedimentation occurred in the system. More physical sediments are captured at the soil surface and it is trapped at a few centimetres below the soil surface. Relationship between both hydraulic and treatment performance are well established using regression model. The data are fitted with the suggested model with adjusted R^2 being more than 0.7 that indicated that hydraulic conductivity can be predicted by water quality performance for mainly TSS and TP removal. Based on this study, Hence, the optimum depth of 400mm was suggested in this study for the design purposes by relating to both hydraulic and water quality performance.

ACKNOWLEDGEMENTS

The research is funded by Ministry of Higher Education under Long Term Research Grant (LRGS) No. 203/PKT/672004 entitled Urban Water Cycle Processes, Management and Societal Interactions: Crossing from Crisis to Sustainability. The authors also acknowledge River Engineering and Urban Drainage Research Center (REDAC), Higher Institution Centre of Excellence (HICoE) for Service and Universiti Teknologi PETRONAS (UTP) for giving full support for the success of this project.

REFERENCES

- American Public Health Association (APHA). (2005) *Standard Methods for the Examination of Water and Wastewater*. American Water Works Association, Water Environment Federation.
- Blecken, G.T., Zinger, Y., Muthanna, T.M., Deletic, A., Fletcher, T.D. & Viklander, M. (2007). The Influence of Temperature on Nutrient Treatment Efficiency in Stormwater Biofilter Systems. *Water Sci. Technol.*, 56(10), 83-91.
- Bozorg, A., Gates, I.D. & Sen, A. (2015). Using Bacterial Bioluminescence to Evaluate the Impact of Biofilm on Porous Media Hydraulic Properties. *Journal of Microbiological Methods*, 109, 84-92.
- Bratieres, K., Fletcher, T.D., Deletic, A. & Zinger, Y. (2008). Nutrient and Sediment Removal by Stormwater Biofilters: A Large-Scale Design Optimisation Study. *Water Res.*, 42(14), 3930-3940, doi: 10.1016/j.watres.2008.06.009.
- Brown, R. & Hunt, W. (2009). Effects of Media Depth on Bioretention Performance in the Upper Coastal Plain of North Carolina and Bioretention Construction Impacts Study, In *World Environmental and Water Resources Congress 2009: Great Rivers*, 1-10.
- Brown, R.A. (2011). Evaluation of Bioretention Hydrology and Pollutant Removal in the Upper Coastal Plain of North Carolina with Development of a Bioretention Modeling Application in DRAINMOD, *PhD Thesis*. North Carolina State University, Raleigh, North Carolina.
- Brown, R.A. & Hunt, W.F. (2011). Impacts of Media Depth on Effluent Water Quality and Hydrologic Performance of Undersized Bioretention Cells. *Journal of Irrigation and Drainage Engineering*, 137(3), 132-143.
- Carpenter, D.D. & Hallam, L. (2010). Influence of Planting Soil Mix Characteristics on Bioretention Cell Design and Performance. *Journal of Hydrologic Engineering*, 15(6), 404-416.
- Clar, M., Laramore, E. & Ryan, H. (2007). Rethinking Bioretention Design Concepts, In *Proceedings of the Second National Low Impact Development Conference*, North Carolina, 119-127.
- Davis, A.P. & McCuen, R.H. (2005). *Stormwater Management for Smart Growth*. Springer Science & Business Media, New York, Chapter C9.
- Davis, A.P., Shokouhian, M., Sharma, H. & Minami, C. (2006). Water Quality Improvement Through Bioretention Media: Nitrogen and Phosphorus Removal. *Water Environment Research*, 78(3), 284-293.
- Department Irrigation and Drainage for Malaysia (DID). (2012). *Urban Stormwater Management Manual for Malaysia*, Department of Irrigation and Drainage (DID), Kuala Lumpur, Malaysia.
- Erickson, A.J., Gulliver, J.S. & Weiss, P.T. (2007). Enhanced Sand Filtration for Storm Water Phosphorus Removal. *Journal of Environmental Engineering*, 133(5), 485-497.
- Glaister, B.J., Fletcher, T.D., Cook, P.L. & Hatt, B.E. (2014). Co-Optimisation of Phosphorus and Nitrogen Removal in Stormwater Biofilters: The Role of Filter Media, Vegetation and Saturated Zone. *Water Science & Technology*, 69(9), 1961-1969.
- Good, J.F., O'Sullivan, A.D., Wicke, D. & Cochrane, T.A. (2012). Contaminant Removal and Hydraulic Conductivity of Laboratory Rain Garden Systems for Stormwater Treatment. *Water Sci. Technol.*, 65(12), 2154-2161.
- Guo, H., Lim, F.Y., Zhang, Y., Lee, L.Y., Hu, J.Y., Ong, S.L., Yau, W.K. & Ong, G.S. (2015). Soil Column Studies on the Performance Evaluation of Engineered Soil Mixes for Bioretention Systems. *Desalination and Water Treatment*, 54(13), 3661-3667.
- Heasom, W., Traver, R.G. & Welker, A. (2006). Hydrologic Modelling of a Bioinfiltration Best Management Practice. *Journal of the American Water Resources Association (JAWRA)*, 42(5), 1329-1347.

- Hou, L., Yang, H. & Li, M. (2014). Removal of Chemical Oxygen Demand and Dissolved Nutrients by a Sunken Lawn Infiltration System During Intermittent Storm Events. *Water Sci. Technol.*, 69(2), 398-406, doi: 10.2166/wst.2013.728.
- Hunt, W., Jarrett, A., Smith, J. & Sharkey, L. (2006). Evaluating Bioretention Hydrology and Nutrient Removal at Three Field Sites in North Carolina. *Journal of Irrigation and Drainage Engineering*, 132(6), 600-608.
- Kandra, H.S., McCarthy, D., Fletcher, T.D. & Deletic, A. (2014). Assessment of Clogging Phenomena in Granular Filter Media Used for Stormwater Treatment. *Journal of Hydrology*, 512, 518-527.
- Li, H., Sharkey, L., Hunt, W. & Davis, A. (2009). Mitigation of Impervious Surface Hydrology Using Bioretention in North Carolina and Maryland. *Journal of Hydrologic Engineering*, 14(4), 407-415.
- Low Impact Development (LID). (2007). *Bioretention Specifications*, Urban Design Tools, Low Impact Development. Retrieved 21 January 2015, from http://www.lid-stormwater.net/biohighres_specs.htm.
- Lucas, W.C. & Greenway, M. (2008). Nutrient Retention in Vegetated and Nonvegetated Bioretention Mesocosms. *Journal of Irrigation and Drainage Engineering*, 134(5), 613-623.
- Mangangka, I.R., Liu, A., Egodawatta, P. & Goonetilleke, A. (2015). Performance Characterisation of a Stormwater Treatment Bioretention Basin. *J. Environ. Manage.*, 150, 173-178.
- Melbourne Water (2005). *WSUD Engineering Procedures, Stormwater*. CSIRO Publishing, Melbourne, Australia.
- North Shore City (2008). *Bioretention Guidelines*, North Shore City, Auckland, New Zealand.
- O'Neill, S.W. & Davis, A.P. (2012). Water Treatment Residual as a Bioretention Amendment for Phosphorus. II: Long-Term Column Studies. *Journal of Environmental Engineering*, 138(3), 328-336.
- Passeport, E., Hunt, W.F., Line, D.E., Smith, R.A. & Brown, R.A. (2009). Field Study of the Ability of Two Grassed Bioretention Cells to Reduce Storm-Water Runoff Pollution. *Journal of Irrigation and Drainage Engineering*, 135(4), 505-510.
- Public Utilities Board (PUB). (2011). *Engineering Procedures for ABC Waters Design Features*. Public Utilities Board, Singapore, Chapter C7.
- Sidek, L., Mohiyaden, H.A., Lee, L.K. & Foo, K.Y. (2016). Potential of Engineered Biomedia for the Innovative Purification of Contaminated River Water. *Desalination and Water Treatment*, 57(51), 24210-24221.
- Takaijudin, H., Ghani, Ab. A, ZAkaria, N.A, Lau, T.L., (2015). The Influence of Filter Depths in Capturing Nutrient Contaminants for Non-Vegetated Bioretention Column: A Preliminary Study, In *36th IAHR World Congress*, The Hague, Netherlands.
- The Prince George County (2009). *The Bioretention Manual*. Environmental Services Division, Department of Environmental Resources, Maryland Chapter C4.

PREPARATION OF ECO-FRIENDLY CARBON AEROGEL VIA AMBIENT PRESSURE DRYING FOR THE EFFECTIVE REMEDIATION OF PHARMACEUTICAL CONTAMINANT, METFORMIN

KIRUSHANTINI BALAKRISHNAN⁽¹⁾, NOR AZAZI ZAKARIA⁽²⁾ & KENG YUEN FOO⁽³⁾

^(1,2,3) River Engineering and Urban Drainage Research Centre (REDAC),
Universiti Sains Malaysia, Engineering Campus, Nibong Tebal, Penang, Malaysia
tina25282@yahoo.com, redac01@usm.my, k.y.foo@usm.my

ABSTRACT

The orally administered drug metformin for diabetes type II has spiked in huge production according to the estimation by World Health Organization (WHO), with the reported patients of more than 350 million annually. The prevalence of metformin is frequently detected in the aquatic environment, specifically at the surface level of water supplies, groundwater and stormwater discharge. If poorly managed, the presence of metformin may become a source of hydro-geological contaminant to the natural environment, with a multiple, acute and synergistic toxicity. Metformin is a recalcitrant, accumulative and persistent toxic chemical, with high mobility, solubility and low degradability. In view of the above matter, a broad range of treatment technology has been abounded. In particular, carbon aerogels, a new generation of eco-friendly carbon adsorbents, has received wide concern due to the favourable capability for the treatment of a variety of pharmaceutical contaminants. In this work, the preparation of low cost carbon aerogel (CA) from natural pectin was attempted via ambient pressure drying. The physical, chemical and physiochemical properties of CA were characterized by Scanning Electron Microscopy (SEM), Fourier Transform Infrared spectroscopy (FTIR), nitrogen adsorption-desorption curve and zeta potential measurements. The adsorptive behavior for the treatment of metformin was investigated by varying the initial concentration, solution pH and operating temperatures. Equilibrium data were simulated using the nonlinear Langmuir, Freundlich and Tempkin isotherm models, while the adsorption kinetics were fitted to the pseudo-first-order and pseudo-second-order kinetic equations. SEM images projected a well-developed porous structure, with the specific surface area of 584.19 m²/g. The removal of metformin was dependent on the variation of pH, in accordance to the Langmuir isotherm model, denoted a maximum adsorption capacity of 224.81 mg/g. The research findings verified the potential of natural apple pectin derived carbon aerogel as an effective solution for the successive treatment of metformin contaminated water.

Keywords: Adsorption; Carbon Aerogel; Metformin; Pectin; Pharmaceutical pollutant.

1 INTRODUCTION

Metformin (MTF) is a highly consumed pharmaceutical with the prescribed quantities of exceeding 4500 tonnes per year (Armbruster et al., 2015; Sargen et al., 2012; ter Laak and Baken, 2014). MTF has been the orally approved antihyperglycemic drug applied for the treatment of diabetes mellitus type II, a complex disease induced by the disruption of insulin secretion, and governed by genetic factor, obesity and inactive behaviour of the urban dwellers. For years, MTF and its metabolites, have been deposited to the water channels, and accumulated in the natural ecosystems. It has been detected in the urban runoff in Germany at the concentration of 102 – 472 ng/L, in the surface water and groundwater at approximately 100 ng/L and 10 ng/L in France, and up to 150 ng/L in the United States (Kolpin et al., 2002; Schuster et al., 2008). It is highly persistent and constitutes a detrimental deterioration to the molecular pathways of flora and fauna, to induce biomolecules, cells or tissue damages in grains, seeds, fruits, beans and vegetables, and signifies adverse effects on the compositions of soil structure (Eggen et al., 2011; Eggen and Lillo, 2012). This has attracted a growing treatment technology for the innovative handling of these pharmaceutical effluents.

Today, carbon aerogel is a new emerging carbonaceous adsorbent, characterized by a well-developed porosity, with specific applications in the construction, aeronautics, biomedicine and environmental remediation. The preparation of carbon aerogels is conducted by suitable drying of wet gels from resorcinol-formaldehyde under supercritical condition to avoid the collapse of the pore structure. This preparation process is subjected to the utilization of hazardous raw precursors, involve high energy consumption, longer processing time and huge production cost. Therefore, the development of a new eco-friendly carbon aerogel would be an interesting strategy to lower the production cost, and enable the on-site remediation of water pollutants.

In this work, the preparation of carbon aerogel from natural apple pectin (CA) via ambient pressure drying has been attempted. The best preparation conditions were optimized. This newly prepared CA was characterized using the Scanning Electron Microscopy (SEM), Fourier Transform Infrared Spectroscopy (FTIR), and nitrogen adsorption-desorption curve. The adsorptive capability was analyzed for the treatment of pharmaceutical contaminant, MTF. The effects of initial concentration, solution pH and operating temperatures on the adsorption process were examined. The isotherm modelling for the adsorption process was elucidated.

2 MATERIALS AND METHOD

2.1 Adsorbate

Analytical grade metformin (MTF), with the chemical structure of $C_4H_{11}N_5$, molecular weight of 129.2 g/mole and pK_a of 11.61, respectively was selected as the template drug molecule. A standard solution of 500 mg/L was initially prepared and working solution were prepared by a series of serial dilutions, using the ultra pure water provided by Thermo Scientific water treatment system (Barnstead Smart2Pure).

2.2 Preparation and characterization of carbon aerogel

Food grade apple pectin was applied as the initial raw precursor for the preparation of carbon aerogels. The preparation of aerogel was conducted by mixing 15 g pectin powder with 100 mL of deionized water until a transparent wet gel was acquired. The wet gel was stabilized at room temperature for 24 h, and solvent exchanged with alcohol-water bath at the concentration range between 10 % and 100 %. The obtained alcogel was oven dried at 50 °C, carbonized at 600 to 1000 °C and activated for 30 to 115 minutes under the flow of carbon dioxide.

The surface physical properties of the newly prepared carbon aerogel was assessed using the nitrogen adsorption-desorption curve. The surface functionality was evaluated by the Fourier transform infrared spectroscopy (FT-IR) using the KBr method in the scanning range of 400 – 4000 cm^{-1} , while the morphological structure was examined by using the scanning electron microscopy (SEM). The pH_{zpc} was determined by adjusting the pH of the 0.01 M NaCl solution between 2 to 12. 0.15 g of carbon aerogel was added, and the pH_{zpc} is denoted as the value $pH_{initial} - pH_{final} = 0$ after 48 h of agitation.

2.3 Batch adsorption studies

The batch adsorption studies were conducted in a set of 250 mL Erlenmeyer flasks containing 0.05 g of CA and MTF solutions within the concentration range of 50 – 500 mg/L. The solution mixtures were agitated at 120 rpm and 30 °C in a water bath shaker until the equilibrium was reached. The residual concentration was determined using a UV-Vis spectroscopy (Shimadzu UV-1800) at the maximum wavelength of 232 nm given by:

$$q_e = \frac{(C_0 - C_e)V}{W} \quad [1]$$

which, C_0 (mg/L) and C_e (mg/L) are the concentrations of MTF at initial and equilibrium, respectively, V (L) is the volume of the solution, and W (g) is the mass of the CA used. The effect of pH on the adsorptive removal of MTF solution was conducted by adjusting the solution pH from 2-12 using 0.1 M of HCl or NaOH solutions. The solution pH was measured using a pH meter (Fisher Scientific Accumet XL200).

3 RESULTS AND DISCUSSION

3.1 Preparation of CA

During the preparation process, the powdered apple pectin applied in this study undergone polymerization process with the formation of strong $-(C-C)$ covalent bonds. The cooling process allowed the formation of transparent gel, and the covalent bonds were rearranged and restructured, with the gradual formation of hydrogen bonds, and the compact bundle, by twisting the pectin molecules into double helixes to provide a perfectly coalesced gel (Pierre and Pajonk, 2002). The effect of different pyrolytic temperatures on the activation process in response to the adsorptive uptake of MTF is given in Figure 1. Increasing the pyrolytic temperature from 600 to 800 °C showed a dramatic increase in the adsorption uptake of MTF from 79.68 to 193.8 mg/g. Activation temperature is recognized as a tailoring factor affecting the quality of the prepared carbon aerogels, usually at temperatures above 500 °C. During the reaction, the aerogel was subjected to the loss of bonded water molecules, with the generation of CO and CO₂, formation of benzene rings, and dehydrogenation of aromatic rings to form a well-developed carbonaceous adsorbent (White et al., 2014). At the pyrolytic temperature between 600 to 800 °C, the micropore volume increased proportionally to the rising temperature, with a greater adsorptive uptake of MTF. However, further gasification at temperatures beyond 800 °C would lead to the widening of the micropores to mesopores structure, with a reduction of the

adsorptive uptake of MTF. Similar observation has been reported by Sudaryanto et al. (2006) for the preparation of cassava peel derived activated carbon. The optimum pyrolytic temperature of 800 °C has been identified to be the best activation temperature for the preparation of high quality CA.

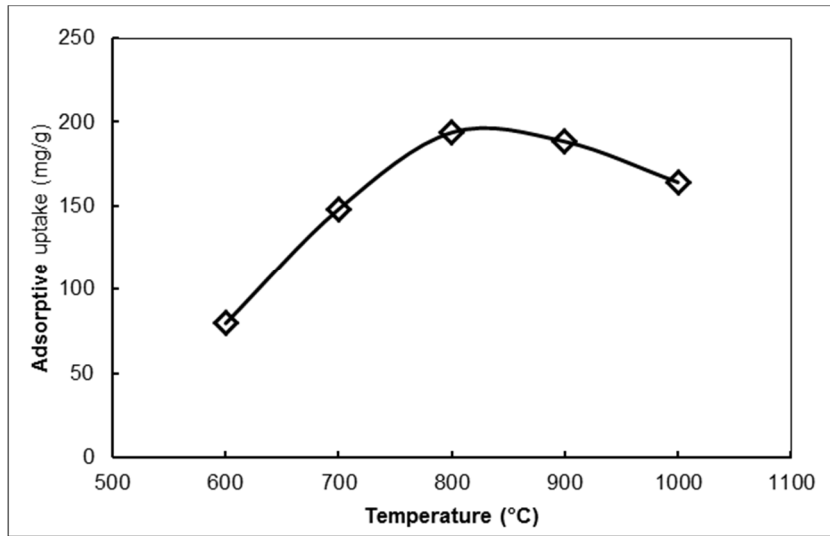


Figure 1. Effect of pyrolytic temperatures on the activation process in response to the adsorptive uptake of MTF.

The effect of activation time on the adsorptive uptake of MTF is depicted in Figure 2. Increasing the activation time from 30 to 75 minutes projected an increase of the adsorptive uptake of MTF from 84.15 to 193.8 mg/g, mainly ascribed to the intense formation of microstructure during the activation stage, with the erosion of carbon surface, expansion of pores, and oxidation of thin walls, and formation of new functionalities. Longer activation time beyond 75 minutes presented a gradual decrease in the adsorptive uptake of MTF, primarily attributed to the external ablation and collapse of the carbon framework reducing the accessibility of the surface active sites. Similar finding was reported by Chang et al. (2010) for the preparation of starch derived carbon aerogel. Therefore, the best preparation conditions were identified to be the activation temperature and time of 800 °C and 75 minutes, respectively.

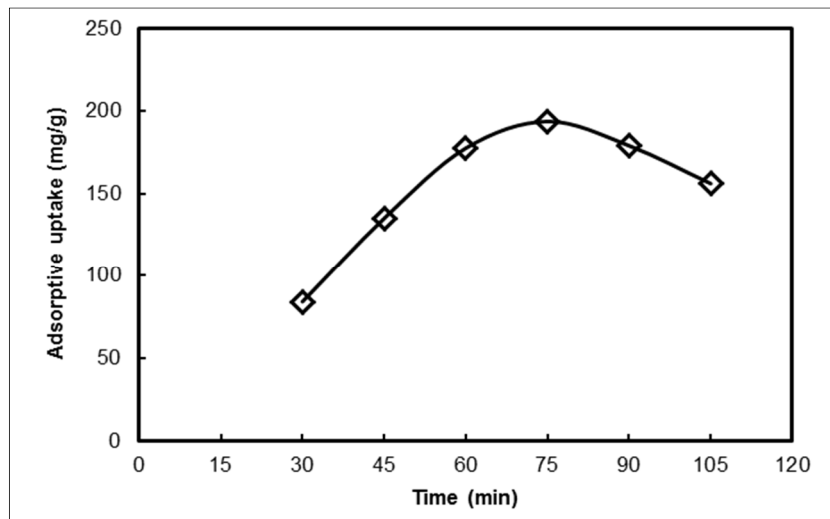


Figure 2. Effect of activation time on the activation process in response to the adsorptive uptake of MTF.

3.2 Characterization of CA

Nitrogen adsorption-desorption curve is a valuable tool in accessing the porosity structure of the carbonaceous adsorbent. The BET surface area, Langmuir surface area and total pore volume of the newly prepared CA were found to be 584.19 m²/g, 656.52 m²/g and 0.263 cm³/g, respectively. The micropores accounted approximately 70 % of the total pore volume, indicating the great feasibility for the adsorptive removal of MTF from the aqueous solutions. A comparative evaluation of the BET surface area for different pectin derived carbon aerogels is reported in Table 1. The CA prepared in this work showed relatively well developed porosity as compared with previous researches.

Table 1. A comparative evaluation of specific surface area for different pectin derived carbon aerogels.

Raw precursor	Type of aerogel	Drying method	Specific surface area (m ² /g)	Reference
Apple pectin	Carbon aerogel	Ambient pressure drying	584	This Study
Citrus and apple pectin	Pectin aerogel	Supercritical	230-270	Rudaz et al. (2014)
Amidated pectin	Pectin aerogel	Supercritical	350-50	Subrahmanyam et al. (2016)
Pectin-alginate-divalent ions	Composite aerogel	Supercritical	272-417	Tkalec et al. (2016)
Pectin-aniline	Composite aerogel	Supercritical	207-331	Zhao et al. (2016)

The morphological development of CA was ascertained by the scanning electron micrograph (SEM), as illustrated in Figure 3. A series of well pronounced microporous and mesoporous cavities were found over the uneven surface of CA, illustrating pore development during the activation stage. The surface functionality of the prepared CA were represented by the FTIR spectra. The broad band between 3412 and 3249 cm⁻¹ could be related to the presence of –OH group. The signals at 2920 and 2851 cm⁻¹ is assigned to -CH symmetric bonds, while the sharp peak at 1634 cm⁻¹ is due to the presence of C=O stretching, ascribed to the carbonyl group. The stretching of C≡O is indicated by the intensity at 1400 cm⁻¹, and the transmittance at 1051 cm⁻¹ is corresponded to the C- N stretching of the amine group.

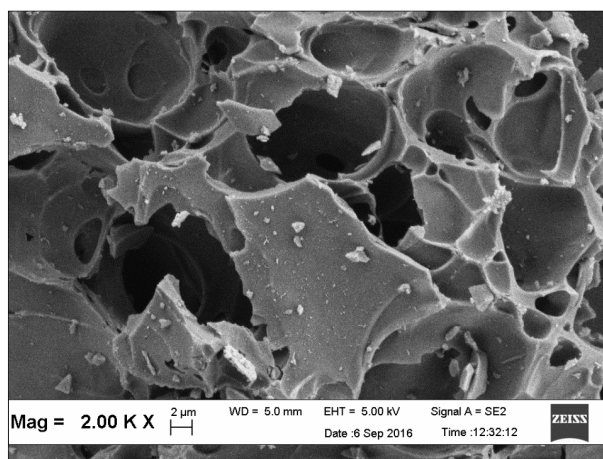


Figure 3. Scanning electron micrograph of CA.

3.3 Batch adsorption equilibrium

The curves adsorption equilibrium (q_e) versus the equilibrium concentration (C_e) for the adsorption of MTF onto CA at the operating temperatures of 30, 40 and 50 °C, respectively is shown in Figure 4. Increasing the initial concentration from 50 mg/L to 500 mg/L illustrated the intensification of the adsorption uptakes from 71.46 – 81.33 mg/g to 193.71 – 215.44 mg/g. The greater adsorption uptake at higher initial concentration is credited to the higher concentration gradient that serves as a major driving force to support the adsorption process. From Figure 4, it is clearly revealed that the adsorption of MTF onto CA was highly dependent on the changing operating temperatures, with a greater adsorptive uptake of MTF at higher temperatures, that could be due to the higher mobility of the adsorbate molecules, which in turn increased the adsorptive uptake. The finding also illustrated a higher operating temperature which enhanced the diffusion rate of the MTF molecules across the external boundary layer, and in the internal pores of the CA.

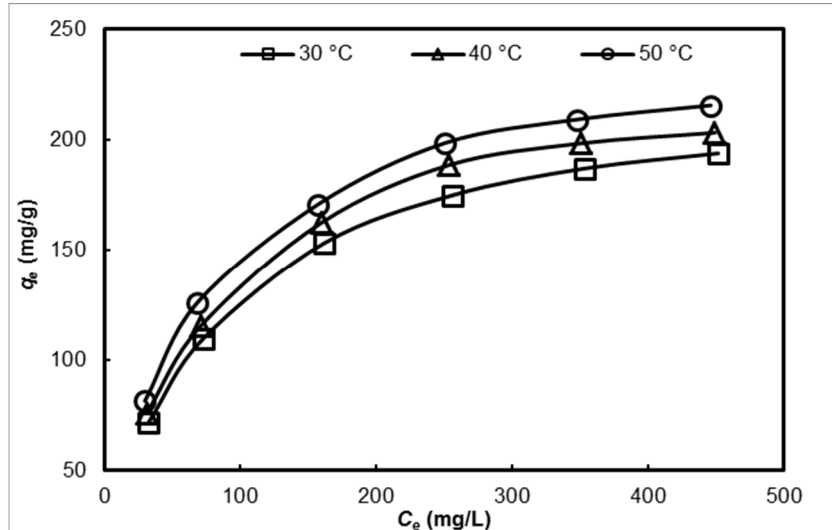


Figure 4. Adsorption equilibrium (q_e) versus equilibrium concentration (C_e) for the adsorption of MTF onto CA at the operating temperatures of 30, 40 and 50 °C.

The adsorptive behaviour of MTF onto CA as a function of solution pH is displayed in Figure 5. Generally, MTF shows positively charged, negatively charged and zwitterionic species at different pH range, due to the variations of pK_a 's values. The molecules exist mainly as cations at $pH < 2.97$, dominated as anions at $pH > 11.61$ and zwitterion in the pH range from 2.97 to 11.61. The pH_{zpc} of CA was identified to be 7.82. When the solution $pH < pH_{zpc}$, the CA surface would exhibit positive charge due to the protonation of the CA's hydrated surface. However, it turns into negative charge at $pH > pH_{zpc}$ due to the deprotonation of the hydrated surface. Accordingly, the lower adsorptive uptake at the low pH of 1-3 was mainly attributed to the strong repulsive force between the cationic MTF and the positively charged CA. The better adsorptive uptake of MTF at the solution pH between 4-7 was ascribed to the zwitterionic characters which enhanced the attraction of MTF onto the positively charged CA. The adsorptive uptake of MTF projected a sharp decline at pH 8, near to the pH_{zpc} of the CA. At the zwitterionic phase between pH 9 – 11, the adsorptive uptake of MTF increased, corresponding to the negatively charged CA. The sharp decline of the MTF uptake at pH 12 could be owing to the significant electrostatic repulsive force between the negatively charged CA and the anions of the MTF species. Similar observation has been reported by Huang et al. (2016) for the adsorption of MTF onto *Alternanthera philoxeroides*, an aquatic plant biomass derived porous carbon.

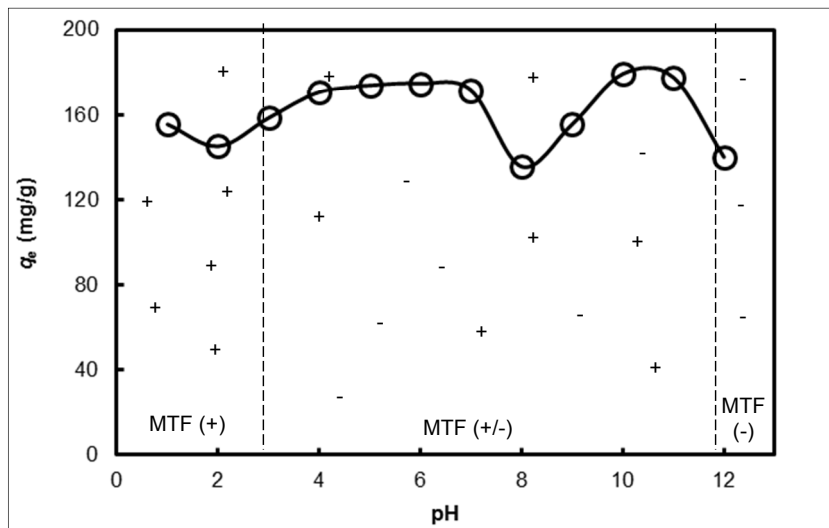


Figure 5. Effect of solution pH on the adsorptive uptake of MTF onto CA at 30 °C.

3.4 Adsorption Isotherm

Adsorption isotherm is essential for the establishment of technical design and practical application of the adsorption system. In the present work, the equilibrium data were simulated using the non-linear Langmuir (Langmuir, 1916), Freundlich (Freundlich, 1906), and Tempkin (Tempkin and Pyzhev, 1940) isotherm models expressed by:

$$q_e = \frac{Q_0 K_L C_e}{1 + K_L C_e} \quad [2]$$

$$q_e = K_F C_e^{1/n} \quad [3]$$

$$q_e = B \ln(AC_e) \quad [4]$$

where Q_0 (mg/g) and K_L (L/g) are denoted as the Langmuir isotherm constants related to the adsorption capacity and energy of adsorption, respectively; K_F (mg/g) (L/mg)^{1/n} is the Freundlich isotherm constant related to adsorption capacity, and $1/n$ is a measure of the adsorption intensity; and $B = RT/b$, which b , A , R and T are the Tempkin isotherm constants related to heat of sorption (J/mole), equilibrium binding constant (L/g), universal gas constant (8.314 J/mole K) and absolute temperature (K), respectively. The non-linear regression method was applied as opposed to the linearized regression as it implicates the step for the minimization of error distribution between the experimental data and the predicted isotherm, and the bias from the linearized form of the isotherm model (Foo and Hameed, 2010). The validity of the isotherm models was verified using the correlation coefficient, R^2 and root-mean-square deviation ($RMSD$), a common statistical tool to measure the predictive power of a model derived as:

$$r^2 = \frac{(q_{e,exp} - \overline{q_{e,calc}})^2}{\sum (q_{e,exp} - \overline{q_{e,calc}})^2 + (q_{e,exp} - q_{e,calc})^2} \quad [5]$$

$$RMSD = \frac{\sqrt{\sum_{i=1}^n (q_{e,exp} - q_{e,calc})^2}}{n - 1} \quad [6]$$

which $q_{e,exp}$ (mg/g), $q_{e,calc}$ (mg/g) and $\overline{q_{e,calc}}$ (mg/g) are the experimental, theoretical and average theoretical adsorption capacity of MTF, respectively. The isotherm parameters at the operating temperatures of 30, 40 and 50 °C, respectively, are presented in Table 2. The results were best confronted to the Langmuir isotherm model, with the maximum adsorption capacities for MTF of 224.81 – 248.91 mg/g. Conformation into the Langmuir isotherm model illustrated monolayer adsorption of MTF onto CA with equal activation energy, and no interaction between the adsorbing molecules with the neighbouring surface. Table 3 provides a comparison of the monolayer adsorption capacity for the adsorption of MTF onto various adsorbents. The adsorption capacity of the adsorbent prepared in this work was comparable with previous studies as reported in the literature.

Table 2. Adsorption isotherm parameters for the adsorption of MTF onto CA at 30, 40 and 50 °C.

Isotherms	Constants			
Langmuir	Q_0 (mg/g)	K_L (L/mg)	R^2	$RMSD$
30 °C	224.81	0.0136	0.999	0.696
40 °C	236.85	0.0142	0.997	1.086
50 °C	248.91	0.0147	0.995	1.442
Freundlich	K_F (mg/g)(L/mg)^{1/n}	n	R^2	$RMSD$
30 °C	25.11	2.924	0.961	3.171
40 °C	27.62	2.976	0.952	3.758
50 °C	29.59	2.994	0.967	3.647
Tempkin	A (L/g)	B	R^2	$RMSD$
30 °C	0.142	47.63	0.994	1.181
40 °C	0.151	49.85	0.989	1.819
50 °C	0.161	51.90	0.999	1.773

Table 3. A comparison of the monolayer adsorption capacity for the adsorption of MTF onto different adsorbents.

Adsorbents	Monolayer adsorption capacity (mg/g)	References
CA	225	This study
Activated carbon	73	Lotfi et al. (2015)
Carbon nanotube	80	
Molecular imprinter polymer	80	Kyzas et al. (2015)
Biomass derived porous carbon	81	Huang et al. (2016)

4 CONCLUSION

The preparation of apple pectin derived carbon aerogel via ambient pressure drying has been attempted. The best pyrolytic temperature of 800 °C and activation time of 75 min has been identified to be the best preparation conditions. This newly prepared carbon aerogel (CA) showed a high BET surface area and total pore volume of 584.19 m²/g, and 0.263 cm³/g respectively, with predominantly microporous in nature. CA demonstrated great feasibility for the adsorptive removal of MTF from the aqueous solution, with a monolayer adsorption capacity of 224.81 mg/g at 30 °C. The equilibrium data were best described by the Langmuir isotherm model, which was substantiated by the correlation coefficient of 0.999 and *RMSD* of 0.696. The findings demonstrated the great feasibility of CA for the adsorptive treatment of MTF from water stream.

5 ACKNOWLEDGEMENT

The authors acknowledge the financial support provided by Universiti Sains Malaysia and Ministry of Higher Education under the Research University (Project No. 1001/PREDAC/814272) and FRGS (Project No. 203/PREDAC/6171157) grant schemes.

REFERENCES

- Armbruster, D., Happel, O., Scheurer, M., Harms, K., Schmidt, T.C. & Brauch, H.J. (2015). Emerging Nitrogenous Disinfection Byproducts: Transformation of the Antidiabetic Drug Metformin During Chlorine Disinfection of Water. *Water Research*, 79, 104-118.
- Chang, X., Chen, D. & Jiao, X. (2010). Starch-Derived Carbon Aerogels with High-Performance for Sorption of Cationic Dyes. *Polymer*, 51(16), 3801-3807.
- Eggen, T. & Lillo, C. (2012). Antidiabetic II Drug Metformin in Plants: Uptake and Translocation to Edible Parts of Cereals, Oily Seeds, Beans, Tomato, Squash, Carrots, and Potatoes. *Journal of Agricultural and Food Chemistry*, 60(28), 6929-6935.
- Eggen, T., Asp, T.N., Grave, K. & Hormazabal, V. (2011). Uptake and Translocation of Metformin, Ciprofloxacin and Narasin in Forage- and Crop Plants. *Chemosphere*, 85(1), 26-33.
- Foo, K.Y. & Hameed, B.H. (2010). Insights into the Modeling of Adsorption Isotherm Systems. *Chemical Engineering Journal*, 156(1), 2-10.
- Freundlich, H.M.F. (1906). Over the Adsorption in Solution. *The Journal of Physical Chemistry*, 57(385), 385-471.
- Huang, X., Liu, Y., Liu, S., Li, Z., Tan, X., Ding, Y., Zeng, G., Xu, Y., Zeng, W. & Zheng, B. (2016). Removal of Metformin Hydrochloride by Alternanthera Philoxeroides Biomass Derived Porous Carbon Materials Treated with Hydrogen Peroxide. *Research Advances*, 6(83), 79275-79284.
- Kolpin, D.W., Furlong, E.T., Meyer, M.T., Thurman, E.M., Zaugg, S.D., Barber, L.B. & Buxton, H.T. (2002). Pharmaceuticals, Hormones, and Other Organic Wastewater Contaminants in US Streams, 1999– 2000: a National Reconnaissance. *Environmental Science & Technology*, 36(6), 1202-1211.
- Kyzas, G.Z., Nanaki, S.G., Koltzakidou, A., Papageorgiou, M., Kechagia, M., Bikiaris, D.N. & Lambropoulou, D.A. (2015). Effectively Designed Molecularly Imprinted Polymers for Selective Isolation of the Antidiabetic Drug Metformin and its Transformation Product Guanylurea from Aqueous Media. *Analytica Chimica Acta*, 866, 27-40.
- Langmuir, I. (1916). The Constitution and Fundamental Properties of Solids and Liquids. *Journal of the American Chemical Society*, 38(11), 2221-2295.
- Pierre, A.C. & Pajonk, G.M. (2002). Chemistry of Aerogels and Their Applications. *Chemical Reviews*, 102(11), 4243-4266.
- Rudaz, C., Courson, R., Bonnet, L., Calas-Etienne, S., Sallée, H. & Budtova, T. (2014). Aeropectin: Fully Biomass-Based Mechanically Strong and Thermal Superinsulating Aerogel. *Biomacromolecules*, 15(6), 2188-2195.
- Sargen, M.R., Hoffstad, O.J., Wiebe, D.J. & Margolis, D.J. (2012). Geographic Variation in Pharmacotherapy Decisions for US Medicare Enrollees with Diabetes. *Journal of Diabetes and its Complications*, 26(4), 301-307.
- Subrahmanyam, R., Gurikov, P., Meissner, I. & Smirnova, I. (2016). Preparation of Biopolymer Aerogels Using Green Solvents. *Journal of Visualized Experiments: JoVE*, (113).

- Sudaryanto, Y., Hartono, S.B., Irawaty, W., Hindarso, H. & Ismadji, S. (2006). High Surface Area Activated Carbon Prepared from Cassava Peel by Chemical Activation. *Bioresource Technology*, 97(5), 734-739.
- Tempkin, M.I. & Pyzhev, V. (1940). Kinetics of Ammonia Synthesis on Promoted Iron Catalyst. *Acta Physiochimica URSS*, 12(3), 327-356.
- ter Laak, T. & Baken, K. (2014). The Occurrence, Fate and Ecological and Human Health Risks of Metformin and Guanylurea in the Water Cycle – a Literature Review. *Watercycle Research Institute. KWR*, 24.
- Tkalec, G., Knez, Ž. & Novak, Z. (2016). PH Sensitive Mesoporous Materials for Immediate or Controlled Release of NSAID. *Microporous and Mesoporous Materials*, 224, 190-200.
- White, R.J., Brun, N., Budarin, V.L., Clark, J.H. & Titirici, M.M. (2014). Always Look on the “Light” Side of Life: Sustainable Carbon Aerogels. *ChemSusChem*, 7(3), 670-689.
- Zhao, H.B., Yuan, L., Fu, Z.B., Wang, C.Y., Yang, X., Zhu, J.Y., Qu, J., Chen, H.B. & Schiraldi, D.A. (2016). Biomass-Based Mechanically Strong and Electrically Conductive Polymer Aerogels and Their Application for Supercapacitors. *ACS Applied Materials & Interfaces*, 8(15), 9917-9924.

SYNTHESIS AND ACTIVITY EVALUATION OF INCENSE ASH SUPPORTED SnO₂ NANOCOMPOSITE FOR THE PHOTOCATALYTIC DEGRADATION OF WATER POLLUTANT

PEI TENG LUM ⁽¹⁾, NOR AZAZI ZAKARIA ⁽²⁾ & KENG YUEN FOO ⁽³⁾

^(1,2,3) River Engineering and Urban Drainage Research Centre (REDAC),
Universiti Sains Malaysia, Engineering Campus, Nibong Tebal, Penang, Malaysia
peiteng_1118@hotmail.com; redac01@usm.my; k.y.foo@usm.my

ABSTRACT

In this work, the preparation of an incense ash (IA) supported tin oxide (SnO₂) nanocomposite via ultrasonication technique has been attempted. The physical and chemical properties were characterized by scanning electron microscopy (SEM) and Fourier Transform Infrared Spectroscopy (FT-IR). The photocatalytic activity was examined using Acid Red 88 (AR 88) as the model pollutant. The operational parameters including the effects of catalyst loadings, initial concentration, contact time and solution pH and on the photocatalytic degradation process were evaluated. The characterization results verified the successful and homogenous deposition of SnO₂ on the surface matrix of IA to promote the synergistic implication on the adsorption-photodegradation process. A complete decolorization of the AR 88 has been achieved with a short duration of 95 minutes, with the high concentration of 500 mg/L. Regeneration analysis revealed that this newly prepared nanocomposite demonstrated a high stability and greater than 80% of degradation efficiency even after five degradation successive cycles. The findings illustrated the potential SnO₂/IA nanocomposite as a promising candidate for the innovative treatment of water pollutants.

Keywords: Acid red 88; Incense ash; Nanocomposites; Photocatalysis; Tin oxide.

1. INTRODUCTION

Today, water photocatalysis reaction has been recognized to be a new emerging environmental purification process, owing to the high efficacy for complete mineralization of the recalcitrant pollutants to carbon dioxide and water that involves the generation of highly reactive radicals species by using a renewable energy resource (Foo and Hameed, 2011). A variety of active metal oxides including titanium dioxide (TiO₂), zinc oxide (ZnO), iron (III) oxide (Fe₂O₃), cerium (IV) oxide (CeO₂), tin oxide (SnO₂), and cadmium sulphide (CdS) have been identified as the dynamic photocatalysts for the degradation of different pollutants based on their band gap energies and irradiation wavelengths (Abdelkader et al., 2016).

SnO₂, with a rutile structure is a n-type semiconductor with a wide band gap of 3.6 eV at 300 K, and high binding energy of 130 meV (Abdelkader et al., 2016). It is characterized by the intriguing properties of high photoelectrical, great thermal, and physiochemical stability, non-toxic, acid and alkaline resistance, and excellent gas sensitivity (Manjula et al., 2012; Tammina and Mandal, 2016). SnO₂ has been extensively applied as the gas or biosensors, sensitized solar cells, lithium-ion batteries, light emission displays, transparent conducting electrode, and luminescent devices (Entradas et al., 2014; Abdelkader et al., 2016).

It has attracted a great deal of interest to be an alternative semiconductor photocatalyst to the commercial TiO₂, due to the stronger oxidative ability than TiO₂ (Abdel-Messih et al., 2013), and the higher photocatalytic activity under the irradiation of ultraviolet (UV). As SnO₂ particles are activated by the light with an energy equal or greater than its band gap, the electrons in the valence band

- (h_{VB}^+) would be excited to the conduction band
- (e_{CB}^-) with the generation of an electron-hole pairs.

Some of these photogenerated electron-hole pairs might migrate to the surface of catalyst, and react with water and oxygen, to initiate the redox reaction for the degradation of water pollutants.

It is noteworthy that UV light accounts only for a small fraction with merely 4% as compared to the visible light. Under this condition, the broad band gap energy of SnO₂ would restrict the applications under visible light, and the rapid recombination of electron-hole pairs would hinder the efficiency of photodegradation reaction. To circumvent with the above drawbacks, a developing research for the preparation of different composites via different preparation techniques: hydrothermal, sol-gel, precipitation, electro-deposition and pyrolysis have been established (Hung-Low et al., 2016; Singh et al., 2014). However, there are limited researches on the synthesis of ash supported SnO₂ photocatalyst.

Within this framework, incense ash (IA), a by-product abundantly available from incense burning, is highly generated among the Asian countries, reported that generation rate of exceeding 75 million tons/year. This raises a matter of aesthetic concern on the daily generation of incense ash, which might contribute to the environmental deterioration if proper waste management strategy are not well implemented. Motivated by the phenomenon, a first attempt is now proposed for the synthesis of incense ash incorporating SnO₂ derived photocatalyst for the effective treatment of dye contaminant.

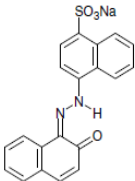
Hence, in present work, a newly developed Sn/IA derived nanocomposite was prepared by simple ultrasonication technique for the photocatalytic degradation of acid red 88, a commercial azo dye extensively applied in a wide range of food processing, pharmaceutical, dyeing and textile industries. The morphological, functional and surface characterizations of the newly prepared composite were examined. The effects of catalyst loading, initial concentration, contact time and solution pH treatment on the performance were evaluated. Moreover, the reusability of the nanocomposite was elucidated.

2 MATERIALS AND METHODS

2.1 Model contaminants

Acid Red 88 (AR 88), an azo anionic textile dye was chosen as the model pollutants in this study. The chemical structure and physiochemical properties of AR88 are given in Table 1. A standard stock solution of 500 mg/L was prepared in deionized water, and the working solutions were prepared by a series of successive dilutions.

Table 1: Chemical structure and physiochemical properties of AR 88.

Dyes	Chemical structure	Molecular formula	Molecular weight (g/mole)	Classes	λ_{max} (nm)	C.I. number
Acid Red 88		C ₂₀ H ₁₃ N ₂ O ₄ SNa	400.8	Azo	505	15620

2.2 Preparation of incense ash based photocatalytic nanocomposite

Incense ash (IA), a by-product of incense burning, was selected as the initial raw precursor in this work. The collected IA was washed thoroughly with deionized water to remove adhering dirt particles, dried and sieved to the particles of 250-500 μ m. The modification process was performed by immersing the IA in the hydrochloric acid with the initial concentration of 1 M for 24 h. This acid treated IA was rinsed and washed with a copious amount of deionized water until a constant pH was acquired in the washing solution. The preparation of IA/SnO₂ derived nanocomposite was conducted by ultrasonating the incense ash in a dissolved SnCl₂ solution with a requisite amount of tin (II) chloride dehydrate solution with the mass ratio (SnO₂: IA) of 1:1 to 1:5. The suspension was filtered, washed sequential with deionized water, and dried at 80 °C.

2.3 Characterizations

The raw IA and newly synthesized Sn/IA nanocomposite were examined with respect to the surface morphological changes and surface functional properties using the scanning electron microscopy (SEM, Zeiss Supra 35 VP, Germany) and Fourier Transform Infrared (FTIR) Spectroscopy (FTIR-2000, PerkinElmer) in the scanning range of 4000–400 cm⁻¹, using the potassium bromide (KBr) discs.

2.4 Photocatalytic activity

The photocatalytic performance of the as-prepared nanocomposites were assessed by the photodegradation of AR 88 in a photoreactor, equipped with circulating water jackets, cooling fan and a visible light irradiation source. For each experiment, a prefixed amount of photocatalyst and 100 mL of AR 88 solution were stirred in the darkness for 30 min until the adsorption-desorption equilibrium was reached prior to the irradiation. The supernatant solutions were withdrawn at different time intervals, and the concentration of AR 88 solution was measured, using a UV-Vis spectrophotometer (UV-1800 Shimadzu, Japan) at 506 nm. The effects of the catalyst loading, initial concentration, contact time and solution pH on the photocatalytic activity was evaluated. The reusability study was conducted by performing sequential degradation cycles, and the degradation rate was given by:

$$\text{Degradation rate (\%)} = 1 - \left(\frac{C_t}{C_0} \right) \times 100 \% \quad (1)$$

Where C_0 and C_t are concentrations of AR 88 at initial and time t .

3. RESULTS AND DISCUSSIONS

3.1 Physical and chemical characterization

The morphological characteristic and microstructure of IA and Sn/IA nanocomposite were revealed by the scanning electron micrographs, with a magnification of 500 X, as depicted in Figure 1. It could be found that incense ash consisted predominantly irregular and spherical shaped particles, with a highly porous structure, to provide greater surface area and surface active sites for the deposition of SnO₂ (Zhang et al., 2013). The SEM micrograph of Sn/IA nanocomposite visualized from Figure 1(b), showed that these SnO₂ sphere-like nanoparticles were well distributed around the surface of IA, illustrating the formation of a thin film of SnO₂ particulates that served as the high availability of surface active sites for the enhance adsorption and degradation of water pollutants.

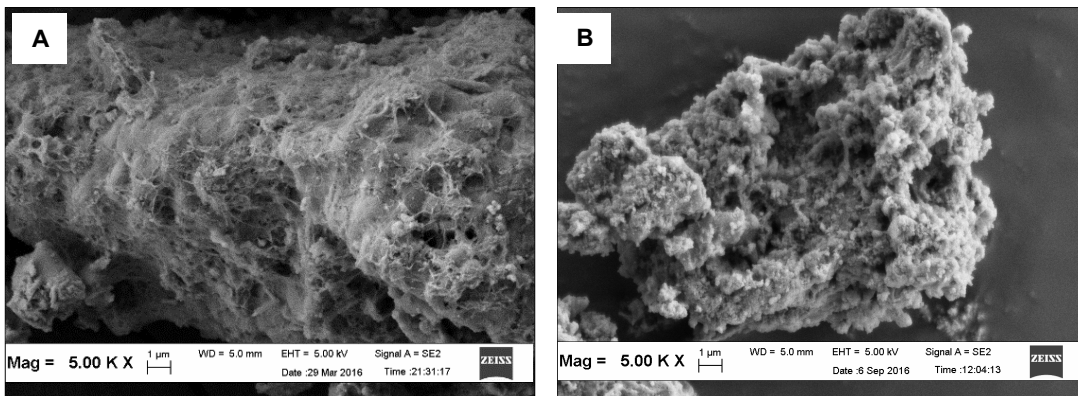


Figure 1: Scanning electron micrographs of (a) IA and (b) SnO₂/IA derived nanocomposite.

The FT-IR spectra of IA and Sn/IA derived nanocomposite are shown in Figure 2. The broad band at 3446 cm⁻¹ and 3400 cm⁻¹ is assigned to the stretching of O-H, attributed to the adsorption of moisture content (Kim et al., 2015). The IR peak at the region 2950-2800 cm⁻¹ reveals the vibration of C-H bond, and the signal at 1450-1350 cm⁻¹ corresponds to the symmetrical Si-O-Si bond (Zhao et al., 2015). The transmittance at 1050-950 cm⁻¹ is associated with the bending vibration of Al-O bond (Liu et al., 2014), and the presence of tin oxide was ascertained by the vibrations at 480 cm⁻¹ (Dharmaraj et al., 2006). This findings verified the homogeneous deposition of SnO₂ on the surface of IA as illustrated from the SEM image (Kim et al., 2015), and supported that the formation of nanocomposite was governed mainly via the van der Waals interaction (Kim et al., 2015).

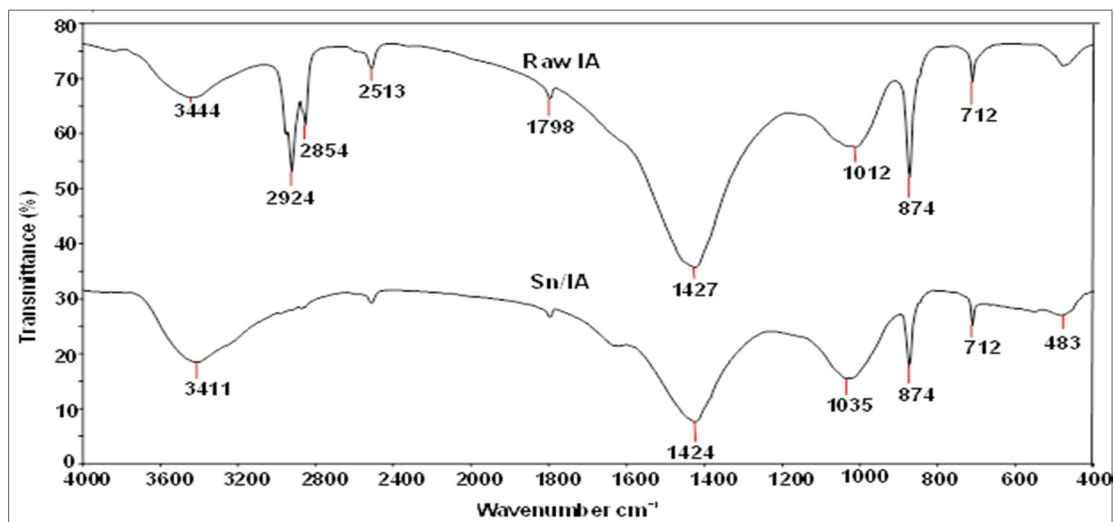


Figure 2: FTIR of IA, and SnO₂/IA derived nanocomposite.

3.2 Photodegradation process

3.2.1 Effect of catalysts

The variation of photocatalytic activity for the raw IA and the IA/SnO₂ derived nanocomposites is presented in Figure 3. It was noticeable that the SnO₂/IA supported photocatalyst demonstrated a greater removal efficacy of 41 to 56%, while the pure IA showed a negligible removal efficacy of lesser than 13%. The result was in agreement with the photocatalytic evaluation of pure fly ash cenosphere (Wang et al., 2011). The findings ascertained the synergetic effect of IA and SnO₂ to improve the photocatalytic activity and strengthen the photoreaction system by providing more active sites for AR 88 adsorption in the vicinity of the photocatalyst onto IA, and SnO₂ that serves as the photoactive centers in generating electron-hole pair for the photo-decolourization of AR 88 (Darvishi et al., 2016).

It could be deduced that the incorporation of IA in the nanocomposite could reduce the agglomeration, and improve the dispersion of SnO₂ particles, which in turn increase the photons transport over the surface of photocatalyst, contributing to the full application of the visible light for the photocatalysis process (Zhang et al., 2014). The findings could also be explained by the well-developed porous structure of the IA that served as a medium carrier for the interaction of dyes molecules with the catalyst in the photodegradation process (Lv et al., 2013). Amongst all, composite 3 showed the best photocatalytic performance, with approximately 56% of degradation efficiency after the irradiation time of 30 minutes. Increasing the content of IA showed a better degradation efficiency till the optimum ratio of 1:3, and the photodegradation process was gradually reduced. This can be ascribed to the excessive IA content beyond the optimum ratio that confines the path of light from reaching the SnO₂ catalyst, resulting in the lower generation of activation energy, and photogenerated electron-hole pairs to affect the degradation process (Behnajady et al., 2009).

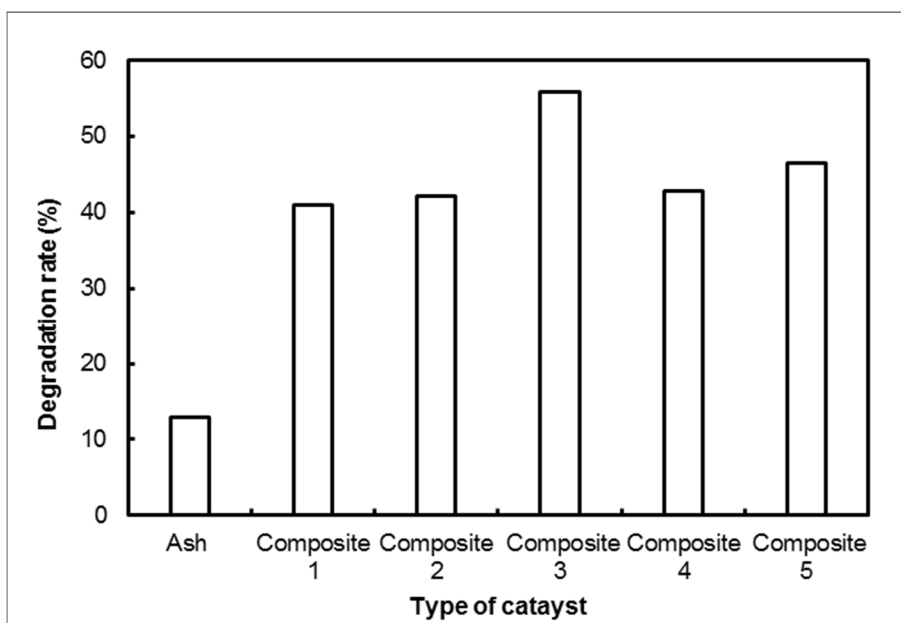


Figure 3: Effect of catalysts on the photodegradation of AR 88 (catalyst loading = 0.01 g /100 mL, $C_0 = 500$ mg/L; $t = 30$ min).

3.2.2 Effect of catalyst loading

Effect of catalyst loading is a predominant factor which affects the optimization of the photodegradation process. The effect of catalyst loading for the degradation of AR 88 was examined from 0.01 g to 0.06 g/100 mL, as depicted in Figure 4. Increasing the catalyst loading from 0.01 to 0.03 g/100 mL showed a superior improvement on the degradation process, from 56 % to 80 % under the illumination of 30 minutes. This finding was in agreement with the photodegradation experiment conducted by Kumar et al. (2009), which reported that increasing the catalyst dosage would enhance the availability of the surface binding sites, and promote the greater generation of hydroxyl or superoxide radicals, to improve the degradation efficiency (Thejaswini et al., 2016). Beyond the catalyst loading of 0.03 g/100 mL, the degradation process only increased slightly from 80 % to 92 %, which could be related to the higher solution turbidity and dispersion of catalyst particles to retard the penetration of light, hindering the photocatalysis process (Thejaswini et al., 2016). Additionally, higher catalyst loading may promote the aggregation of catalyst particles to reduce the number of surface active sites with higher generation of radical intermediates by the excessive amount of photocatalyst, to trigger the recombination of these immediate radicals (Balachandran et al., 2014). In this sense, the optimum catalyst loading in this work was identified to be 0.03 g/100 mL.

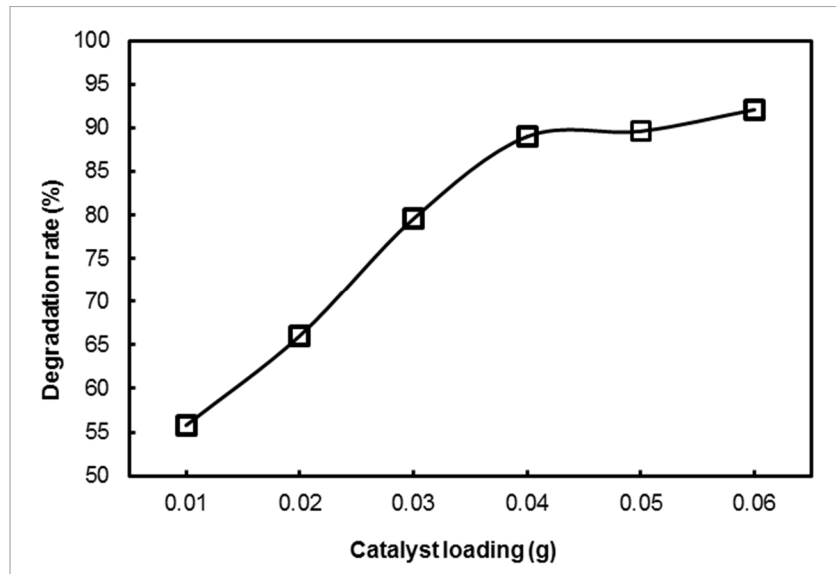


Figure 4: Effect of catalyst loading on the photodegradation of AR 88 ($C_0 = 500$ mg/L; $t = 30$ min).

3.3.3 Effect of initial concentration and contact time

The photodegradation of AR 88 as a function of initial concentration and contact time is provided in Figure 5. Noticeably, increasing the initial concentration showed a gradual reduction of the degradation efficiency, evidenced from the higher contact time required for the complete mineralization of AR 88, which increased from 1 to 95 minutes.

As the initial dye concentration is increased, the solution would turn to be impermeable to the penetration of light, to hinder the photons from reaching to the catalyst surface for light activation. Similarly, these dyes molecules could be adsorbed onto the catalyst surface to block most of the active sites responsible for the photocatalytic degradation process. These factors would limit the generation of hydroxyl and superoxide radicals, which is necessary for the typical photocatalytic reaction. In this context, the photolysis rather than the photocatalysis of AR 88 might take part (Kumar et al., 2009; Darvishi et al., 2016). Meanwhile, the competition between the excessive dye molecules would lead to the saturation of catalyst surface at a constant catalyst loading (Kumar et al., 2008). As a result, a lower decolourization rate was observed at the higher initial concentration of AR 88.

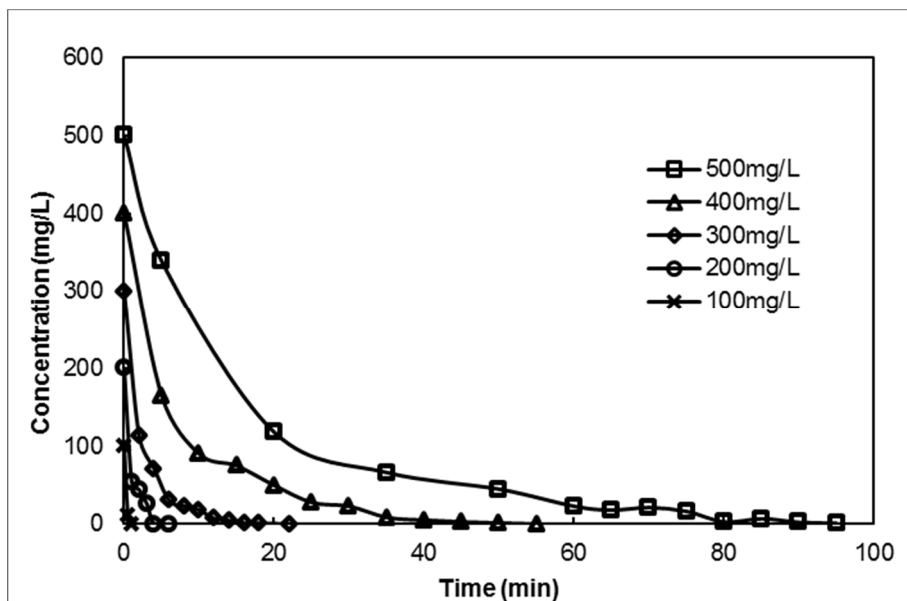


Figure 5: Effect of initial concentration and contact time on the photodegradation of AR 88 (catalyst loading = 0.03 g/100 mL; $t = 30$ min).

3.3.4 Effect of solution pH

The effect of solution pH on the photodegradation of AR 88 was evaluated at the pH range of 2-10. It can be clearly found from Figure 6 that the degradation rate was almost not affected by the alteration of solution pH, ranging within 94 to 100%. The present result demonstrated the high stability of the nanocomposite that was pH independent with the changing solution pH to affect degradation process (Subash et al., 2013). The finding differed from the experimental data presented by Saharan et al. (2012), which reported that the decolourization process was favourable under acidic medium. The data implied that the molecular structure of the AR 88 dye pollutants was not significantly affected (Sheng et al., 2014), and the photocatalytic activity of the Sn/IA nanocomposite remained extremely stable throughout the pH range of 2-10.

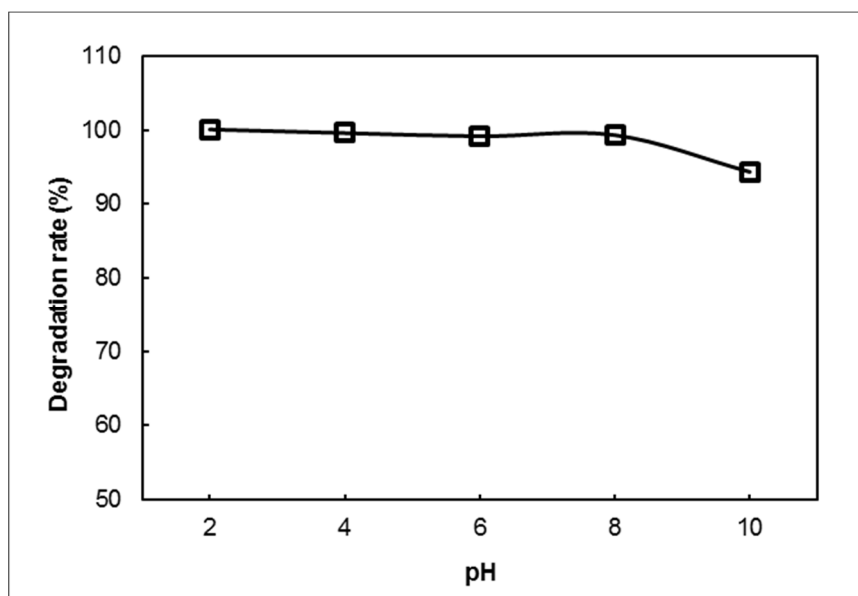


Figure 6: Effect of solution pH on the photodegradation of AR 88 (catalyst loading = 0.03 g/100 mL, $C_0 = 500$ mg/L; $t = 30$ min).

4. REUSABILITY STUDY

The stability of the catalyst is another important key characteristic to ascertain the long term application for the photocatalytic process. The reusability test was accessed by performing five successive cyclic experiments under the optimized conditions. For each experiment, the nanocomposite was filtered and regenerated by washing with a copious amount of deionized water, subsequently followed by drying at 120 °C for 3 h. The result is displayed in Figure 7. It has clearly revealed that the degradation efficiency could maintain at above 80% even after the fifth regeneration cycle.

The findings showed that the photocatalytic activity of Sn/IA derived nanocomposite was relatively stable against the degradation reaction. This could be ascribed by the low density and good dispersion property of this newly developed nanocomposite that can be easily recovered without the agglomeration reaction (Zhang et al., 2014). The slight reduction after a few regeneration runs was probably due to an inevitable loss of the fragment of the photocatalyst during each sampling and filtration, and the accumulation of dye molecules on the active surface site of the catalyst (Hassan and El-Salamony, 2014). The findings demonstrated the great efficacy of the newly prepared photocatalyst with high reusability potential. A comparison of the photocatalytic performance of different catalysts for the degradation of AR 88 is provided in Table 2. The Sn/IA derived nanocomposite prepared in this work showed relatively high photocatalytic performance, with the complete removal of AR 88 at the concentration of 100 mg/L within 1 minute, as compared with previous researches.

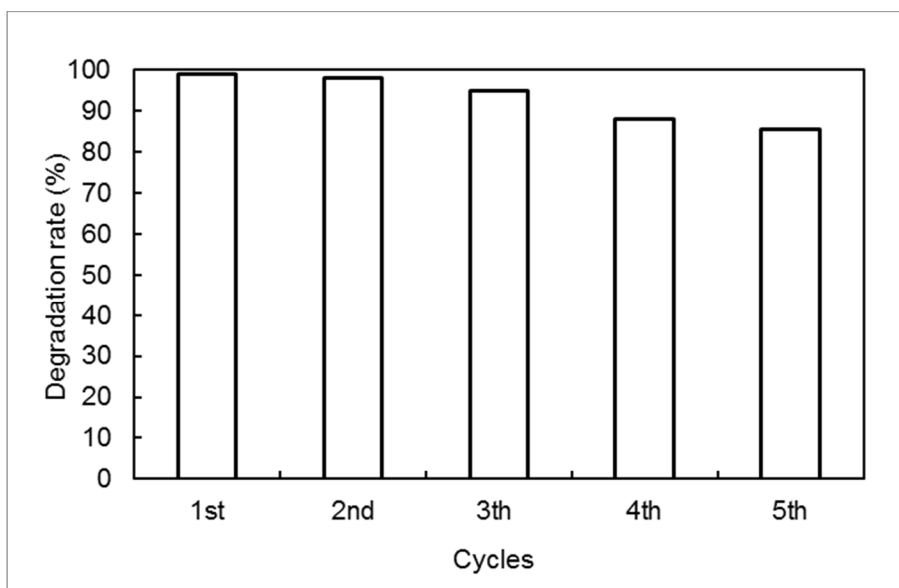


Figure 7: Reusability study on the photodegradation of AR 88 (catalyst loading = 0.03 g/100 mL, $C_0 = 200$ mg/L; $t = 30$ min).

Table 2: A comparison of the photocatalytic performance of different catalysts for the photocatalytic degradation of AR 88.

Photocatalyst	Initial concentration (mg/L)	Irradiation time (min)	Removal (%)	Reference
Sn/IA nanocomposite	100	1	100	Present study
ZnO/biosilica nanocomposite	20	30	96	Darvishi et al. (2016)
TiO ₂ /AC-Darco-G60	40	180	93	Gao et al. (2011)
TiO ₂	20	90	93	Behnajady et al. (2008)

5. CONCLUSION

In this work, a new IA supported SnO₂ nanocomposite has been successfully synthesized. The composite illustrated a good photocatalytic activity on the decolourization process to completely degrade AR 88 with the high concentration of 500 mg/L within 100 minutes. It showed an extremely high stability and reusability, with the degradation efficiency of higher than 80 % even after 5 regeneration runs. The findings demonstrated its unique feasibility to be a highly valuable and environmental friendly photocatalyst.

ACKNOWLEDGEMENTS

The authors acknowledge the financial support provided by Universiti Sains Malaysia, Malaysia under the Research University (Project No. 1001/PREDAC/814272) grant scheme.

REFERENCES

- Abdelkader, E., Nadjia, L., Naceur, B. & Nouredine, B. (2016). SnO₂ Foam Grain-Shaped Nanoparticles: Synthesis, Characterization and UVA Light Induced Photocatalysis. *Journal of Alloys and Compounds*, 679, 408-419.
- Abdel-Messih, M.F., Ahmed, M.A. & El-Sayed, A.S. (2013). Photocatalytic Decolorization of Rhodamine B Dye using Novel Mesoporous SnO₂-TiO₂ Nano Mixed Oxides Prepared by Sol-Gel Method. *Journal of Photochemistry and Photobiology A: Chemistry*, 260, 1-8.
- Balachandran, K., Venkatesh, R., Sivaraj, R. & Rajiv, P. (2014). TiO₂ Nanoparticles versus TiO₂-SiO₂ Nanocomposites: A Comparative Study of Photo Catalysis on Acid Red 88. *Spectrochimica Acta Part A: Molecular and Biomolecular Spectroscopy*, 128, 468-474.
- Behnajady, M.A., Modirshahla, N., Mirzamohammady, M., Vahid, B. & Behnajady, B. (2008). Increasing Photoactivity of Titanium Dioxide Immobilized on Glass Plate with Optimization of Heat Attachment Method Parameters. *Journal of Hazardous Materials*, 160(2), 508-513.
- Behnajady, M.A., Modirshahla, N., Shokri, M., Zeininezhad, A. & Zamani, H.A. (2009). Enhancement Photocatalytic Activity of ZnO Nanoparticles by Silver Doping with Optimization of Photodeposition Method Parameters. *Journal of Environmental Science and Health, Part A*, 44(7), 666-672.

- Dharmaraj, N., Kim, C.H., Kim, K.W., Kim, H.Y. & Suh, E.K. (2006). Spectral Studies of SnO₂ Nanofibres Prepared by Electrospinning Method. *Spectrochimica Acta Part A: Molecular and Biomolecular Spectroscopy*, 64(1), 136-140.
- Foo, K.Y. & Hameed, B.H. (2011). The Environmental Applications of Activated Carbon/Zeolite Composite Materials. *Advances in Colloid and Interface Science*, 162(1), 22-28.
- Gao, B., Yap, P.S., Lim, T.M. & Lim, T.T. (2011). Adsorption-Photocatalytic Degradation of Acid Red 88 by Supported TiO₂: Effect of Activated Carbon Support and Aqueous Anions. *Chemical Engineering Journal*, 171(3), 1098-1107.
- Hassan, S.A. & El-Salamony, R.A. (2014). Photocatalytic Disc-Shaped Composite Systems for Removal of Hazardous Dyes in Aqueous Solutions. *Canadian Chemical Transactions*, 2, 57-71.
- Hung-Low, F., Ramirez, D.A., Peterson, G.R., Hikal, W.M. & Hope-Weeks, L.J. (2016). Development of a Carbon-Supported Sn-SnO₂ Photocatalyst by a New Hybridized Sol-Gel/Dextran Approach. *RSC Advances*, 6(25), 21019-21025.
- Kim, H.J., Joshi, M.K., Pant, H.R., Kim, J.H., Lee, E. & Kim, C.S. (2015). One-Pot Hydrothermal Synthesis of Multifunctional Ag/ZnO/Fly Ash Nanocomposite. *Colloids and Surfaces A: Physicochemical and Engineering Aspects*, 469, 256-262.
- Kumar, P.S.S., Manivel, A. & Anandan, S. (2009). Synthesis of Ag-ZnO Nanoparticles for Enhanced Photocatalytic Degradation of Acid Red 88 in Aqueous Environment. *Water Science and Technology* 59(7), 1423-1430.
- Kumar, P.S.S., Sivakumar, R., Anandan, S., Madhavan, J., Maruthamuthu, P. & Ashokkumar, M. (2008). Photocatalytic Degradation of Acid Red 88 Using Au-TiO₂ Nanoparticles in Aqueous Solutions. *Water Research*, 42(19), 4878-4884.
- Liu, Z., Liu, Z., Cui, T., Li, J., Zhang, J., Chen, T., Wang, X. & Liang, X. (2014). Photocatalysis of Two-Dimensional Honeycomb-Like ZnO Nanowalls on Zeolite. *Chemical Engineering Journal*, 235, 257-263.
- Lv, J., Sheng, T., Su, L., Xu, G., Wang, D., Zheng, Z. & Wu, Y. (2013). N, S Co-Doped-TiO₂/Fly Ash Beads Composite Material and Visible Light Photocatalytic Activity. *Applied Surface Science*, 284, 229-234.
- Manjula, P., Boppella, R. & Manorama, S.V. (2012). A Facile and Green Approach for the Controlled Synthesis of Porous SnO₂ Nanospheres: Application as an Efficient Photocatalyst and an Excellent Gas Sensing Material. *ACS Applied Materials & Interfaces*, 4(11), 6252-6260.
- Saharan, V.K., Pandit, A.B., Satish Kumar, P.S. & Anandan, S. (2012). Hydrodynamic Cavitation as an Advanced Oxidation Technique for the Degradation of Acid Red 88 Dye. *Industrial & Engineering Chemistry Research*, 51(4), 1981-1989.
- Sheng, F., Zhu, X., Wang, W., Bai, H., Liu, J., Wang, P., Zhang, R., Han, L. & Mu, J. (2014). Synthesis of Novel Polyoxometalate K₆ZrW₁₁O₃₉Sn·12H₂O and Photocatalytic Degradation Aqueous Azo Dye Solutions with Solar Irradiation. *Journal of Molecular Catalysis A: Chemical*, 393, 232-239.
- Singh, L., Luwang, M.N. & Srivastava, S. (2014). Luminescence and Photocatalytic Studies of Sm³⁺ Ion Doped SnO₂ Nanoparticles. *New Journal of Chemistry*, 38(1), 115-121.
- Subash, B., Krishnakumar, B., Sreedhar, B., Swaminathan, M. & Shanthi, M. (2013). Highly Active WO₃-Ag ZnO Photocatalyst Driven by Day Light Illumination. *Superlattices and Microstructures*, 54, 155-171.
- Tamma, S.K. & Mandal, B.K. (2016). Tyrosine Mediated Synthesis of SnO₂ Nanoparticles and Their Photocatalytic Activity Towards Violet 4 BSN Dye. *Journal of Molecular Liquids*, 221, 415-421.
- Thejaswini, T.V.L., Prabhakaran, D. & Maheswari, M.A. (2016). Soft Synthesis of Bi Doped and Bi-N Co-Doped TiO₂ Nanocomposites: A Comprehensive Mechanistic Approach Towards Visible Light Induced Ultra-Fast Photocatalytic Degradation of Fabric Dye Pollutant. *Journal of Environmental Chemical Engineering*, 4(1), 1308-1321.
- Wang, B., Li, Q., Wang, W., Li, Y. & Zhai, J. (2011). Preparation and Characterization of Fe³⁺-Doped TiO₂ On Fly Ash Cenospheres for Photocatalytic Application. *Applied Surface Science*, 257(8), 3473-3479.
- Zhang, J., Cui, H., Wang, B., Li, C., Zhai, J. & Li, Q. (2013). Fly Ash Cenospheres Supported Visible-Light-Driven BiVO₄ Photocatalyst: Synthesis, Characterization and Photocatalytic Application. *Chemical Engineering Journal*, 223, 737-746.
- Zhang, J., Cui, H., Wang, B., Li, C., Zhai, J. & Li, Q. (2014). Preparation and Characterization of Fly Ash Cenospheres Supported CuO-BiVO₄ Heterojunction Composite. *Applied Surface Science*, 300, 51-57.
- Zhao, L., Liu, Z.C. & Liu, Z.F. (2015). Synthetic Zeolite Supported ZnO Nanoparticle Materials for Photocatalytic Applications. *Materials Technology*, 30(1), 60-64.

UTILIZATION OF NATURAL CLAY AS A RELIABLE SOLUTION FOR THE ADSORPTIVE TREATMENT OF METOLACHLOR CONTAMINATED STORMWATER

SITI FAIROS AB SHATTAR⁽¹⁾, NOR AZAZI ZAKARIA⁽²⁾ & KENG YUEN FOO⁽³⁾

^(1,2,3)River Engineering and Urban Drainage Research Centre (REDAC),
Universiti Sains Malaysia, Engineering Campus, Nibong Tebal, Penang, Malaysia.
ctfairosz89@yahoo.com.my; redac01@usm.my; k.y.foo@usm.my

ABSTRACT

Pesticide is a diverse group or mixture of chemical substances, intentionally applied for selective attenuation against controlling pest, vectors and animal disease. Today, the presence of pesticide derivatives in the urban and suburban stormwater has attracted aesthetic attention among the scientific community. Among various available water treatment technologies, adsorption process, notably using low cost, renewable, eco-friendly, and natural adsorbent has gained important credibility. In this sense, in this study, a new route for the conversion of natural clay into a functionalized adsorbent via simple chemical treatment has been presented. The treatment potential for the adsorptive removal of metolachlor was attempted. The physical and chemical properties were evaluated by Fourier Transform Infrared (FTIR) Spectroscopy, scanning electron microscopy (SEM), and nitrogen adsorption-desorption curve. The effects on adsorption behavior as a function of initial concentration, contact time and solution pH were examined. Equilibrium data were fitted to the Langmuir, Freundlich, and Temkin isotherm models, while the kinetic data were simulated using the pseudo-first order and pseudo-second order kinetic equations. Results demonstrated that the equilibrium data was well fitted to the Langmuir isotherm model, with a maximum monolayer adsorption capacity of 38.55 mg/g. The good correlation coefficient, R^2 was found following closely to the pseudo-second order kinetic model, and the morphological study provided a strong evidence support to the presumption that the intercalation of hexadecyltrimethylammonium bromide (HDTMA) with the natural clay was successfully obtained. The findings revealed the great feasibility of natural clay derivative as a viable treatment technique for the effective remediation of pesticides contaminated stormwater.

Keywords: Adsorption; metolachlor; natural clay; pesticide; water pollution.

1 INTRODUCTION

Metolachlor, also known as 2-chloro-N-(2-ethyl-6-methylphenyl)-N-(2-methoxy-1-methylethyl) acetamide, is a nonionizable substituted methoxyacetamide widely applied to control annual broadleaf weeds and grasses in the agriculture crops, including corn (*Zea mays* L.), soybean (*Glycine max* (L) merr), bean (*Phaseolus vulgaris* L.) and potato (*Solanum tuberosum* L.) (Buttle, 1990). It is applied as a pre- and post-emergence, to be incorporated to the natural soil to inhibit the cell growth, and prevents the synthesis of long-chain fatty acids, with a recommended dosage of 0.7-1.4 L/acre at 4623-9246 ppm. Metolachlor (MW=283.8 g/mole) is a hydrophobic herbicide with a moderate vapor pressure of 1.7 mPa at 20 °C, to hinder the elongation of roots and shoots by the inhibition of amino acid glutathione, which takes place in the protein synthesis.

It is highly persistent in the colloidal soil structure, with slow microbial and anaerobic degradation rate, and extremely stable in water under regular sunlight. The leaching potential of metolachlor in the groundwater soil column with a shallow aquifer was 4.18×10^{16} , with the dissipation rate constant and half-life of 0.140 week⁻¹ and 5 weeks, respectively. It has the highest persistency among the acetanilide herbicides, with the $t^{1/2}$ of 200 days in highly acidic water, and 97 days in highly alkaline water, with a water solubility of 530 mgL⁻¹ at 20 °C. Metolachlor has been recognized as the major non-point source pollutant in urban environment. It was detected in all depth (up to 160 cm) even after two week of its recorded application, with the greatest concentration in soil water of 845 µg/L (Vryzas et al., 2012). The half-life (DT₅₀) values of metolachlor range from 48-162 days, with the persistency of up to 10 µg/L, 18 months after its application. The Environmental Protection Agency (EPA) of the United States has reported that metolachlor was detected in 2091 out of 4161 of tested surface water samples. Similar statement has been coded by EPA for the subsequent study, which found that 1644 samples of metolachlor was identified from 312 locations at 14 states, at a maximum concentration of 138 µg/L against the permissible limit of 100 µg/L.

One of the critical approaches pursued to reduce the migration of metolachlor in natural soil is adsorption process. It is the most important process affecting the biological activity and environmental fate of most organic and inorganic water pollutants. The clay fraction and the associated mineral contents in soil (Koskinen and Harper, 1990), play a key role to govern the mobility, preferential flow properties, and leaching

potential of a variety of water contaminants to the subsurface (Obrigawitch et al., 1981; Singh et al., 2002; Weber et al., 2003; Goldreich et al., 2011). Johnson et al. (2011) found that the adsorption of metolachlor onto Sharkey clay was higher and more consistent as compared to the commercial silt loam soils. They stated that, although both of the tested samples were alluvials Mississippi Delta Soils, Sharkey clay with 4 times higher clay content than the commercial silt loam soil showed a better adsorptive potential. Si et al. (2009), in another study reported that the greatest adsorption capacity of metolachlor occurred at the 300-425 cm of soil depth, which contained the highest smectite clay and extractable iron oxalate. Previous researchers have suggested the suitability of clays as a filter media to reduce the infiltration of pesticides contaminated water into the groundwater and receiving waterways, which might induce detrimental and threatening implications to the environment and aquatic ecosystem (Shattar et al., 2016). Within this framework, this study was undertaken to evaluate the viability of locally available natural clay for the innovative treatment of water pollutant, particularly for the removal of metolachlor. The significant influences of initial concentration, contact time and solution pH on the adsorption process were analyzed. Textural, functional and surface chemistry of the prepared adsorbent was performed. The adsorption isotherms and kinetics are elucidated.

2 EXPERIMENTAL WORK

2.1 Adsorbent

The natural clay (NC) applied in this study was acquired from a local paddy field. The collected sample was purified under vigorously stirring at 90 °C in hydrogen peroxide (H₂O₂) and acetic acid (CH₃COOH) solution. The purified sample was filtered, washed thoroughly with double distilled water, dried at 105 °C, and crushed, grounded and sieved to the particle sizes of 20-45 µm. The purified clay was dispersed in 0.5 dm³ of deionized water, and the quaternary ammonium bromide, C₁₉H₄₂NBr, a cationic surfactant with an average molar mass of 364.45 g/mole was added to the NC dispersion by mixing at 75 °C for 3 h. The suspension (HNC) was filtered using a hot sintered disc filter funnel, and rinsed with double distilled water until no chloride ions were detected by the silver nitrate (AgNO₃) solution.

2.2 Adsorbate

Analytical grade substituted metolachlor (97.8% purity), with a chemical formula of C₁₅H₂₂ClNO₂ was applied as the model adsorbate. The standard stock solution was prepared in the aqueous calcium chloride of 0.01 M, and working solutions with the desired concentrations were prepared by a series of successive dilutions.

2.3 Adsorption equilibrium and kinetic studies

The adsorption experiments were performed in a set of Erlenmeyer flasks containing 0.2 g of HNC and 200 mL of metolachlor solutions with the concentration range of 50-400 mg/L. The flasks were kept in an isothermal shaker at 30 °C and 120 rpm until equilibrium was attained. All samples were filtered prior to analysis to minimize the interference of the HNC fines particles. Each experiment was duplicated under identical conditions, and the concentrations of metolachlor in the supernatant solutions before and after the adsorption experiments were analyzed using a double beam UV-vis spectrophotometer (Shimadzu-1800, Japan) at 194 nm. The adsorptive uptake of metolachlor at the equilibrium, q_e (mg/g), was calculated by:

$$q_e = \frac{(C_0 - C_e)V}{W} \quad [1]$$

where C_0 and C_e (mg/l) are the liquid-phase concentrations of metolachlor at initial and equilibrium, respectively. V (L) is the volume of the solution and W (g) is the dry mass of HNC.

The effect of solution pH on the adsorptive uptake of metolachlor was examined by varying the solution pH from 2 to 12, at the fixed concentration of 400 mg/L, adsorbent dosage of 0.2 g/200 mL and adsorption temperature of 30 °C. The initial pH of the metolachlor solution was adjusted by the addition of 0.10 M of hydrochloric acid (HCl) or sodium hydroxide (NaOH). The procedure of adsorption kinetic test was identical to the batch equilibrium studies, where the aqueous samples were withdrawn at different time intervals, and the concentrations of metolachlor were similarly measured. The amount of adsorption at time t , q_t (mg/g), was calculated by:

$$q_t = \frac{(C_0 - C_t)V}{W} \quad [2]$$

where C_t (mg/l) are the liquid-phase concentrations of metolachlor at time t (hour).

2.4 Adsorption isotherms

The establishment of the most appropriate isotherm model is an important procedure for upscaling of the adsorption systems. It describes the interaction between the solute molecules with the adsorbents, and is critical for the optimization use of the adsorbents (Foo and Hameed, 2010). In this work, three major isotherm models: the Langmuir, Freundlich and Temkin isotherm models were established. The applicability of the models was verified by the determination of correlation coefficient, R^2 and the root-mean-square deviation (RMSD), the commonly used statistical tool measuring the predictive power of a model derived as:

$$R^2 = \frac{(\overline{q_{e,meas}} - \overline{q_{e,calc}})^2}{\sum (q_{e,meas} - q_{e,calc})^2 + (\overline{q_{e,meas}} - \overline{q_{e,calc}})^2} \quad [3]$$

$$RMSD = \frac{\sqrt{\sum_{i=1}^n (q_{exp} - q_p)^2}}{n-1} \quad [4]$$

where $q_{e,meas}$, $q_{e,calc}$, and $\overline{q_{e,calc}}$ (mg/g) are the measured, calculated and average mean of adsorbate concentration, while q_{exp} (mg/g) and q_p (mg/g) are the experimental and predicted adsorption capacity, respectively.

2.5 Adsorption kinetic

Adsorption kinetic provides an invaluable insight into the controlling mechanism of an adsorption process, which in turn governs the residence time of adsorbates at the solid-liquid interface (Foo, 2016). The applicability of the kinetic model to describe the adsorption process was validated by judging the values of the correlation coefficient, R^2 as well as the normalized standard deviation, Δq (%) defined as:

$$\Delta q(\%) = \sqrt{\frac{\sum \left[\frac{(q_{e,exp} - q_{e,cal})^2}{q_{e,exp}} \right]^2}{N - 1}} \quad [5]$$

where $q_{e,exp}$ (mg/g) and $q_{e,cal}$ (mg/g) are referred to the experimental and calculated value for the metolachlor adsorption at equilibrium, respectively and N is the number of data points.

2.6 Physical and chemical characterizations

The textural characterization of the prepared adsorbents was carried out by nitrogen (N_2) adsorption-desorption curve at 77K using a Micromeritics ASAP 2020 analyzer. The determination of Brunauer-Emmett-Teller (BET) surface area, total pore volume and pore size distribution was deduced using the BET equation, by converting the amount of N_2 gas adsorbed at a relative pressure of 0.95 to equivalent liquid volume of the adsorbate (N_2). The surface morphology was examined by using the scanning electron microscope (Zeiss Supra 35VP). The Fourier Transform Infrared (FTIR) Spectroscopy analysis was conducted using a FTIR spectrophotometer (Perkin Elmer-1600) within the wavelength of 4000-400 cm^{-1} . The determination of pH_{pzc} was conducted by using the titrimetric method, in which 0.15 g of HNC was mixed with 0.01 M of sodium chloride (NaCl) solution. The solution pH was adjusted between 2 and 12. These flasks were kept for 48 h, and the solution pH was measured using a two point calibration pH meter. The intersection of the curves of " pH_{final} vs $pH_{initial}$ ", is the pH_{pzc} of HNC.

3 RESULTS AND DISCUSSION

3.1 Adsorption equilibrium studies

The batch adsorption experiments as a function of initial concentration and contact time were carried out at the initial concentration of 50-400 mg/L, with the adsorbent dosage of 0.2 g/200 mL [(Figure 1 (a))]. Initial concentration presents a driving force to alleviate the mass transfer between the metolachlor molecules of the bulk solution with the adsorbent surface. The adsorptive uptake of metolachlor increased from 7.32 to 26.15 mg/g with increasing the initial concentration from 50 to 400 mg/L. At the beginning, the metolachlor were adsorbed rapidly onto the exterior surface of adsorbent. When the adsorption of the exterior surface reached to the saturation, the metolachlor would need to penetrate into the interior surface of the adsorbent. This phenomenon takes relatively longer contact time. The amount of metolachlor adsorbed at the equilibrium time

reflects the maximum adsorption capacity of the adsorbent under those operating conditions (Foo et al., 2013a). During this time, the amount of metolachlor adsorbing to the surface of HNC is in a dynamic equilibrium with the amount of metolachlor desorbing from the surface. The equilibrium time required for the adsorption of metolachlor onto HNC was approximately 3 h for the initial concentrations below 200 mg/L. However, longer equilibrium time of 5 h was required for the higher concentrations to reach to the equilibrium.

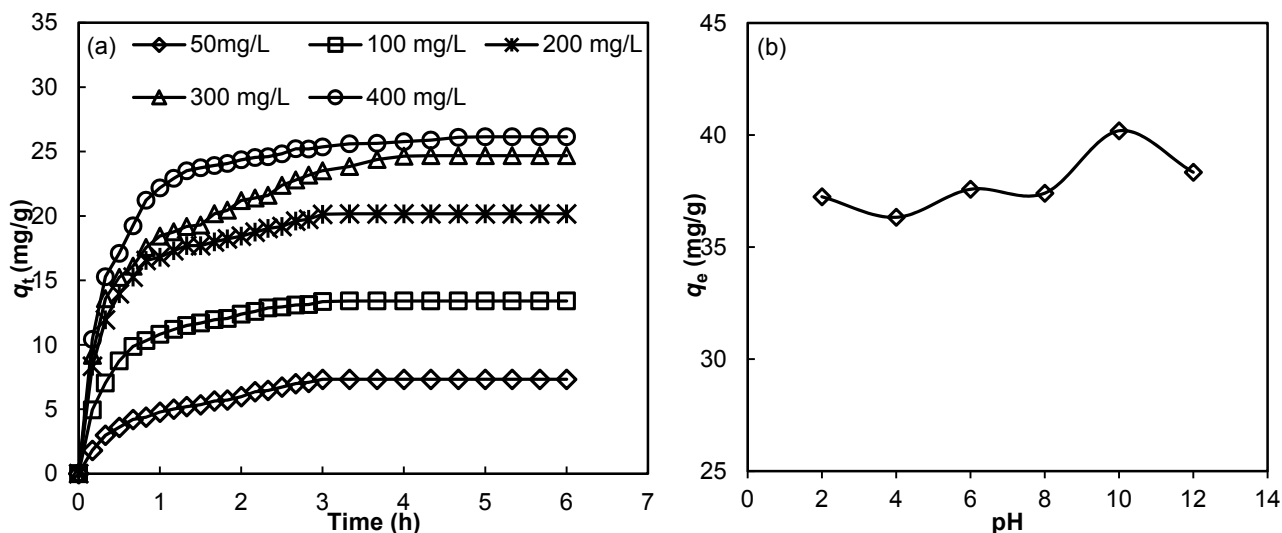


Figure 1. Effect of (a) initial concentration and contact time and (b) solution pH on the adsorptive uptake of metolachlor onto HNC at 30 °C.

Solution pH exerts a profound influence on the adsorptive uptake of adsorbate molecule by regulating the surface charge and ionization/dissociation of the adsorbate molecules. The adsorption behaviour of metolachlor over a broad pH range of 2-12 is depicted in Figure 1(b). It can be observed that the adsorption of metolachlor remain almost unaltered with the changing solution pH. However, the equilibrium adsorption of metolachlor was found to decrease slightly from 37.25 to 36.33 mg/g as the initial pH of the aqueous solution increased from 2 to 4. This may be due to the presence of excess H^+ ions which accelerates the removal of metolachlor anions in the aqueous solution. At the very low solution pH, the surface of adsorbent would be surrounded by hydronium ions, which may enhance the adsorbate interaction with the surface binding sites, by greater attractive forces to improve the uptake for the polar molecules (Akhtar et al., 2007). The adsorption process could be explained in term of zero point of charge pH_{pzc} . HNC has a pH_{pzc} value of 4.01. At the acidic pH, the surface of HNC was positively charged, and this suggested that the main interactions between HNC and metolachlor at $pH < 4.01$ is governed mainly by electrostatic interaction between the positive charge of the adsorbent surface and electron-rich regions of the adsorbed molecules. At $pH=4.01$, the surface of HNC was essentially neutral, leading to the weakening of the interactions with the metolachlor molecules, to decrease the degree of adsorption. From pH 4 to 12, there was a slight increase in the adsorption. Similar finding was found by Otero et al. (2012), who reported that the adsorption of metolachlor onto organohydrotalcites was not pH dependent. This finding was mainly due to the buffering effect of the hydrotalcite-like equilibrated suspensions.

3.2 Adsorption isotherm

Adsorption isotherm elucidates the distribution of adsorbate molecules between the liquid phase and the solid medium when the adsorption process reaches to the equilibrium. The equilibrium data were fitted to three different isotherm models, the Langmuir, Freundlich and Temkin isotherm models. Langmuir isotherm model was derived based on the assumption that the adsorption process takes place at the specific homogeneous sites within the adsorbent, and the monolayer adsorption onto a surface that contains a finite number of adsorption sites, with uniform adsorption energy and no transmigration of adsorbates in the plane of the adsorbing surface (Langmuir, 1918). The non-linear form of Langmuir isotherm equation is given by:

$$q_e = \frac{Q_0 K_L C_e}{1 + K_L C_e} \quad [6]$$

which Q_0 (mg/g) and K_L (L/g) are the Langmuir isotherm constants related to adsorption capacity and rate of adsorption, respectively.

The essential characteristics of the Langmuir isotherm model can be expressed in terms of a dimensionless parameter (R_L) defined as:

$$R_L = \frac{1}{1 + K_L C_e} \quad [7]$$

The value of R_L would verify either the adsorption process to be unfavorable ($R_L > 1$), linear ($R_L = 1$), favorable ($0 < R_L < 1$) or irreversible ($R_L = 0$) (Weber and Chakkravorti, 1974).

Freundlich isotherm model assumes heterogeneous surface energy, in which the energy could vary as a function of surface coverage. The well-known nonlinear form of Freundlich isotherm model (Freundlich, 1906) is derived as:

$$q_e = K_F C_e^{1/n} \quad [8]$$

where K_F (mg/g)(L/mg)^{1/n} and n are the Freundlich isotherm constants that indicate favourably of the adsorption process. K_F is defined as the adsorption or distribution coefficient, and represents the quantity of metolachlor adsorbed onto HNC for a unit of equilibrium concentration.

Another popular equation for the isotherm analysis was given by Temkin (Temkin and Pyzhev, 1940). Temkin isotherm model assumes that the heat of adsorption (function of temperature) of all molecules in the layer would decrease linearly rather than logarithmically with surface coverage. Its derivation is characterized by a uniform distribution of binding energies (up to some maximum binding energy). The Temkin isotherm model has been used in the form of:

$$q_e = \frac{RT}{b_T} \ln A_T C_e \quad [9]$$

where $B = RT/b$, and b , A , R and T are the Temkin isotherm constant related to heat of sorption (J/mole), equilibrium binding constant (L/g), gas constant (8.314 J/mole K) and absolute temperature (K), respectively.

Table 1. Isotherm parameters for the adsorption of metolachlor onto HNC at 30 °C.

Isotherm models	Isotherm constants			
Langmuir	Q_0 (mg/g)	K_L (L/mg)	R^2	$RMSD$
	38.55	0.006	0.997	0.206
Freundlich	K_F (mg/g).(L/mg) ^{1/n}	n	R^2	$RMSD$
	1.303	1.941	0.958	0.563
Temkin	A (L/g)	B	R^2	$RMSD$
	0.053	8.949	0.993	0.258

The isotherm constants, correlation coefficients, R^2 and $RMSD$ values obtained for the three isotherm models are summarized in Table 1. Langmuir isotherm model yielded the best fit with the greatest R^2 values and the lowest $RMSD$ values of 0.997 and 0.206 respectively as compared to the other models. Similar result was reported for the adsorption of metolachlor onto fly ash amended soils (Ghosh and Singh, 2012) and organosilica (Otero et al., 2013), respectively. Conformation of the experimental data into Langmuir isotherm equation indicated homogeneous nature of the metolachlor molecules onto the surface of HNC, with equivalent activation energy of adsorbing molecules. The results also demonstrated no interaction and transmigration of pesticide molecules in the plane of the neighbouring surface, and monolayer coverage of metolachlor molecules at the outer surfaces of HNC. Table 2 summarizes a comparison of the adsorption capacity for metolachlor onto different adsorbents. The adsorbent prepared in this work showed relatively high adsorption capacity as compared to the previous researches.

Table 2. Comparison of adsorption capacities for metolachlor onto different adsorbents.

Adsorbent	Activating agent	Adsorption capacity (mg/g)	Reference
Natural clay	HDTMA	38.55	Present study
Activated charcoals	-	0.14-0.16	Bosetto et al. (1992)
Wyoming bentonite	-	0.05	Nennemann et al. (2001)
Fly ash	-	1.0	Singh (2009)
Clay loam soil	-	0.01	Si et al. (2009)
Soil	Fly ash	15.87-27.03	Ghosh and Singh (2012)
Granular carbon	-	3.33	Kumar et al. (2013)

Organosilica	Benzene	0.21	Otero et al. (2013)
--------------	---------	------	---------------------

3.3 Kinetic modeling

The adsorption of metolachlor from the liquid phase to the solid medium can be considered to be a reversible reaction with equilibrium established between the two phases. The adsorption kinetic of metolachlor onto HNC was simulated using two kinetic equations, the pseudo-first order and pseudo-second order kinetic models. The pseudo-first order equation given by Lagergren and Svenska (1898) is represented by:

$$\ln(q_e - q_t) = \ln q_e - k_1 t \quad [10]$$

where k_1 (1/h) is the pseudo-first order kinetic rate constant. The value of k_1 was deduced from the slopes of the linear plots of $\ln(q_e - q_t)$ versus t . The pseudo-second order chemisorption kinetic equation (Ho and McKay, 1998) is expressed by:

$$\frac{1}{q_e} = \frac{1}{k_2 q_e^2} + \frac{1}{q_e} t \quad [11]$$

where k_2 (g/mg h) is the pseudo-second order kinetic rate constant. The linear plot of t/q_t versus t would provide the value of q_e and k_2 from the slope and the intercept. This procedure is more likely to predict the behaviour over the whole range of adsorption.

The adsorption kinetic parameters for the two kinetic models are summarized in Table 3. The correlation coefficient, R^2 for the pseudo-second order equation were higher at all the tested concentration. The suitability of the model was further justified based on the value of Δq (%). The pseudo-second order kinetic model was found to provide the lowest Δq (%) values which ranged between 5.76-10.21 % as compared to 22.69-35.69 % for the pseudo-first order kinetic model. These findings ascertained the suitability of the pseudo-second order kinetic model to describe the adsorption process, based on the assumption that chemisorption is the rate limiting step. The result was in agreement with the previous work which evaluated the adsorption of metolachlor onto organosilica (Otero et al., 2013).

Table 3. Kinetic model parameters for the adsorption of metolachlor onto HNC.

C_0 (mg/g)	$q_{e,exp}$ (mg/g)	Pseudo-first order				Pseudo-second order			
		$q_{e,cal}$ (mg/g)	k_1 (1/h)	R^2	Δq (%)	$q_{e,cal}$ (mg/g)	k_2 (g/mg h)	R^2	Δq (%)
50	7.32	4.71	1.406	0.681	35.69	6.98	0.307	0.999	5.76
100	13.41	9.38	2.038	0.815	30.02	14.49	0.208	0.999	8.05
200	20.17	15.59	2.723	0.829	22.69	21.46	0.175	0.999	6.40
300	24.69	17.58	3.079	0.779	28.78	22.68	0.182	0.997	8.14
400	26.15	19.49	3.346	0.964	25.48	28.82	0.112	0.995	10.21

3.4 Adsorption mechanism

The Weber and Morris intraparticle diffusion model (Weber and Morris, 1963), derived from the Fick's second diffusion law was applied to analyze the kinetic results. It is an empirically found functional relationship, common to the most adsorption processes, where the uptake varies proportionally to $t^{0.5}$ rather than linearity with the contact time, t . According to this theory:

$$q_t = K_{pi} t^{0.5} + C_i \quad [12]$$

where K_{pi} (mg/g h^{0.5}) is the diffusion rate constant, and C_i gives an idea about the thickness of the boundary layer. If intraparticle diffusion occurs, then q_t versus $t^{0.5}$ will be linear, and intraparticle diffusion is the sole rate limiting step, if the plot passes through the origin. Otherwise, some other mechanism along with intraparticle diffusion may involve.

Refer to the intraparticle diffusion plots (Figure 2a), the first sharper region is the instantaneous adsorption or external surface adsorption. The second region is the gradual adsorption stage where intraparticle diffusion is the rate limiting. In some cases, the third region exists, which is the final equilibrium stage where intraparticle diffusion starts to slow down due to the extremely low adsorbate concentrations left in the solutions. For all initial concentrations, the first stage was completed within the first 1 hour, representing the different stages of the mass transfer of adsorbate molecules from bulk solution to the adsorbent surface.

Table 4. Intraparticle diffusion model constants for the adsorption of metolachlor onto HNC at 30 °C.

C_0 (mg/L)	Intraparticle diffusion model constant								
	K_{p1} (mg/g h ^{1/2})	K_{p2} (mg/g h ^{1/2})	K_{p3} (mg/g h ^{1/2})	C_1	C_2	C_3	$(R_1)^2$	$(R_2)^2$	$(R_3)^2$
50	4.923	2.777	-	0	1.85	-	0.991	0.950	-
100	11.169	2.975	-	0	8.34	-	0.987	0.937	-
200	17.287	3.686	-	0	11.40	-	0.972	0.960	-
300	18.504	5.373	0.094	0	13.32	23.76	0.987	0.986	0.448
400	22.415	3.362	1.039	0	19.45	24.47	0.987	0.945	0.801

From Figure 2(a), the linear lines of all stages did not pass through the origin, and this deviation from the origin or near saturation might be due to the difference of the mass transfer rate in the initial and final stages of the adsorption process (Mohanty et al., 2005). The findings further illustrated that intraparticle diffusion was not the only rate limiting mechanism in the adsorption process. The values of k_{pi} , C_i and correlation coefficient R^2 obtained for the plots are given in Table 4. Increasing bulk liquid metolachlor concentrations from 50 to 400 mg/L showed an enhancement of pore diffusion rate and intercept, indicative of the increase of thickness of the boundary layer and driving force for the sorption process.

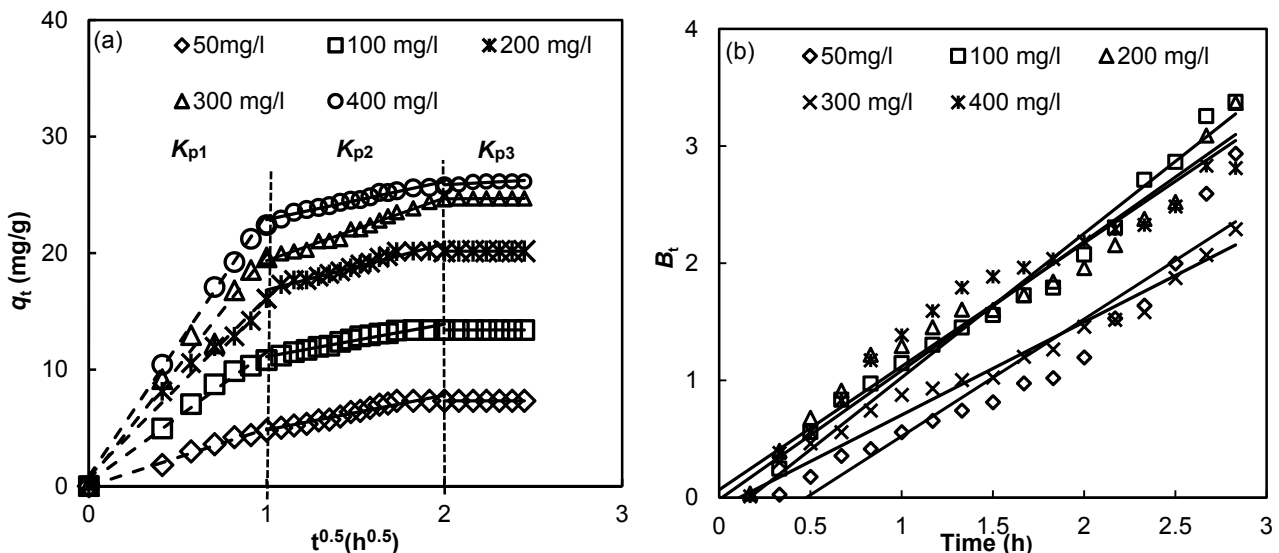


Figure 2. Plots of (a) intraparticle diffusion and (b) Boyd plot models for the adsorption of metolachlor onto HNC at 30 °C.

Generally, the three sequential steps in the adsorption process are film diffusion, where adsorbate ions will travel towards the external surface of the adsorbent, particle diffusion, where adsorbate ions will travel within the pores of the adsorbent, excluding a small amount of adsorption that occurs on the exterior surface of the adsorbent, and adsorption of the adsorbate ions into the interior surface of the adsorbent. The third step is considered to be very fast, and thus it cannot be treated as the rate limiting step. If external transport > internal transport, this rate is governed by particle diffusion. If external transport < internal transport, the rate is governed by film diffusion, and if external transport ≈ internal transport, the transport of the adsorbate ions to the boundary may not be possible at a significant rate. Therefore, the formation of a liquid film surrounding the adsorbent particles would take place through a proper concentration gradient (Mittal et al., 2008). The data was further analyzed by the Boyd model (Boyd et al., 1947) given by:

$$B_t = -0.4977 - \ln(1 - F) \quad [13]$$

which B_t is the mathematical function of F , and F represents the fraction of solute adsorbed at time, t (h), defined as:

$$F = \frac{q_t}{q_e} \quad [14]$$

According to the Boyd model, if the plot B_t versus t passes through the origin, pore diffusion is the rate-limiting step. Conversely, the adsorption process is film diffusion controlled. The calculated B_t values were plotted against time t (h), as illustrated in Figure 2(b). From the curve, it can be found that, the linear lines did not pass through the origin, and the points were scattered around the curve. This indicated that the adsorption of metolachlor onto HNC was mainly governed by the external mass transport mechanism, where particle diffusion was the rate limiting step.

3.5 Physical and chemical characterizations

Nitrogen adsorption-desorption technique provides qualitative information on the adsorption mechanism and porous structure of the clay based adsorbents (Foo et al., 2013b). The BET surface area, Langmuir surface area, and total pore volume of the virgin natural clay were identify to be 32.31 m²/g, 41.50 m²/g, and 0.120 cm³/g, respectively. However, HNC demonstrated a lower BET surface area, Langmuir surface area, and total pore volume of 2.84 m²/g, 3.43 m²/g, and 0.007 cm³/g, respectively, mainly attributed to the exchangeable surface sites satisfied by HDTMA with larger molecular size, resulting in inaccessibility of the internal surface to nitrogen gas, and the blocking of the micropores during the modification stage. The finding was in accordance with the conclusions drawn by the previous researches (Xi et al., 2010; Burns et al., 2006; Seki and Yurdakoç, 2005). The micrograph images for NC and HNC are presented in Figure 3. It can be found that the virgin NC showed the presence of massive and curve plates with a dense and compact structure. In contrast, HDTMA modified-NC showed significant changes to progressively turn into a relatively flat and slick surface, with a series of mesoporous structure among these aggregated particles.

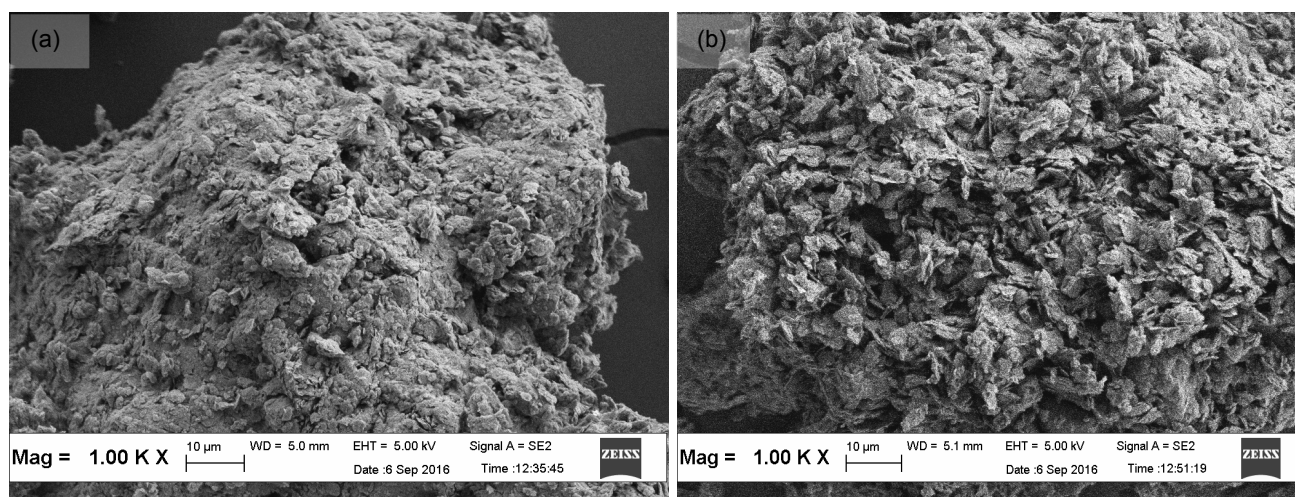


Figure 3. SEM micrographs of (a) NC and (b) HNC.

FTIR spectroscopy is a sensitive tool to evaluate the surface functionalities of the intercalated surfactant within the natural clay based adsorbent (Foo and Hameed, 2012). A comparison of the FTIR spectra for both NC and HNC is depicted in Figure 4. Generally, the transmittance of NC and HNC demonstrated a series of changes, with distinct difference between the intensity and band width. It can be observed that the 3621 and 3697 cm⁻¹ band resolved in both samples, which is due to the presence of hydroxyl structural group corresponded to O-H stretching vibrations. Examination of the clay samples illustrated the ionic vibrations at 3435-3455 cm⁻¹, 1881-1890 cm⁻¹, 1618-1634 cm⁻¹, 1027-1031 cm⁻¹, 912-913 cm⁻¹, 796-779 cm⁻¹, 694-695 cm⁻¹, and 472-535 cm⁻¹, corresponding to the H-O-H stretching, Si-OH stretching mode in quartz, H-O-H bending vibration of H₂O, Si-O stretching vibrations, Al-Al-OH deformation, Si-O stretching vibration, Si-O-Si stretching, and asymmetric and symmetric bending of O-Si-O, respectively. Relatively, for the HDTMA modified-NC, the weak singlet band was detected at 1472 cm⁻¹ resulting from HDTMA methyl group vibrations (Gładysz-Płaska et al., 2012), while the vibrations bands at 2922 and 2852 cm⁻¹ indicated the formation of C-H₂ and C-H₃ groups, from the symmetric and asymmetric stretching of the organo-surfactant methylene group. These findings have clearly shown that the intercalation of the quaternary ammonium cation within the interlamellar spaces of the natural clay has been successfully obtained.

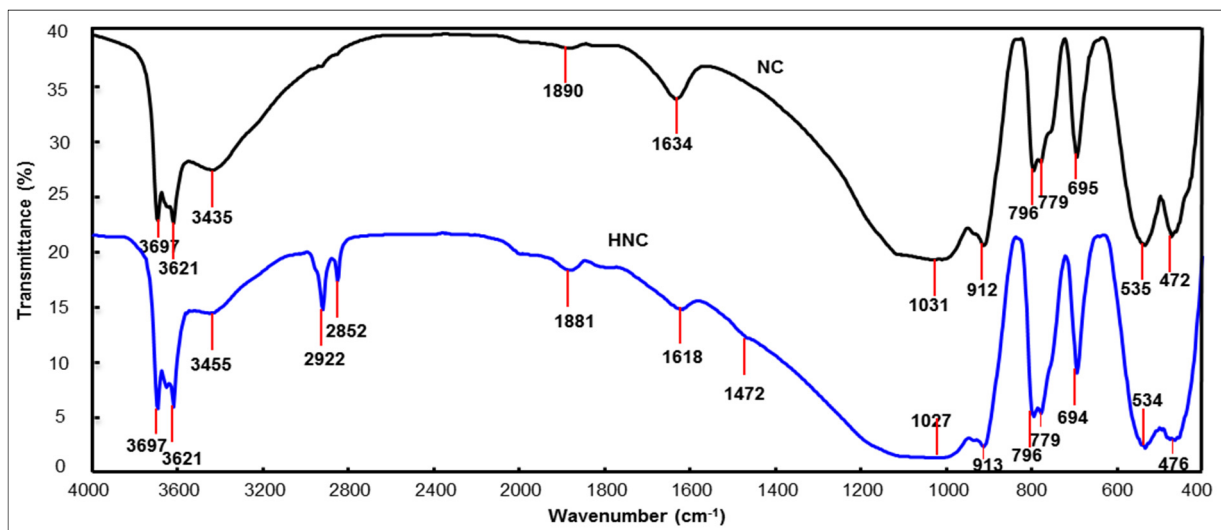


Figure 4. FTIR spectra of NC and HNC.

4 CONCLUSIONS

The present investigation verified the viability of natural clay as a promising alternative technique for the adsorptive removal of metolachlor from the aqueous solution. The intercalation of HDTMA into the interlayer of NC has significantly improved the Van der Waals forces between the organophilic properties and hydrocarbon chains. Adsorption of metolachlor was found to increase with increasing initial concentration and contact time. The equilibrium data were best described by the Langmuir isotherm model, with a maximum monolayer adsorption capacity for metolachlor of 38.55 mg/g. Kinetic data were best confronted to the pseudo-second order kinetic equation, assuming that the chemisorption is the rate controlling step. Mechanism studies ascertained that the adsorption process was governed primarily by the external mass transport mechanism, with particle diffusion as the rate controlling step.

ACKNOWLEDGEMENTS

The authors acknowledge the financial support provided by the Ministry of Higher Education of Malaysia and Universiti Sains Malaysia under the Research University (Project No. 1001/PREDAC/814272) and FRGS (Project No. 304/PREDAC/6171157) research grant schemes.

REFERENCES

- Akhtar, M., Hasany, S.M., Bhangar, M.I. & Iqbal, S. (2007). Low Cost Sorbents for the Removal of Methyl Parathion Pesticide from Aqueous Solutions. *Chemosphere*, 66, 1829–1838.
- Bosetto, M., Arfaio, P. & Fusi P. (1992). Adsorption of the Herbicides Alachlor and Metolachlor on Two Activated Charcoals. *The Science of the Total Environment*, 123/124, 101–108.
- Boyd, G.E., Adamson, A.W. & Myers Jr., L.S. (1947). The Exchange Adsorption of Ions from Aqueous Solutions by Organic Zeolites. II. Kinetics. *Journal of the American Chemical Society*, 69, 2836–2848.
- Burns, S.E., Bartelt-Hunt, S.L., Smith, J.A. & Redding, A.Z. (2006). Coupled Mechanical and Chemical Behavior of Bentonite Engineered with a Controlled Organic Phase. *Journal of Geotechnical and Geoenvironmental Engineering*, 132(11), 1404–1412.
- Buttle, J.M. (1990). Metolachlor Transport in Surface Runoff. *Journal of Environmental Quality*, 19, 531–538.
- Foo, K.Y. (2016). Value-Added Utilization of Maize Cobs Waste as an Environmental Friendly Solution for the Innovative Treatment of Carbofuran. *Process Safety and Environmental Protection*, 100, 295–304.
- Foo, K.Y. & Hameed, B.H. (2010). Insights into the Modeling of Adsorption Isotherm Systems. *Chemical Engineering Journal*, 156, 2–10.
- Foo, K.Y. & Hameed, B.H. (2012). Coconut Husk Derived Activated Carbon Via Microwave Induced Activation: Effects of Activation Agents, Preparation Parameters and Adsorption Performance. *Chemical Engineering Journal*, 184, 57–65.
- Foo, K.Y., Lee, L.K. & Hameed, B.H. (2013a). Preparation of Banana Frond Activated Carbon by Microwave Induced Activation for the Removal of Boron and Total Iron from Landfill Leachate. *Chemical Engineering Journal*, 223, 604–610.
- Foo, K.Y., Lee, L.K. & Hameed, B.H. (2013b). Preparation of Activated Carbon from Sugarcane Bagasse by Microwave Assisted Activation for the Remediation of Semi-Aerobic Landfill Leachate. *Bioresour Technol*, 134, 166–172.
- Freundlich, H.M.F. (1906). Over the Adsorption in Solution. *Journal of Physical Chemistry*, 57, 385–470.

- Ghosh, R.K. & Singh, N. (2012). Sorption of Metolachlor and Atrazine in Fly Ash Amended Soils: Comparison of Optimized Isotherm Models. *Journal of Environmental Science and Health, Part B: Pesticides, Food Contaminants, and Agricultural Wastes*, 47, 718–727.
- Gładysz-Płaska, A., Majdan, M., Pikus, S. & Sternik, D. (2012). Simultaneous Adsorption of Chromium (VI) and Phenol on Natural Red Clay Modified by HDTMA. *Chemical Engineering Journal*, 179, 140–150.
- Goldreich, O., Goldwasser, Y. & Mishaël, Y.G. (2011). Effect of Soil Wetting and Drying Cycles on Metolachlor Fate in Soil Applied as a Commercial or Controlled-Release Formulation. *Journal of Agricultural and Food Chemistry*, 59, 645–653.
- Ho, Y.S. & McKay, G. (1998). A Comparison of Chemisorption Kinetic Models Applied to Pollutant Removal on Various Sorbents. *Process Safety and Environmental Protection*, 76, 332–340.
- Johnson, A.B., Rowe, D.E. & Tsegaye, T. (2011). Adsorption and Degradation of Metolachlor in Alluvial Soils: Effect of Poultry Litter. *Journal of Sustainable Watershed Science and Management*, 1, 31–35.
- Koskinen, W.C. & Harper, S.S. (1990). The Retention Process: Mechanisms. *Pesticides in the soil environment: processes, impacts, and modeling.*, 51-77.
- Kumar, Y.B., Singh, N. & Singh, S.B. (2013). Removal of Atrazine, Metribuzin, Metolachlor and Alachlor by Granular Carbon. *Journal of Environmental and Analytical Toxicology*, 3, 1–5.
- Lagergren, S. & Svenska, B.K. (1898). Zur theorie der sogenannten adsorption gelöster stoffe, *Kungliga Vetenskapsakademiens Handlingar*, 24, 1–39.
- Langmuir, I. (1918). The Adsorption of Gases on Plane Surfaces of Glass, Mica and Platinum. *Journal of the American Chemical Society*, 40, 1361–1403.
- Mittal, A., Gajbe, V. & Mittal, J. (2008). Removal and Recovery of Hazardous Triphenylmethane Dye, Methyl Violet through Adsorption over Granulated Waste Materials. *Journal of Hazardous materials*, 150, 364–375.
- Mohanty, K., Das, D. & Biswas, M.N. (2005). Adsorption of Phenol from Aqueous Solutions using Activated Carbons Prepared from Tectona Grandis Sawdust By $ZnCl_2$ Activation. *Chemical Engineering Journal*, 115, 121–131.
- Nennemann, A., Mishaël, Y., Nir, S., Rubin, B., Polubesova, T., Bergaya, F., van Damme, H. & Lagaly, G. (2001). Clay-based Formulations of Metolachlor with Reduced Leaching. *Applied Clay Science*, 18, 265–275.
- Obrigawitch, T., Hons, F.M., Abernathy, J.R. & Gipson, J.R. (1981). Adsorption Desorption and Mobility of Metolachlor in Soils. *Weed Science*, 29, 332–336.
- Otero, R., Esquivel, D., Ulibarri, M.A., Jiménez-Sanchidrián, C., Romero-Salguero, F.J. & Fernández, J.M. (2013). Adsorption of the Herbicide S-Metolachlor on Periodic Mesoporous Organosilicas. *Chemical Engineering Journal*, 228, 205–213.
- Otero, R., Fernández, J.M., Ulibarri, M.A., Celis, R. & Bruna, F. (2012). Adsorption of Non-Ionic Pesticide S-Metolachlor on Layered Double Hydroxides Intercalated with Dodecylsulfate and Tetradecanedioate Anions. *Applied Clay Science*, 65–66, 72–79.
- Seki, Y. & Yurdakoç, K. (2005). Paraquat Adsorption onto Clays and Organoclays from Aqueous Solution. *Journal of Colloid and Interface Science*, 287, 1–5.
- Shattar, S.F.A., Zakaria, N.A. & Foo, K.Y. (2016). Feasibility of Montmorillonite-Assisted Adsorption Process for the Effective Treatment of Organo-Pesticides. *Desalination and Water Treatment*, 57, 13645–13677.
- Si, Y., Takagi, K., Iwasaki, A. & Zhou, D. (2009). Adsorption, Desorption and Dissipation of Metolachlor in Surface and Subsurface Soils. *Pest Management Science*, 65, 956–962.
- Singh, N. (2009). Adsorption of Herbicides on Coal Fly Ash from Aqueous Solutions. *Journal of Hazardous Materials*, 168, 233–237.
- Singh, N., Kloeppel, H. & Klein, W. (2002). Movement of Metolachlor and Terbutylazine in Core and Packed Soil Columns. *Chemosphere*, 47, 409–415.
- Tempkin, M.I. & Pyzhev, V. (1940). Kinetics of Ammonia Synthesis on Promoted Iron Catalyst. *Acta Physicochim URSS*, 12, 217–222.
- Vryzas, Z., Papadakis, E.N. & Papadopoulou-Mourkidou, E. (2012). Leaching of Br, Metolachlor, Alachlor, Atrazine, Deethylatrazine and Deisopropylatrazine in Clayey Vadoze Zone: A Field Scale Experiment in North-East Greece. *Water Research*, 46, 1979–1989.
- Weber, J.B., McKinnon, E.J. & Swain, L.R. (2003). Sorption and Mobility of ^{14}C -Labeled Imazaquin and Metolachlor in Four Soils as Influenced by Soil Properties. *Journal of Agricultural and Food Chemistry*, 51, 5752–5759.
- Weber, T.W. & Chakravorti, R.K. (1974). Pore and Solid Diffusion Models for Fixed-Bed Adsorbers. *AIChE Journal*, 20(2), 228–238.
- Weber, W.J. & Morris, J.C. (1963). Kinetics of Adsorption on Carbon from Solution. *Journal of the Sanitary Engineering Division*, 89, 31–60.
- Xi, Y., Mallavarapu, M. & Naidu, R. (2010). Preparation, Characterization of Surfactants Modified Clay Minerals and Nitrate Adsorption. *Applied Clay Science*, 48, 92–96.

EXPERIMENTAL INVESTIGATION OF THE EFFECT OF TEMPERATURE DIFFERENTIALS ON HYDRAULIC PERFORMANCE OF A SEDIMENT RETENTION POND

EHSAN HENDI⁽¹⁾, ASAAD Y. SHAMSELDIN⁽²⁾, BRUCE W. MELVILLE⁽³⁾ & STUART E. NORRIS⁽⁴⁾

^(1,2,3) University of Auckland, Department of Civil and Environmental Engineering, Auckland, New Zealand, ehen327@aucklanduni.ac.nz; a.shamseldin@auckland.ac.nz; b.melville@auckland.ac.nz

⁽⁴⁾ University of Auckland, Department of Mechanical Engineering, Auckland, New Zealand, s.norris@auckland.ac.nz

ABSTRACT

Sediment retention ponds (SRPs) are widely used for control of water quality and quantity. Previous studies have examined the effect on the performance of SRPs of physical parameters such as positioning and orientation of pond inlets and outlets, pond geometry, and the location and orientation of baffles. However, the effect of a temperature difference between the pond and the inflow, an environmental parameter, is often neglected. This paper reports on a study of the effect of temperature on the performance of a model SRP, using two heat exchangers to create a temperature difference between the inflow and the water in the pond. The effect of inflow temperature is investigated, for different temperature differentials. For influent colder than the pond water, the inflow tended to sink to the bottom of the pond and move rapidly towards the outlet; for influent hotter than the pond water, the inflow tended to flow on the top of the pond. The positive or negative buoyancy-driven flow significantly reduced the hydraulic performance of the pond, and it also caused severe short-circuiting. At the end of each test, the flow became stratified, illustrating the long-term effect of temperature differentials. But, however, this stratification reduces with time.

Keywords: Sediment retention ponds; hydraulic performance; temperature differential; residence time; buoyancy driven flow.

1 INTRODUCTION

Sediment retention ponds (SRPs) have been used for many years, to minimise the adverse impacts of urbanization (ARC, 2003; Khan et al., 2013; Vymazal, 2014). The treatment efficiency of the pond is directly linked to its hydraulic efficiency. The amount of mixing in SRPs is a major factor that can affect the hydraulic performance of the ponds. The no-mixing condition, which is known as plug flow, is the most efficient hydraulic condition and deviation from plug flow reduces hydraulic efficiency (von Sperling, 2002). The design of stormwater ponds is currently based primarily on the assumption that plug flow conditions prevail in the pond and that 100% of the pond volume is used. This is not the case for most ponds, as the flow structure is normally composed of zones of recirculation and eddies (Kadlec, 1994).

Several factors affect the hydrodynamics of a pond which can be divided into physical and environmental parameters. Physical parameters are characteristics of the ponds such as positioning and orientation of pond inlets and outlets, pond geometry, and the location and orientation of baffles. Environmental parameters of the ponds are external driving forces such as wind and temperature (Shilton, 2005). Most of the open literature on the hydraulic performance of SRPs has been focused on the physical parameters. Previous research concerning the effect of physical parameters on pond hydraulic efficiency has investigated pond layout (Persson, 2000; Su et al., 2009), inlet and outlet design (Bodin et al., 2012; Pearson et al., 1995; Persson, 2000), floating treatment wetlands (Khan et al., 2013) and baffles (De Oliveira et al., 2011; Farjood et al., 2015). Regarding temperature differences as an environmental parameter, the results of tracer studies indicate that temperature variation causes short-circuiting in ponds (Macdonald et al., 1986; Pedahzur et al., 1993). Goula et al. (2008), also numerically investigated the effect of influent temperature variations in a sedimentation tank for potable water treatment and found that "only 1 °C between influent and tank content is enough to induce a density current". Few studies have been found to experimentally investigate the temperature influence on stormwater ponds. One, however, is Watters (1972a) who investigated the effect of influent temperature variations in a waste stabilization pond. In his research, the temperature differences have been experimentally investigated by changing the density of the influent using salt water and there appears to be no choice but to accept the results with certain approximations when using salt (mass transfer) as a method of creating density stratified flows. Therefore, systematic studies on temperature difference effects are still needed to have better understanding of the hydrodynamics of SRPs.

The primary aims of this study are to investigate how a buoyant, neutrally buoyant or negatively buoyant inflow affects the residence time and flow pattern in a modeled retention pond.

2 MATERIALS AND METHODS

2.1 Tracer studies

Hydraulic residence time (HRT) is a key factor in investigating the treatment efficiency of ponds and wetlands. The HRT delineates the time a parcel of water spends within a system, and it depends on the streamline of each particle (Nix, 1985; Thackston et al., 1987). Since each particle of water pursues a particular path, there is a specific HRT for each of the water parcels. These variations in HRT can be explained by generating the residence time distribution (RTD) curves which represent the temporal probability distribution of non-reacting tracer particles within the system (Van de Vusse, 1959).

The tracer such as the cation lithium (Kadlec, 1994), the anion bromide (Grismer et al., 2001), or fluorescent dyes (Khan, 2012) can be added to the system inlet as an impulse or step change (Werner et al., 1996) to create RTD curves. In this study Rhodamine WT (RWT) was selected as the tracer dye due to the numerous advantages over the other tracers such as being readily soluble in water, highly detectable by fluorometers, mostly unaffected by background fluorescence, minimally degradable in short times, harmless in low concentrations (Wilson et al., 1968) and cost effective.

2.2 Hydraulic performance

Hydraulic performance of ponds can be evaluated by analysing the residence time distribution (RTD) curve. In this study, the hydraulic performance of the pond was assessed using the hydraulic indices recommended by Farjood et al. (2014) which are t_5 for short-circuiting (SC). The moment index (MI) for the hydraulic efficiency, and the Morril index (M_o) for mixing. t_5 is the normalised time for passage of 5% of added tracer to exit through the outlet. The Morril index, M_o , is defined as t_{90}/t_{10} , where t_{10} and t_{90} are the times for 10% and 90% of the added tracer to exit the system, respectively. M_o values close to 1 show a more plug flow like regime, and it increases with increase in the degree of mixing. The moment index proposed by Wahl et al. (2010) is defined as:

$$MI = 1 - \int_0^1 (1 - t' C'(t')) dt' \quad [1]$$

where $C' = C / C_0$, C is the concentration of tracer, C_0 is the amount of tracer added to the pond divided by the pond volume, $t' = t / t_n$ is normalised time which is the measured time divided by the nominal residence time, and MI is bounded from zero to one. To reflect the effective volume of the pond and the distribution of hydraulic residence time, it is beneficial to measure (λ) as the second hydraulic efficiency measure, given by:

$$\lambda = \frac{t_p}{t_n} \quad [2]$$

where t_p is the peak time, and t_n is nominal residence time.

2.3 Experimental setup

The physical model is a trapezoidal pond made from transparent acrylic sheets fitted on a steel frame with top dimensions of 4.1m × 1.6m, 0.3m deep, and bank slope of 2:1. The pond was preceded by a rectangular tank of 0.3 × 1.6 × 0.2m serving as the sediment forebay (Figure 1) (Farjood et al., 2015; Khan et al., 2011). The facility was designed so that the temperature differential could be created using two separate systems and monitored with a thermometer. Before starting the experiments, the water in the tank was pumped to the forebay and over a level spreader into the retention pond. The effluent at this stage is carried by a 40mm pipe to the waste. After ensuring steady flow conditions in the pond, the effluent of the pond and the water in the tank are recirculated in two different systems. Each system consists of two heater/chiller units to change the temperature of the water. After changing the temperature of the water, the water in the tank was pumped to the pond and the tracer experiments were conducted by adding Rhodamine WT uniformly across the spread inlet width. For the outlet, three perforated T-bars are fixed to an outlet riser to model a floating decant dewatering system. The perforated T-bars were constructed from PVC pipe with a diameter of 48mm. Five rows of 6mm diameter holes on each of the T-bars allow the water to leave the pond. The T-bars were fixed to a 250mm long, vertical PVC pipe with 200mm internal diameter, which serves as the outlet riser (Farjood et al., 2015). The T-bars are fixed to the outlet riser at 220mm from the bottom and are about 80% submerged in the 245mm water depth during the tests for 1l/s and fully submerged in the 265mm water depth for 2l/s. The tracer concentration in the outflow was continuously measured using a Cyclops-7TM fluorometer manufactured by Turner Designs.

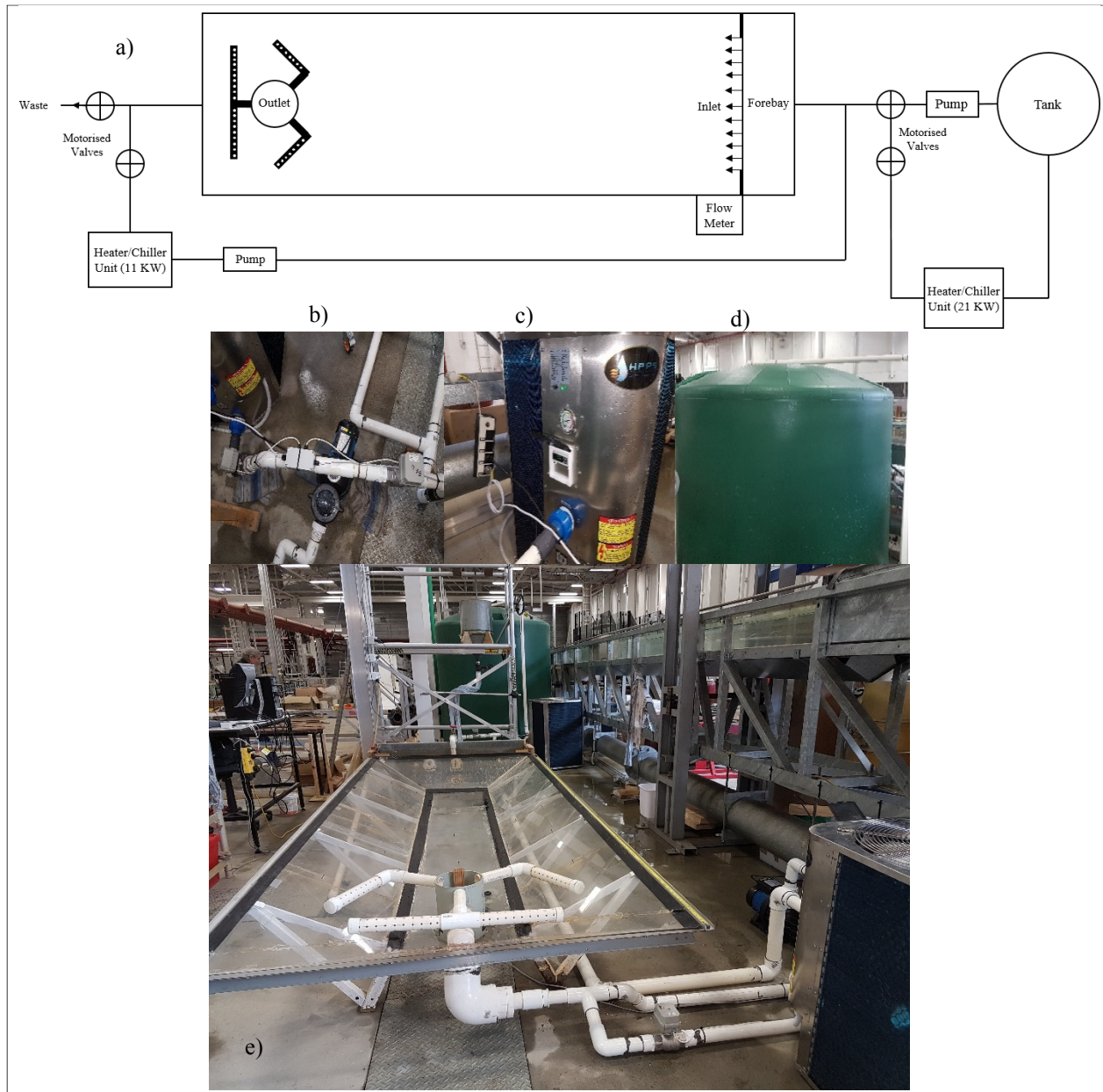


Figure 1. a) Schematic diagram of the experimental setup, b) Pump and motorized valves, c) Heater/Chiller unit, d) Tank, e) The physical model viewed from the outlet.

3 RESULTS AND DISCUSSIONS

To test the effect of temperature variations on the performance of the pond, two cases were selected. In the first case, the temperature of water in the pond was hotter than the influent (positive values of ΔT where $\Delta T = \text{Initial temperature of water in the pond} - \text{Inflow temperature}$). In the second case, the temperature of water in the pond was colder than the influent (negative values of ΔT). Tables 1 and 2 give a list of the density stratified flow experiments with the experimental results that were performed at different temperatures. The temperature of the inflow for cases 2-6 was lower than the temperature of the pond fluid while the reverse was true for the experiments of cases 7-11. Figures 2-3 illustrated some typical RTD curves for the two cases above. Also shown in Figures 2-3 are the uniform temperature experiment ($\Delta T = 0$). It can be seen from these figures that temperature differences between the pond water and inlet can cause significant changes in RTD curves and consequently can change the hydraulic efficiency of the retention pond. For both $+\Delta T$ and $-\Delta T$ temperature differences, when the temperature differences increase, the RTD curves have a sharper peak and the maximum normalised concentration was also increased. There is also a clear trend of decreasing time to reach the peak which shows the poor efficiency and short-circuiting.

The reasons for these differences are given as follows. When $\Delta T > 0$ the inflow tracer flows along the bottom of the pond due to its higher density. The movement through the pond was faster due to the higher velocities that occur near the pond bottom due to the influence of the confinement of the inflow. The inflow, in this case, rises up at the end of the pond and exit through the outlet. This causes the tracer to take a shorter time to reach

the outlet. The same is true when $\Delta T < 0$. The tracer is concentrated in the top of the pond, and it thus reaches the outlet in a shorter time interval.

Table 1. Hydraulic index values for different temperatures (1l/s).

Model Case	ΔT (°C)	SC (%)	MI (%)	Mo (%)
1	0	47.63	84.29	27.57
2	+1	38.24	71.68	20.50
3	+2	30.09	66.35	18.43
4	+4	25.95	63.09	14.58
5	+6	21.46	58.77	13.17
6	+8	21.02	56.34	13.96
7	-1	37.32	71.62	21.54
8	-2	32.94	65.60	20.40
9	-4	30.34	63.52	17.57
10	-6	22.43	57.78	12.65
11	-8	22.04	55.85	12.40

Table 2. Hydraulic index values for different temperatures (2l/s).

Model Case	ΔT (°C)	SC (%)	MI (%)	Mo (%)
1	0	48.60	87.56	21.82
2	+1	42.26	80.27	21.62
3	+2	42.02	80.03	20.49
4	+4	40.06	76.99	19.21
5	+6	33.35	70.79	14.68
6	+8	31.38	70.31	13.42
7	-1	37.72	80.51	16.69
8	-2	31.98	70.66	17.69
9	-4	27.05	65.43	14.77
10	-6	24.52	65.40	13.17
11	-8	25.70	62.54	12.73

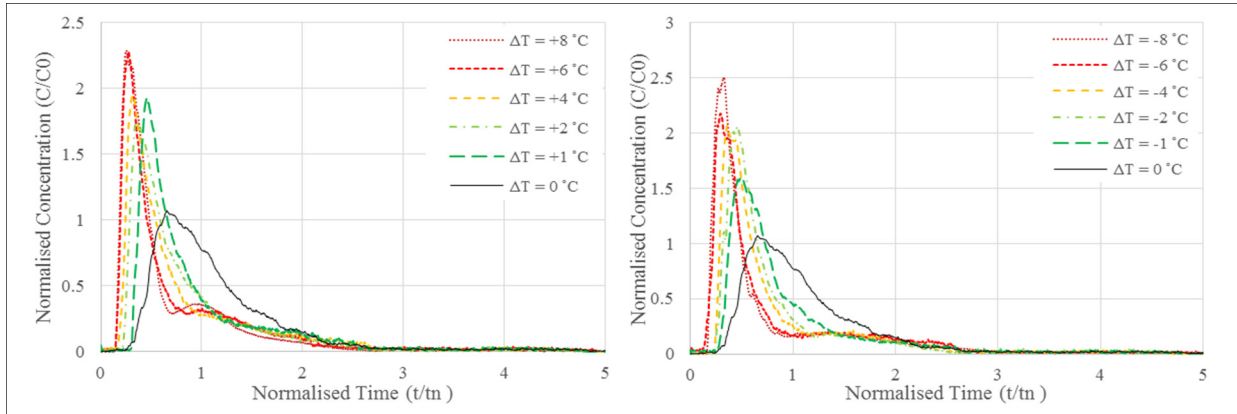


Figure 2. RTD curves with constant inlet temperature and different colder and hotter initial pond temperatures (1l/s).

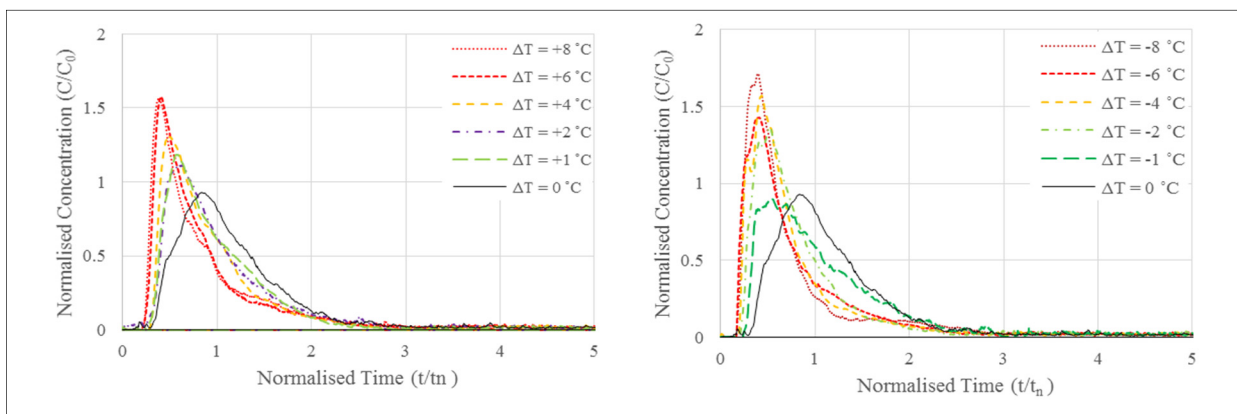


Figure 3. RTD curves with constant inlet temperature and different colder and hotter initial pond temperatures (2l/s).

The relationships between the RTD curves and temperature differences are shown graphically in Figures 4-5. As shown in these figures, there is a clear trend of all index values decreasing with the increase of the temperature difference emphasising the importance of temperature effects on the hydraulic behaviour of retention ponds. It is apparent from these figures that even a one-degree temperature difference can significantly reduce the hydraulic efficiency and can cause severe short-circuiting. This finding is consistent with that of Goula et al. (2008) study, who concluded that “only 1°C between influent and tank content is enough to induce a density current”. The temperature difference also decreases the Morrill index, which is indicative of decreased mixing levels in the pond for both hot and cold influent. It is also clear that the slope of these trends decreases with increasing temperature difference for both 1l/s and 2l/s. For the flowrate of 1l/s, the hydraulic indices rapidly decrease for 1°C - 2°C. Temperature difference between the influent and the pond, while decreasing is lower from 2°C - 8°C. For the flowrate of 2l/s, the same trend was observed in the hot influent case while the initial rapid decreasing trend for the hydraulic indices was detected only up to 1°C temperature difference between the influent and the pond for cold influent.

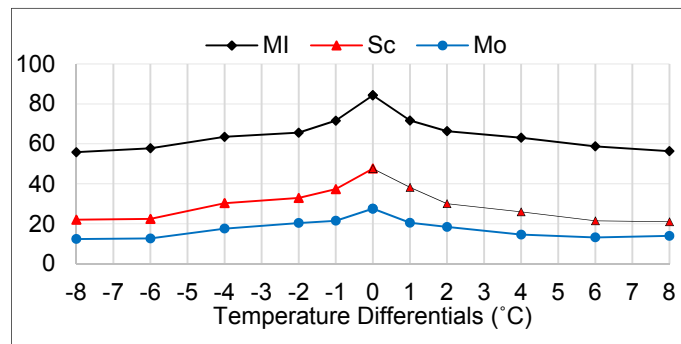


Figure 4. Relationships between the hydraulic index values and temperature differences (1l/s).

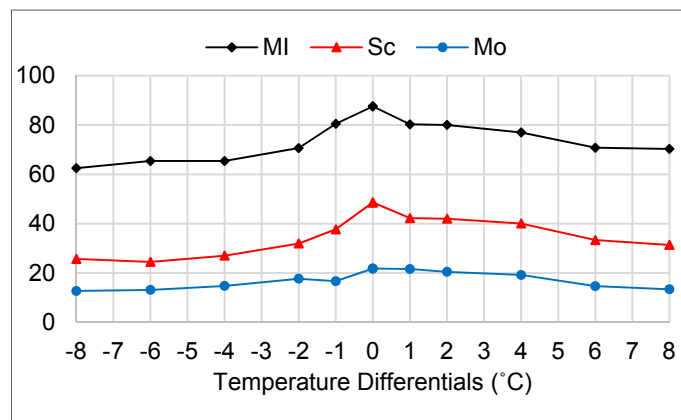


Figure 5. Relationships between the hydraulic index values and temperature differences (2l/s).

4 CONCLUSIONS

The following conclusions are drawn from this study:

- 1 This study is aimed at showing that the geometric features of SRPs, such as inlet and outlet configurations, pond layouts and baffles are not the only parameters that need to be considered in the design of sediment retention ponds. The most obvious finding to emerge from this study is that the temperature variations in a pond can significantly change the hydraulic performance of the pond. Even with one degree of Celsius temperature difference between the pond water and inlet, the hydraulic efficiency, short-circuiting, and mixing indices are reduced significantly;
- 2 It is shown that the decrease of hydraulic efficiency in the pond could be attributed to the temperature induced flow pattern, which has a significant role in creating short-circuiting. The study has found that for colder influent, the inflow tended to sink to the bottom of the pond and move rapidly towards the outlet, while in the case of hotter influent the inflow tended to move to the top of the pond.

The results presented show sensitivity of the hydraulic performance of ponds and wetlands to temperature variations, and highlight the need for physical modeling and investigations.

REFERENCES

- Auckland Regional Council (ARC). (2003). *TP10 Design Guideline Manual Stormwater Treatment Devices*. Auckland, New Zealand.
- Bodin, H., Mietto, A., Ehde, P.M., Persson, J. & Weisner, S.E.B. (2012). Tracer Behaviour and Analysis of Hydraulics in Experimental Free Water Surface Wetlands. *Ecological Engineering*, 49, 201-211, <http://dx.doi.org/10.1016/j.ecoleng.2012.07.009>.
- De Oliveira, R., Pearson, H.W., Silva, J.V., Sousa, J.T., Leite, V.D. & Lopes, W.S. (2011). Baffled Primary Facultative Ponds with Inlets and Outlets Set at Different Levels Treating Domestic Wastewater in Northeast Brazil. *Water Sci. Technol.*, 63(6), 1183-1187, 10.2166/wst.2011.105.
- Farjood, A., Melville, B.W. & Shamseldin, A.Y. (2014). A Study in Hydraulic Performance Indices for Sediment Retention Ponds. *River Flow*, 251-257.
- Farjood, A., Melville, B.W. & Shamseldin, A.Y. (2015). The Effect of Different Baffles on Hydraulic Performance of a Sediment Retention Pond. *Ecological Engineering*, 81, 228-232, <http://dx.doi.org/10.1016/j.ecoleng.2015.04.063>.
- Goula, A.M., Kostoglou, M., Karapantsios, T.D. & Zouboulis, A.I. (2008). The Effect of Influent Temperature Variations in a Sedimentation Tank for Potable Water Treatment—A Computational Fluid Dynamics Study. *Water Research*, 42(13), 3405-3414, <http://dx.doi.org/10.1016/j.watres.2008.05.002>.
- Grismer, M.E., Tausendschoen, M. & Shepherd, H.L. (2001). Hydraulic Characteristics of a Subsurface Flow Constructed Wetland for Winery Effluent Treatment. *Water Environment Research*, 73(4), 466-477.
- Gu, R. & Chung, S.W. (1998). Reservoir Flow Sensitivity to Inflow and Ambient Parameters. *Journal of Water Resources Planning and Management*, 124(3), 119-128.
- Kadlec, R.H. (1994). Detention and Mixing in Free Water Wetlands. *Ecological Engineering*, 3(4), 345-380, [http://dx.doi.org/10.1016/0925-8574\(94\)00007-7](http://dx.doi.org/10.1016/0925-8574(94)00007-7).
- Khan, S. (2012). Hydrodynamics of Sediment Retention Ponds, *PhD Thesis*. The University of Auckland, New Zealand.
- Khan, S., Melville, B. & Shamseldin, A. (2013). Design of Storm-Water Retention Ponds with Floating Treatment Wetlands. *Journal of Environmental Engineering*, 139(11), 1343-1349, 10.1061/(ASCE)EE.1943-7870.0000748.
- Khan, S., Melville, B.W. & Shamseldin, A.Y. (2011). Retrofitting a Stormwater Retention Pond Using a Deflector Island. *Water Science and Technology*, 63(12), 2867-2872, 10.2166/wst.2011.569.
- Macdonald, R.J. & Ernst, A. (1986). Disinfection Efficiency and Problems Associated with Maturation Ponds. *Water Science & Technology*, 19(3-4), 557-567.
- Nix, S.J. (1985). Residence Time in Stormwater Detention Basins. *Journal of Environmental Engineering*, 111(1), 95-100.
- Pearson, H., Mara, D.D. & Arridge, H. (1995). The Influence of Pond Geometry and Configuration on Facultative and Maturation Waste Stabilisation Pond Performance and Efficiency. *Water Science and Technology*, 31(12), 129-139.
- Pedahzur, R., Nasser, A.M., Dor, I., Fattal, B. & Shuval, H. (1993). The Effect of Baffle Installation on the Performance of a Single-Cell Stabilization Pond. *Water Science & Technology*, 27(7-8), 45-52.
- Persson, J. (2000). The Hydraulic Performance of Ponds of Various Layouts. *Urban Water*, 2(3), 243-250, [http://dx.doi.org/10.1016/S1462-0758\(00\)00059-5](http://dx.doi.org/10.1016/S1462-0758(00)00059-5).
- Shilton, A. (2005). *Pond Treatment Technology*. IWA publishing.
- Su, T.M., Yang, S.C., Shih, S.S. & Lee, H.Y. (2009). Optimal Design for Hydraulic Efficiency Performance of Free-Water-Surface Constructed Wetlands. *Ecological Engineering*, 35(8), 1200-1207.
- Thackston, E.L., Shields Jr, F.D. & Schroeder, P.R. (1987). Residence Time Distributions of Shallow Basins. *Journal of Environmental Engineering*, 113(6), 1319-1332.
- Van de Vusse, J. (1959). Residence Times and Distribution of Residence Times in Dispersed Flow Systems. *Chemical Engineering Science*, 10(4), 229-233.
- von Sperling, M. (2002). Relationship between First-Order Decay Coefficients in Ponds, for Plug Flow, CSTR and Dispersed Flow Regimes. *Water Science & Technology*, 45(1), 17-24.
- Vymazal, J. (2014). Constructed Wetlands for Treatment of Industrial Wastewaters: A Review. *Ecological Engineering*, 73, 724-751, <http://dx.doi.org/10.1016/j.ecoleng.2014.09.034>.
- Wahl, M.D., Brown, L.C., Soboyejo, A.O., Martin, J. & Dong, B. (2010). Quantifying the Hydraulic Performance of Treatment Wetlands Using the Moment Index. *Ecological Engineering*, 36(12), 1691-1699, <http://dx.doi.org/10.1016/j.ecoleng.2010.07.014>.
- Watters, G.Z. (1972a). *The Hydraulics of Waste Stabilization Ponds*.
- Watters, G.Z. (1972b). *The Hydraulics of Waste Stabilization Ponds*, Reports. Paper 18, Utah Water Research Laboratory, College of Engineering, Utah State University.
- Werner, T.M. & Kadlec, R.H. (1996). Application of Residence Time Distributions to Stormwater Treatment Systems. *Ecological Engineering*, 7(3), 213-234.
- Wilson, J.F., Cobb, E.D. & Kilpatrick, F.A. (1968). *Fluorometric Procedures for Dye Tracing*. US Government Printing Office.

PERCENTILE ANALYSIS OF RAINFALL DEPTH ESTIMATION ON PERFORMANCE OF CONSTRUCTED WETLAND

MAZLINA ALANG OTHMAN⁽¹⁾, AMINUDDIN AB. GHANI⁽²⁾, KENG YUEN FOO⁽²⁾ & CHUN KIAT CHANG⁽⁴⁾

^(1,2,3,4) River Engineering and Urban Drainage Research Centre (REDAC),
Universiti Sains Malaysia, Engineering Campus, Nibong Tebal, Penang, Malaysia
emona1510@gmail.my; redac02@usm.my; K.y.foo@usm.my; redac10@usm.my
⁽¹⁾ Polytechnic Kuching Sarawak, Sarawak, Malaysia

ABSTRACT

Water quality volume (WQV) is a storage that captures pollutant generated from stormwater. Maximized WQV should be greater or equal to 75 to 90 percentile runoff volume and these design volume are required to achieve specific reduction of pollutant. Percentile approach is used in WQV estimation because it determines the rainfall depth in term of water quality depth (WQD) for a specified percentage. Therefore, an investigation is conducted in the constructed wetland to investigate the relationship between WQD and constructed wetland performance. From the percentile analysis, WQD at 75th percentile is 24 mm. This is followed by 29 mm, 33mm, 42 mm and 54 mm for 80th, 85th, 90th and 95th percentile respectively. As stormwater went through the constructed wetland, Total Suspended Solid (TSS), Total Nitrogen (TN) and Total Phosphorus (TP) are reduced by 53%, 28% and 10% on average respectively. However, the design goal of 80% (TSS), 50% (TN) and 40% (TP) reduction are not accomplished because of low concentration of inflow that went through the wetland. The effect of rainfall depth on the performance of constructed wetland differs in every parameters. TSS recorded the highest performance in 86% with rainfall depth of 30 mm (between 80th to 85th percentile). TN and TP recorded higher performance as rainfall depth is more than 50 mm and ranged from 6 months and 50 year average recurrence interval (ARI). Therefore, it is recommended that WQD in the study area to be in the range of 29 to 33 mm (80th to 85th percentile). To determine the applicability of this range, a case study should be carried out in differing sizes, geographic locations, site conditions and types of BMPs facilities.

Keywords: Water quality volume; water quality depth; percentile analysis; stormwater constructed wetland.

1 INTRODUCTION

BMPs (best management practices) is a structure used to control non-point sources pollution caused by variety of human activities. One of the functions is to improve water quality by capturing and retaining sediments and other pollutants that are present in the stormwater runoff. When a BMPs facilities captures a portion of runoff volume and infiltrates it into the soil, the pollutants in that portion are prevented from entering a reserving water body. Hence, captured runoff volume, plays a significant role in the pollutant load reduction. It represents the volume that is fully infiltrated and captures the majority of the pollutants generated from the site. Furthermore, this volume requires to achieve a specific pollutant reduction. The capture runoff volume approach also copes with the difficulties in the design of BMPs facilities in term of variation in flow rate and pollutant concentration (Niu et al., 2016). The term 'water quality volume' or WQV refers to captured runoff volume to be treated and water quality depth (WQD) is a unit WQV per catchment area. The recommended WQV largely originated from temperate climates countries including Australia and United State.

Maximized WQV should be greater or equal to 75 to 90 percentile of runoff volume (Collins et al., 2010). Percentile approach is used in WQV estimation because it determines the rainfall depth in term of WQD for a specified percentage. The value of WQD plays important roles because captured runoff volume is related to it. This value also varies depending on local rainfall data. In the case of percent capture option among other country and city, Georgia (2001) has suggested using an 85% runoff volume from the annual event to treat Total Suspended Solid (TSS) loadings by 80%. However, UDFCD (2010) has used an 80th percentile runoff volume to remove between 80 and 90% of the annual TSS. Singapore required to treat 90% rainfall event together with 80% removal of TSS, 45 % removal of TN and 45% removal of TP (PUB, 2011). In Malaysia, the BMPs facilities are recommended to use 40 mm of WQD with the design goal of 80% removal of TSS, 50% removal for TN and 40% removal for TP (MSMA, 2011). Furthermore, this value is applied to all areas in Peninsular Malaysia.

A varying rainfall event is one of the factors that influence BMPs performance. In tropical climate country, WQD in the range of 10 to 30 mm is needed in order to meet removal targets of the bioretention basin (Wang et al., 2017). In case of constructed wetland performance, it has been demonstrated that small rainfall event treated better in the beginning of a runoff event while the pollutant reduction of large rainfall event is lower at the beginning and gradually increase towards the end (Mengangka et al., 2015). There has been a lack of field study in the relationship between removal of pollutant and rainfall characteristic of the tropic country (Wang et

al., 2017). Moreover, the relation between WQD and BMPs facilities treatment performance has not been identified yet in Malaysia. Realizing these necessities, a study was conducted in the constructed wetland to investigate the relationship between WQD and constructed wetland performance.

2 METHODOLOGY

2.1 Site description

The studied free water surface constructed wetland was completely constructed in Jun 2014 in Universiti Sains Malaysia (USM) Engineering Campus at Seberang Perai Selatan District, Pulau Pinang. The wetland area was included with a forebay zone, macrophyte zone (high marsh, low marsh and deep marsh) followed by micropoll zone (Figure 1). The high marsh area was mainly covered with *Donax grandis* and *Eleocharis variegata*, the low marsh area dominated by *Phragmites karka* and the deep marsh area was surrounded by *Typha angustifolia*. The wetland system was designed to treat stormwater from 0.0712 km² catchment area which consist of faculty buildings and car park area.

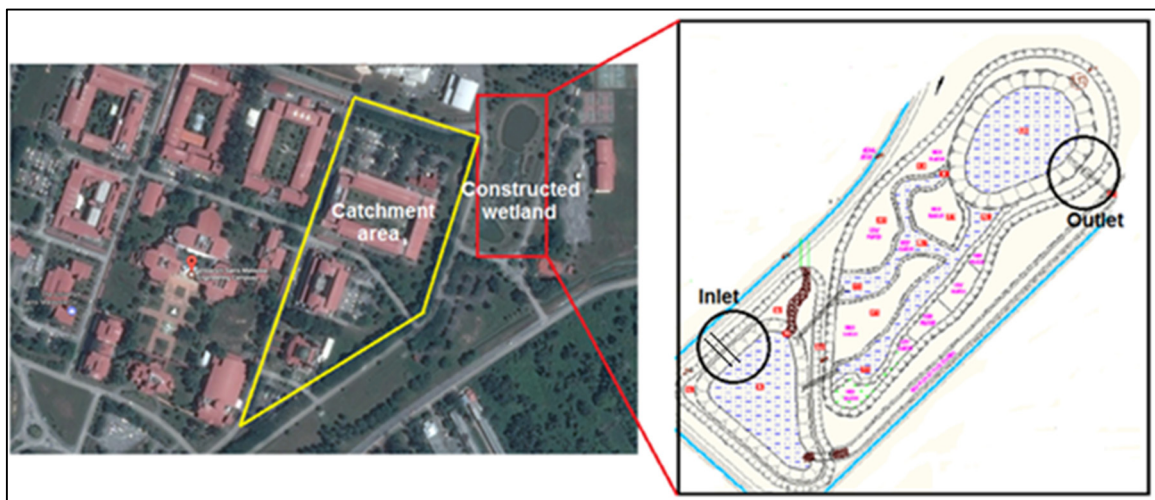


Figure 1. Location of study area and sampling location

2.2 Percentile analysis

In this paper, the capture target for runoff volume was based on percentile analysis suggested from USEPA (2009). Percentile analysis concepts determines a WQD for a specified percentage. Historical rainfall data from Sg. Simpang Ampat rainfall station was obtained from Water Resources Management and Hydrology Division, Drainage and Irrigation Department (DID), Malaysia. The station was chosen because it is the nearest rainfall station from the study area which had rainfall record for more than 20 years. This study used six (6) hour separation time as minimum inter event time (MIT) and 2.5 mm initial runoff as suggested by Guo and Urbonas (2002). Firstly, a visual basic command in Excel Macro mode was developed to separate continuous rainfall record into a single rainfall event. After that, rainfall depths from the rainfall record were then sorted in ascending order and the nth percentile was determined. The percentage capture target was chosen from 75th, 80th, 85th, 90th and 95th percentile of rainfall event (Collins et al., 2010).

2.3 Sampling analysis

A total nine (9) rainfall event that were monitored from 2014 to 2015 are presented in Table 1. Rainfall data were collected using a rain gauge located in the constructed wetland. Average recurrence interval (ARI) from rainfall event was obtained from Intensity-Duration-Frequency (IDF) curve for Sg. Simpang Ampat rainfall station (Figure. 2). Sampling was conducted at the inlet and outlet of the wetland (Figure 1). The sample was collected 24 hours after a rainfall event (Niu et al., 2015) and TSS, TN and TP of the water samples were analyzed following HACH, Water Analysis Handbook 5th edition. The removal efficiencies of the different pollutants were estimated based on differences between pollutant concentration in inflow and outflow and were calculated using the following equations:

$$Removal(\%) = \frac{Inflow - Outflow}{Inflow} \times 100 \quad [1]$$

Table 1 listed comparisons between pollutant concentration in the inflow and outflow in every parameter. Statistical differences between inflow and outflow of pollutants were examined using paired sample t-test in Minitab 2016.

Table 1. Inflow and outflow pollutant

Event date	Rainfall parameter			TSS		TN		TP	
	Depth (mm)	Duration (min)	ARI	In (mg/L)	Out (mg/L)	In (mg/L)	Out (mg/L)	In (mg/L)	Out (mg/L)
24.08.2014	50.0	85	12 months	25	6	3.6	3.5	0.53	0.31
19.09.2014	64.4	115	12 months	22	9	1.4	1.9	0.52	0.37
23.09.2014	113.4	480	2 years	14	8	3.4	1.6	0.31	0.27
20.10.2014	84.1	125	50 years	21	10	1.1	0.1	0.44	0.36
12.11.2014	30.4	130	1 month	14	2	3.6	3.1	0.40	0.37
08.12.2014	161.5	225	20 years	31	9	1.7	4.9	0.36	0.35
28.10.2015	31.7	50	6 months	14	11	6.5	4.3	0.23	0.48
07.12.2015	26.9	45	3 months	17	11	1.8	1.4	0.29	0.30
17.12.2015	49.2	115	2 years	11	9	2.5	1.4	0.34	0.44

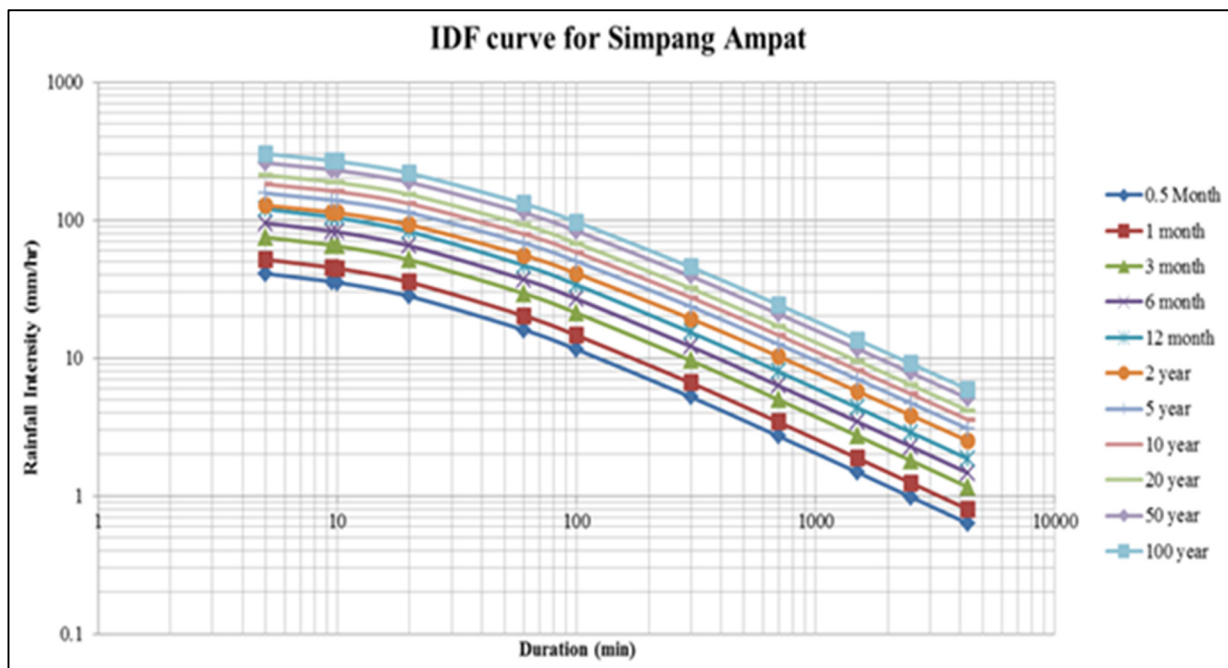


Figure 2. IDF Curve for Sg. Simpang Ampat Tangki rainfall station (Beh, 2014)

3 RESULTS AND DISCUSSIONS

3.1 WQD from percentile analysis

Using historical data from the year 1988 to 2014, total 4 466 individual rainfall event was founded with 6 hours MIT and 2.5 mm initial runoff. From the rainfall event distribution (Figure 3 (a)), 39% (1 739) of rainfall event consist rainfall depth below than 2.5 mm and were excluded from the data set. From USEPA (2009), this value generally does not produce runoff due to rainfall losses. The remaining 60% were rainfall depth in the range of 2.6 mm to 100 mm and only 1% were more than 100 mm. It shows that WQV must be designed for more that 60% of rainfall event from the study area. From the percentile analysis (Figure 3 (b)), WQD at the 75th percentile is 24 mm followed by 29 mm, 33mm, 42 mm and 54 mm for 80th, 85th, 90th and 95th percentile respectively. These results indicated that WQD in percentile analysis gives a different value compared to the one recommended by MSMA (40 mm). It is suggested to use percentile approach in WQD estimation because it represents the volume that fully is infiltrated and thus gives an exact amount that need to be retained in order to meet the removal target. WQD also should be analyzed based on the local historical rainfall data. This is because every rainfall station has different rainfall pattern due to the effect of topography and geographical area as well as the influence of the monsoons over the Peninsula (Suhaila et al., 2011). To ensure the WQD value is appropriate for all areas, the percentile analysis should be carried out for all rainfall stations in Peninsular Malaysia.

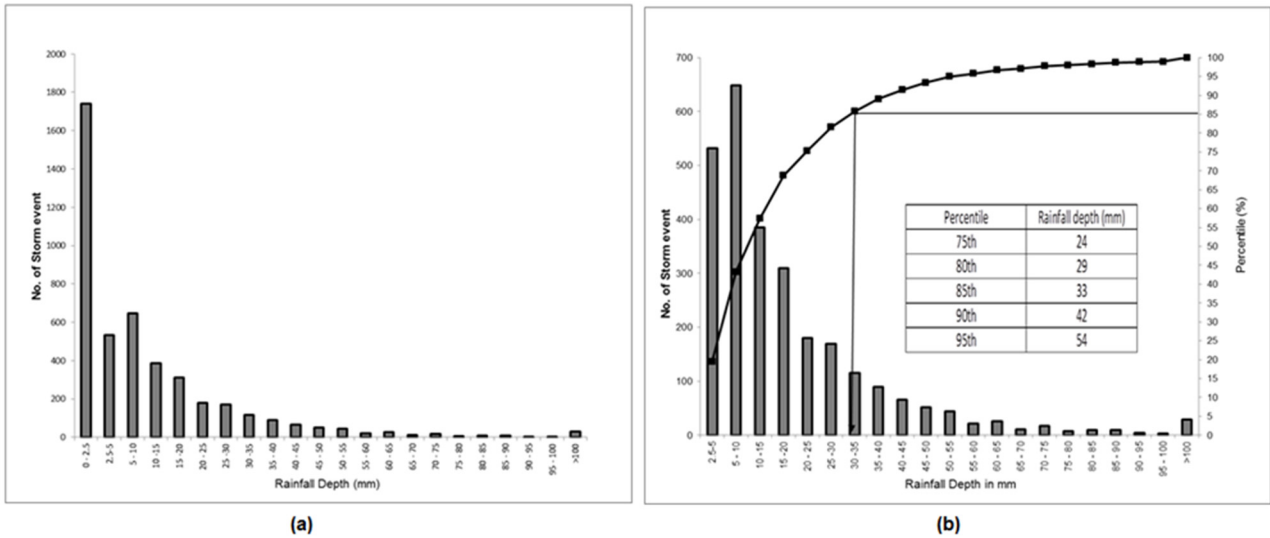


Figure 3. (a) Rainfall distribution (b) Percentile analysis

3.2 Performance of the wetland

Comparisons between pollutant concentrations in the inflow and outflow are shown in Figure 4. A paired Student's t test was performed to test differences between inflow and outflow pollution concentrations. The results showed that TSS was significantly lower than inflow concentrations (0.01; $p < 0.05$). However TN and TP are not significant with a value of 0.46 and 0.66. These results indicated that the wetland was effective at removing solid particles. The measured pollution removal performance of the constructed wetland was calculated by an average of 53% for TSS, 28% for TN and 10% for TP (Figure 5). It was not accomplished for the design goal of 80% (TSS), 50% (TN) and 40% (TP) as required in MSMA (2011). Small catchment area and limited source of pollutant causes studied wetland to received low concentration of pollutant and leading to low performance of wetland. As mentioned by Tony (1999), concentration levels and input concentration are factors that influence the performance of a wetland. Therefore, studied area should be carried out at bigger size of catchment area with high concentration of pollutant.

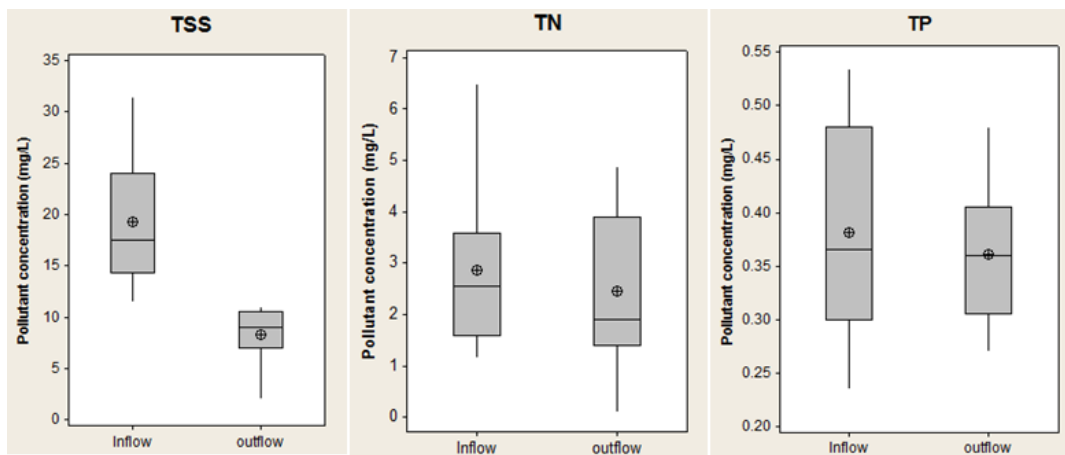


Figure 4. Boxplot of inflow and outflow pollutant

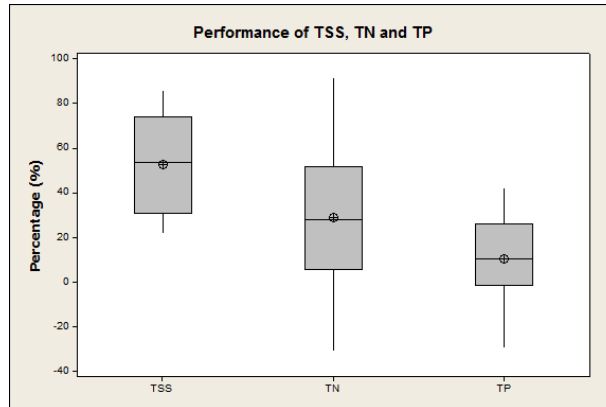


Figure 5. Performance of TSS, TN and TP

3.3 Effect of the rainfall depth on the wetland performance

Rainfall depth is an important parameter for the design capture volume in terms of WQV. Therefore, it was necessary to investigate its effects on wetland performance. It was observed that the effect of rainfall depth on the inflow and outflow pollution was different in every parameter (Figure 6). Heavy rain results in higher inflow and outflow concentration of TSS (Figure 6 (a) and (b)). High inflow occurred where the rainfall depth was at 113 mm (more than 95 percentile) and considered as an extreme event with 20 year ARI. The effect of rainfall depth on the inflow of TN was different (Figure 6 (d)). As the rainfall depth increase, the inflow of TN was decreased. The higher inflow occurred at rainfall depth of 31.74 mm (between 80 to 85 percentile). The inflow pollutant of TP was initially increased, after which it decreases with an additional increase of rainfall depth (Figure 6 (g)). The higher inflow occurred at rainfall depth of 50 mm (between 90th to 95th percentiles). These results suggested that heavy rain may result in higher pollutant. However, too heavy rain likely leads to low pollutant concentration and these results was comparable to the one obtained by Niu et al., (2016). Higher pollutant likely occurs at rainfall depth with more than 80th percentile. Hence, the selection of a proper percentile for the design volume of the BMPs facilities is very important.

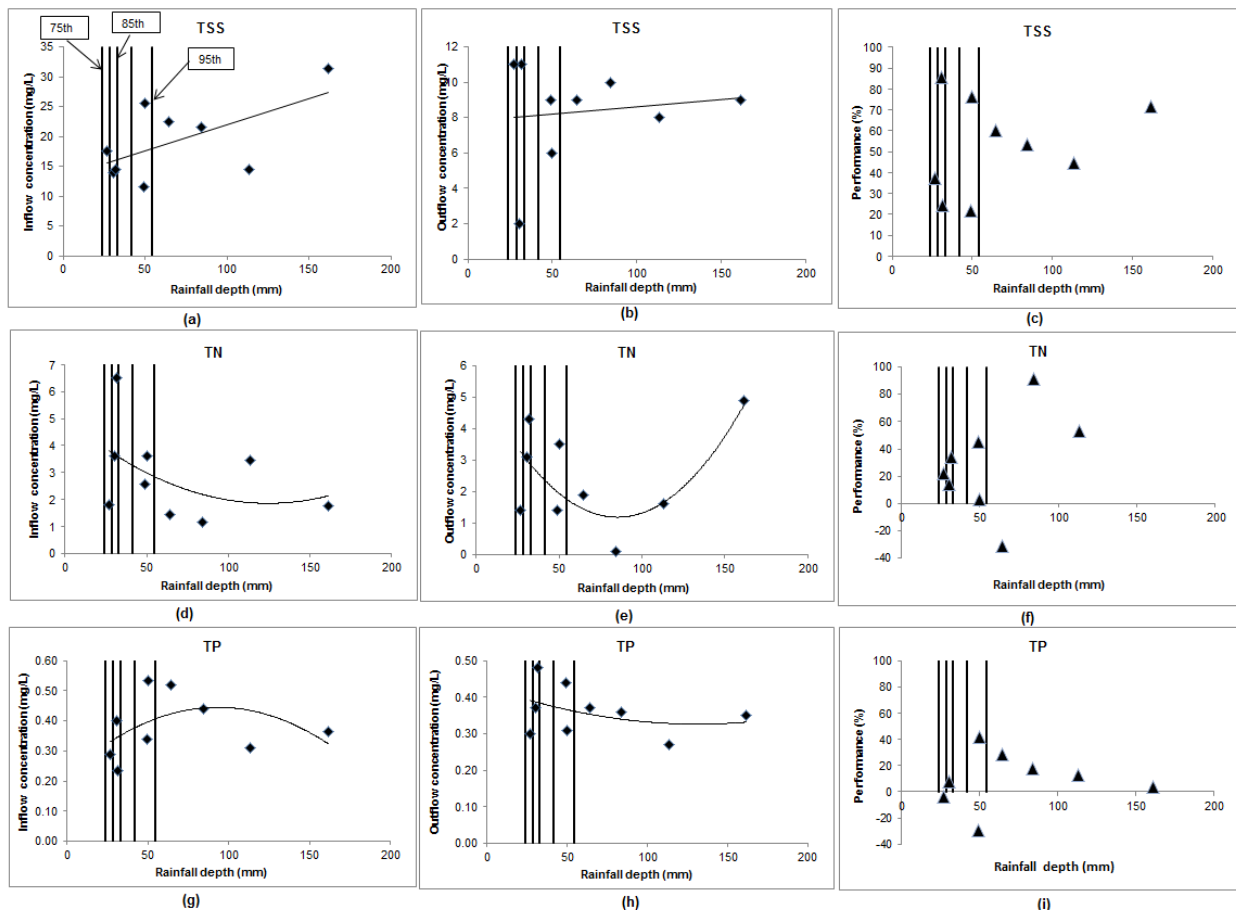


Figure 6. Relationship between rainfall depth and inflow, outflow and wetland performance.

The effect of rainfall depth on the performance of constructed wetland was also different in every parameter. TSS was recorded as the higher performance at 86% with rainfall depth of 30 mm (between 80th to 85th percentile) at 1 month ARI rainfall event. As for other parameters, TN recorded 91% with rainfall depth at 84 mm (more than 95th percentile) and TP recorded 42% with rainfall depth at 50 mm (between 90th to 95th percentile). TN and TP recorded higher performance as rainfall depth was more than 50 mm and ranged from 6 months to 50 year ARI. It was contrary to 3 month ARI suggested in MSMA (2000). Therefore, it was more reasonable to design the captured volume of the wetland according to TSS performance with WQD range of 29 to 33 mm (80th to 85th percentile). This range was slightly higher to the one obtained by Wang et al., 2017. However, the conclusion was obtained only based on nine rainfall event with small catchment area. To determine the applicability of this range, a case study should be carried out in differing sizes, geographic locations, site conditions and types of BMPs facilities. Hydrologic analysis and water quality modelling also need to be done in order to meet the percentage removal target.

4 CONCLUSIONS

The primary conclusions of this study are as follows:

- i. From the percentile analysis, WQD at the 75th percentile is 24 mm followed by 29 mm, 33mm, 42 mm and 54 mm for 80th, 85th, 90th and 95th percentile respectively. This study recommended that percentile analysis approach should be carried out for all rainfall stations in Peninsular Malaysia. It is because it represents the volume that fully is infiltrated and thus gives an exact amount that need to be retained in order to meet the removal target;
- ii. Pollutant removal performances are 53% for TSS, 28% for TN and 10% for TP and it is not accomplished with the design goal required in MSMA (2010). Small catchment area and limited sources of pollutant causes studied wetland to receive low concentration of pollutant and this leads to low performance of wetland. However, statistical analysis confirmed that constructed wetland provides effective treatment for TSS concentration;
- iii. Based on nine rainfall event, this study recommended a WQD in the range of 29 to 33 mm (80th to 85th percentile). To determine the applicability of this range, a case study should be carried out in differing sizes and geographic locations, site conditions and different types of BMPs facilities.

ACKNOWLEDGEMENTS

The author would like to acknowledge the financial assistance from the Ministry of Higher Education Malaysia under the Long Term Research Grant (LRGS) No. 203/PKT/672004 entitled Urban Water Cycle Processes, Management and Societal Interactions: Crossing from Crisis to Sustainability. Special thanks also to Water Resources Management and Hydrology Division, Department of Irrigation and Drainage, Malaysia for providing the historical rainfall data for this study.

REFERENCES

- Atlanta Regional Commission (ARC) (2001). *Georgia Stormwater Management Manual, Volume 2*. Technical Handbook. Atlanta Regional Commission. Atlanta, GA.
- Beh, C.H. (2014). Water Quantity and Quality Assessments of Stormwater Purification in BIOECODS. *Masters Thesis*. Universiti Sains Malaysia, Malaysia.
- Collins, K. A., Lawrence, T. J., Stander, E. K., Jontos, R. J., Kaushal, S. S., Newcomer, T. A., Grimm & Ekberg, M. L. C. (2010). Opportunities and Challenges for Managing Nitrogen in Urban Stormwater: A Review and Synthesis. *Ecological Engineering*, 36(11), 1507-1519.
- Department of Irrigation and Drainage or DID, (2000). *Urban Stormwater Management Manual for Malaysia (MSMA)*. DID, Kuala Lumpur.
- Department of Irrigation and Drainage or DID, (2011). *Second Edition of Urban Stormwater Management Manual for Malaysia (MSMA 2nd Edition)*. DID, Kuala Lumpur.
- Guo, J.C.Y. & Urbonas, B. (2002). Runoff Capture and Delivery Curves for Storm-Water Quality Control Designs. *J. Water Resour. Plann Manage.*, 128(3), 208-215.
- Mangangka, I.R., Liu, A., Egodawatta, P. & Goonetilleke, A. (2015). Sectional Analysis of Stormwater Treatment Performance of a Constructed Wetland. *Ecological Engineering*, 77, 172-179.
- Niu, S., Park, K. & Kim, Y. (2015). Effect of Sampling Duration On The Performance Evaluation Of A Stormwater Wetland. *Water Science and Technology*, 71(3), 373-381.
- Niu, S., Park, K., Cheng, J. & Kim, Y. (2016). An Investigation Into The Relationship Between Water Quality Volume (Design Storage Volume) and Stormwater Wetland Performance. *Water Science and Technology*, 73(6), 1483-1491.
- Public Utilities Board (PUB), (2011). *ABC water design guidelines – second edition*. Singapore.
- Suhaila, J., Jemain, A.A., Hamdan, M.F. & Zin, W.Z.W. (2011). Comparing Rainfall Patterns Between Regions in Peninsular Malaysia via a Functional Data Analysis Technique. *Journal of hydrology*, 411(3), 197-206.

- Technical Guidance on Implementing the Stormwater Runoff Requirements for Federal Projects Under Section 438 of the Energy Independence and Security Act, (2009). United States Environmental Protection Agency, Washington, DC 20460. Available from <https://www.epa.gov/sites/production/files/2015-09/documents/eisa-438.pdf> [15 Desember 2016]
- Tony, H.F.W., CRC Cooperative Research Centre for Catchment Hydrology & Wong, T.H.F. (1999). Managing Urban Stormwater Using Constructed Wetlands. *Cooperative Research Centre for Catchment Hydrology*.
- Urban Drainage Flood Control District (UDFDC), (2010). *Urban Storm Drainage Criteria Manual – Volume 3*. Denver, CO.
- Urban Storm Drainage Criteria Manual - Volume 3 Best Management Practices, (2010). *Urban Drainage and Flood Control District*, Denver, Colorado.
- Wang, J., Chua, L.H. & Shanahan, P. (2017). Evaluation of Pollutant Removal Efficiency of a Bioretention Basin and Implications for Stormwater Management in Tropical Cities. *Environmental Science: Water Research & Technology*, 3(1), 78-91.

EFFECT OF DESIGN CRITERIA FOR THE PERFORMANCE ON CONSTRUCTED WETLANDS

NUR ASMALIZA MOHD NOOR⁽¹⁾, LARIYAH MOHD SIDEK⁽²⁾, SIMON BEECHAM⁽³⁾ & AMINUDDIN AB GHANI⁽⁴⁾

⁽¹⁾ Faculty of Civil Engineering, Universiti Teknologi MARA, Pahang,
asmalizamn@gmail.com

⁽²⁾ Centre for Sustainable Technology and Environment, Universiti Tenaga Nasional,

⁽³⁾ School of Natural and Built Environments, University of South Australia,

⁽⁴⁾ River Engineering and Urban Drainage Research Centre (REDAC), Universiti Sains Malaysia, Engineering Campus

ABSTRACT

The progressive development in urban area has drastically changed land use and deteriorated the quality of source water. The contribution towards higher intensity of rainfall will also increase the problem and affects the quality of water, social and financial situations of the country. The installation of BMPs has been the alternative approach in reducing the effects from rapid urban development. Constructed wetland has been selected under BMPs with the target to enhance the quality of water. It is widely used in developed countries with tropical climate for improving the quality of stormwater. However, constructed wetland is being considered as a new innovation, which is not implemented throughout Malaysia. The main objective of this paper is to evaluate the effect of design criteria on the performance of constructed wetland. Three locations of constructed wetland in Malaysia were selected, which are situated at Putrajaya, Universiti Sains Malaysia Engineering Campus and Humid Tropic Center. The selection of design criteria is based on the length to width ratio, detention time and average water depth. The results indicated that the Biochemical Oxygen Demand, Chemical Oxygen Demand and Total Phosphorus removal were affected with pollutant removal of 48%, 37% and 64%, respectively. However, Total Nitrogen and Total Suspended Solids analysis showed percentage of removal to be around 74% and 71%, respectively. The findings can be significantly used to enhance knowledge in constructing wetland under tropical climate where it can serve effectively for managing urban runoff using control at source approach.

Keywords: Best Management Practices (BMPs); constructed wetlands; design criteria; water quality; pollutant removal.

1 INTRODUCTION

The urbanization process has changed the land use pattern and the urban structure. Urban development adds impervious surfaces, increases runoff, decreases infiltration, ground water recharge and has negative effects on the local water quality and quantity balance. A large portion of former forest and agricultural areas have been cleared and replaced by concrete buildings, roads and drainage systems which are impermeable. The rivers flowing along the urban area are choked up with sediment from mining, housing and other development areas. The problem of silting in rivers and drains together with high rainfall intensity causes flash floods. Flash floods not only cause problems to commuters who are usually caught in traffic jams but at times, the residents of some settlements have also been evacuated to relief centres (Yong and Mohd Noh, 2004). Flash flood incidences in urban areas become more severe year by year. Some 29, 720 km² or 9% of the Malaysia land is flood prone and about 4.915 million people or 21% of the population reside in these areas (Abdullah, 2007). The average annual damage and economic losses due to flood are estimated at RM 915 million with another RM 1.83 billion estimate consequential to economic drag effect losses (Abdullah, 2007). In addition, the phenomenon of these flash floods has become more common as the surface runoff from developed urban and industrial areas has fully increased the peak discharges entering the rivers with shortened time of detention to peak flow (Abdullah, 2007).

Conventional land development practices required rapid removal of the runoff, causing a loss of water for ground water recharge (Carmon and Shamir, 1997). In order to overcome flash flood problems, Department of Irrigation and Drainage (DID) has taken a step ahead by introducing the Stormwater Management Manual for Malaysia (MSMA). MSMA is a guideline published by the Department of Irrigation and Drainage Malaysia (DID) in 2000 and was revised with the MSMA 2nd Edition in 2012 to align with long term nationwide directions and needs in ensuring that sustainable urban drainage systems are fully utilized.

Constructed wetlands can be used for water quality improvement and it is widely used for stormwater improvement and domestic wastewater. Constructed wetlands are man-made wetlands developed and managed to treat contaminants in stormwater and wastewater. Successful application of constructed wetlands for wastewater has led to the exploration of the treatment for different sources such as stormwater, industrial,

agricultural, urban, airport runoff and acid mine drainage (Kadlec and Knight, 1996; Scholz et al., 2007; Vymazal, 2009; Mohd Noor et al., 2013). The constructed wetlands have been evolved recently to the hybrid system with the application to treat various industrial wastewater (Jing et al., 2001; Oovel et al., 2007; Camino et al., 2011; Serrano et al., 2011; Kato et al., 2010).

1.1 Design criteria

Design criteria, vegetation and organic loading are the ultimate factors which affect the performance of constructed wetlands as water quality improvement. Design criteria can be evaluated as length to width ratios, wide uniform depths and wide wetlands with transverse baffles that contribute to making the wetlands more efficient (Persson et al., 1999). Therefore, a perfect combination of these factors will contribute to the better performance of constructed wetlands.

Persson and Wittgren (2003) suggested that there are eight aspects that will influence all the wetlands such as topography, shape of wetlands (e.g; circular, rectangular or curved shape), depth of wetlands, length to width ratio, flat or angled bottom, baffles, inlet and outlet structure and vegetation. Department of Planning and Local Government (2009) stated that the considered designs are hydrology, water quality, maintenance, safety and landscape and vegetation. Removal efficiency was found to be dependent upon such factors as soil type, wetlands surface area, flow depth, Hydraulic Residence Time (HRT) and plant species. Persson et al. (1999) concluded that large length to the width ratios, wide uniform depth and wide wetlands with traverse baffles are the key characteristics that make efficient wetlands.

1.1.1 Length to the width ratio

Flow distribution and hydraulic short circuiting are affected by length to width ratio where a high length to width ratio is suggested by the necessity to minimize short circuiting and maximize water contact (Giuseppe et al., 2000). Free Water Surface (FWS) treatment wetlands with high length to width ratio are the greatest concern with respect to head loss. The minimum length to width ratio (2:1) is recommended for an economical point of view and the maximum length to the width ration is 10:1. However, some studies showed that for the nutrient removal, the optimum length to width ratio is 10:1 (Hammer, 1989). Some early researchers reported that the treatment performance of FWS constructed wetlands is better at higher aspect ratio (Giuseppe et al., 2000).

1.1.2 Detention time

Theoretical hydraulic detention time can be defined as time taken for water to pass through the wetlands system. The volume reducing effect of vegetation which is related to the porosity was included. A more realistic measure of detention time can be computed using the average flow rate to account for the effect of the water gain and losses that occur in the wetlands. The detention time can be varied between three days to 15 days to achieve adequate treatment (Crites, 1994). However, the hydraulic residence time greater than 10 days is considered optimum to ensure that pathogens are reduced by sunlight exposure or natural die off (Crites, 1994). Estimation detention time is much larger than actual detention time, and in many cases, water can flow at high velocities through a small portion of the total wetlands volume, significantly lowering the hydraulic detention time. For example, for Boggy Gut in South Carolina, the estimation of theoretical detention time was to be 19 days and when it was measured using tracer, it was approximately two days (Knight and Ferda, 1989).

1.1.3 Depth

Wetlands can be designed to incorporate features that allow the system to be operated over a wide range of depth from less than 10.0 cm to 1.5 m (USEPA, 1999). Water depth in FWS should be considered an operational characteristic as well as a design characteristic. The effective depth of wetlands will change with time as litter fall below the water surface and detritus build up on the bottom begin to reduce the depth therefore reducing the effective hydraulic volume. Persson et al. (1999) deduced that depth also plays an important role in the removal performance.

The main objective of this paper is to evaluate the effect of design criteria on the performance of constructed wetland in Malaysia and this will contribute towards increasing local knowledge and optimization of constructed wetland effectiveness. This paper will discuss according to the stormwater constructed wetland which are situated at Putrajaya Wetland, Universiti Sains Malaysia (USM) Engineering Campus, Pulau Pinang and Humid Tropic Centre (HTC) Kuala Lumpur.

1.2 Study area

1.2.1 Putrajaya Wetland

Putrajaya, strategically located at the south of the popular Klang Valley, is being developed by the Federal Government. The Putrajaya lake catchment, which is also known as the Sg. Chuau catchment, is

2. METHODOLOGY

Water quality data from the three locations had been collected at the inlet and the outlet point of constructed wetland during rainfall event. The parameters measured and discussed in this paper were Total Suspended Solids (TSS), Total Nitrogen (TN), Total Phosphorus (TP), Biochemical Oxygen Demand (BOD) and Chemical Oxygen Demand (COD). However, other parameters such as temperature, heavy metals, Dissolved Oxygen, and Total Coliform were also measured and analyzed. The sampling and testing procedures conducted were in accordance with the *Standard Method for Examination of Water and Wastewater 20th Edition* (APHA, 1998).

3. RESULTS AND DISCUSSIONS

3.1 Length to the width ratio

Length to the width ratio is an element in wetlands design that contributes to the effect of flow distribution and hydraulic circuits. Previously, the earlier design ratio of some wetlands with a recommendation at least 10:1, was expected to have plug flow conditions in wetlands, thus avoiding short circuits and maximizing the water contact with the biofilm substrate for the biological removal of nutrients (Reed et al., 1995). However, the major problem with this approach is the resistance of flow increases as the length of the flow path increases and this contributes to the higher aspect ratios but increases the area of berm. Berm must be constructed to enclose the given wetland area, and as a consequence, the high cost of construction (Reed et al., 1995; Kadlec and Knight, 1996).

Figure 2 shows the average percentage of pollutant removal over the length to the width ratio for the different water quality parameters based on selected study areas. The results indicated that the Putrajaya Wetlands had the highest length to width ratio (6:1) which contributed to the highest average percentage of pollutant removal efficiency compared to HTC and the USM Engineering Campus for BOD, COD and TP with an average percentage pollutant removal efficiency of around 48%, 37% and 64%, respectively. The USM Engineering Campus with the length to the width ratio (5:1) contributed to the highest average percentage of pollutant removal efficiency for TN and TSS compared to the other selected study areas with an average percentage pollutant removal efficiency of around 74% and 71%, respectively.

Some studies indicated that for the removal of nutrients, the optimum length/width ratio is 10:1, but in order to maintain the effective flow distribution, the recommended structures, such as adequate inlet, deep zone and islands are needed (Persson et al., 1999; Hammer, 1989). Therefore, Reed et al. (1995) recommended that ratios of less than 1:1 up to about 3:1 or 4:1 are acceptable. Overall, Figure 2 shows the constructed wetland is effective to remove TN, TSS, TP, BOD, and COD with the average removal efficiency of 60%, 56%, 53%, 44% and 37% respectively.

3.2 Detention time

A detention time of six to seven days has been reported to be optimal for the treatment in constructed wetlands. Shorter detention times do not provide adequate time for pollutant degradation to occur; longer detention times can lead to stagnant, anaerobic conditions. However, the estimation on detention time in the wetland system faces several difficulties such as the large dead spaces that may exist in the wetlands due to differences in topography, plant growth, solid sedimentation and the degree of flow channelization (Kadlec and Wallace, 2009).

Figure 2 indicates the average percentage of pollutant removal efficiency over detention time for different water quality parameters for selected study areas. The findings indicated that the Putrajaya Wetlands, with the highest detention time (12.2 days), contributed to the highest average pollutant removal efficiency for BOD, COD and TP, with the recorded average percentage removal efficiency at around 48%, 37% and 64% respectively. The USM Engineering Campus, with the detention time of three days indicated the highest average percentage of pollutant removal efficiency for TSS and TN, with the percentage of pollutant removal at around 74% and 71% respectively.

Overall, Figure 2 shows the constructed wetland is effective to remove TN, TSS, TP, BOD and COD with the average removal efficiency of 60%, 56%, 53%, 44% and 37% respectively. The finding had been confirmed with the similar trend by a conducted study during the summer time, the approximate 100 mm water depth should be increased to minimize the effect of climate on detention time (Kadlec and Wallace, 2009). Moreover, a study conducted by Akratos and Tsihrintzis (2007) with the different HRT of 8, 14 and 20 days indicated that the BOD removal for an HRT of 8, 14 and 20 was 91.9%, 90.6% and 91.9%, respectively.

In a certain location, a higher Area of wetland/Area of catchment ratio increases the retention time of the water, allowing more time for particles to settle and sorption to occur. This also decreases the resuspension and loss of TP already captured in the wetlands (Koskiaho, 2006), resulting in a more efficient relative retention (in % of Phosphorus load). In contrast, the area-specific retention will be lower because there is a positive relationship between the Phosphorus load and the area-specific Phosphorus retention (Braskerud, 2002; Kadlec, 2005). However, the nitrogen removal efficiency varies greatly with flow conditions and residence time (Kadlec and Wallace, 2009).

The performance of TSS is influenced by the moderate to long detention time process of generation and resuspension incoming solids. The effect of larger open water area in marshes-pond cells was to raise the TSS concentration due to generation and resuspension (Kadlec and Wallace, 2009).

3.3 Water depth

The actual water depth is not known with a high degree of accuracy due to basin bottom irregularities. Sometimes, the water depth in the wetlands may decrease due to the formation of peat from the process of deposition of detritus and settled solid buildup (Mitch and Gosselink, 2000). In order to solve this problem, the increase in water depth by changing the outlet weir elevation, can help offset the decrease in water depth. Water depth may also influence the TP removal by affecting the amount of submersed biota and the hydraulic flow with considerable topography, irregularity, and allowing island and deeper zones that may cause short circuiting (Kadlec and Wallace, 2009).

Previously, the performance of BOD in constructed wetlands may be reduced as the depth increases. However, new finding indicated, the performance can be increased as the depth of water is increased (Kadlec and Wallace, 2009). The removal efficiency of TP in constructed wetlands depends on area, water flow, inlet concentration, vegetation type, depth and event pattern. Low retention for TP may also be due to lower settling velocity in the high temperature (Braskerud, 2002).

Figure 2 indicates the average percentage of pollutant removal over different depths of water for different water quality parameters. The findings indicate that the Putrajaya Wetlands with an average depth of 1.0 m contributed to the highest average percentage of pollutant removal efficiency for BOD, COD and TP compared to the other selected study areas with an average percentage of around 48%, 37% and 64%, respectively. For TSS and TN, the highest average pollutant removal efficiency was contributed by the USM Engineering Campus with an average depth of 1.12 m and percentage of 74% and 71%, respectively.

Overall, Figure 2 shows the constructed wetland is effective to remove TN, TSS, TP, BOD, and COD with average removal efficiency around 60%, 56%, 53%, 44% and 37% respectively. The finding was confirmed with others' studies on the wetlands that had been operating for 15 years which indicated that the change in depth of about 0.08 to 0.12 m was due to plant detritus along the initial vegetated zone in FWS wetlands (USEPA, 1999). The operating water depths, based on experience in North America, have ranged from approximately 0.1 to over 2.0 m with typical depths of 0.15-0.60 m. Operating depths are generally different for the area with emergent plants (0.6 m) than those areas with submerged plants (1.2 m) (USEPA, 1999). Water level variation will be one of the effects towards hydraulic residence time, atmospheric oxygen diffusion and plant covers which are all the factors that influence wetlands performance. Water depth manipulations, drawdown and uneven bed surfaces can be used to moderate or encourage the colonization rate and select specific vegetation communities (Bachand et al., 1999). During the early stage of constructed wetlands, lower water levels are required to avoid flooding of the newly emergent plants (Allen et al., 1998). The depth of a constructed wetlands is contained in a narrow range, typically from 0.2 to 0.8 m and, in most cases, less than 0.4 m (Cooper et al., 1996). Depending on climatic conditions, wetlands water levels can be varied on a seasonal basis. Maintaining a high-water depth could increase detention time and surface area for attached microbial growth (Kadlec, 2005). However, during high temperature and when the plant productivity is the highest, the water levels should be lowered to promote better oxygen diffusion to the wetlands sediments and plant roots (Kadlec and Knight, 1996).

However, the performance of constructed wetlands in terms of design criteria effects does not solely depend on one element, but the combination of more than one element. Different water quality parameters may require different combinations of design criteria elements in order to optimize the performance of constructed wetlands. The differences from previous studies conducted may be due to influent characteristics, size, shape of the pilot unit and operating conditions.

3.4 Enhancement of pollutant removal reduction chart

In MSMA 2nd Edition, the preliminary check to confirm the required area from the concept design whether it is adequate to deliver the required level of stormwater quality improvement is the first step before the detailed design for constructed wetlands can be proceeded. The pollutant reduction curve for constructed wetlands as function of catchment impervious area can be used for verification. The main point of this curve is to provide an indication only for appropriate sizing and do not function as additional for detailed design process.

Based on MSMA 2nd Edition, the highest wetlands area as percentage of contributing impervious area is 5%, however based on Malaysian condition, the wetlands area as percentage of contributing impervious area are 20% for Putrajaya, 12% for HTC and 4% for USM Engineering Campus. New percentage of contributing impervious for different parameter such as TSS, TP and TN was developed based on the data obtained from Putrajaya, HTC and USM Engineering Campus. Figures 3, 4, and 5 show the pollutant reduction based on wetlands area as percentage of contributing impervious for different parameter such as TSS, TP and TN respectively with Malaysian condition.

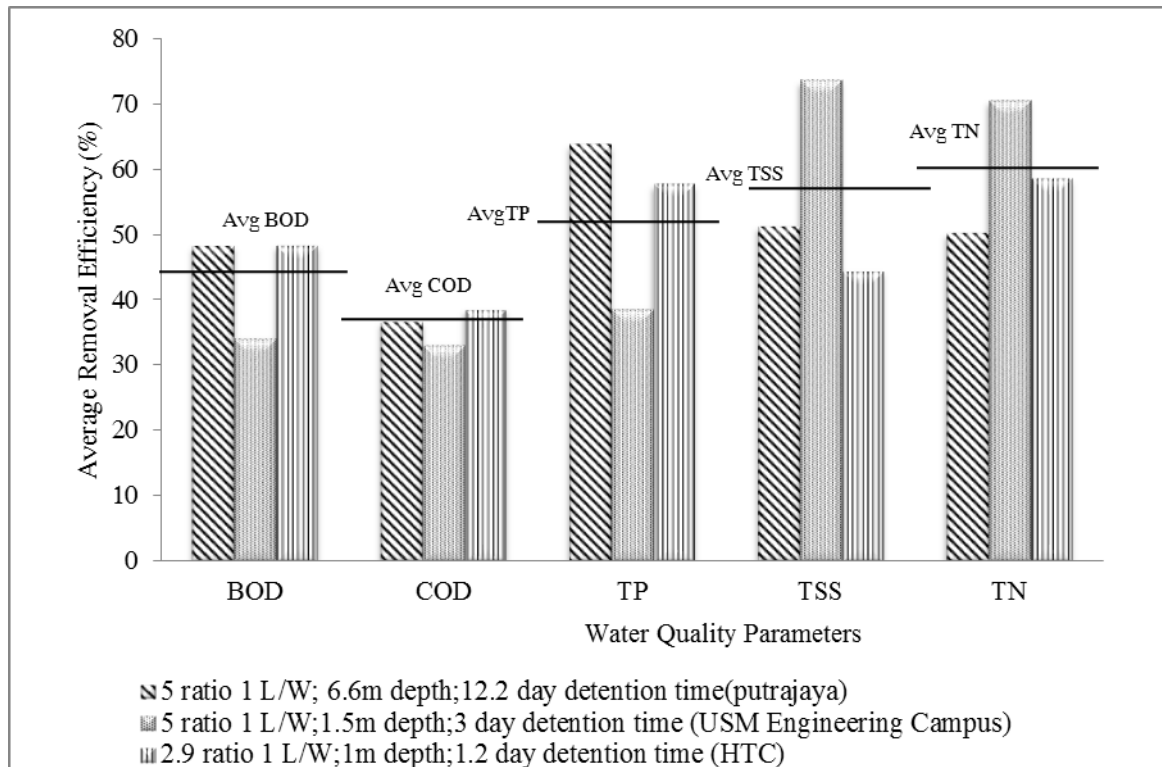


Figure 2. Average percentage of pollutant removal efficiency over the different length to the width ratio, detention times and depths of water for different water quality parameters.

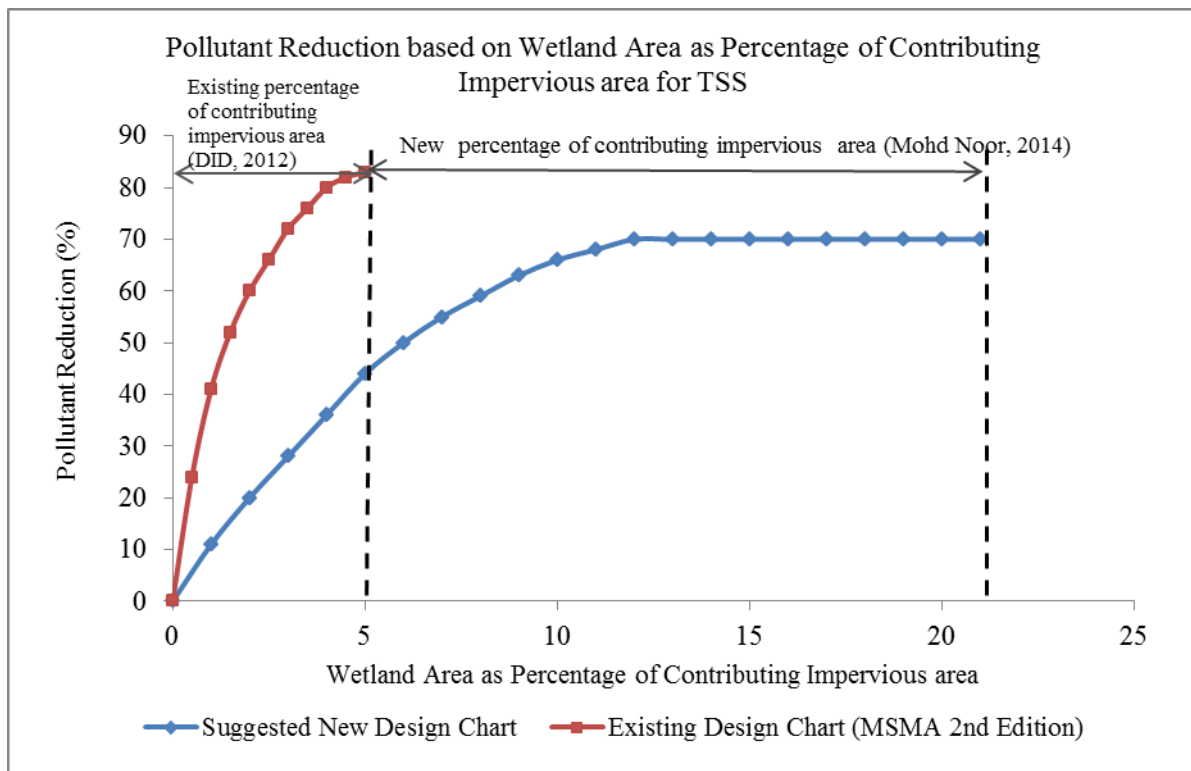


Figure 3. Pollutant reduction based on wetlands area as percentage of contributing impervious for TSS.

Figure 3 indicates that lower percentage pollutant removal for the Suggested New Design Pollutant Chart as compared to the Existing MSMA 2nd Edition TSS Design Pollutant Chart with the higher percentage of constructed wetland. Figures 4 and 5 indicate slightly higher of percentage pollutant removal for Suggested New Design Pollutant Chart as compared to the MSMA 2nd Edition TP and TN Design Pollutant Chart respectively.

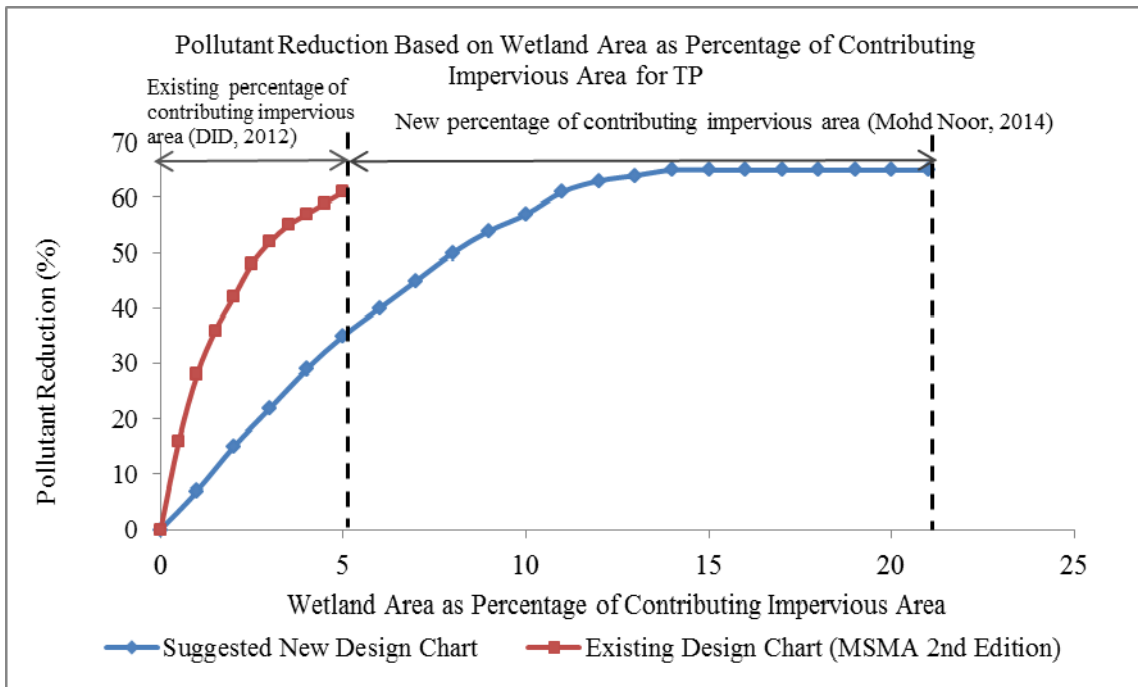


Figure 4. Pollutant reduction based on wetlands area as percentage of contributing impervious for TP.

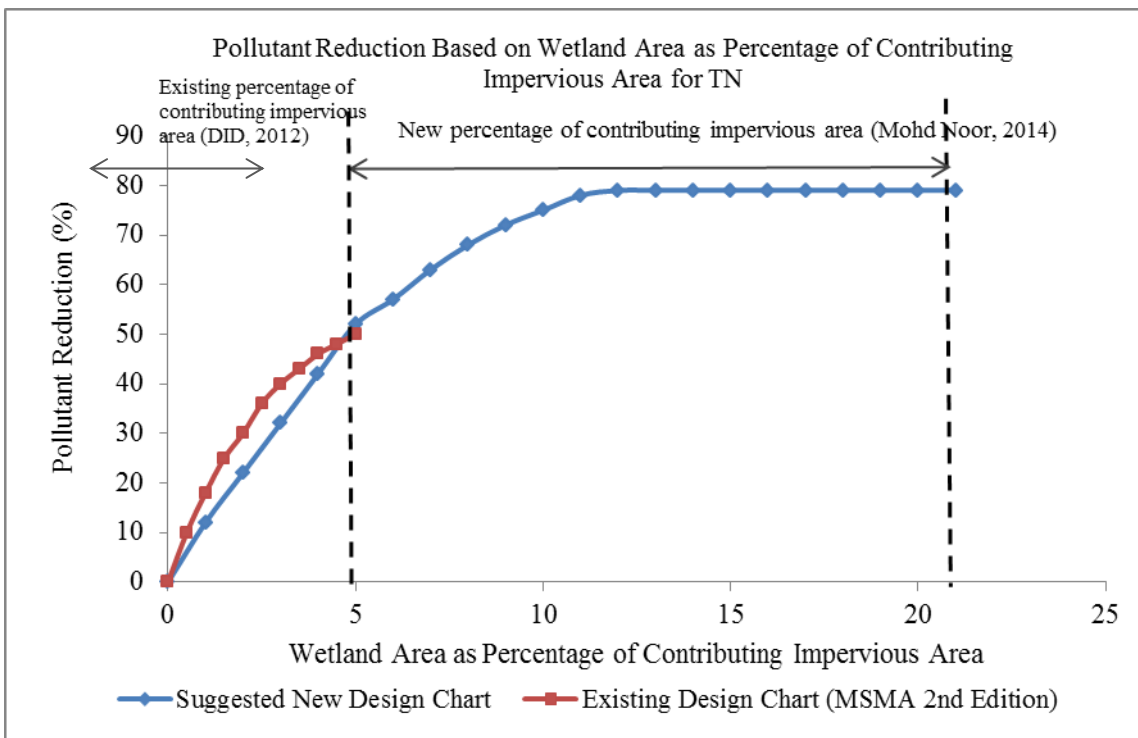


Figure 5. Pollutant reduction based on wetlands area as percentage of contributing impervious for TN.

4 CONCLUSIONS

The findings indicated that various factors influence the removal efficiency of constructed wetland in tropical climate such as hydraulic retention time, depth of water and length to width ratio. The efficacy of these constructed wetlands to treat stormwater from different sources varied, and modified wetland designs or active management may be necessary to improve water quality even further. The findings can be used significantly to enhance the knowledge in constructed wetland under tropical climate where it can serve effectively for managing urban runoff using control at source approach.

ACKNOWLEDGEMENTS

The authors would like to express gratitude towards Ministry of Higher Education, Universiti Tenaga Nasional, Universiti Teknologi MARA, Universiti Sains Malaysia, Perbadanan Putrajaya and Humid Tropic Center for supporting this study.

REFERENCES

- Abdullah, K. (2007). Water Resources Management in Malaysia. *International Conference on Water Resource Management in the Islamic Countries*, 19-20 February 2007, Tehran Iran.
- Akratos, C.S. & Tsihrintzis, V.A. (2007). Effect of Temperature, HRT, Vegetation and Porous Media on Removal Efficiency of Pilot-Scale Horizontal Subsurface Flow Constructed Wetlands. *Ecological Engineering*, 29(2), 173-191.
- Allen, R.G., Pereira, L.S., Raes, D. & Smith, M. (1998). Crop Evapotranspiration-Guidelines for Computing Crop Water Requirements-FAO Irrigation and Drainage Paper 56. *FAO, Rome*, 300(9), D05109.
- American Public Health Association (APHA), American Water Works Association and Water Environment Federal. (1998). *Standard Methods for the Examination of Water and Wastewater 20th Edition* APHA. Washington DC.
- Bachand, P.A.M. (1999). *Low Intensity Chemical Dosing of Stormwater Treatment Areas: An Approach to Enhance Phosphorus Removal Capacity of Stormwater Treatment Areas*. Florida Department of Environmental Protection.
- Bendoricchio, G., Cin, L.D. & Persson, J. (2000). Guidelines for Free Water Surface Wetland Design. *EcoSys Bd*, 8, 51-91.
- Braskerud, B.C. (2002). Factors Affecting Phosphorus Retention in Small Constructed Wetlands Treating Agricultural Non-Point Source Pollution. *Ecological Engineering*, 19(1), 41-6.
- Carmon, N. & Shamir, U. (1997). *Water Sensitive Urban Planning: Concept and Preliminary Analysis. In Groundwater in Urban Environment: Problem, Processes and Management*. Eds J chilton, K Hiscock, P. Younger, B. Morris, S. Puri, S W. Kirkpatrick, H Nash W Armstrong, Paldous, T Water, J. Tellman, R Kimblin and S Hennings. London, Balkema, Rotterdam, Brookfield.
- Comino, E., Riggio, V. & Rosso, M. (2011). Mountain Cheese Factory Wastewater Treatment with the Use of a Hybrid Constructed Wetland. *Ecological Engineering*, 37(11), 1673-1680.
- Cooper, P.F., Job, G.D., Green, M.B. & Shutes, R.B.E. (1996). *Reed Beds and Constructed Wetlands for Wastewater Treatment*. Swindon, UK: Water Research Centre, 184.
- Crites, R.W. (1994). Design Criteria and Practice for Constructed Wetlands. *Water Science and Technology*, 29(4), 1-6.
- Department of Planning and Local Government. (2009). *Water Sensitivity Urban Drainage for Greater Adelaide Region Technical Manual*, Department of Planning and Local Government. July 2009.
- Drainage and Irrigation Department Malaysia (DID). (2012). *Stormwater Management Manual for Malaysia 2nd Edition*. Drainage and Irrigation Department Malaysia.
- Hammer, D.A. (1989). *Constructed Wetlands for Wastewater Treatment*. Lewis Publishers: Chelsea, USA
- Jing, S.R., Lin, Y.F., Lee, D.Y. & Wang, T.W. (2001). Nutrient Removal from Polluted River Water by Using Constructed Wetlands. *Bioresource Technology*, 76(2), 131-135.
- Kadlec, R.H. & Knight, R.L. (1996). *Treatment Wetlands*. CRC Press-Lewis Publishers: New York.
- Kadlec, R.H. & Wallace, S.D. (2009). *Treatment Wetlands 2nd Edition* CRC Press-Lewis Publishers: New York.
- Kadlec, R.H. (2005). Constructed Wetlands to Remove Nitrate. *Nutrient Management in Agricultural Watersheds: A Wetlands Solution*. Wageningen Academic Publishers, the Netherlands, 132-143.
- Kato, K., Inoue, T., Ietsugu, H., Koba, T., Sasaki, H., Miyaji, N. & Nagasawa, T. (2010). Design and Performance of Hybrid Reed Bed Systems for Treating High Content Wastewater in the Cold Climate. In *12th international conference on Wetland systems for water pollution control*.
- Knight, R.L. & Ferda, K.A. (1989). Performance of the Boggy Gut Wetland Treatment system, Hilton Head, South Carolina. Wetlands: Concerns and Successes. *American Water Resources Association, United States*, 439-450.
- Koskiaho, J. (2006). Retention Performance and Hydraulic Design of Constructed Wetlands Treating Runoff Waters from Arable land.
- Koskiaho, J. (2006). *Retention performance and hydraulic design of constructed wetlands treating runoff waters from arable land*. Unpublished PhD Thesis, Oulu University, Finland, 68, 1.
- Mitch, W.J. & Gosselink, J.G. (2000). *Wetlands. 3rd. Edition*. John Willey and Son.
- Noor, N.M., Sidek, L.M., Abdullah, R. & Ab Ghani, A. (2013). Performance of Artificial Wetland in Removing Contaminants from Stormwater under Tropical Climate. *IAHS Publication*, 357, 208-216.
- Mohd Noor, N.A. (2014). Evaluation on Hydrologic and Environmental Performance of Three Constructed Wetlands in Malaysia. Unpublished PhD Thesis, Universiti Tenaga Nasional, Malaysia.
- Öövel, M., Tooming, A., Mäuring, T. & Mander, Ü. (2007). Schoolhouse Wastewater Purification in a LWA-Filled Hybrid Constructed Wetland in Estonia. *Ecological Engineering*, 29(1), 17-26.

- Persson, J., Somes, N.L.G. & Wong, T.H.F. (1999). Hydraulics Efficiency of Constructed Wetlands and Ponds. *Water Science and Technology*, 40(3), 291-300.
- Persson, J. & Wittgren, H.B. (2003). How Hydrological and Hydraulic Conditions Affect Performance of Ponds. *Ecological Engineering*, 21(4), 259-269.
- Reed, S.C., Middlebrooks, E.J. & Crites, R.W. (1995). *Natural Systems for Waste Management and Treatment*. (431). McGraw-Hill: New York.
- Scholz, M., Harrington, R., Carroll, P. & Mustafa, A. (2007). The Integrated Constructed Wetlands (ICW) Concept. *Wetlands*, 27(2), 337-354.
- Serrano, L., De la Varga, D., Ruiz, I. & Soto, M. (2011). Winery Wastewater Treatment in a Hybrid Constructed Wetland. *Ecological Engineering*, 37(5), 744-753.
- USEPA. (1999). *Free Water Surface Wetland for Waste Water Treatment*. USEPA
- Vymazal, J. (2009). The Use Constructed Wetlands with Horizontal Sub-Surface Flow for Various Types of Wastewater. *Ecological engineering*, 35(1), 1-17.
- Yong, R. & Md Noh, M.N. (2004). *Stormwater Management: Manual Saliran Mesra Alam*. Buletin Inginieur, 48-52. Available at: www.bem.org.my/publication/dec04-feb05.

EMULATOR-AIDED OPTIMIZATION OF DETENTION TANKS FOR FLOOD REDUCTION

WEI LU⁽¹⁾, XIAOSHENG QIN⁽²⁾ & JIANJUN YU⁽³⁾

^(1,2) School of Civil and Environmental Engineering, Nanyang Technological University, Singapore,
xsqin@ntu.edu.sg

⁽³⁾ Environmental Change Institute, School of Geography and the Environment, University of Oxford, Oxford, UK.

ABSTRACT

Stormwater detention tank is widely used as an effective measure in improving the performance of an urban stormwater drainage system (USDS) and mitigating urban flood risk during intensive storm events. Different layouts of detention tanks can largely affect their efficiency; therefore, it is crucial to determine their appropriate locations. This study investigates the feasibility of integrating urban hydrological simulation into an optimization model, meanwhile taking into consideration the constraints of realistic flooding control criteria, for the purpose of developing a general methodology for the optimal location design of detention tanks. For demonstration of the proposed method, the Storm Water Management Model (SWMM) is run on a hypothetical urban catchment, concerning different specifications of detention tanks in the USDS. The performance criteria of the nominated detention tanks are set as the computed value of the total flood volume in the USDS, as these criteria are closely connected to the loss ratio of property assets and infrastructures in an urban flood event. An artificial neural network (ANN) model is then established as an emulator to save the computational effort in hydrological simulation. Genetic algorithm (GA) is employed to automatically search the optimal solution in the optimization process. The optimal design of detention tanks could lead to a reasonable reduction of flood volume with a relatively lower cost when compared to an empirical design. The proposed study could help water management authorities or governmental agencies in reaching a more cost-effective decision-making.

Keywords: Storm water detention tank; flood mitigation; optimization; genetic algorithm (GA); artificial neural network.

1 INTRODUCTION

Urban drainage system is one of the most critical urban infrastructures to accommodate extensive rainfall to avoid urban flooding that cause severe damage to property assets, industrial manufacturing, transportation and human lives. However, the increasing climatic extremes and urbanization have challenged the existing drainage systems in most places as they may not have sufficient capacity to adapt to the rapid environmental change (Yu et al., 2015a). Among various measures in the urban drainage upgrades for flood defense, implementation of storage structures such as storm water detention tank is of particular importance for peak flow and flood reduction (Lee and Li, 2009; Chapman and Horner, 2010). For the sake of pursuing a tradeoff between affordable flood damage and construction cost, optimization techniques have been widely developed and applied to the design process of detention tanks (Oxley and Mays, 2014; Zhang and Hu, 2014; Li et al., 2015). These studies have demonstrated the feasibility of applying both simulation and optimization techniques. However, the computational burden of running the simulation-aided optimization models is high and this has limited the method being widely adopted. This study aims to propose an optimization model for the design of storm water detention tanks aided by using artificial neural network (ANN) and genetic algorithm (GA). ANN is used as a surrogate model to replace a hydrological model to provide flood information as it runs faster. The proposed model could help minimize the construction cost and meanwhile meet the local criteria of flood mitigation. A hypothetical urban catchment is used for demonstration.

2 DESCRIPTION OF METHODOLOGY

2.1 Optimization framework of for storm water detention tank

Figure 1 shows the framework for the proposed optimization process. Firstly, the essential data (e.g., hydrological, meteorological data and layout of drainage system) should be available for the study area. These datasets were used to generate design rainfalls and set up the hydrological simulation model. In this study, the Storm Water Management Model (SWMM) developed by U.S. EPA (Rossman, 2010) was chosen to model the study basin. SWMM is a dynamic rainfall-runoff model for collecting rainfall and generating runoff through the drainage networks of conduits, storage units and other hydraulic structures (Aad et al., 2009). Also, the quality and quantity of runoff generated within each sub-catchment can be tracked. Secondly, the model was tested by a design rainfall, thus an original scenario was generated, from which the potential locations of detention tanks were assumed to be determined. A limited number (*i.e.*, 100 scenarios in this

study) of samples about specifications of detention tanks on these locations were generated from the predetermined sampling space. They were simulated directly using the SWMM and the results were used to train and validate the ANN emulator, which was used to approximate the relationship between the design parameters and simulated floods. Thirdly, an optimization model was built to minimize the objective (e.g., construction cost) and meanwhile satisfy the constraints (e.g., total flood volume within the drainage network and dimensional limit of detention tanks). Finally, GA was applied to solve the optimization model to yield the optimal design, where the emulator (i.e., ANN) instead of SWMM was linked to provide the flooding information.

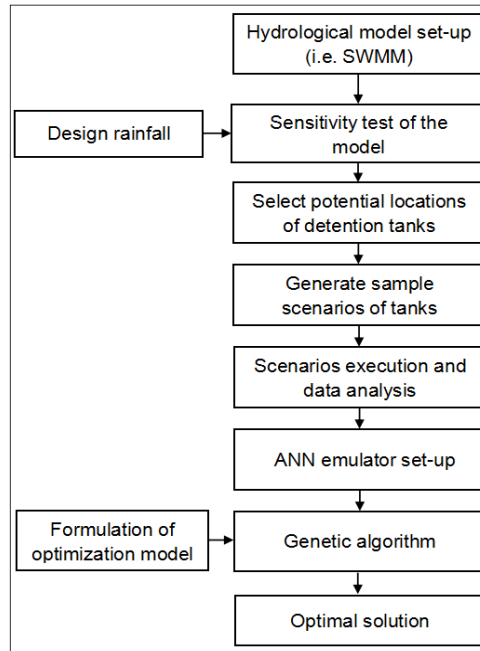


Figure 1. The framework of the proposed method.

2.2 Formulation of optimization model

The proposed optimization model is formulated as follows:

$$\text{Min } C = c \cdot \sum_{i=1}^n (A_i \cdot h_i) + b \quad [1a]$$

subject to:

$$V = \sum V_j = a(r, A_i) \leq \gamma \quad [1b]$$

$$\delta \leq A_i \leq \varphi \quad [1c]$$

where in Eq.1a, A_i and h_i represent area and depth of the i^{th} detention tank, respectively; n denotes the total number of tanks; C represents total construction cost of detention tank implementation, which is estimated by the product of the corresponding unit cost by volume (c) and the total volume of tanks, plus a management cost of the project (b). In constraint 1b, V represents the simulated total flood volume, which is determined by ANN emulator (a), design rainfall (r), specification of detention tanks (A_i), and an affordable threshold (γ) according to local design criteria. V_j denotes the flood volume of the j^{th} junction or detention tank (if any). Constraint 1c gives the predetermined range of area of the proposed detention tanks. The parameters (δ and φ) are expected to be decided from on-site investigation and land use condition. In the process of applying GA to solve the model, in case there was any violation of constraints, a penalty will be adopted to the total construction cost to ensure the faulty candidate solution is rejected.

2.3 ANN emulator

The ANN is employed in this study as an emulator to approximate the flood volume of different scenarios. In recent decades, ANN had gained its popularity for prediction and forecasting in many areas including environmental science and water resources (Maier and Dandy, 2000). ANN has the capability of self-learning and can fit complex nonlinear relationships (Yu et al., 2015b). Figure 2, as adapted from Stergiou and Siganos (2010) illustrates a common structure of a simple ANN.

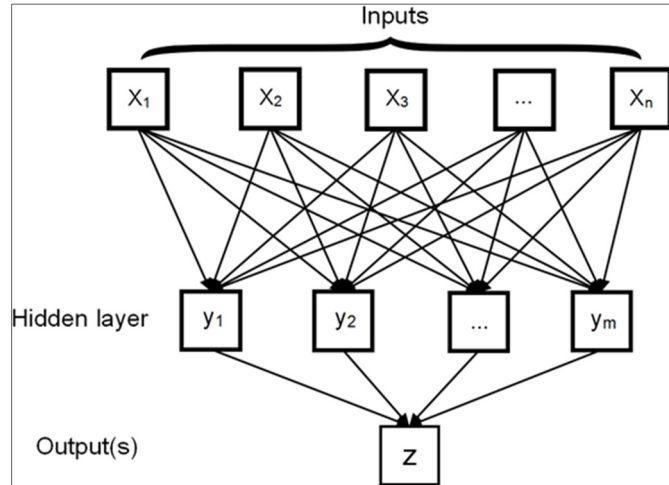


Figure 2. A common structure of simple neural network.

3 CASE STUDY

3.1 Case background and setup

A hypothetical urban catchment with an area of 560 hectares, adapted from PCSWMM workbook (CHI, 2014), was selected for demonstrating the proposed optimization framework. Figure 3 illustrates the layout of the drainage system within this catchment, which consists of 16 sub-catchment, 172 junctions, 175 conduits and 1 outfall. A SCS 24-hour design storm distribution (Smithers and Schulze, 2003) was used to derive a 20-year-return design rainfall in 5-minute interval with a total depth at 149.7mm (see Figure 4). Under such an event, the total flooding in the system, with an original scenario of no detention tanks was being implemented, with the volume of 3,907m³ (see Figure 3). There are 8 junctions suffering from heavy flooding (*i.e.*, $V_j \geq 100\text{m}^3$), which are considered to be the potential locations to deploy detention tanks. In order to limit the excavation work, the depth of the potential tanks (h_i) is set to be equal to the corresponding junctions. The shape of tanks was set to rectangular with constant cross section area. An optimization model (Eq. 1) is set up with a unit cost (c) of 200 dollar/m² and a management cost (b) of 0. The area of tanks ranges from 100-1,000m².

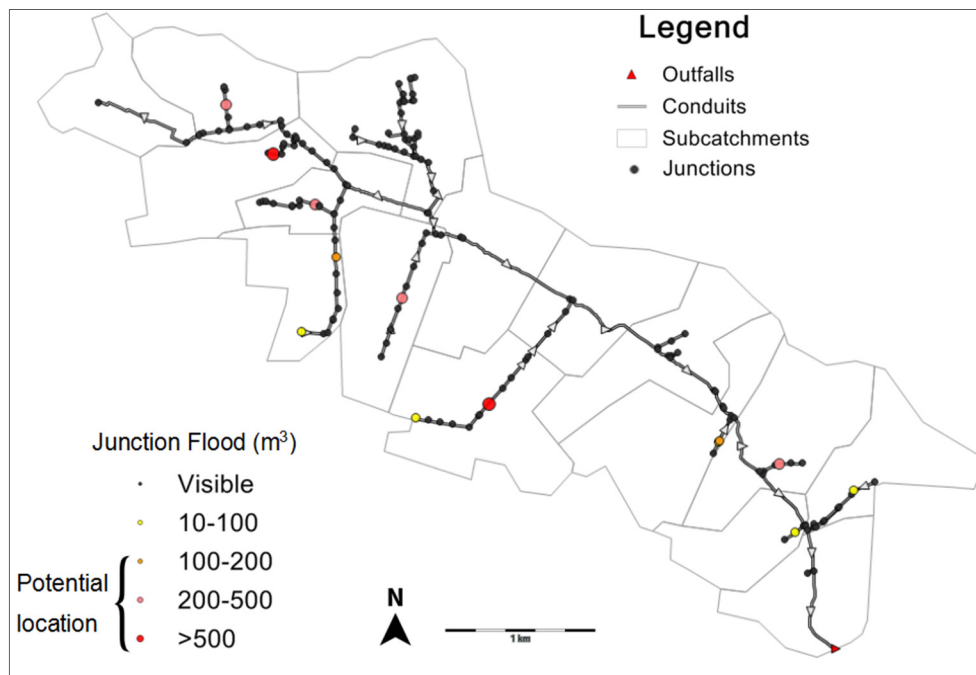


Figure 3. Case study and flooded volumes of junctions (without detention tanks).

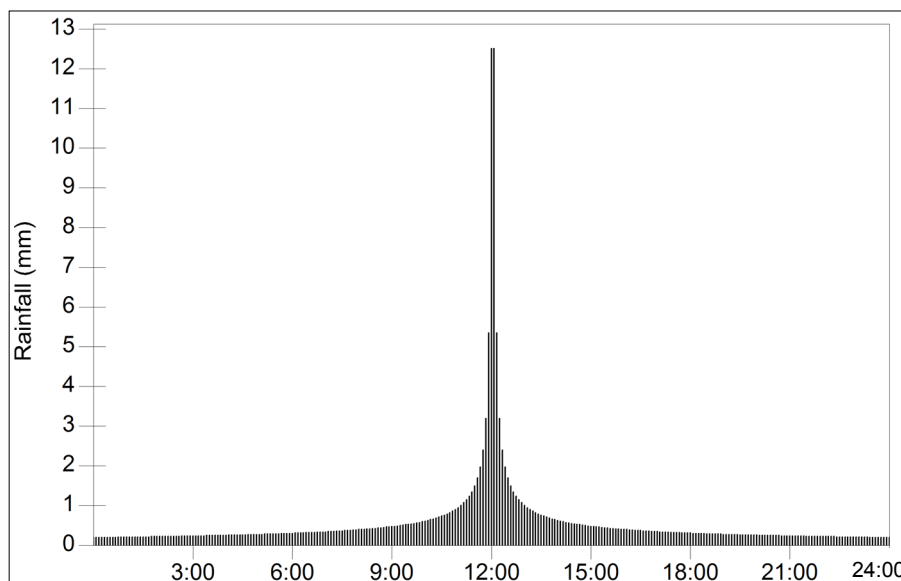


Figure 4. Design rainfall for the study area.

3.2 Results and discussion

Figure 5 shows the training, validation and test results of the ANN emulator based on 100 simulation results directly using SWMM. The surrogate model achieved a good fitness (with correlation coefficient, R , being 0.959 for all sets) of hydrological model. Table 1 summarizes the optimization results under the 20-year-return rainfall for various settings of affordable threshold, where ST_i denotes the area of the i^{th} detention tank (unit in m^2). An investment of 1.696 million dollars is required to construct the proposed detention tank networks in order to control the total flood volume at a level of less than $200m^3$. The cost decreases notably to 1163.2, 1002.1 and 790.4 thousand dollars as the threshold increases to 500, 800 and 1000, respectively. By testing, the construction cost would not decrease much when the flood threshold is larger than $1,000m^3$. By comparing these optimal solutions with the original scenario (*i.e.*, without tank implementation), which would generate a flood volume of $3,907m^3$, the situation had improved significantly. It is also noted that, for each GA optimization, the simulated flood volume of the optimal solution was close to its threshold. This demonstrates the effectiveness of constraint 1b during GA operations. Figure 6 shows the areas of concerned tanks under different flood thresholds. Some detention tanks lose their dominance at a relatively larger flood threshold (*e.g.*, ST_1 and ST_8), while others have a stable performance across the entire range of threshold (*e.g.*, ST_4 and ST_5).

Table 1. Optimized layout of detention tanks and the cost under various flood thresholds.

Total flood threshold γ (m^3)	ST_1	ST_2	ST_3	ST_4	ST_5	ST_6	ST_7	ST_8	Cost (10^3 dollar)	Flood volume V (m^3)
200	944.3	342.1	437.0	474.5	343.8	110.1	429.8	612.4	1695.8	199.9
500	905.8	125.2	212.7	320.3	283.4	100.0	107.9	782.4	1163.2	494.0
800	944.5	135.3	112.2	311.1	460.8	104.8	122.6	230.7	1002.1	798.9
1000	228.1	113.0	134.3	342.9	450.2	149.8	115.8	107.3	790.4	996.3

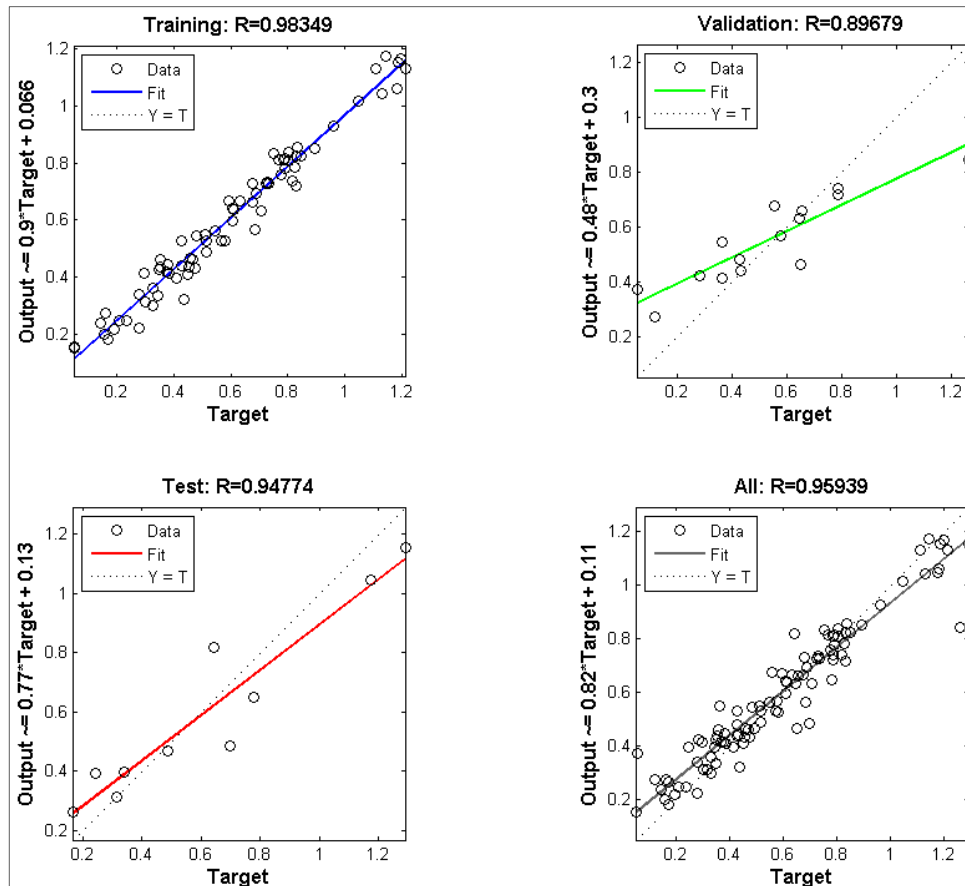


Figure 5. Performance test of the ANN emulator.

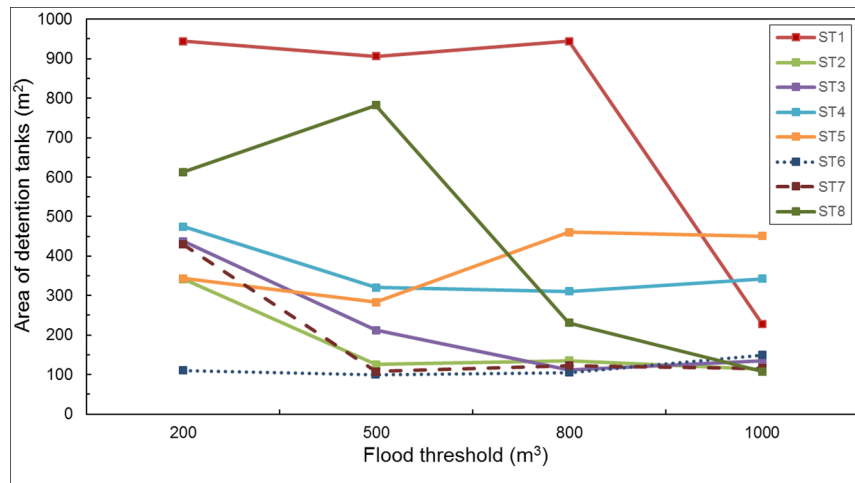


Figure 6. The detention tank areas under different flood thresholds.

4 CONCLUSIONS

This study proposed an emulator-based optimization framework to identify the optimal layout of storm water detention tanks. An ANN emulator was established based on the results simulated by SWMM to approximate the relationship between the design parameters of detention tanks with surcharge volumes. The ANN emulator was then embedded in the optimization model, aiming to minimize the construction cost while satisfying the constraint of flood thresholds. Compared to traditional optimization techniques, the proposed method could yield optimal solutions at a lower computational power, which allowed the proposed method to be applied in relatively large study cases. The effectiveness of user-defined constraints (i.e. total flood volume of drainage system) was also demonstrated during the optimization process. For future works, we believe the proposed method could be more valuable if a hydraulics model (like flood inundation model) is involved in the optimization framework. Also, how to address the uncertainty issues should also be taken into consideration.

ACKNOWLEDGEMENTS

The research work is supported by Nanyang Technological University (NTU) Start-Up Grant (WBS No.: M4081327.030) and partly supported by Singapore's Ministry of Education (MOE) AcRF Tier 1 Project (Ref No. RG170/16; WBS No.: M4011766.030). The authors also would like to thank Computational Hydraulics International (CHI) for providing PCSWMM software under CHI University Grant Program.

REFERENCES

- Aad, M.P.A., Suidan, M.T. & Shuster, W.D. (2009). Modeling Techniques of Best Management Practices: Rain Barrels and Rain Gardens Using EPA SWMM-5. *Journal of Hydrologic Engineering*, 15(6), 434-443.
- Chapman, C. & Horner, R.R. (2010). Performance Assessment of a Street-Drainage Bioretention System. *Water Environment Research*, 82(2), 109-119.
- Computational Hydraulics International (CHI). (2014). *Urban Drainage Modeling Workbook* (2014). <https://support.chiwater.com>, (accessed Jan. 1, 2017).
- Lee, J.S. & Li, M.H. (2009). The Impact of Detention Basin Design on Residential Property Value: Case Studies Using GIS in the Hedonic Price Modeling. *Landscape and Urban Planning*, 89(1), 7-16.
- Li, F., Duan, H.F., Yan, H.X. & Tao T. (2015). Multi-Objective Optimal Design of Detention Tanks in the Urban Stormwater Drainage System: Framework Development and Case Study. *Water Resources Management*, 29(7), 2125–2137, <https://doi.org/10.1007/s11269-015-0931-0>.
- Maier, H.R. & Dandy, G.C. (2000). Neural Networks for the Prediction and Forecasting of Water Resources Variables: A Review of Modelling Issues and Applications. *Environmental Modelling & Software*, 15(1), 101-124.
- Oxley, R.L. & Mays, L.W. (2014). Optimization–Simulation Model for Detention Basin System Design. *Water Resources Management*, 28(4), 1157–1171.
- Rossmann, L.A. (2010). *Stormwater Management Model User's Manual, Version 5.0: Water Supply and Water Resources Division*. National Risk Management Research Laboratory, U.S. Environmental Protection Agency, Cincinnati.
- Smithers, J.C. & Schulze, R.E. (2003). *Design Rainfall and Flood Estimation in South Africa*. Water Research Commission, Pretoria.
- Stergiou, C. & Siganos, D. (2010). Neural Networks, Imperial College London.
- Yu, J.J., Qin, X.S. & Min, R. (2015a). Optimal Sizing of Urban Drainage Systems Using Heuristic Optimization. *Resources, Environment and Engineering II: Proceedings of the 2nd Technical Congress on Resources, Environment and Engineering*, 111-116, CRC Press, <https://doi.org/10.1201/b19136-18>.
- Yu, J.J., Qin, X.S. & Larsen, O. (2015b). Applying ANN Emulators in Uncertainty Assessment of Flood Inundation Modelling: A Comparison of Two Surrogate Schemes. *Hydrological Sciences Journal*, 60(12), 2117-2131.
- Zhang, X. & Hu, M. (2014). Effectiveness of Rainwater Harvesting in Runoff Volume Reduction in a Planned Industrial Park, China. *Water Resources Management*, 28(3), 671–682.

RAPID ASSESSMENT OF HYDROLOGIC PERFORMANCE OF LOW IMPACT DEVELOPMENT PRACTICES AT DIFFERENT IMPLEMENTATION LEVELS

YANG YANG⁽¹⁾ & TING FONG MAY CHUI⁽²⁾

^(1,2) Department of Civil Engineering, The University of Hong Kong, Pokfulam, Hong Kong SAR, China
yyang90@connect.hku.hk; maychui@hku.hk

ABSTRACT

In recent years, low impact development (LID) practices have been widely used to manage stormwater and to restore natural hydrologic regimes. During preliminary design, it is often necessary to identify the required LID practice area that can meet the control target of peak flow and runoff volume. Currently, equation-based methods (e.g. the Rational and the Curve Number method) and hydrological models are often used. However, the coefficients required by the equation-based methods are often site-specific and inaccurate. On the other hand, the hydrological models may not provide direct and intuitive results due to model complexity. This study employed EPA SWMM, a dynamic hydrologic/hydraulic model, to investigate the surface peak flow and surface runoff volume reductions of various LID implementation levels. A MATLAB code was developed to automate the processes of input file modification, model execution, result extraction and post-processing. A few commonly used LID practices, e.g. porous pavement and bio retention cells, were examined. The results were summarized as performance curves which can be used to quickly assess the hydrologic performance of the preliminary designs. Furthermore, a few equations based on the concept of water balance were proposed, which can be used to quickly estimate the required LID practice area using hand calculations. Finally, sensitivity analysis was performed on design storm characteristics, catchment hydrological properties and LID design configurations, etc.

Keywords: Low impact development; sustainable drainage system; performance assessment; SWMM; stormwater management.

1 INTRODUCTION

Low impact development (LID) practices, also known as green infrastructure (GI), sustainable drainage system (SuDS) or water sensitive urban design (WSUD), are considered as environmentally-friendly alternatives of the conventional stormwater drainage structures. Through decades of research and implementation, their effectiveness in stormwater runoff quantity and quality control has been generally recognized (Ahiablame et al., 2012). Commonly used LID practices include green roofs, bio retention cells and porous pavements, etc.

During preliminary design, it is important to select the suitable LID practice types and their implementation levels (i.e. the ratio of the LID practices surface area to the impervious area) to achieve the desirable hydrologic performance. Peak surface flow and surface runoff volume are commonly considered in urban hydraulic structure designs, and are thus chosen as performance indicators in this study (Debo and Reese, 2002). Few empirical or model-based methods are currently used to estimate the hydrologic performance of the LID practices. Commonly used process-based simulation models include Storm Water Management Model (SWMM) (Rossman, 2010), HYDRUS model (Simunek et al., 2006), Model for Urban Stormwater Improvement Conceptualization (MUSIC) (Wong et al., 2002), etc. However, the model set-up is relatively complex and also the data requirement is high. Recently, several tools have been developed to assist practitioners to draft initial designs and to visualize simulation results. For example, National Storm Water Calculator (SWC) (EPA, 2013) was developed to enable end users to quickly estimate the hydrologic performance of certain LID design for particular sites.

This study aims to generate a set of performance curves relating the hydrologic performance to LID implementation levels and catchment imperviousness. By referring to these curves, practitioners can easily select the type and implementation level of the LID practice that meet the hydrologic performance requirement for their specific sites. Furthermore, few equations based on the concept of water balance were proposed, which can be used to quickly estimate the required LID practice area using hand calculations. This study further analyzes the sensitivity of the performance to design storm characteristics and LID design configurations.

2 METHODOLOGY

In this study, the hydrologic performance of three types of LID practice: green roofs, bio retention cells and porous pavements were investigated. The effectiveness of each LID practice type under different

implementation levels and catchment imperviousness was examined. A conceptual catchment representing a generic city block was set up in EPA SWMM. The catchment area is 20,234 m² (or 5 acres), which is similar to the average block size obtained from Ewing et al. (2003). The slope of the catchment is 2%. In SWMM, different subareas (i.e., pervious and impervious subareas) within a catchment were assumed to have the same routing width if only one lump catchment was modeled. Since a wide range of catchment imperviousness (i.e. every percent between 1% and 100%) was examined in this study, the routing lengths for the pervious or impervious areas can change dramatically and sometimes become unrealistic because of the constant width. Therefore, for consistency, this study modeled the pervious and impervious areas as two separate sub catchments in SWMM, allowing the catchment width to vary. In this study, the routing length was set to be 30 m (or 100 feet) as suggested in USDA (2014). The parameters of the LID practices followed the recommendations in Rossman and Huber (2016) and Qin et al. (2013). The catchment components and the surface runoff routing directions are shown in Figure 1.

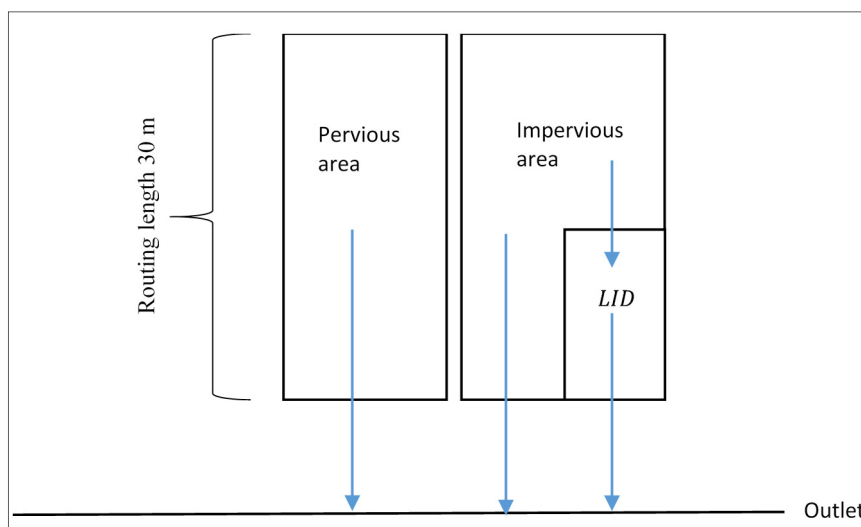


Figure 1. Schematic of SWMM catchment model. The arrows represent the flow directions of surface runoff.

Design storms were obtained from the SCS 24-hour design storms (NRCS, 1986), which are commonly used in the U.S. First this study investigated the performance of various LID practices under 24-hour SCS type III storm with a depth of 7.6 cm (3 inches). It then examined the impacts of using different storm types and depths in the sensitivity analysis. A MATLAB toolbox for controlling and monitoring SWMM simulations was developed. The toolbox can automatically change the SWMM input files according to user-defined rules, control SWMM simulations, extract and analyze the results. In each simulation, only one type of LID practice was placed in the catchment. The scenarios with LID practices occupying 1% to 100% of impervious areas were run automatically for catchments whose imperviousness range between 1% to 100%.

3 RESULTS AND DISCUSSIONS

3.1 Performance curves of green roofs

Green roofs, also known as living roofs or vegetation roofs, are rooftops that are covered by plants (VanWoert et al., 2005). They have been widely used to control stormwater and also to mitigate the urban heat island effect. They are normally designed to treat rainfall that falls directly onto them. Figure 2 shows the relationship between runoff reduction percentages, green roof implementation levels and catchment imperviousness. Given the imperviousness of the catchment of interest, practitioners can quickly estimate the reductions in both peak flow and runoff volume for different green roof implementation levels (i.e., percentages of impervious areas implemented with green roofs). Since green roofs can only treat rainfall that falls onto them and do not have external contributing areas, large green roof implementation levels are required to effectively reduce surface runoff.

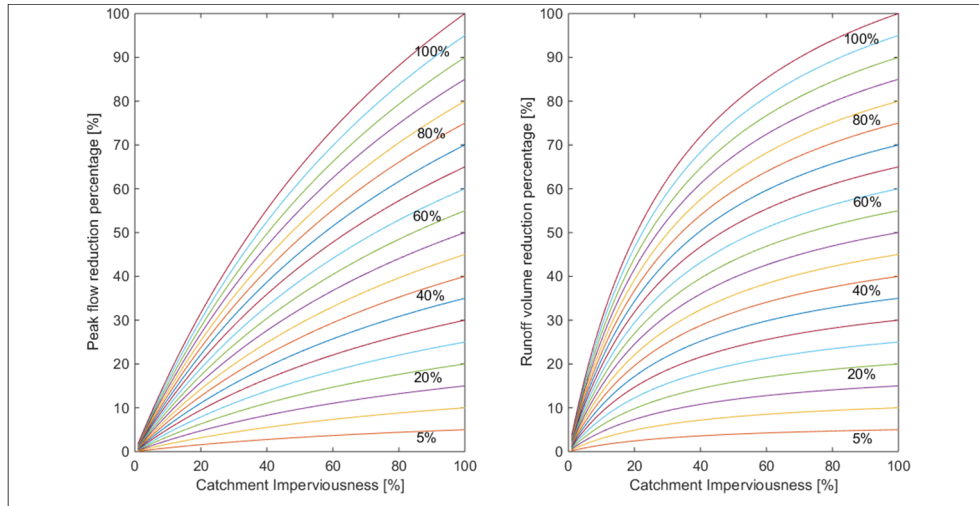


Figure 2. Peak flow and runoff volume reduction percentages for different catchment imperviousness under 7.6 cm (3 inches) type III design storms. Different curves from bottom to top correspond to different green roof implementation levels of every 5 percent between 5% and 100%.

3.2 Performance curves of porous pavements

Porous pavements, also known as pervious pavements or permeable pavements, are pavements with infiltration capacity and are equipped with underground storage and drainage facilities (Pagotto et al., 2000). The external contributing areas of porous pavements are normally small (Virginia Department of Conservation and Recreation, 2010a). The reductions in peak flow and runoff volume for different porous pavement implementation levels at different catchment imperviousness are shown in Figure 3. This study assumed that at maximum, porous pavements receive runoff from external contributing areas that are twice their own areas. Therefore, all the surface runoff from the impervious area drains to porous pavements when the implementation level exceeds 33%. Simulation results indicate that porous pavements can fully store surface runoff from twice of its surface area without overflowing.

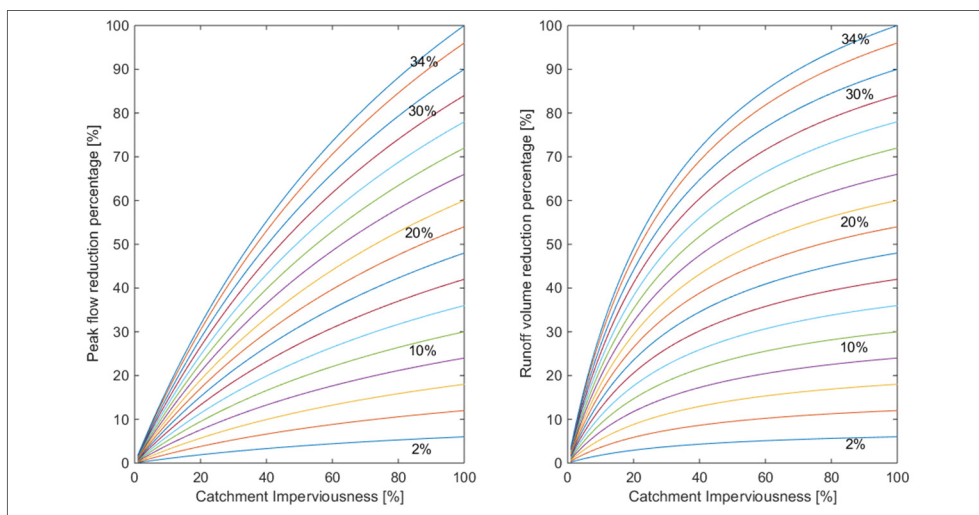


Figure 3. Peak flow and runoff volume reduction percentages for different catchment imperviousness under 7.6 cm (3 inches) type III design storms. Different curves from bottom to top correspond to different porous pavement implementation levels of every 2 percent between 2% and 34%.

3.3 Performance curves of bio retention cells

Bio retention cells are defined as soil-vegetation based stormwater infiltration and treatment facilities (Kim et al., 2003). Bio retention cells enhance infiltration and storage, and can be designed to treat runoff from external contributing areas of 30 times of the bioretention cell areas (Virginia Department of Conservation And Recreation, 2010b). The underdrain systems of bioretention cells are designed to drain the design volume within 24 hours, according to Maine Department of Environmental Protection (2014). This study assumed that at maximum, bioretention cells can receive surface runoff from external catchments that are 30 times of their surface areas. Figure 4 shows the percentage of peak flow and runoff volume reductions at different implementation levels of bioretention cells at different catchment imperviousness. Simulation results indicate

that, at 12% implementation level, bioretention cells can fully store the runoff drained to them without overflowing.

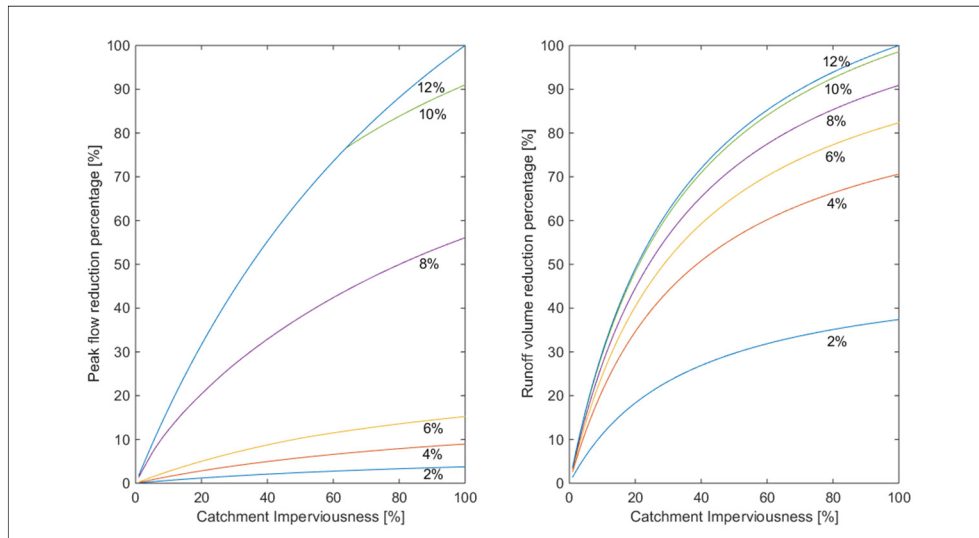


Figure 4. Peak flow and runoff volume reduction percentages for different catchment imperviousness under 7.6 cm (3 inches) type III design storms. Different curves from bottom to top correspond to different bioretention cell implementation levels of every 2 percent between 2% and 12%.

3.4 Runoff reduction estimations using equations

Qin et al. (2013) defined the effective storage depth (S_e) as the void storage depth (V) provided by the LID practices divided by the contributing area ratio, $A_{LID}/A_{catchment}$ (Eq. [1]). S_e represents the depth of the stormwater that can be potentially stored in the LID practices without overflowing.

$$S_e = \frac{V}{A_{LID}/A_{catchment}} \quad [1]$$

However, the actual storage volume during storm events might differ from S_e . It is because some LID practices, e.g. bioretention cells, can drain out the infiltrated stormwater through exfiltration and underdrain. Based on Qin et al. (2013), a new variable R_c is defined in this study, which is the actual storage depth provided by the LID practices during storm event (Eq. [2]).

$$R_c = S_e + R_i + R_d \quad [2]$$

where, R_i and R_d are the depths of stormwater converted to exfiltration and underdrain flows, respectively. In EPA SWMM, Green-Ampt equation, orifice flow equation, water balance equations, etc. are used to model the infiltration process and the underdrain flow. For a given inflow hydrograph (determined by design storm and catchment characteristics), it is possible to use EPA SWMM to derive the correlation between inflow depth and R_c .

In order to provide sufficient peak flow and runoff volume reductions during storm events, the LID practices should be designed to provide enough storage upon the arrival of peak inflow. Since the shape of design storm type III is symmetrical, peak rainfall intensity occurs in the middle of the storm event. In other types of design storm, the proportion of storm depth accumulated before the arrival of the peak intensity can be calculated. In this study, the correlation between storm depth D and R_c , peak flow and runoff volume reductions can then be estimated as follows:

- i. When $R_c > D$, LID practices can fully store the surface runoff from the catchment, thus surface runoff volume and peak flow reductions are 100%;
- ii. When $R_c < 0.5 * D$, peak overflow rate from the LID practice is $Q_t - I - U$, where Q_t is the peak surface runoff rate from the catchment, I and U are the exfiltration rate and the underdrain flow rate of the LID practice, respectively. When overflow occurs, the soil layer and the storage layer are normally fully saturated. Therefore I can be approximated as the saturated hydraulic conductivity of the bottom layer, and U can be simply calculated using the orifice flow equation at the fully saturated status of the LID practice (the total underdrain flow from an LID practice can be modelled using simple orifice flow equation in SWMM (Rossman, 2010)). R_c can be roughly regarded as the reduction in runoff volume;

- iii. When $0.5 * D < Rc < D$, peak overflow rate from the LID occurs after the arrival of peak inflow. Peak runoff can also be calculated as $Q_{tr} - I - U$, but Q_t is the catchment surface runoff rate when the LID practice is filled up. The reduction in runoff volume can also be approximated as Rc .

3.5 Sensitivity analysis

The LID performance curves are sensitive to storm types and storm depths, and therefore there is a need to derive different performance curves for different design storms. As an example, Figure 5 shows the performance curves under 5.1 cm (2 inches) type III storms for bioretention cells. The reduction rate is generally higher under this storm, and the required bioretention cell implementation level to store all runoff from the impervious area reduces from 12% in the base case to 7%.

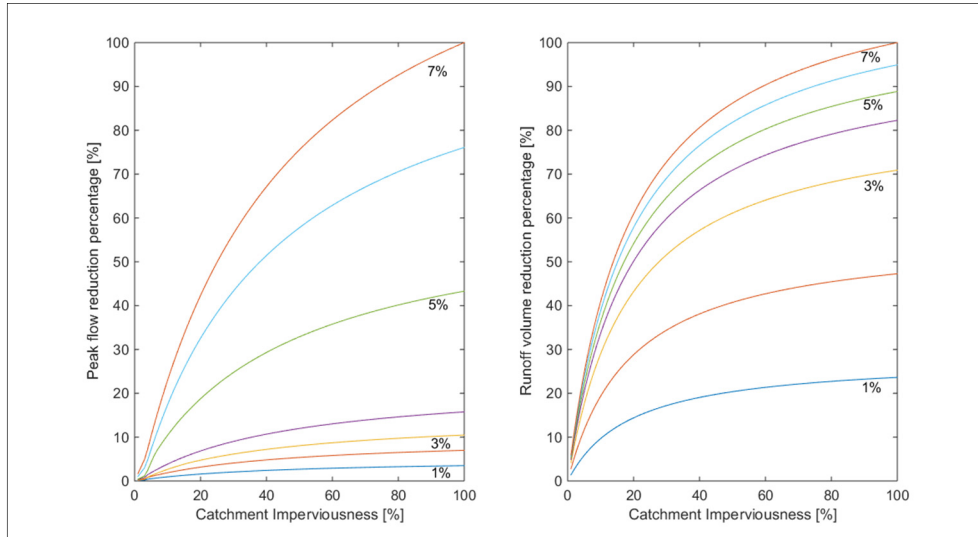


Figure 5. Peak flow and runoff volume reduction percentages for different catchment imperviousness under 5.1 cm (2 inches) type III design storms. Different curves from bottom to top correspond to different bioretention cell implementation levels of every 1 percent between 1% and 7%.

Performance curves of bioretention cells under 7.6 cm (3 inches) type II storm are shown in Figure 6. The curve patterns are different from those of the type III storm in the base scenario.

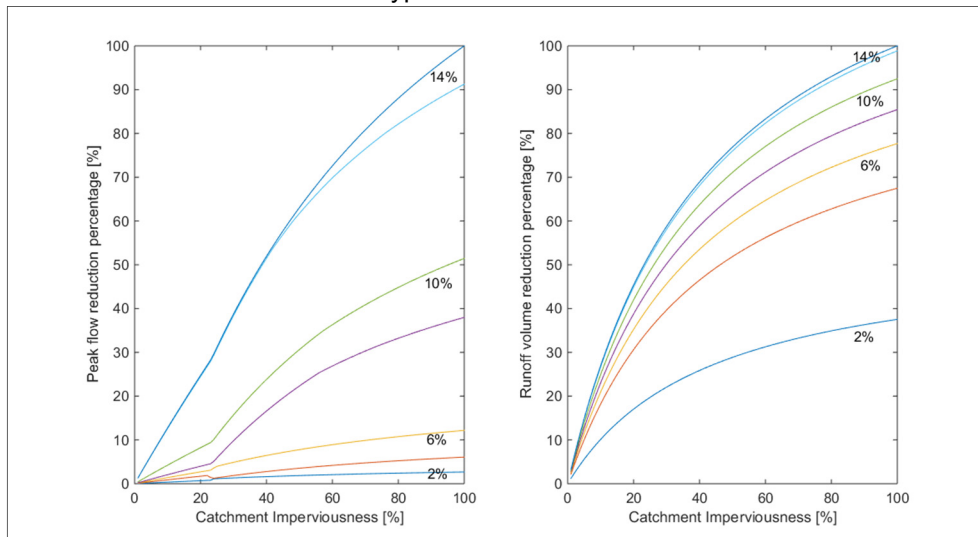


Figure 6. Peak flow and runoff volume reduction percentages for different catchment imperviousness under 7.6 cm (3 inches) type II design storms. Different curves from bottom to top correspond to different bioretention cell implementation levels of every 1 percent between 1% and 7%.

Other than the design storms, the performance curves are also different when the design configurations of the LID practices are different. For example, Figure 7 shows the performance curves for bioretention cells under 7.6 cm (3 inches) type III design storms. The maximum surface ponding depth of the bioretention cells was changed from 15.2 cm (6 inches) in the base case to 10.2 cm (4 inches). The shapes of these curves are slightly different from those of the base case. Also, as a result of the thinner surface ponding depth, the

required bioretention cell implementation level to store all runoff from the impervious area increases from 12% to 14%.

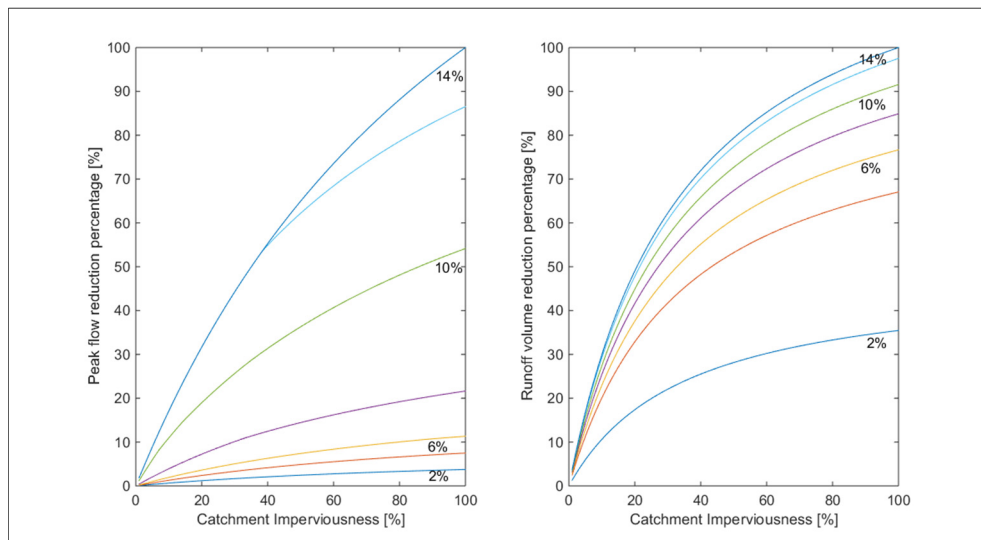


Figure 7. Peak flow and runoff volume reduction percentages for different catchment imperviousness under 7.6 cm (3 inches) type III design storms. Different curves from bottom to top correspond to different bioretention cell (with 10.2 cm ponding depth) implementation levels of every 2 percent between 2% and 14%.

4 CONCLUSIONS

This study used a dynamic hydrologic/hydraulic model, EPA SWMM, to evaluate the peak flow and runoff volume reductions at various catchment imperviousness and LID implementation levels. The results are especially useful when empirical coefficients for other equation-based methods (i.e., runoff coefficient and curve numbers) are not available. In general, for the same level of implementation, bioretention cells are the most effective LID practices, followed by porous pavements and then green roofs, mostly due to their large external drainage contributing areas. The pattern of peak runoff reduction in bioretention cells is more complex and varies more among different design storms because the peak runoff is governed by several hydrological processes, such as surface routing, ponding, and infiltration.

The performance curves derived in this study can serve as look-up curves, enabling practitioners to quickly assess the hydrologic performance of different LID implementation levels for their specific catchments. The curves only consider one type of LID practices within the catchment. However, if several LID practices are used in parallel, the catchment can be divided into several smaller subcatchments with each sub catchment equipped with only one type of LID practices. A quick assessment can then be performed for each sub catchment, and the overall performance is the weighted sum of the results from all subcatchments. The performance curves are also simple and can be coupled with other models to support more comprehensive decision making. For example, they can be coupled with cost estimation models for cost-benefit analysis.

This study aims to provide generic and widely applicable results. The model therefore simulated a typical urban catchment equipped with standard LID practices with design parameters derived from literature and design manuals. Therefore, model calibration is not applicable and necessary. However, sensitivity analysis reveals that the model results can be influenced by design storms and LID design configurations. Therefore, different performance curves are needed for different design storms and different LID design configurations. To fully understand the interactions and correlations among the model parameters and their impacts on the model results, a global sensitivity analysis is recommended.

ACKNOWLEDGMENTS

The work described in this paper was partly funded by Seed Funding Programme for Basic Research of The University of Hong Kong (Project code: 201411159159), and partly supported by a grant from the Research Grants Council of the Hong Kong Special Administrative Region, China (Project No. HKU17255516).

REFERENCES

- Ahiablame, L.M., Engel, B.A. & Chaubey, I. (2012). Effectiveness of Low Impact Development Practices: Literature Review and Suggestions for Future Research. *Water, Air, & Soil Pollution*, 223(7), 4253-4273.
- Debo, T.N. & Reese, A. (2002). *Municipal Stormwater Management*. CRC Press.
- Environmental Protection Agency, (EPA), (2013). *National Stormwater Calculator User's Guide*.

- Ewing, R., Pendall, R. & Chen, D. (2003). Measuring Sprawl and Its Transportation Impacts. Transportation Research Record. *Journal of The Transportation Research Board*, 1831, 175-183.
- Kim, H., Seagren, E.A. & Davis, A.P. (2003). Engineered Bioretention for Removal of Nitrate From Stormwater Runoff. *Water Environment Research*, 75(4), 355-367.
- Maine Department of Environmental Protection (2014). *Maine Stormwater Best Management Practices Manual*.
- NRCS (Natural Resources Conservation Service) (1986). *Technical Release 55 (TR-55)*.
- Pagotto, C., Legret, M. & Le Cloirec, P. (2000). Comparison of the Hydraulic Behaviour and the Quality of Highway Runoff Water According to the Type of Pavement. *Water Research*, 34(18), 4446-4454.
- Qin, H.-P., Li, Z.-X. & Fu, G. (2013) The Effects of Low Impact Development on Urban Flooding Under Different Rainfall Characteristics. *Journal of Environmental Management*, 129, 577-585.
- Rossman, L.A. (2010). *Storm Water Management Model User's Manual, Version 5.0*.
- Rossman, L.A. & Huber, W.C. (2016) *Stormwater Management Model Reference Manual Volume III – Water Quality*.
- Simunek, J., Van Genuchten, M.T. & Sejna, M. (2006). *The HYDRUS Software Package for Simulating Two and Three-Dimensional Movement of Water, Heat, and Multiple Solutes in Variably-Saturated Media*, Technical Manual, 1.
- USDA (U.S. Department Of Agriculture) (2014). *National Engineering Handbook Hydrology Chapters*.
- Vanwoert, N.D., Rowe, D.B., Andresen, J.A., Rugh, C.L., Fernandez, R.T. & Xiao, L. (2005). Green Roof Stormwater Retention. *Journal of Environmental Quality*, 34(3), 1036-1044.
- Virginia Department of Conservation and Recreation (2010). *Virginia DCR Stormwater Design Specification*, 7.
- Virginia Department of Conservation and Recreation (2010). *Virginia DCR Stormwater Design Specification*, 9.
- Wong, T.H., Fletcher, T.D., Duncan, H.P., Coleman, J.R. & Jenkins, G.A. (2002). A Model for Urban Stormwater Improvement Conceptualisation. *Global Solutions for Urban Drainage*, 813.

PERFORMANCE OF GROSS POLLUTANT TRAP IN URBAN RIVER CATCHMENT FOR KLANG RIVER BASIN

NUR FARAZUIEN MD SAID⁽¹⁾, LARIYAH MOHD SIDEK⁽²⁾, HIDAYAH BASRI⁽³⁾, NAZIRUL MUBIN ZAHARI⁽⁴⁾,
MOHD AZMI HAJI ISMAIL⁽⁵⁾, NORLIDA MOHD. DOM⁽⁶⁾, LLYOD CHUA⁽⁷⁾ & SIMON BEECHAM⁽⁸⁾

^(1,2,3,4)Sustainable Technology & Environment Group, Institute for Energy Infrastructure, Universiti Tenaga Nasional, Selangor, Malaysia

⁽⁵⁾River Basin Management Division, Department of Irrigation and Drainage, Kuala Lumpur, Malaysia

⁽⁶⁾Humid Tropics Centre, Kuala Lumpur, Malaysia

⁽⁷⁾School of Engineering, Deakin University, Australia

⁽⁸⁾School of Natural and Built Environments, University of South Australia.

ABSTRACT

Flooding problem is often associated with clogging of drainage system contributed by large amount of litter. Gross Pollutant Traps (GPTs) function to trap gross pollutants and have been installed in urban waterways. However, the performances of GPTs are strongly dependent on the specific site criteria including type of land use, hydrological regime and maintenance frequency. The local authority is facing problems in conducting maintenance for the installed GPTs resulting in the clogging of system clogging. This leads to the flooding and contaminating of water at the downstream area. The current study aims to propose a proper management and planning tool for 151 units of proprietary GPTs installed in the urban areas under the project of River of Life (ROL). This study involves data collection of gross pollutants wet load trapped inside GPTs from 3 different types of land use (residential, commercial and mixed development). It takes into consideration of the cost associated in relation to Life Cycle Cost (LCC) and Cost Effectiveness Ratio (CER) of the installed GPTs in the study area. The results obtained from this study will help in assisting the engineers and local authorities to implement appropriate strategies for trapping gross pollutants in urban area, expanding the sources for managing gross pollutants in order to rehabilitate the river system and preparing budget allocation for GPTs operation and maintenance.

Keywords: Gross pollutant trap (GPT); pollutants; river catchment; life cycle cost (LCC); cost effectiveness ratio (CER); stormwater management.

1 INTRODUCTION

The growing population and migration towards built areas are driving land use change in the form of urbanization across the globe and by the year 2050, some 70% of the world's population is expected to live in urban areas. Urbanization often relates to deterioration of storm water quality due to many factors such as uncontrolled pollution and waste disposal (Lariyah et al., 2006). Pollutants carried by urban storm water runoff are considered as significant contributor for the degradation of receiving waters. The term "gross pollutants" derived as large pieces of silt, trash, and particulate matters, either as floating or bed loads in urban conveyance system (Madhani and Brown, 2015).

In Malaysia, gross pollutants such as litter, debris and sediments are one of the main causes of river pollution and flooding problem and, as a result, there is a widespread degradation of the river, which is often the source of the flooding problems (Lariyah et al., 2011). These accumulated pollutants are not only aesthetically unattractive, but also demonstrate environmentally threatening and devastating effect to the natural equilibrium, and impede hydraulic performance of the urban drainage system (Ghani et al., 2011). There are now large numbers of trapping devices with different trapping mechanism available in the market. Efforts have been made by the authority to install the Gross Pollutant Trap (GPT) for trapping the gross pollutants from entering the river system (Smith, 2010). It has been proven in many studies that these devices are able to reduce significant amount of gross pollutants before entering the river system. It is also important to note that these devices function well with periodic and proper maintenance method (DID, 2012).

The performance of GPTs is strongly dependent upon the specific site criteria including type of land use, hydrological regime and maintenance frequency. As maintenance cost is significant in the life cycle cost of GPTs, the local authority is facing issues of conducting proper maintenance frequency for installed GPTs, resulting in system clogging which lead to flooding and contaminating the water at the downstream area. In view of this challenge, the Humid Tropics Centre (HTC) has appointed UNITEN R&D Sdn Bhd (URND), Malaysia to provide services to carry out the research on performance of proprietary gross pollutant trap (GPT) trapping devices versus life cycle cost and gross pollutant management strategies knowledge database for River of Life (ROL) Project. In this study, URND characterized and estimated the gross pollutants trapped using different type of proprietary GPT's, quantified life cycle cost associated with various types of proprietary

GPTs and developed Gross Pollutant Management Strategies Knowledge Database for managing the gross pollutants. This study mainly aims to provide better management and planning tool for the gross pollutants to be used in the urban areas specifically in ROL Project.

2 METHODOLOGY

2.1 Location of study area

The study area is located in Sungai Klang upper catchment, which flows through Kuala Lumpur and Selangor in Malaysia and eventually flows into the Straits of Malacca as shown in Figure 1. The Klang River drains an area of 1,288 km² from the steep mountain rainforests of the main central range along Peninsular Malaysia to the river mouth in Port Klang, spanning a distance of 120 km. Klang River has 11 major tributaries including Sungai Ampang, Sungai Gombak, Sungai Kerayong, Sungai Damansara, Sungai Keroh, Sungai Kuyuh and Sungai Penchala. This study focus on River of Life (ROL) project catchment which is a Malaysian Government idea under Economic Transformation Program to reach greater Klang Valley through transforming Klang River into a vibrant and liveable waterfront by the year 2020. The main tributaries in ROL catchment are Sungai Klang (upper catchment), Sungai Gombak, Sungai Batu, Sungai Jinjang, Sungai Keroh, Sungai Bunus, Sungai Ampang and Sungai Kerayong.

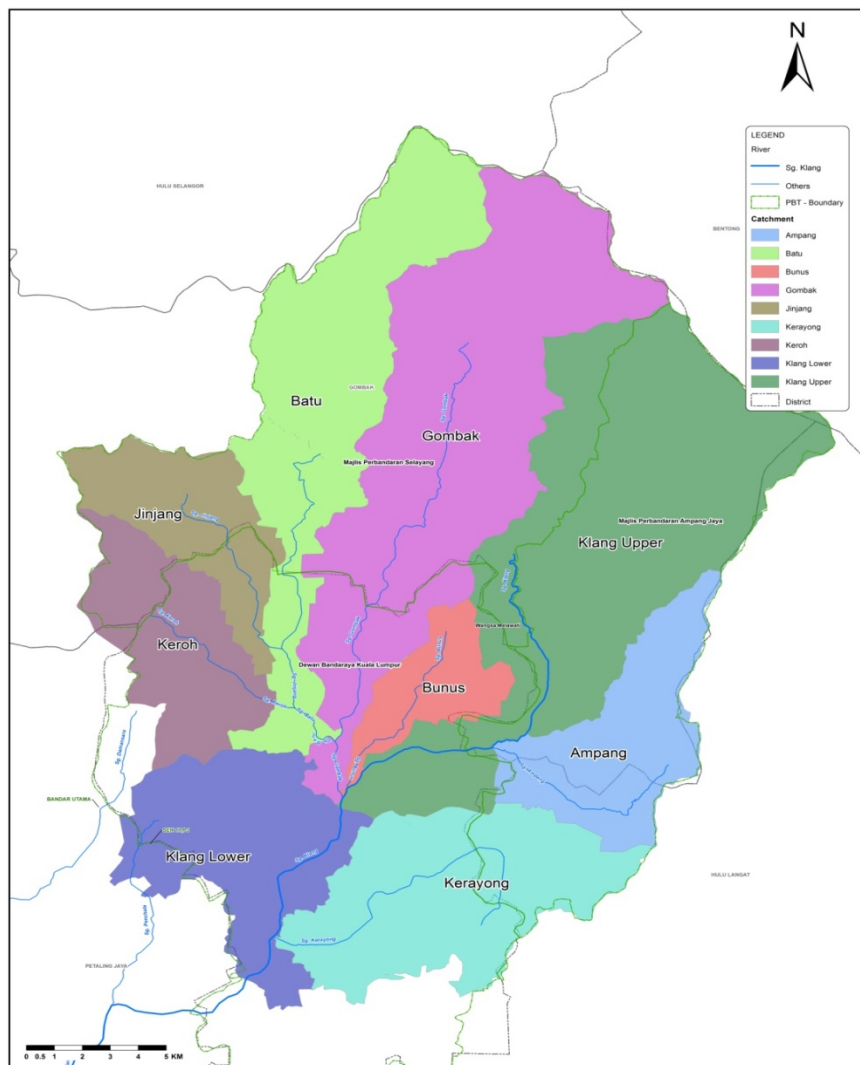


Figure 1. Location of ROL Project and the Klang River Basin (DID, 2012).

2.2 Gross pollutant monitoring

This study consists of monitoring process for assessment of gross pollutant traps for 5 types of proprietary GPTs from 3 different types of land use (residential, commercial and mixed development) at Sungai Klang, Sungai Gisir, Sungai Sering, Sungai Kemensah and Sungai Kerayong. The data collection process was divided into desktop data collection and field data collection. Desktop data collection involved information gathering of hydrological data, GPT inventory database, GIS mapping and also operation and maintenance cost data. For field data collection, there were three activities involved on-site, which are

weighting of gross pollutant wet load trapped in GPTs, gross pollutant sorting and water quality sampling at selected locations. All data and information were finally incorporated into the gross pollutant management strategies database.

2.3 Estimation of life cycle cost analysis, cost effectiveness ratio

The estimate life cycle cost of GPTs, costing data was obtained from Pejabat Lembaga Sungai Klang (PLSK). The data includes installation cost, inspection cost and cleaning cost. LCC for each trap is using the appropriate Australian Standard (AS/NZS, 1999). This process used Excel spreadsheet to calculate the GPTs LCC. A 10 years and 40-years' service life were used as GPTs life duration as recommended from previous study (Taylor, 2005).

3 RESULTS AND DISCUSSION

3.1 Life cost analysis (LCA)

The life cycle cost for all GPT in the study area was analysed. The analysis included Equivalent Annual Cost (EAC) derived from the life cycle cost, based on different project duration. The project duration selected was 10 and 40 years based on the literature review. The analysis assumed the maintenance of all GPTs was performed monthly. From the analysis, LCC of GPTs in the study area is ranging from RM 157,750 to RM 297,086 for duration of 10 years. However, for project duration of 40 years, the LCC of GPTs ranged from RM 315,358 to RM 616,694. The main factor contributing to the value of life cycle cost is maintenance frequency, which also takes into account the maintenance method.

The analysis from this study shows that manual maintenance of GPTs (using manpower to take out the rubbish from GPTs) is having among the lowest life cycle cost, with the LCC value of RM 157,750. The second lowest life cycle cost is using suction truck, while the highest LCC is maintenance using crane. At least two vehicles are required during maintenance i.e., crane and lorry to transport gross pollutants to the dumping area. This explains the higher LCC required for this type of maintenance. It is important to note that more frequent maintenance will increase the total life cycle cost. Therefore, in order to decide on the maintenance frequency of GPTs, it is important to identify the total loading coming from each catchment. Table .1 shows the maintenance method conducted during the maintenance activities in the study area.

Table 1. LCC and EAC of GPTs for the frequency of monthly maintenance.

Maintenance Method	Type of Proprietary GPTs	LCC (RM)		EAC (RM/yr)	
		10 years	40 years	10 years	40 years
Manual	Neutralizing Turbulent Vortex System (NTVS)	157,750.00	315,358.50	15,775.05	7,883.96
Suction Truck	Continuous Separation (CDS)	163,054	to 387,712	to 17,808.90	to 10,462
		270,686	511,094	27,068.60	12,777.35
	Deflective	170,364	410,772	17,036.40	10,269.30
Crane	Solid Interceptor (SI)	163,054	to 387,712	to 16,305.40	to 9,692.80
	Downstream Defender (DD)	479794	479794	25,513.6	11,994.85
	CleansAll (CA)	297,086	616,694	29,708.60	15,417.35

3.2 Determination of cost effectiveness ratio (CER)

CER provides a simple tool to assess management options for pollution trap operations. This study provide an opportunity to showcase the use of the CER tool.

CER was defined by Brisbane City Council (2002) as:

$$\text{CER} = \text{LCC (RM/yr)} / \text{Pollutant Removal Efficiency (kg/ha/yr)} \quad [1]$$

where,

PRE is the pollutant removal efficiency for the GPT (kg/ha/yr)

The Pollutant Removal Efficiency is calculated through a simple calculation of:

$$\text{PRE} = \text{WPR} / \text{CA} \quad [2]$$

where,

PRE is pollutant removal efficiency (kg/ha/yr)

WPR is weight of pollutants removed (kg/yr)

CA is catchment area (ha)

These equations provided a maintenance effectiveness ranking that could be used in considering future GPT selection. Generally devices with the lowest CER are preferred, meaning that they captured more

pollution and were not excessively priced to clean. The important criterion in assessing the performance of GPTs is the cost analysis. The analysis involved is quantifying the value for money for each device, using the “Cost Effectiveness Ratio” analytical technique. The Cost Effectiveness Ratio (CER) takes into account the life cycle cost and pollutant removal efficiency. The important advantage of the CER is that it provides a simple tool to assess management options for pollution trap operations.

The CER for all 151 GPTs in the study area was calculated and it was found that more than 50% of proprietary GPTs in the study area has the cost effectiveness ratio between RM 1,001 to RM 10,000. Another 30% of GPTs are seen to have CER value less than RM 1,000, whereas only 11% of GPTs have CER of more than RM 10,000. In general devices with lowest CER is preferred, which means it can capture more amount of pollutants and more excessively priced to clean (Dean, 2007). The percentage of GPTs with different range of Cost Effectiveness Ratio is shown in Figure 2.

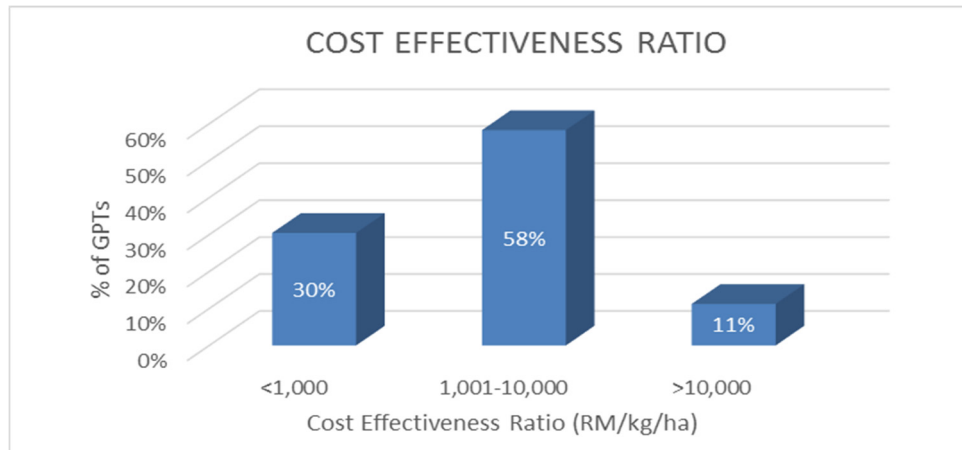


Figure 2. Percentage of GPTs with different range of cost effectiveness ratio.

The CER for each model installed in study area catchments was also calculated. Top 25 for the CER value as well as three lowest CER values have been selected for each type of land use, shown in Table 2. The result shows that NTVS has the smallest CER value in comparison with other GPT types.

Table 2. Top 3 for lowest CER ratio based on land use of proprietary GPTs installed in Upper Sg Klang and Kerayong catchments based on 10 years.

GPT ID	L*	Maintenance Method	Maintenance Costs (Rm/Yr)	Pollutant Removed (Kg/Yr)	Wet Load (Kg/Ha)	Pollutant Removal Efficiency (Kg/Ha/Yr)	Life Cycle Cost (Rm/Yr)	Equivalent Annual Cost (Rm/Yr)	Cost Effectiveness Ratio (Rm/Kg/Ha)
							10 years	10 years	10 years
GPT/SKER2/CA/3	R	Crane	RM10,653.60	957.83	1419.6	1710.36	RM297,086.00	RM29,708.60	RM173.70
GPT/SK/CDS/94	R	Suction truck	RM8,013.60	215.00	895.8	895.83	RM178,089.00	RM17,808.90	RM198.80
GPT/SK/NTV S/102	R	Manual	RM5,253.60	255.66	608.7	608.71	RM157,750.50	RM15,775.05	RM259.15
GPT/SK/NTV S/43	C	Manual	RM5,253.60	297.27	1189.1	1189.08	RM157,750.50	RM15,775.05	RM132.67
GPT/SKER1/CDS/4	C	Suction truck	RM8,013.60	133.3	1000.0	1333.33	RM178,089.00	RM17,808.90	RM133.57
GPT/SKER1/CDS/5	C	Suction truck	RM8,013.60	186.7	864.20	1152.27	RM178,089.00	RM17,808.90	RM154.56
GPT/SK/NTV S/107	M	Manual	RM5,253.60	560.14	1018.4	1018.44	RM157,750.50	RM15,775.05	RM154.89
GPT/SG/NTV S/108	M	Suction truck	RM5,253.60	562.90	987.54	987.54	RM157,750.50	RM15,775.05	RM159.74
GPT/SK/NTV S/96	M	Manual	RM5,253.60	403.13	937.5	937.51	RM157,750.50	RM15,775.05	RM168.27

*Landuse: R: Residential C: Commercial M: Mixed Development

CONCLUSIONS

The aim of this study was to improve the understanding on the loads of gross pollutant trapped in 151 GPTs in the study area. This information was further analysed in terms of cost effectiveness by calculating the Cost Effectiveness Ratio (CER) and Life Cycle Cost. The cost effectiveness ratio (CER) shows more than 50% of proprietary GPTs in the study area having cost effectiveness ratio between RM 1,001 to RM 10,000, 30% of GPTs CER value is less than RM 1,000 and only 12% of GPTs have CER of more than RM 10,000. LCC of GPTs in the study ranged from RM 157,750 to RM 297,086 for the project duration of 10 years. However, for project duration of 40 years, the LCC of GPTs ranged from RM 315,358 to RM 616,694. This study shows that manual maintenance of GPTs (using manpower to take out the rubbish from GPTs) is having among the lowest life cycle cost, with the LCC value of RM 157,750. The second lowest life cycle cost is using suction truck, while the highest LCC is for maintenance using crane.

REFERENCES

- AS/NZS 4536. (1999). *Life Cycle Costing – An Application Guide*, Standards Australia.
- Dean, D.K., Natalie, P. & Murray, P. (2007). *Auditing and Maintenance Costing of Gross Pollutant Traps*, Protecting our Urban Waterways - Water Quality and Managing Flow Impacts, Blacktown City Council, Australia.
- DID. (2012). *Chapter 10, Storm Water Management Manual For Malaysia 2nd Edition*, Department of Irrigation and Drainage (DID), Malaysia.
- Ghani, A.A., Azamathulla, H.M., Lau, T.L., Ravikanth, C.H., Zakaria, N.A., Leow, C.S. & Yusof, M.A.M. (2011). Flow Pattern and Hydraulic Performance of the REDAC Gross Pollutant Trap. *Flow Measurement and Instrumentation*, 22(3), 215-224.
- Lariyah, M.S., Nor, M.D.M., Khairudin, K.M., Chua, K.H., Norazli, O. & Leong, W.K. (2006). Development of Stormwater Gross Pollutant Traps (GPT's) Decision Support System for River Rehabilitation. In *National Conference on Water for Sustainable Development towards a Developed Nation by* (Vol. 2020).
- Lariyah, M.S., Nor M.D.M, Norazli O., Nasir M.N.M., Hidayah, B. & Zuleika, Z. (2011). Gross Pollutants Analysis in Urban Residential Area for a Tropical Climate Country. *12th International Conference on Urban Drainage*, Porto Alegre/Brazil.
- Madhani, J.T. & Brown, R.J. (2015). The Capture and Retention Evaluation of a Stormwater Gross Pollutant Trap Design. *Ecological Engineering*, 74, 56-59.
- Smith, D.P. (2010). New Approach to Evaluate Pollutant Removal by Storm-Water Treatment Devices. *Journal of Environmental Engineering*, 136(4), 371-380.
- Taylor, A. (2005). Structural Stormwater Quality BMP Cost-Size Relationship Information from the Literature. *Cooperative Research Centre for Catchment Hydrology*, Melbourne, 53-64.

THE APPLICABILITY OF AGRICULTURE-BASED EQUATIONS FOR THE ESTIMATION OF EVAPOTRANSPIRATION FROM RAINGARDENS

TINGTING HAO ⁽¹⁾, ASAAD SHAMSELDIN ⁽²⁾, KEITH ADAMS ⁽³⁾ & BRUCE MELVILLE ⁽⁴⁾

^(1,2,3,4) Department of Civil and Environmental Engineering, Auckland University, Auckland, New Zealand
thao073@aucklanduni.ac.nz

⁽¹⁾ Key Laboratory of Urban Stormwater System and Water Environment, Beijing University of Civil Engineering and Architecture, China

ABSTRACT

There are many equations for estimating evapotranspiration (ET). Many have been developed for agriculture, and are possibly only reliable in the regions and over the periods for which they were developed. It is difficult to say whether these equations are appropriate for raingardens, because they were developed with specific assumptions, such as idealized climate, a well-watered condition, and a monoculture vegetation of uniform height. Raingardens do not always meet these requirements because they often have complex structure, a variety of vegetation types and uncertain water availability. This research aims to determine if common agriculture-based ET equations can be successfully applied in raingardens. Similar research would also be appropriate for other low-impact development (e.g., green roofs, or bioswales).

Keywords: Raingardens; evapotranspiration; agriculture-based equations; low-impact development; stormwater management.

1 INTRODUCTION

The significant signs of urbanization are the changes of regional underlying surface conditions represented by the sharp increase in impermeable area and intense use of land resources. These changes have modified the natural hydrological cycle mechanism, resulting in water quantity and water quality effects.

Since the mid-1990's, low impact development stormwater management has developed all around the world. Its goals are to minimize negative influences by avoiding them as much as possible in the design phase, and to promote new, ecologically sound practices for storm water management.

Rain gardens are one of several versatile low impact design approaches; they have a significant effect on controlling runoff, groundwater recharge, and water quality. Rain gardens can provide a wide variety of worthy benefits, one of which is reducing runoff by increasing evapotranspiration (ET).

Estimating the amount of ET is necessary for predicting and quantifying such benefits. Study of the hydrology of rain gardens, including seasonal and diurnal effects, will provide a theoretical basis for their design.

2 EXPERIMENTAL SITES

The Hooton Reserve Raingarden (North Shore, Auckland, New Zealand) was selected as the experimental site. This raingarden has dimensions of 60m length by 22 m width and an area of about 1300 m². It is on the northern side of Oteha Valley Road (36.719021° S, 174.710952° E).

The research involves the deployment of a wide variety of sensors for the measurement of hydrological, meteorological, soil and plant variables (Figure 1). Site access and personal security are good, but there is no existing data.

Although field hydrology is more expensive than computing power and is accompanied by many risks and difficulties, field research can bring new fundamental understanding and mechanistic explanations of processes. It thereby contributes to hypothesis development (Burt and McDonnell, 2015).

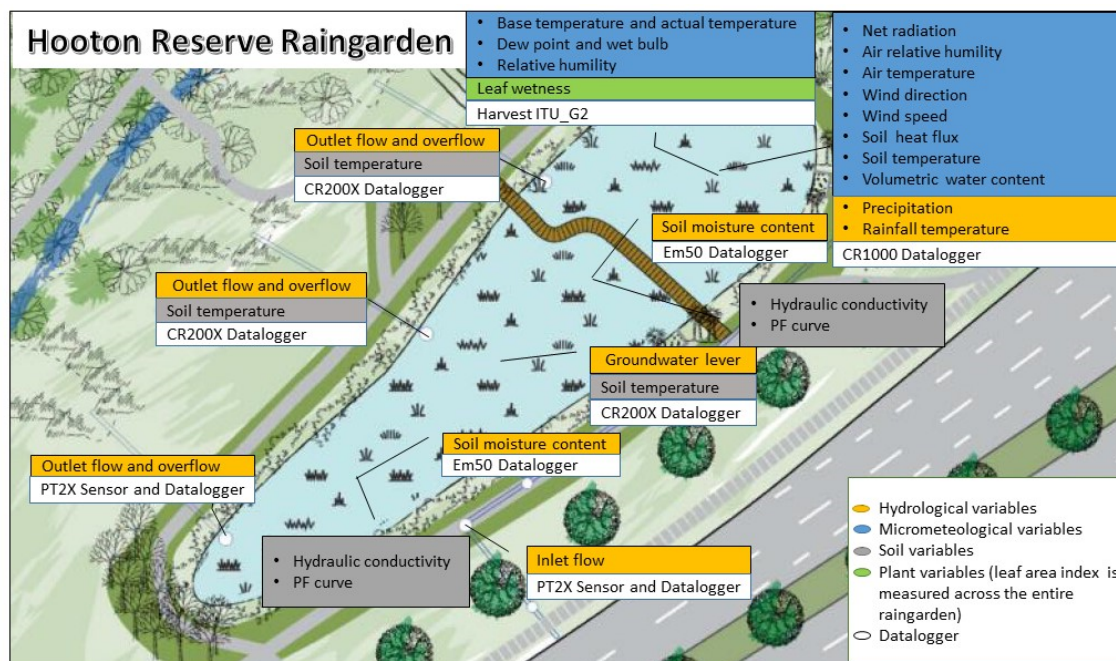


Figure 1. Deployment of sensors for experiments in the Hooton Reserve Raingarden.

3 METHODS

3.1 Evapotranspiration from raingardens

Evapotranspiration (ET) is the sum of evaporation and transpiration. Raingarden design allows for some reduction in the total volume of stormwater through evaporation and transpiration.

- Evaporation: When heated by the sun, evaporation is the process of water changes from liquid to water vapor as it moves from the ground surface, or from the temporary ponding, or from vegetation interception, into the atmosphere.
- Transpiration: raingarden plants use their leaves but also the stems, flowers and fruits, to transpire stormwater back into the atmosphere.

It is difficult to measure evaporation and transpiration directly and separately. Evapotranspiration is commonly estimated using mathematical models of varying complexity. The commonly used estimation methods can be categorized as temperature-based, radiation-based, and combination methods (Xu & Singh, 2002).

3.2 Evapotranspiration calculated using different equations

This paper aims to determine if common agriculture-based evapotranspiration equations can be successfully applied in raingardens.

At present, the National Institute of Water and Atmospheric Research of New Zealand is using the Penman (1963) method (combination) and Priestley-Taylor methods (Flint and Childs, 1991) for calculation of potential evapotranspiration for the National Climate Database, but they are currently evaluating adding the FAO 56 Penman-Monteith method (Allen et al., 1998) as an alternative method.

And based on the previous literature, in this paper six different methods were used to calculate evapotranspiration: Hamon Method, Makkink Method, Hargreaves Method, Jensen-Haise Method, Turc Method and FAO-56 Penman-Monteith Method. The variables and parameters required for each method are shown in the Table 1.

All the estimation methods were evaluated against the AET determined using the Bowen Ratio method. Evapotranspiration was calculated at a daily resolution, over a four-week period (04/08/2016-31/08/2016).

Required input for each method was data collected onsite, with quality control and gap filling using data from New Zealand's National Climate Database. The nearest climate station from the field study site is the North Shore Albany Ews Station (Agent Number 37852, 36.74827° S, 174.71377° E).

Table 1. Variables and parameters required by six different methods.

	Temperature	Radiation	Humidity	Others
Hamon (1963)	√			calibration constant (1.2), daytime length
Makkink (1957)	√	√		
Hargreaves (1985)	√	√		calibration constant (0.0023)
Jensen & Haise (1963)	√	√		actual hours of sunshine, possible hours of sunshine
Turc (1961)	√	√	√	
FAO 56 PM (1998)	√	√	√	wind speed

3.2.1 FAO56 Penman-Monteith Method

FAO56 Penman-Monteith equation is a widely accepted method and is recommended by the American Society of Civil Engineers (ASCE) to determine the reference evapotranspiration (Allen et al., 1998). It is a combination method and was derived from the original Penman equation. It assumes that the hypothetical reference crop has a height of 0.12 m, a fixed surface resistance of 70 s/m and an albedo value of 0.23 (Allen et al., 2005).

The equation can be expressed for daily values as:

$$ET_0 = \frac{0.408\Delta(R_n - G) + \gamma \frac{900}{T + 273} u_2 (e_s - e_a)}{\Delta + \gamma(1 + 0.34u_2)} \quad [1]$$

Where, ET_0 is the reference evapotranspiration rate [mm day^{-1}]; R_n is the net radiation [$\text{MJm}^{-2}\text{day}^{-1}$]; G is the soil heat flux density [$\text{MJm}^{-2}\text{day}^{-1}$]; γ is the psychrometric constant [$\text{kPa}^\circ\text{C}^{-1}$]; T is the mean daily air temperature at 2 m height [$^\circ\text{C}$]; u_2 is the wind speed at 2 m height [ms^{-1}].

e_a is the actual vapor pressure [kPa]; it is derived from relative humidity and air temperature:

$$e_a = \frac{e(T_{\min}) \left[\frac{RH_{\max}}{100} \right] + e(T_{\max}) \left[\frac{RH_{\min}}{100} \right]}{2} \quad [2]$$

Where, T_{\max} is the maximum daily air temperature [$^\circ\text{C}$], T_{\min} is the minimum daily air temperature [$^\circ\text{C}$], RH_{\max} is the maximum relative humidity [%], RH_{\min} is the minimum relative humidity [%].

e_s is the mean saturated vapor pressure [kPa], computed as the mean between the saturation vapor pressure at the mean daily maximum and minimum air temperatures:

$$e_s = 0.5 \left[e(T_{\max}) + e(T_{\min}) \right] \quad [3]$$

The function to calculate saturation vapor pressure at a particular temperature (t) is

$$e(t) = 0.6108 \exp \left[\frac{17.27t}{t + 237.3} \right] \quad [4]$$

Where, t is the air temperature [$^\circ\text{C}$].

Δ in the equation [1] is the slope of the relationship between saturation vapor pressure and temperature [$\text{kPa}^\circ\text{C}^{-1}$], given by

$$\Delta = \frac{4098 \cdot \left[0.6108 \exp \left(\frac{17.27T}{T + 237.3} \right) \right]}{(T + 237.3)^2} \quad [5]$$

Where, T is the mean daily temperature [$^\circ\text{C}$], \exp is the base of natural logarithm (2.7183).

3.2.2 Makkink Method

This method is radiation-based, using grass as a reference crop (Makkink, 1957). It is calculated by:

$$ET_0 = 0.61 \frac{\Delta}{\Delta + \gamma} \frac{R_s}{\lambda} - 0.12 \quad [6]$$

Where, R_s is the global solar radiation [$\text{MJm}^{-2}\text{day}^{-1}$]; λ is the latent heat of vaporization [MJkg^{-1}].

3.2.3 Turc Method

This method given by Turc (1961) is radiation-based and is expressed as (when the relative humidity is above 50%):

$$ET_0 = 0.013 \frac{T}{T + 15} \cdot \frac{23.8856R_s + 50}{\lambda} \quad [7]$$

3.2.4 Jensen-Haise Method

This approach is expressed as (Jensen and Haise, 1963):

$$ET_0 = 0.87(0.025T - 0.075) * 0.408 * (0.25 + 0.5 \frac{n}{N}) R_a \quad [8]$$

Where, R_a is the extraterrestrial radiation [$Mm^{-2}day^{-1}$]; n is the actual hours of sunshine, N is the possible hours of sunshine.

3.2.5 Hargreaves Method

This method is used for estimating grass reference evapotranspiration; it is expressed as (Hargreaves et al., 1985):

$$ET_0 = 0.0023 \cdot R_a \cdot \sqrt{T_{max} - T_{min}} (T + 17.8) \quad [9]$$

3.2.6 Hamon Method

Hamon (1963) proposed a simple temperature –based method for use when the mean air temperature is more than 0°C, it can be expressed as:

$$ET_0 = 0.1651 \cdot L_d \cdot 216.7 \cdot \frac{e(T)}{T + 273.3} \cdot 1.2 \quad [10]$$

Where, L_d is the daytime length, it is time from sunrise to sunset in multiples of 12 hours.

4 RESULTS AND DISCUSSIONS

4.1 Daily PET calculated by six different agriculture-based equations

As shown in the Figure 2, the PET results obtained using six different agriculture-based methods were compared with one another. It is evident that they show considerable variations. It should, however, be noted that they have similar patterns.

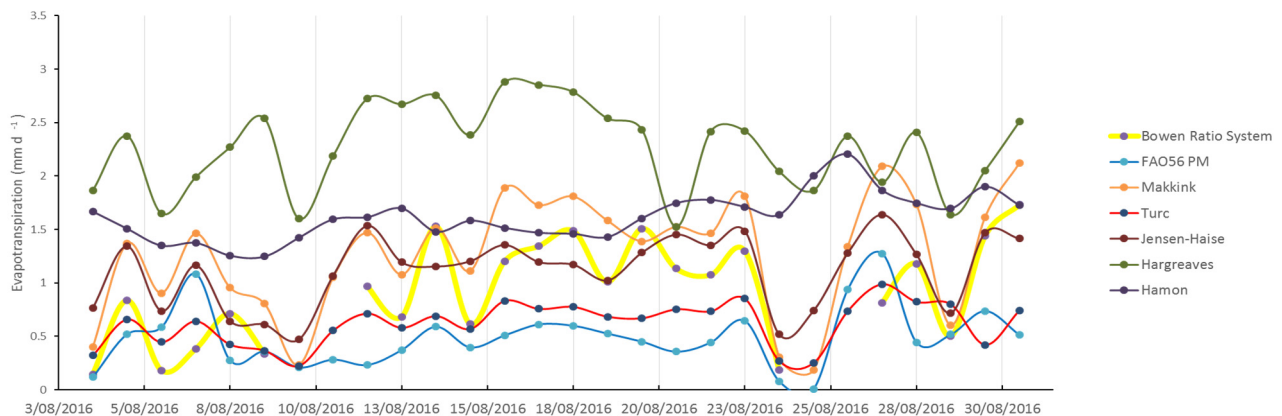


Figure 2. ET calculation using different equations (compared with the results from Bowen Ratio method).

On the dates of 10/08/2016, 11/08/2016, 25/08/2016 and 26/08/2016, the actual ET results measured by Bowen Ratio method are below zero, so they are eliminated.

The Hargreaves method gives the highest evapotranspiration estimates. The FAO56 Penman-Monteith method and Turc Method give the lowest estimates, and, most of the time, only their estimates were lower than the actual field ET for the same period, which was determined by the Bowen Ratio method as part of a related research project.

4.2 Simple linear regression analysis

Correlation coefficients, from simple linear regression analysis, are shown in the Figure 3. The evapotranspiration estimated by the Bowen Ratio System was taken as the independent variable while the evapotranspiration estimated by six different agriculture-based methods were taken as the dependent variable.

The Makkink method achieved the best performance, with the highest coefficient of determination ($R^2=0.6384$). The Jensen-Haise Method presented the second-best behavior ($R^2=0.452$), followed by the Turc Method ($R^2=0.3301$). For these three methods, Pearson's correlation coefficients are significant at 0.01 level.

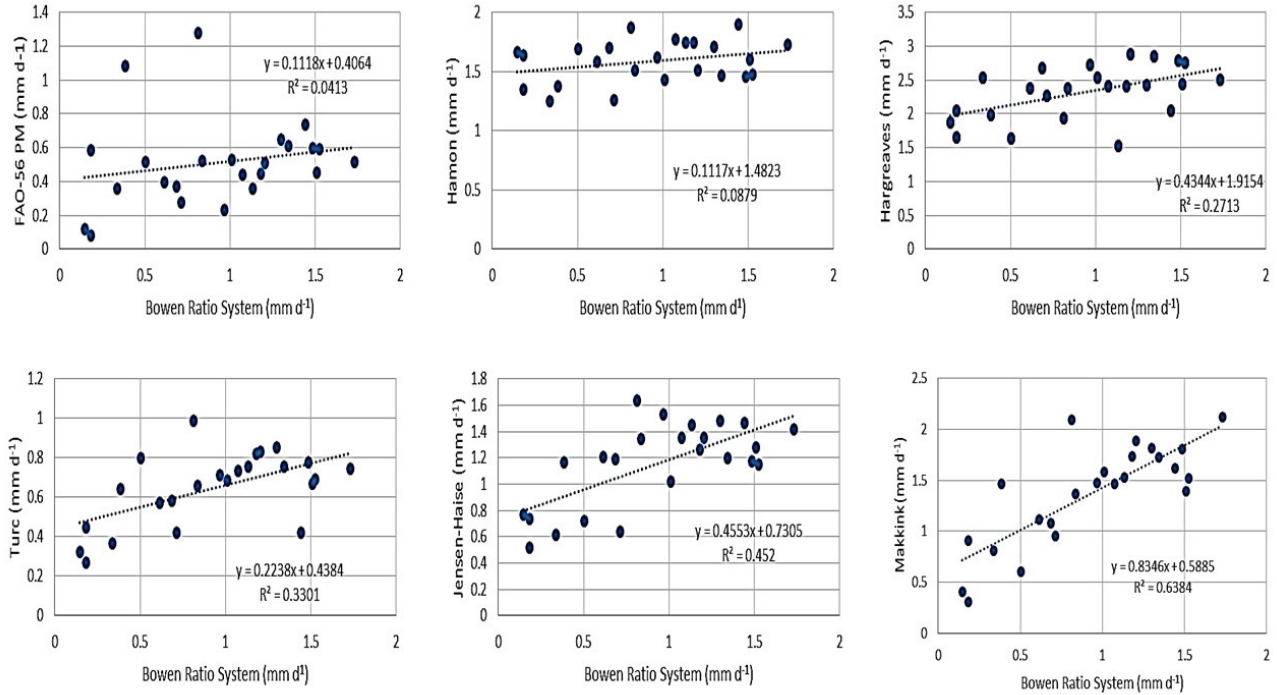


Figure 3. Correlations between daily values of ET estimated from the six agriculture-based equations and the from the Bowen Ratio system.

4.3 Statistical analysis using different types of performance indicators

For further comparison of Makkink method, Jensen-Haise Method and Turc Method, four types of performance indicators were used, namely, mean absolute error (MAE), root mean squared error (RMSE), coefficient of residual mass (CRM) and Nash-Sutcliffe equation (NSE).

$$MAE = \frac{1}{n} \sum_{i=1}^n |ET_{br,i} - ET_{est,i}| \quad [11]$$

$$RMSE = \sqrt{\frac{\sum_{i=1}^n (ET_{br,i} - ET_{est,i})^2}{n}} \quad [12]$$

$$CRM = \frac{\sum_{i=1}^n ET_{br,i} - \sum_{i=1}^n ET_{est,i}}{\sum_{i=1}^n ET_{br,i}} \quad [13]$$

$$NSE = 1 - \frac{\sum_{i=1}^n (ET_{br,i} - ET_{est,i})^2}{\sum_{i=1}^n (ET_{br,i} - \overline{ET_{br}})^2} \quad [14]$$

Where, $ET_{br,i}$ is the measured daily AET using Bowen Ratio method at i day [mm day⁻¹]; $ET_{est,i}$ is the estimated daily PET using Makkink method, Jensen-Haise Method or Turc Method at i day [mm day⁻¹]; $\overline{ET_{br,i}}$ is the average measured AET using Bowen Ratio method, and n is the number of days. The results are shown in Table 2 below.

Table 2. Statistical analysis using four types of performance indicators

	MAE [mm day ⁻¹]	RMSE [mm day ⁻¹]	CRM	NSE
Makkink Method	0.446	0.530	-0.468	-0.293
Jensen-Haise Method	0.345	0.411	-0.241	0.221
Turc Method	0.390	0.483	0.305	-0.074

The more the value of MAE is lower, the smaller the error is (Jensen-Haise Method);

The more the value of RMSE is lower; it indicates better performance (Jensen-Haise Method);

The value of CRM is closer to 0, which indicates that the proposed method is close to Perfection (Jensen-Haise Method), the negative value means, the tendency to over-estimate the measured AET.

The value of NSE is closer to 1, which indicates that the estimated PET match perfectly with the measured AET using Bowen Ratio method (Jensen-Haise Method); the negative values means that the results calculated from Makkink Method and Turc Method are worse than simply using average measured AET.

5 CONCLUSIONS

A comparison of different agriculture-based ET methods showed that there are great differences in their performance; overall, the Jensen-Haise Method has the closest relationship with Bowen Ratio method, and it is concluded that it is the most accurate approach for estimating ET from the Hooton Reserve Raingarden (for August 2016).

Future work will involve more agriculture-based ET equations and data collected for a longer period of time.

A similar evaluation for other low impact development applications (vegetated rooftops, vegetated traffic island, etc.) would also produce practical benefits.

ACKNOWLEDGEMENTS

This research is partially funded by the Open Research Fund Program of the Key Laboratory of Urban Stormwater System and Water Environment (Beijing University of Civil Engineering and Architecture), Ministry of Education. The corresponding author gratefully acknowledge the travel grant from New Zealand Hydrology Society. The authors would like to thank the Auckland Council and Auckland Transport for their support in establishing the research site.

REFERENCES

- Allen, R. G., Pereira, L. S., Raes, D & Smith, M. (1998). *Crop Evapotranspiration-Guidelines for Computing Crop Water Requirements – FAO Irrigation and Drainage Paper 56*, FAO, Rome.
- Allen, R. G., Pereira, L. S., Smith, M., Raes, D. & Wright, J. L. (2005). FAO-56 Dual Crop Coefficient Method for Estimating Evaporation from Soil and Application Extensions. *Journal of Irrigation and Drainage Engineering-ASCE*, 131(1), 2-13.
- Burt, T. P. & McDonnell J. J. (2015). Whither Field Hydrology? The Need for Discovery Science and Outrageous Hydrological Hypotheses. *Water Resources Research*, 51, doi: 10.1002/2014WR016839.
- Flint, A.L. & Childs, S.W. (1991). Use of the Priestley–Taylor Evaporation Equation for Soil Water Limited Conditions in a Small Forest Clearcut. *Agricultural and Forest Meteorology*, 56, 247–260.
- Hargreaves, L. G., Hargreaves, G. H. & Riley, J. P. (1985). Irrigation Water Requirements for Senegal River Basin. *Journal of Irrigation and Drainage Engineering-ASCE*, 111(3), 265-275.
- Jensen, M. E. & Haise, H. R. (1963). Estimating Evapotranspiration from Solar Radiation. *Journal of Irrigation and Drainage Engineering-ASCE*, 93(IR3), 15-41.
- Makkink, G. F. (1957). Testing the Penman Formula by Means of Lysimeters. *Journal of the Institution of Water Engineers*, 957(11), 277-288.
- Priestley, C.H.B. & Taylor, R.J. (1972). On the Assessment of Surface Heat Flux and Evaporation Using Large-Scale Parameters. *Monthly Weather Review*, 100(2), 81-92.
- Turc, L. (1961). Estimation of Irrigation Water Requirements, Potential Evapotranspiration: A Simple Climatic Formula Evolved Up to Date. *Advances in Agronomy*, 12, 13-49.
- Xu, C. Y. & Singh, V. P. (2002). Cross Comparison of Empirical Equations for Calculating Potential Evapotranspiration with Data from Switzerland. *Water Resources Management*, 16(3), 197-219.

COMPARISON OF TWO APPROACHES FOR THE MODELLING OF GREEN STORMWATER INFRASTRUCTURES

JULIEN LHOMME⁽¹⁾, JONATHAN KLARIC⁽²⁾ & DAVID FORTUNE⁽³⁾

^(1,3) XP Solutions, Newbury, United Kingdom,
julien.lhomme@xpsolutions.com , david.fortune@xpsolutions.com
⁽²⁾ XP Solutions, Brisbane, Australia,
jonathan.klaric@xpsolutions.com

ABSTRACT

Green Stormwater Infrastructures are now commonly used in urban and peri-urban developments or retro-fitted operations in many countries around the world. However, the representation of the flow and pollutant movements in these structures for design or modelling purposes is still a matter of research, development and investigation. This study compares two approaches for the representation of Green Stormwater Infrastructures as part of a drainage system: (i) a conceptual representation of the hydraulic processes based on a Muskingum routing scheme; and (ii) a physics-based representation of the hydraulic processes using the core calculations of EPA SWMM5 for Low Impact Developments (LID) (although modified to be used as network components and not as part of a catchment). The two approaches are compared on a simple study case featuring a sustainable drainage structure connected to a conventional drainage network. Differences in the respective algorithms are scrutinized to explain the differences in results. The comparison of the results given by the two engines highlight the critical parameters that are common between the two engines which allow the engines to give very similar results with the appropriate setup. Assumptions made in the physics-based approach lead to the absence of attenuation and delay in the outflow hydrograph. This appears to be a deficiency and will be addressed in the future.

Keywords: Sustainable drainage; LIDs; WSUD; SuDS; SWMM.

1 INTRODUCTION

As the use of Green Stormwater Infrastructures become more widespread, there is a growing need to represent numerically these structures for design and modelling purposes. Green Stormwater Infrastructures, are described in the UK as Sustainable Drainage Systems (SuDS), in Australia as Water Sensitive Urban Design (WSUD) and in the United States and other countries area referred to as Low Impact Development (LID), which is the term used in this paper. Although guidelines exist for the design of these structure, for example the SuDS Manual in the UK (Woods Ballard et al., 2015), the New York State Stormwater Management Design Manual (NYS DEC, 2010), the City of Melbourne WSUD Guidelines (City of Melbourne 2009), they are only suited to simple configurations and isolated structures.

There are a number of software tools that can be used to represent the behavior of LIDs and help with the design of such structures. Some software use specific algorithms: for example SWMM (EPA, 2017), Music (eWater, 2017), WinSLAMM (PVA, 2017), and XPDRAINAGE (XP Solutions, 2017). Conversely a number of commercial programs rely, at least partly, on the SWMM computational engine for representing the LIDs.

A number of studies have been done previously looking either at comparing one LID modelling approach with experimental results (Brunetti et al., 2017; Massoudieh et al., 2017; Brown et al., 2013; Dussailant et al., 2004) or comparing “on paper” the abilities of a selection of LID-specific software (Elliott and Trowsdale, 2007). Comparing several modelling approaches dedicated to LIDs is not reported in the literature, unlike for other aspects of stormwater modelling, or more generally hydraulic and hydrological modelling (Fewtrell et al., 2011; Leandro et al., 2009; Lhomme et al., 2006; Horritt and Bates, 2002), and ground water modelling (Sulis et al., 2010; Gandolfi et al., 2006). That may be because of the relative “youth” of such approaches that combine different aspects of surface and groundwater modelling.

In this study, two software with LID capabilities, XPDRAINAGE and a modified version of SWMM, are compared because they use very different representations of the LIDs. The aim is first to see how much difference the two approaches generate in modelling of a simple LID, and secondly to identify if the two computational engines can be configured to give almost identical results and how much change to each engine is needed for this.

The first computational engine considered is the flow routing engine featured in the XPDRAINAGE design software, this is referred to as the “conceptual engine”. The second computational engine considered here is a modified version of the SWMM5 flow engine, this is referred to as the “physics-based engine”.

The two engines are first described in Section 2, then their results are compared on a simple test case in Section 3.

2 DESCRIPTION OF THE COMPUTATIONAL ENGINES

The two computational engines used in this investigation have been developed independently and both have very different approaches to the modelling of hydraulic processes in a drainage network and in Green Stormwater Infrastructures. They have however in common a very detailed description of the LID structures.

2.1 The conceptual engine

LIDs are represented as individual objects in the conceptual engine. Seven types of LIDs were available where each one is made of a combination of a Ponding Area, a Filter Area that can be made of several layers and contain an under-drain, one or several Inlets and Outlets.

Muskingum routing was used in the conceptual engine to represent channeled flow and filtered flow. It is suitable for drainage systems with significant time of travel between inlet and outlet and some flattening of the hydrograph, either because of long channeled flow, or because flow was filtered slowly. It was used to route flow through LIDs and Connections (*i.e.* links). The Muskingum routing method is based on the continuity equation (Eq. [1]) and the equation of storage in the channel/reach/pipe/system (Eq. [2]).

$$I - Q = \frac{dS}{dt} \quad [1]$$

$$S = K(\theta I + (1 - \theta)Q) \quad [2]$$

where I is the inflow, Q is the outflow, S is the reach storage, K represents the travel time through the reach (Retention time), θ is the Retention coefficient. These two equations are combined into a routing equation relating outflow to inflow over the timestep Δt from time t_n to time t_{n+1} :

$$Q_{n+1} = \frac{-K\theta + 0.5\Delta t}{K(1 - \theta) + 0.5\Delta t} I_{n+1} + \frac{K\theta + 0.5\Delta t}{K(1 - \theta) + 0.5\Delta t} I_n + \frac{K(1 - \theta) - 0.5\Delta t}{K(1 - \theta) + 0.5\Delta t} Q_n \quad [3]$$

These simple equations are well suited to represent flow through sustainable drainage systems because of the natural choice of states and parameters (in terms of the design process). Maximum storage is either a design aim or can be estimated easily. Similarly, travel time is either a design aim or can be approximated fairly by using a friction loss equation and length between input and output locations.

The Retention coefficient is less straightforward to estimate. 0.5 is the maximum possible value and gives no attenuation of the hydrograph (*i.e.* translation only). Values between 0.2 and 0.4 are well suited for natural channels. A value of 0.4 would be a reasonable estimate for swales and 0.2 for bioretention systems.

For sustainable drainage systems, the travel time was calculated both along the length of the system and down through the filter layers. This was done as a simple calculation of 'along + down', where along is along the fastest route through the system (along channel for a swale and through bottom drainage layer for bioretention). While the Muskingum method gives the output hydrograph value at every time step, it does not calculate levels. The water levels in each structure were calculated from the current stored volume, after the volumes have been updated. This allows the engine to compute the hydraulic grade line.

A Time of Travel is calculated for pipes and channels using the Manning equation, the routing through the connections is done as a simple translation (*i.e.* no attenuation).

2.2 The physics-based engine

This engine is derived from the open-source SWMM5 engine and includes some additional functionalities such as Hydraulic LIDs, custom hydrology, OpenMI linking. The SWMM5 engine was based on the one-dimensional shallow-water equations (*i.e.* the St Venant equations) and these equations were solved with a finite difference scheme (Rossman, 2006). Although the numerical scheme can solve either the complete equations (*i.e.* dynamic wave) or a simplified set of equations (*i.e.* kinematic wave), only the dynamic wave is considered here.

In the regular SWMM5, LIDs can be specified as part of a catchment characteristics. Eight types of LIDs are available and can be combined in one or several catchments. They receive the catchment outflow and release the flow to the node the catchment drains to. A LID is represented by a set of several layers (typically surface, soil, storage) that have a calculated water depth or moisture content (Figure 1). During the computation, water was moved between the layers or leaves the LID according to the following flow equations (Rossman and Huber, 2016):

- The Green-Ampt equation for the infiltration from the surface layer to the soil layer, Eq. [4];
- The Darcy equation for the percolation through the soil layer, Eq. [5];
- The Manning equation for the outflow from the surface layer, Eq. [6].

Each layer was characterized by a height or a thickness, a porosity or a void ratio, a hydraulic conductivity, a seepage rate or a friction coefficient. Each Hydraulic LID also has a length and a width parameters.

$$f_1 = K_{2S} \left(1 + \frac{(\phi_2 - \theta_{20})(d_1 + \psi_2)}{F} \right) \quad [4]$$

$$f_2 = \begin{cases} K_{2S} \exp(-HCO(\phi_2 - \theta_2)) & \theta_2 > \theta_{FC} \\ 0 & \theta_2 \leq \theta_{FC} \end{cases} \quad [5]$$

$$q_1 = \frac{1}{n} b (d_1 - D_1)^{5/3} S^{1/2} \quad [6]$$

where K_{2S} is the soil saturated hydraulic conductivity (ft/sec), ϕ_2 is the porosity of the soil layer, ψ_2 is the suction head for the soil layer, HCO is referred to as the conductivity slope, D_1 is freeboard height (*i.e.* berm height) for surface ponding, S is the slope of the surface layer, b is the width of the LID, n is the Manning friction coefficient, d_1 is the depth of water stored in the surface layer, θ_{20} is the moisture content at the top of the soil layer, θ_2 is the soil moisture content, θ_{FC} is the soil field capacity moisture content, F is the cumulative infiltration volume per unit area.

In the modified version of SWMM5 considered here, with the Hydraulic LIDs functionality, LIDs can be specified as part of the hydraulic network. This means several LIDs can be combined into a “treatment train”, or one LID can treat the flows from several catchments.

Hydraulic LIDs have been implemented in such a way that they re-use the core computational functions of Catchment LIDs of SWMM5. Like for a Catchment LID, a Hydraulic LID is an “instance” of a LID process as defined in the library of “LID Controls”.

A Hydraulic LID is treated as a Link in the drainage network and in the algorithm. The inflow is taken from the upstream node instead of being the runoff flow from the catchment. The outflow is passed on to the downstream node as for a normal link.

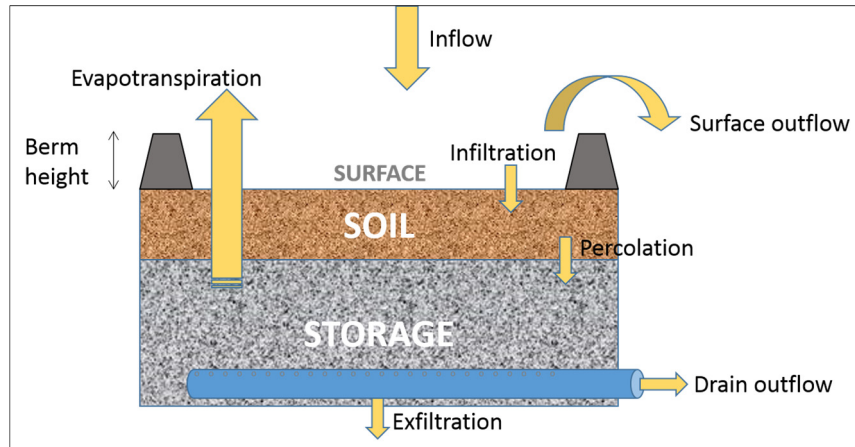


Figure 1. Vertical representation of the LID in the physics-based engine.

3 COMPARISON OF THE TWO ENGINES

3.1 Study case

This is a very simple study case with 1 Bio Retention, or Bio Cell, that is connected to a pipe upstream and downstream (Figures 2 and 3). All parameters for the pipes, manholes and LIDs are the same in both engine setups (see Table 1). The inflow hydrograph is made of two rectangular flow “impulses” (Figure 4).

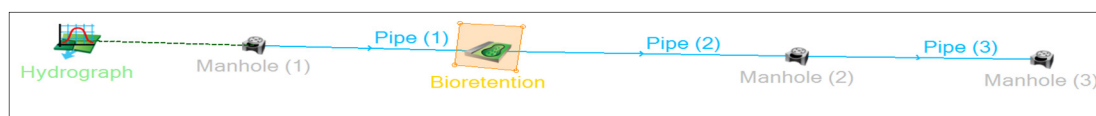


Figure 2. Schematic plan view of the study case as displayed in the XPDRAINAGE software.

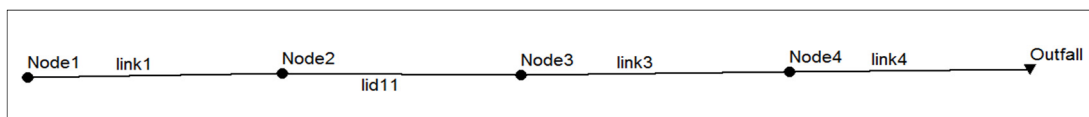


Figure 3. Schematic plan view of the study case as displayed in the EPA SWMM5 interface, where 'lid11' is the Hydraulic LID.

Table 1. Hydraulic properties of the pipes and the Bioretention.

	PROPERTY	VALUE (US UNITS)	VALUE (SI UNITS)
Pipes	Diameter (ft), (m)	1.0	0.305
	Manning n	0.015	0.015
	Slope (ft/ft), (m/m)	0.003	0.003
Bioretention Surface Layer	Length (ft), (m)	30.0	9.14
	Width (ft), (m)	30.0	9.14
	Slope (ft/ft), (m/m)	0.001	0.001
	Manning n	0.1	0.1
	Outlet or Berm height (ft), (m)	3.0	0.91
Bioretention Filter / Soil Layer	Depth (ft), (m)	4.0	1.22
	Filtration rate or conductivity (in/hr), (mm/hr)	5.0	127
	Void ratio or porosity (%)	50	50
	Field Capacity (%)	20	20
	Wilting Point (%)	0	0

Note that the Retention times in the conceptual engine were set to 5 and 120 minutes for the surface layer and the soil layer respectively. These are typical values for a Bioretention. The Retention Coefficients are set to 0.20 for the two layers.

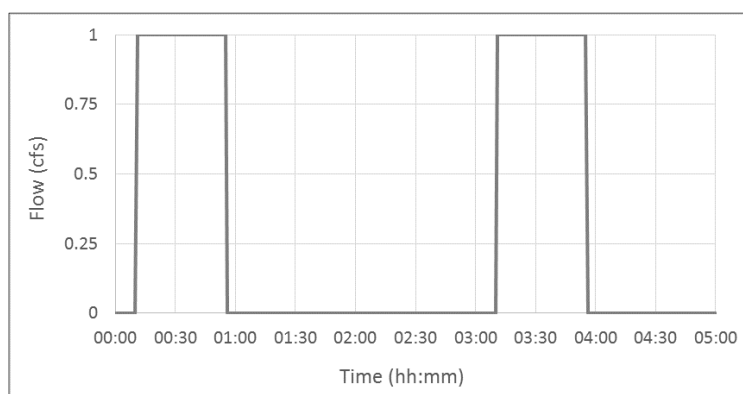


Figure 4. Inflow hydrograph (in cubic feet per second).

3.2 Initial comparison

Following the initial setup, the simulation results from both engines showed very similar outflow hydrographs (Figure 5), but the internal levels were actually quite different (Figure 6). Note that the first “flow impulse” was entirely stored within the Bioretention, but the second impulse generates an outflow as the Bioretention had not yet recovered to its full capacity (there is still water stored in the Surface layer). The differences between the two engines were considered in order to explain different results.

The calculation of infiltration is a significant difference between the 2 engines, a constant infiltration rate is used in the conceptual engine, whereas the physics-based engine uses a Green-Ampt relation. The effective infiltration rate given by the Green-Ampt equation was higher than the hydraulic conductivity, leading to more infiltration with the physics-based engine. This explains why the depth of water stored in the surface layer (eq. to Ponding area) was less than with the conceptual engine.

In the conceptual engine setup, the flow leaving the LID had been configured to be dictated by the downstream pipe. However, the LID outflow was calculated using a Manning relation in the physics-based engine, using the full LID width and the head over the Berm height, regardless of the size of the downstream pipe. This explains why the peak outflow with the conceptual engine is similar to the one with the physics-based engine despite the head being greater (as the wide “channel-type” outflow is greater than the pipe outflow for a given head).

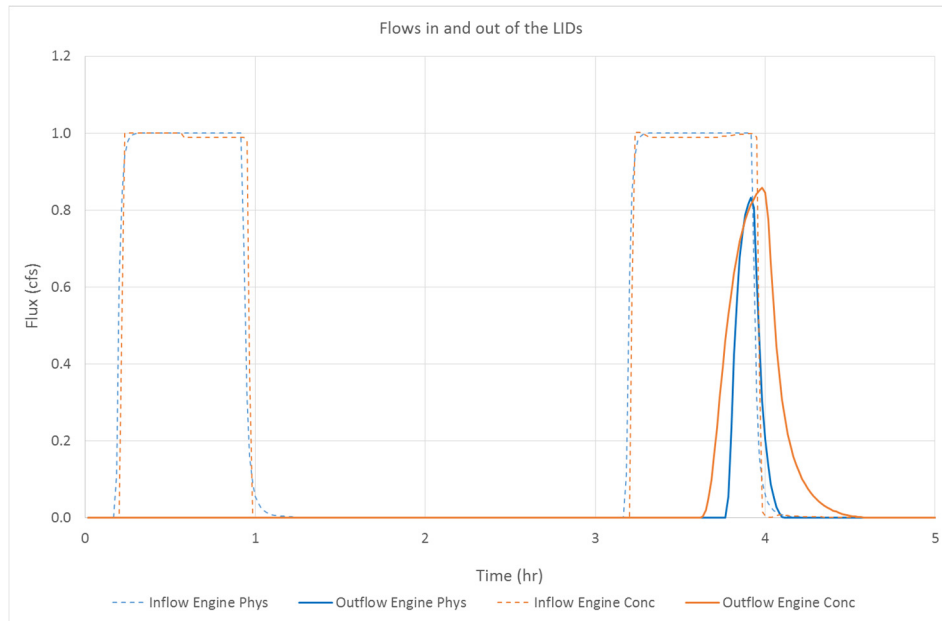


Figure 5. Comparison of inflows and outflows in the LID.

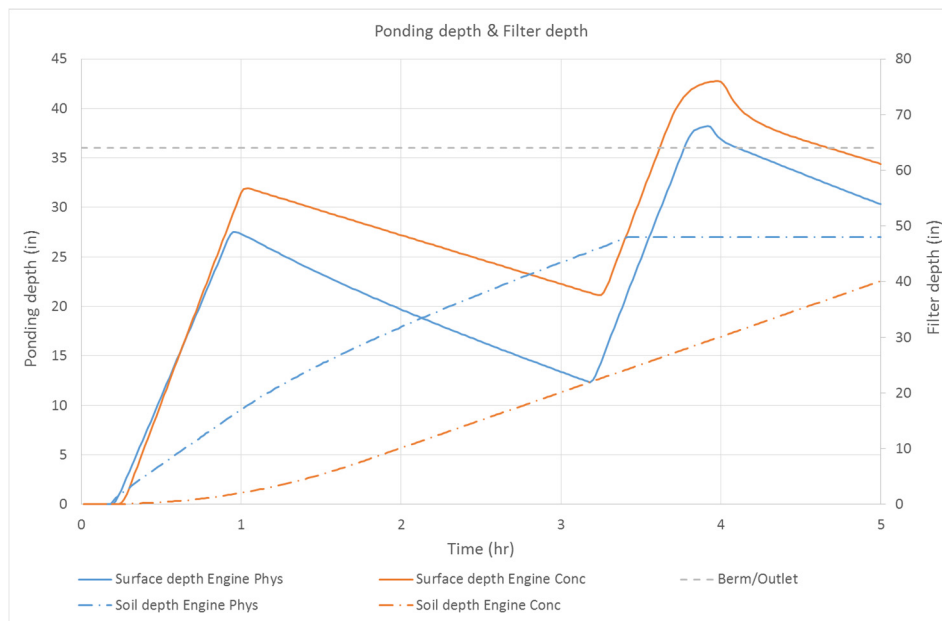


Figure 6. Comparison of water depths in the LID.

3.3 Changes to the setup

Having compared the results given by the two engines when using a default configuration in each of the two tools, an attempt was made to produce more similar results. More than getting similar results from the two engines, the intention was to highlight which were the key parameters and processes in each engine that caused the results to be different.

As mentioned in the previous section, the two main sources of differences between the two engine runs were the calculation of the infiltration rate and the LID outflow.

The conceptual engine does not allow specifying explicitly a channel-type outflow calculation as used by the physics-based engine. However, it is possible to use a depth-flow table to replicate this outflow. Also, the pipes downstream of the Bioretention have been enlarged in the conceptual engine setup to avoid any restriction of the flow leaving the LID.

The physics-based engine cannot be setup with a constant infiltration rate into and through the soil layer. Therefore, the source code is modified to bypass the Green-Ampt infiltration calculation and just use the hydraulic conductivity instead, like the conceptual engine does. Also, the Conductivity slope parameter was set to zero to make the Darcy flow constant and equal to the hydraulic conductivity. This allows the two engines setup to be more similar than previously.

Another aspect of the conceptual engine to be considered is the attenuation and delay introduced by the Muskingum approach in the routing through the LID. Conversely, the physics-based engine makes 2 assumptions for the calculation of water level and fluxes in layers:

- Inflow to the LID was distributed uniformly over the top surface;
- Moisture content was uniformly distributed throughout the soil layer.

This means that there is no delay and attenuation introduced by the physics-based engine through the LID. For the sake of making the two engines setup as close as possible, the retention times for the Ponding and Filter areas are set to zero (*i.e.* no delay) in the conceptual engine, and the retention coefficients are set to the maximum value (0.5 *i.e.* no attenuation).

3.4 Revised comparison

The calculated hydrographs with the revised setup are now very close (Figure 7), mainly with the spread of the hydrographs being more similar than with the initial setup. Also, noticeably the water depths are much closer than previously due to the change in the infiltration calculation for the physics-based engine (Figure 8). This confirms that the key differences in the two engines have been identified: (i) calculation of the infiltration rate; (ii) calculation of the LID outflow; (iii) calculation of the LID routing.

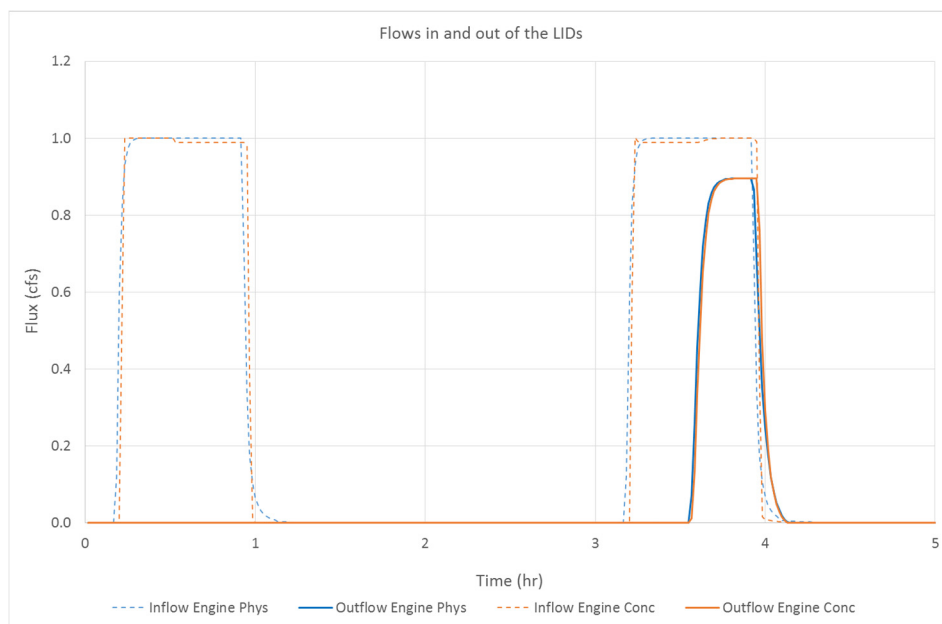


Figure 7. Revised comparison of inflows and outflows in the LID.

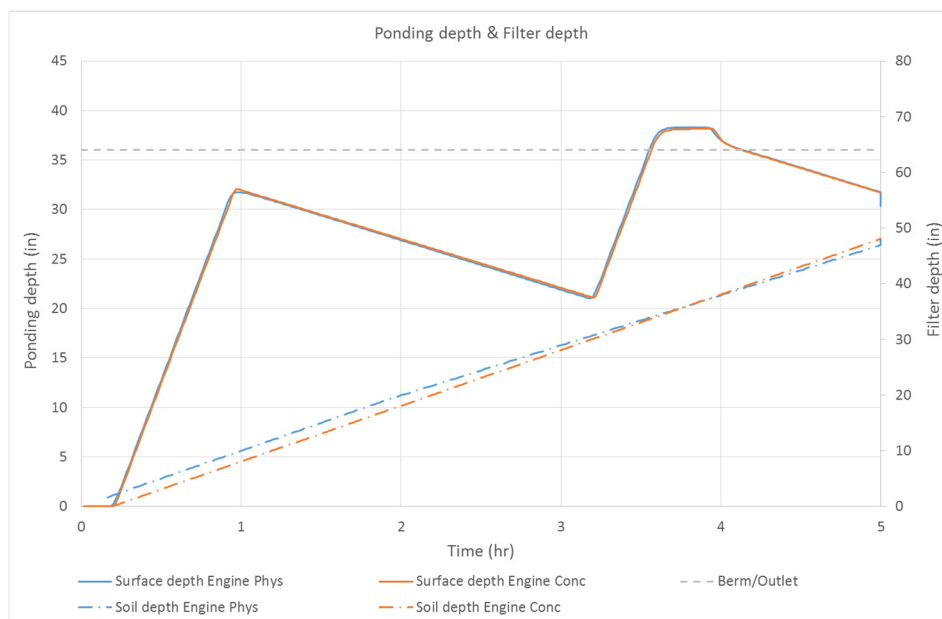


Figure 8. Revised comparison of water levels in the LID.

4 CONCLUSIONS

The comparison of the results given by the two engines and the changes made to the original engines setup have highlighted (i) the critical parameters that are common between the two engines; and (ii) the other parameters that control the processes represented in different ways.

The initial comparison of the two engines on a test Bioretention LID structure shows some clear differences in the results when a typical setup is used for each engine. However, it has been shown that with an appropriate setup the two engines give very similar results. The key differences in the two engines have been identified as: (i) calculation of the infiltration rate; (ii) calculation of the LID outflow; (iii) calculation of the LID routing. The differences in infiltration and outflow calculation are relatively straightforward to reduce as the relevant equations in the engines can be easily altered. For these two processes the physics-based engine is more attractive because of the more advanced equations used.

Regarding the attenuation and delay, it is a process that is currently ignored by the physics-based engine, because of the assumption of uniform distribution of water within the layers. It is likely that this limitation has a limited impact for a Catchment LID (*i.e.* the original application of the LID functions in SWMM5), as the hydrograph coming in the LID is already spread out. However, for a Hydraulic LID this assumption seems too simplistic. It is realistic to think that some degree of attenuation and delay is necessary to represent well the hydrograph transformation through the Hydraulic LID, like what is done in the conceptual engine. This could be achieved by introducing additional routing functions to attenuate the outflow hydrograph, or alternatively by splitting each LID structure in several smaller sub-units.

Future work will involve comparing the engine results with experimental data on LIDs to evaluate how much attenuation and delay is really needed. Also, more LID structures will be tested and a relatively complex, realistic test case with multiple LIDs will be simulated.

ACKNOWLEDGEMENTS

The authors would like to acknowledge the support of the US EPA to the SWMM flow engine and user interface over the years.

REFERENCES

- Brown, R., Skaggs, R.W. & Hunt, W. (2013). Calibration and Validation of DRAINMOD to Model Bioretention Hydrology. *Journal of Hydrology*, 486, 430-442.
- Brunetti, G., Šimůnek, J., Turco, M. & Piro, P. (2017). On the Use of Surrogate-Based Modeling for the Numerical Analysis of Low Impact Development Techniques. *Journal of Hydrology*, 548, 263-277.
- City of Melbourne (2009). *Water Sensitive Urban Design Guidelines*, Melbourne Water, (<http://www.melbourne.vic.gov.au/SiteCollectionDocuments/wsud-full-guidelines.pdf>).
- Dussaillant, A.R., Wu, C.H. & Potter, K.W. (2004). Richards Equation Model of a Rain Garden. *Journal of Hydrologic Engineering*, 9(3), 219-225.
- Elliott, A. & Trowsdale, S. (2007). A Review of Models for Low Impact Urban Stormwater Drainage. *Environmental Modelling & Software*, 22(3), 394-405.
- Environment Protection Agency (EPA). (2017). Homepage for the SWMM5 Software, United States, (<https://www.epa.gov/water-research/storm-water-management-model-swmm>).
- eWater (2017). Homepage for the MUSIC Software, Evolving Water Management, (<http://www.ewater.org.au/products/music/>).
- Fewtrell, T.J., Duncan, A., Sampson, C.C., Neal, J.C. & Bates, P.D. (2011). Benchmarking Urban Flood Models of Varying Complexity and Scale Using High Resolution Terrestrial LiDAR Data. *Physics and Chemistry of the Earth, Parts A/B/C*, 36(7), 281-291.
- Gandolfi, C., Facchi, A. & Maggi, D. (2006). Comparison of 1D Models of Water Flow in Unsaturated Soils. *Environmental Modelling & Software*, 21(12), 1759-1764.
- Horritt, M.S. & Bates, P.D. (2002). Evaluation of 1D and 2D Numerical Models for Predicting River Flood Inundation. *Journal of Hydrology*, 268(1), 87-99.
- Hunter, N.M., Bates, P.D., Neelz, S., Pender, G., Villanueva, I., Wright, N.G., Liang, D., Falconer, R.A., Lin, B., Waller, S., Crossley, A.J. & Mason, D. (2008). Benchmarking 2D Hydraulic Models for Urban Flood Simulations. *Proceedings of the Institution of Civil Engineers: Water Management*, 161(1), 13-30.
- Leandro, J., Chen, A.S., Djordjević, S. & Savić, D.A. (2009). Comparison of 1D/1D and 1D/2D Coupled (Sewer/Surface) Hydraulic Models for Urban Flood Simulation. *Journal of Hydraulic Engineering*, 135(6), 495-504.
- Lhomme, J., Bouvier, C., Mignot, E. & Paquier, A. (2006). One-Dimensional GIS-Based Model Compared with a Two-Dimensional Model in Urban Floods Simulation. *Water Science and Technology*, 54(6-7), 83-91.
- Massoudieh, A., Maghrebi, M., Kamrani, B., Nietch, C., Tryby, M., Aflaki, S. & Panguluri, S. (2017). A Flexible Modeling Framework for Hydraulic and Water Quality Performance Assessment of Stormwater Green Infrastructure. *Environmental Modelling & Software*, 92, 57-73
- Division of Water (2010). *Stormwater Management Design Manual*, Department of Environmental Conservation, New York State.

- PV & Associates (2017). Homepage for the WinSLAMM Software, (<http://www.winslamm.com/>).
- Rossman, L. (2006). *Storm Water Management Model Quality Assurance Report: Dynamic Wave Flow Routing*, US Environmental Protection Agency, Office of Research and Development, National Research Management Research Laboratory.
- Rossman, L. & Huber, W. (2016). *Storm Water Management Reference Manual: Volume III Water Quality*, US EPA.
- Sulis, M., Meyerhoff, S.B., Paniconi, C., Maxwell, R.M., Putti, M. & Kollet, S.J. (2010). A Comparison of Two Physics-Based Numerical Models for Simulating Surface Water–Groundwater Interactions. *Advances in Water Resources*, 33(4), 456-467.
- Ballard, B.W, Wilson, S., Udale-Clarke, H., Illman, S., Scott, T., Ashley, R. & Kellagher, R. (2015). *The SuDS Manual, C753*, CIRIA, London, UK.
- XP Drainage (2017) Documentation for the XPDRAINAGE Software, XP Solutions, (<http://help.xpsolutions.com/display/XDH2017v1>).

HOMOGENEITY TESTING AND TRENDS ANALYSIS IN LONG TERM RAINFALL DATA FOR SUNGAI PAHANG RIVER BASIN OVER 40 YEARS RECORDS

CHUN KIAT CHANG⁽¹⁾, AMINUDDIN AB. GHANI⁽²⁾, HOW TION PUAY⁽³⁾ & MAZLINA ALANG OTHMAN⁽⁴⁾

^(1, 2, 3, 4)River Engineering and Urban Drainage Research Centre (REDAC),
Universiti Sains Malaysia, Engineering Campus, Nibong Tebal, Penang, Malaysia
redac10@usm.my; redac02@usm.my; redac_puay@usm.my; emona1510@gmail.com

ABSTRACT

Current design of infrastructure is primarily based on precipitation Intensity-Duration-Frequency (IDF) curves. For this reason, the accuracy and reliability of the hydrological analysis relied on the quality of the rainfall data used. Rainfall data should be checked and tested for its reliability and homogeneity before being used for further analysis. However, factors such as location of the station, the tool and method of data recording, collection and observation quality will affect the homogeneity of rainfall records. For that reason, a subsample of 9 stations that have more than 40 years of observations obtained from the Department of Irrigation and Drainage (DID) Malaysia located in Sungai Pahang river basin are investigated for homogeneity by using four absolute homogeneity tests. These include the Standard Normal Homogeneity test (SNHT), Pettitt test, Buishand Range test (BRT), and Von Neumann ratio (VNR) test. The result of each method was evaluated at the 95% significance level. The annual rainfall amount was used as testing variable and the results from four tests were then combined into three classes: 'useful', 'doubtful' and 'suspect'. Among all rainfall stations within the river basin, there are only 1 station (Kg Merting, ID = 4223115) was inhomogeneous (labeled as "suspect"), whilst remaining 8 of rainfall stations are homogeneous and considered as "useful". From the analysis of trends, only 2 of the stations (Rumah Pam Pahang Tua, ID = 3533102 and Kg Merting, ID = 4223115) indicate statistically increasing trend. Inhomogeneity of rainfall data at station Kg Merting may correspond to the result of statistically increasing trend in that station. The findings of the study will be useful for planning and designing infrastructure in managing floods, as well as flood risk and infrastructure systems failure risk in Sungai Pahang river basin.

Keywords: Homogeneity test; trend analysis; IDF curves; rainfall extreme; Sungai Pahang river basin.

1 INTRODUCTION

Reliable database for hydrologic analyses depends on the quality of the long-term rainfall record. It is often inconsistent or inhomogeneous caused by changes of the location and measuring and observing techniques of the rainfall station (Peterson et al., 1998). Furthermore, rainfall observation systems were not well distributed or equipped especially before 1980s, leading to the additional potential errors in long term rainfall records (Che Ros et al., 2016). Increased climate variability also leads to changes in the long term of rainfall record and is expected to affect flood/drought events. It is essential to check the inhomogeneity and identify the presence of shifts or trends related to changes of the rainfall records for more reliable hydrologic analyses.

The homogeneity tests of time series are classified in two groups of 'relative method' and 'absolute method'. In relative method, neighboring stations are used in the testing process while the test is applied for each station individually in absolute method. Peterson et al. 1998 suggested using the relative method because this method easily detect inhomogeneity. However, this method did not show how real changes can be distinguished from random fluctuations (Buishand, 1982). Absolute method uses statistical analysis to check inhomogeneity. Different statistical methods have been regularly used by researchers to detect inhomogeneity and break year in rainfall data. Wijngaard et al. (2003) used the standard normal homogeneity test (SNHT), Buishand range test (BRT), Pettitt test and Von Neumann ratio (VNR) test for testing the homogeneity in European climate. The test results were then condensed in a three-class system with categories termed 'useful', 'doubtful' and 'suspect'. This hybrid method seems like a good choice given the fact that different methods have different sensitivity of break.

A trend analysis is one of the tools to provide useful information on tendency change of rainfall data in the future. Different statistical test methods are used to detect trends in hydrological and classified as parametric and nonparametric tests (Chen et al., 2007). Parametric tests require independent data and normally distributed, which is rarely true for hydrological time series data. For nonparametric tests, data must be independent, but the outliers are better tolerated. The most common nonparametric tests for working with time series trends are the Mann-Kendall (Mann, 1945). It is widely used to assess the trend of hydrological time series (Yue et al., 2002; Shadmani et al., 2012). A number of studies have dealt with homogeneity and

trend analysis for rainfall data in Malaysia by using MK test (Suhaila et al., 2010; Mayowa et al., 2015; Che Ros et al., 2016). Their studies vary depending on the duration of the time series, number of rainfall station and the method of statistical tests used. In this study, statistical test was carried out to detect homogeneity and trends of long term rainfall record within the Sungai Pahang River Basin.

2 STUDY AREA

Sungai Pahang river basin is located in the eastern part of Peninsular Malaysia between latitude $02^{\circ} 48' 45''$ N and $04^{\circ} 40' 24''$ N and between longitude $101^{\circ} 16' 31''$ E and $103^{\circ} 29' 34''$ E. Sungai Pahang river basin (Figure 1) drains an area of 29,300 km² of which 27,000 km² lies within Pahang (which is about 75% of the State) and 2,300 km² is located in Negeri Sembilan. Sungai Pahang is the longest river in the Peninsular Malaysia at about 435 km. Sungai Pahang actually begins from Kuala Tembeling at the confluence of two equally large and long rivers. About 304 km from the river mouth in the central north, Sungai Jelai emerges from the Titiwangsa Range at the northwestern tip of the Sungai Pahang Basin, while Sungai Tembeling originates from the Timur Range at the northeastern edge of the basin. Other main tributaries of Sungai Pahang are Semantan, Teriang, Bera and Lepar. Sungai Pahang system begins to flow in the south east and south directions from the north passing along such major towns as Kuala Lipis, Jerantut and Temerloh, finally turning eastward at Mengkarak in the central south flowing through Pekan town near the coast before discharging into the South China Sea.

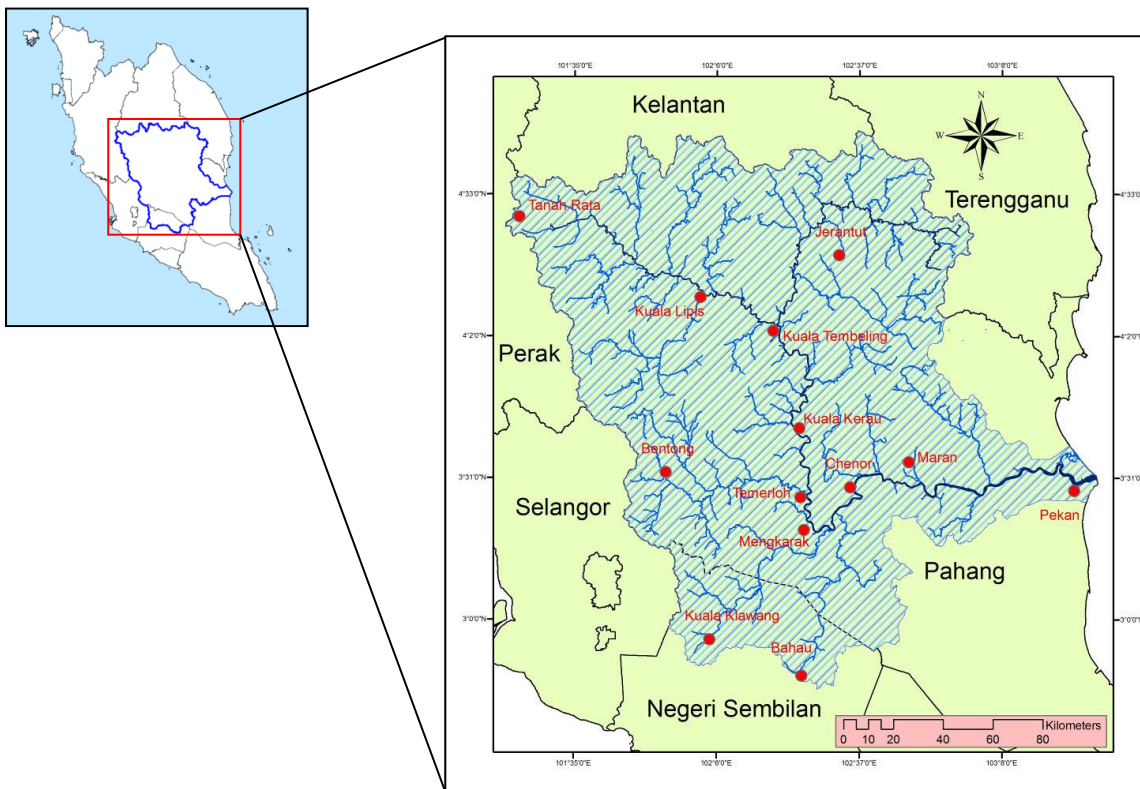


Figure 1. Sungai Pahang River Basin Delineation.

The climate of Pahang river basin is mainly governed by the regime of Northeast and Southwest monsoon winds. Southwest monsoon occurs between March and September. The Northeast monsoon wind lasts from October to January. Northeast monsoon season is mainly responsible for the heavy rain which hits the east coast of Pahang state and causes flooding. The annual rainfall varies from approximately between 1,700 mm to 3,500 mm within the river basin, and relatively high annual rainfalls are observed from Cameron Highlands to the east coast along the north boundary of the river basin. The rainy season starts from September and the maximum monthly average rainfalls are observed in November or December for all the stations, while the driest months are observed in June and July.

3 DATA AND METHODOLOGY

This study examined long term rainfall record in the Pahang river basin for homogeneity and trend analysis. There are about one hundred fifty-nine (159) numbers of rainfall stations within the Sungai Pahang river basin. Due to the accuracy and complete data, only nine (9) rainfall stations were used for the analysis. Rainfall data were obtained from Drainage and Irrigation Department (DID), Malaysia for a period approximately 40 years. Table 1 and Figure 2 show the location of 9 stations in Sungai Pahang river basin

with the geographical coordinates. Most of the rainfall data used in the present study are recorded from the automatic recorded rain gauges where the data are normally measured using a tipping bucket rain gauge with a sensitivity of 0.5 mm per tip. This study used annual rainfall amount as the testing variable and this value was used only if 90% of the daily rainfall data are valid. At the first step in any analysis of homogeneity, the rainfall time series was plotted on a linear scale to check the existence of marked changes in time series. Then, further investigation was done through statistical procedures. The methods proposed by Wijngaard et al. (2003) were used to check the homogeneity of the data and trend detection analysis was then performed through Mann Kendall (MK) non-parametric tests. In addition, the magnitude of the trend was calculated using the Sen's slope approach. Homogeneity and MK test for the time series were conducted using XLSTAT statistical software. XLSTAT is a data analysis and statistical application available for Microsoft Excel.

Table 1. Rainfall stations at study area.

Station ID	Station Name	Latitude	Longitude	Duration
3121143	Simpang Pelangai	03° 10' 30" N	102° 11' 50" E	1975 – 2013
3424081	JPS Temerloh	03° 26' 20" N	102° 25' 35" E	1970 – 2013
3533102	Rumah Pam Pahang Tua	03° 33' 40" N	103° 21' 25" E	1970 – 2013
3628001	Pintu Kawalan Paya Kertam	03° 38' 00" N	102° 51' 20" E	1975 – 2013
3924072	Rumah Pam Paya Kangsar	03° 54' 15" N	102° 26' 00" E	1970 – 2013
4023001	Kg Sungai Yap	04° 01' 55" N	102° 19' 30" E	1973 – 2013
4219001	Bukit Betong	04° 14' 00" N	101° 56' 25" E	1974 – 2013
4223115	Kg Merting	04° 14' 35" N	102° 23' 00" E	1970 – 2013
4513033	Gunung Brinchang	04° 31' 00" N	101° 23' 00" E	1975 - 2013

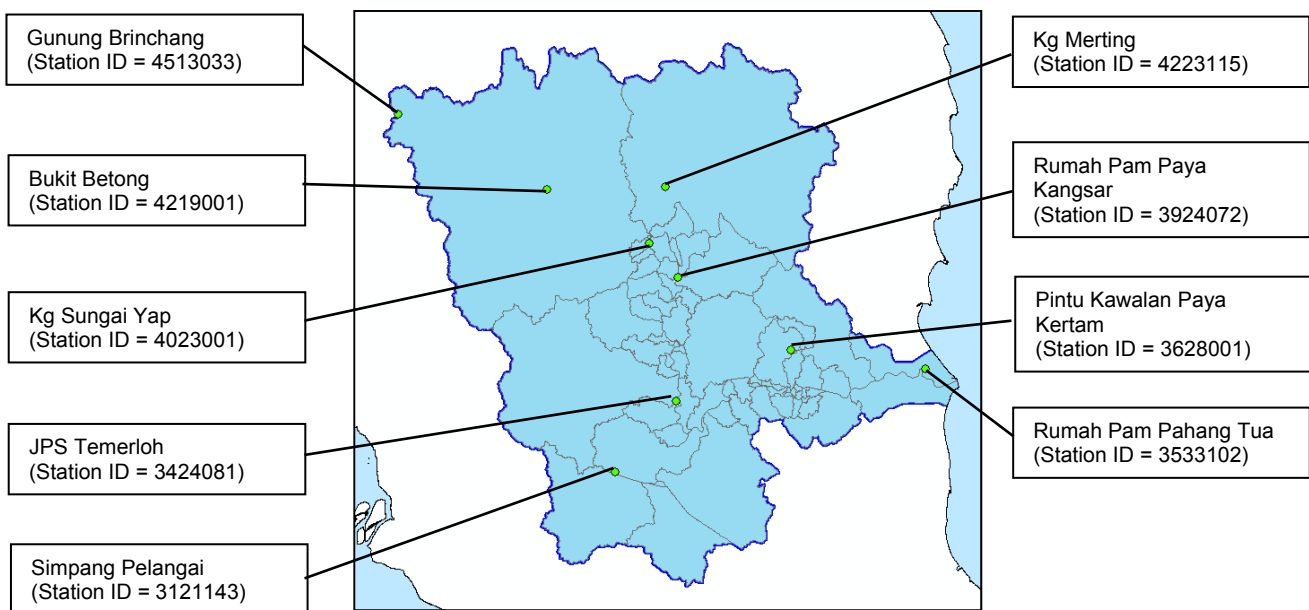


Figure 2. Location and ID numbers of the rainfall station.

4 RESULTS AND DISCUSSIONS

4.1 Linear trend line

A series of graphs showing the annual total rainfall for all rainfall stations are shown in Figure 3. Fitting trend lines show positive magnitude in slope for all stations except station JPS Temerloh (ID = 3424081). Stations Rumah Pam Pahang Tua (ID = 3533102) and Kg Merting (ID = 4223115) shows a higher magnitude compared to the others. In general, Sungai Pahang river basin annual precipitation data in Pahang River Basin show no significant trend. However, it reveals that all of the stations depict clear upward trend and only downward trend for station JPS Temerloh (ID = 3424081). The sign of the slope magnitudes defines the direction of trend variable: increasing if the sign is positive and decreasing if the sign is negative. Annual total rainfall increases at the rate of 16.829 mm per year for Station Rumah Pam Pahang Tua and 26.669 mm per year for station Kg Merting in the last 40 years. Other stations also indicate the increasing magnitude, but only in a low rate.

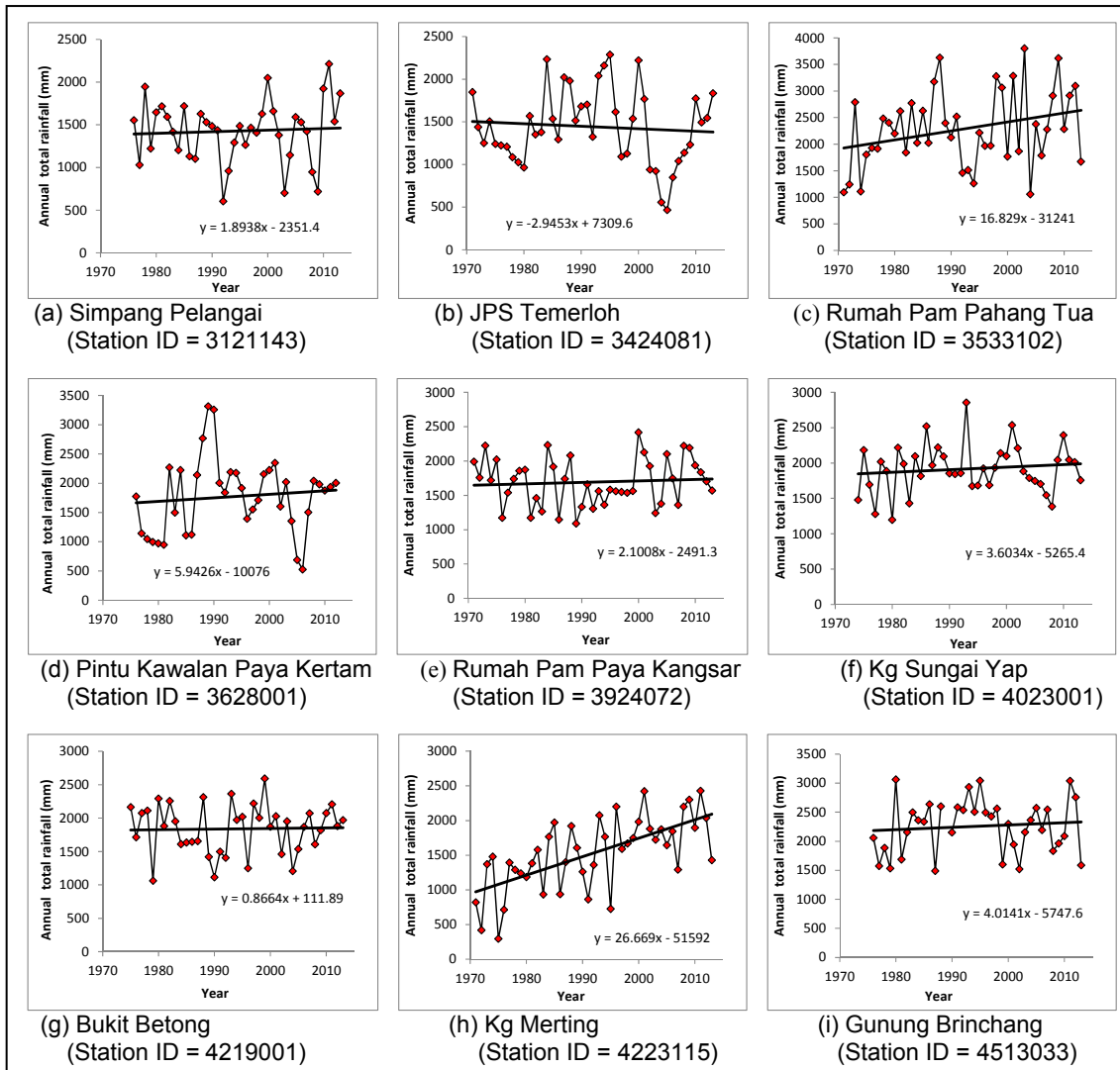


Figure 3. Linear trade line for annual total rainfall series.

4.2 Homogeneity test

The homogeneity of the annual total rainfall was investigated by using statistical analysis tool, XLSTAT 2016, with the following 4 methods of homogeneity test:

- Pettitt's test
- Standard normal homogeneity test (SNHT)
- Buishand's test (BRT)
- Von Neumann's ratio (VNR) test

Under null hypothesis (H_0), the annual values Y_i of the testing variables Y are independent and identically distributed and the series are considered as homogeneous. Meanwhile under alternative hypothesis (H_a), SNHT, BRT and Pettitt test assume the series consisted of break in the mean and considered as inhomogeneous. There are some differences between SNHT, BRT and Pettitt test. SNHT test is known to find change point towards the beginning and the end of the series, whereas BRT and Pettitt tests are sensitive to find the changes in the middle of a series (Martínez et al., 2009). These three tests are capable to detect the year where break occurs. Meanwhile, VRNT assumes the same null hypothesis as the previous three tests but for alternate hypothesis, it assumes that the series is not randomly distributed. VNRT assesses the randomness of the series, but does not give information about the year of the break. For all these four tests, if the test statistic exceeds the critical value at certain confidence level, the null hypothesis will be rejected at that confidence level.

XLSTAT statistical software used hypothesis testing method to detect homogeneity of the rainfall data. The results are categorized into three classes, which are useful, doubtful and suspect according to the number of tests rejecting the null hypothesis. The classification of the test results, according to the methods proposed by Wijngaard et al. (2003), is as follows:

- a) Class A: Useful
The series that rejects one or none null hypothesis under the four tests at 1% significance level are considered. Under this class, the series is grouped as homogeneous and can be used for further analysis.
- b) Class B: Doubtful
The series that reject two null hypotheses of the four tests at 1% significance level is placed in this class. In this class, the series have the inhomogeneous signal and should be critically inspected before further analysis.
- c) Class C: Suspect
When there are three or all of the tests reject the null hypothesis at 1% significance level, then the series is classified into this category. In this category, the series can be deleted or ignored before further analysis.

Based on alpha value of 0.05 (95% significance level), if p value is bigger than alpha value, therefore the series is homogeneous. Table 2 shows the summary result of the test. According to the Wijngaard et al. (2003) classification, 8 rainfall stations were found homogeneous (labeled as “useful”) and only one station (Kg Merting, ID = 4223115) was inhomogeneous (labeled as “suspect”). This may be due to increasing of annual and North East (NE) monsoon rainfall on the east coast of Peninsular Malaysia (Mayowa et al., 2015). Figures 4 and 5 depict the example outputs using 3 different methods of homogeneity test. The plots in Figure 5 show the change point occurred in the year 1992 for Pettitt test and 1996 for SHNT and BRT for station Kg Merting. To confirm the inhomogeneous of this station, the change point year should be compared with those of stations evaluated as homogeneous. If they have similar patterns, thus, it could not be considered as inhomogeneous. It is because the inhomogeneous rainfall data may also be due to the increasing of climate and rainfall variability in the area.

Table 2. Homogeneity test results using different methods at 95% significance level.

Station ID	p value				VNR test	Result
	Pettitt test	SHNT	BRT			
3121143	0.45	0.07	0.38		0.07	Useful
3424081	0.09	0.06	0.06		< 0.0001	Useful
3533102	0.31	0.19	0.22		0.39	Useful
3628001	0.10	0.08	0.09		< 0.0001	Useful
3924072	0.28	0.16	0.27		0.20	Useful
4023001	0.69	0.39	0.35		0.38	Useful
4219001	0.81	0.97	0.78		0.56	Useful
4223115	0.0002	0.0004	0.0001		0.004	Suspect
4513033	0.56	0.60	0.38		0.45	Useful

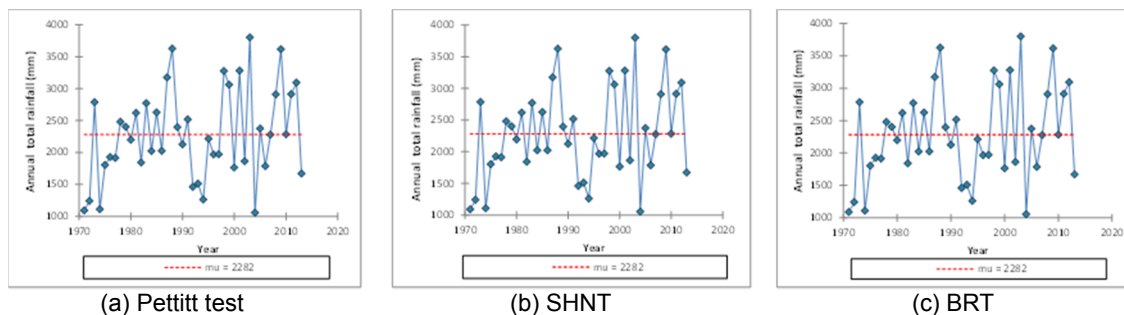


Figure 4. Results for station Rumah Pam Pahang Tua (Station ID = 3533102) using different homogeneity test methods. (*mu represent the mean rainfall).

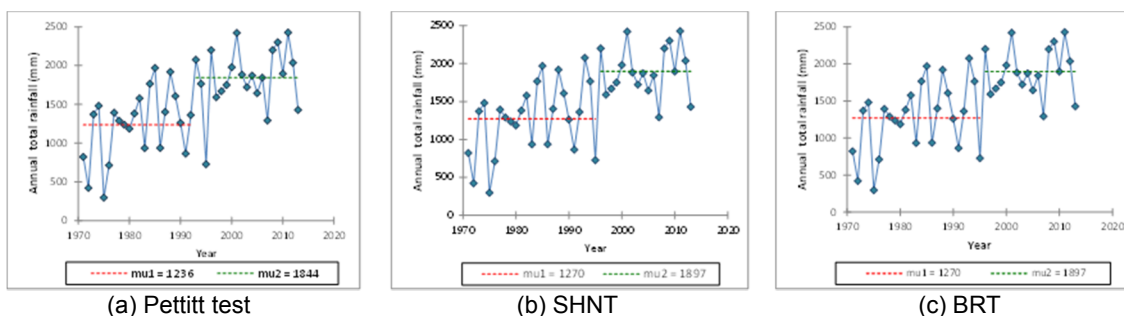


Figure 5. Change year in annual rainfall series / break year for station Kg Merting (Station ID = 4223115) (*mu1 and mu2 represent the mean rainfall before and after the change point.).

4.3 Trend Analysis

A trend analysis of annual rainfall variability was conducted by means of the Mann–Kendall (MK) test using the homogenous time-series rainfall data. In MK test, the positive test statistic, S indicates an increasing trend, while a negative value indicates a decreasing trend in rainfall. When setting up a study, a risk threshold above which H_0 should not be rejected must be specified. This threshold is referred to as the significance level alpha and should lay between 0 and 1. Low alphas are more conservative. The choice of alpha should depend on how dangerous it is to reject H_0 while it is true. Alpha is normally set at 0.05 or 0.01 or 0.001. The statistical test produces a number called p-value (bounded between 0 and 1), which is the probability of obtaining the data or more extreme data under the null hypothesis. More practically, the p-value will be compared to alpha:

- If p-value < alpha, reject H_0 and accept alternative hypothesis (H_a) with a risk proportional to p-value of being wrong.
- If p-value > alpha, do not reject H_0 , but this does not necessarily implying for it to be accepted. It either means that H_0 is true, or that H_0 is false but it shows that the experiment and statistical test were not “strong” enough to lead to a p-value lower than alpha.

In this study, the critical value (alpha) is tested at 95% (0.05) confidence level. XLSTAT 2016 calculated the p-value and if the p-value is less than the critical value (alpha) at the chosen significance levels, H_0 is rejected. Rejecting H_0 indicates that “there is a trend” in the time series, while accepting H_0 indicates “no trend was detected”. On rejecting the null hypothesis, the result is said to be statistically significant. For this test, the Null Hypothesis was accepted for only two (2) stations (Rumah Pam Pahang Tua, ID = 3533102 and Kg Merting, ID = 4223115).

For the analysis of trends, seven (7) rainfall stations indicate increasing trends while only two (2) stations showing decreasing trends. The magnitude of trend was identified using Sen’s slope estimator indicating positive (increasing) and negative (decreasing) magnitudes corresponding to MK test value. Only two (2) stations (Rumah Pam Pahang Tua, ID = 3533102 and Kg Merting, ID = 4223115) indicate a statistically significant trend with value of S and the magnitude of Sen’s slope are higher than the others. The trend results are similar with the finding magnitude in linear trade line (Figures 2(c) and 2(h)). These two stations showing higher magnitude in linear trade line indicate high probability of increasing trend in rainfall record. Inhomogeneity of rainfall data at station Kg Merting may correspond to the result of statistically increasing trend in that station. In particular, this station also indicate statistically increasing trend of extreme rainfall events of various storm durations from the study conducted by Alang Othman et al. (2016). With the increasing trend in annual amount and also extreme event, it may increase the frequency of flood and trigger more natural disaster such as landslide in this area.

Table 3. Mann-Kendall and Sen’s slope estimator test results.

Station ID	Mann-Kendall test				Sen’s slope
	S	p-value	Trend	Test interpretation	
3121143	9	0.82	Increase	No trend was detected	0.57
3424081	-19	0.79	Decrease	No trend was detected	-1.58
3533102	167	< 0.0001	Increase	There is a trend	17.33
3628001	44	0.44	Increase	No trend was detected	6.85
3924072	40	0.46	Increase	No trend was detected	1.39
4023001	30	0.47	Increase	No trend was detected	1.98
4219001	-9	0.80	Decrease	No trend was detected	-0.47
4223115	423	< 0.0001	Increase	There is a trend	25.83
4513033	41	0.17	Increase	No trend was detected	3.50

5 CONCLUSIONS

This study demonstrates the application of statistical tests to identify of homogeneity and trend of rainfall records in Pahang River basin. The major findings and conclusions of this study are as follows:

- Fitting trend lines show positive magnitude in slope for all rainfall stations except station JPS Temerloh (ID = 3424081).
- Eight (8) rainfall stations were found to be homogeneous and only one station (Kg Merting, ID = 4223115) were inhomogeneous. This station is suggested not to be used for further analysis. However, to confirm the inhomogeneous of this station, the break year should be compared with those of stations evaluated as homogeneous. If they have similar patterns, thus, it could not be considered inhomogeneous. It is because the inhomogeneous rainfall data may be also due to the increasing of climate and rainfall variability in the area. Homogeneity testing also can be tested with different variables such as annual mean, annual maximum and annual median.
- MK test for trend analysis showed increased rainfall trends for seven (7) rainfall stations while two (2) of them showing decreasing trends. Only 2 of the stations (Rumah Pam Pahang Tua, ID = 3533102 and Kg Merting, ID = 4223115) indicate statistically increasing trend. Sen’s slope also indicating positive (increasing) and negative (decreasing) magnitudes corresponding to MK test value.

On the basis of trend analysis, most of the rainfall stations in Sungai Pahang river basin showing significant increasing trends over approximately 40 years of records. The findings of the study offers remarkable insights for planning and designing infrastructure in managing floods, as well as flood risk and infrastructure systems failure risk in Sungai Pahang river basin.

ACKNOWLEDGEMENTS

The authors would like to acknowledge the financial assistance from the Ministry of Higher Education Malaysia under the TRGS 2015 Flood Management Grant No. 203/REDAC/6767003 entitled "Model-Based Morphological Prediction for Large Scale River Basin in Raising Flood Protection Levels for Sungai Pahang". Special thanks also to Water Resources Management and Hydrology Division, Department of Irrigation and Drainage (DID), Malaysia for providing the historical rainfall data for this study.

REFERENCES

- Alang Othman, M.A., Zakaria, N.A., Ab. Ghani, A., Chang, C.K. & Chan, N.W. (2016). Analysis of Trend of Extreme Rainfall Events Using Mann Kendall Test: A Case Study in Pahang and Kelantan River Basins. *Jurnal Teknologi*, 78(9-4), 63-69.
- Buishand, T.A. (1982). Some Methods for Testing the Homogeneity of Rainfall Records. *Journal of Hydrology*, 58(1), 11-27.
- Che Ros, F., Tosaka, H., Sidek, L.M. & Basri, H. (2016). Homogeneity and Trends in Long-Term Rainfall Data, Kelantan River Basin, Malaysia. *International Journal of River Basin Management*, 14(2), 151-163.
- Chen, H., Guo, S., Xu, C.Y. & Singh, V.P. (2007). Historical Temporal Trends of Hydro-Climatic Variables and Runoff Response to Climate Variability and Their Relevance in Water Resource Management in the Hanjiang Basin. *Journal of Hydrology*, 344(3-4), 171-184.
- Mann, H. B. (1945). Nonparametric Tests against Trend. *Econometrica*, 13(3), 245-259.
- Martínez, M.D., Serra, C., Burgueño, A. & Lana, X. (2009). Time Trends of Daily Maximum and Minimum Temperatures in Catalonia (Ne Spain) for the Period 1975-2004. *International Journal of Climatology*, 30(2), 267-290.
- Mayowa, O.O., Pour, S.H., Shahid, S., Mohsenipour, M., Harun, S.B., Heryansyah, A. & Ismail, T. (2015). Trends in Rainfall and Rainfall-Related Extremes in the East Coast of Peninsular Malaysia. *Journal of Earth System Science*, 124(8), 1609-1622.
- Peterson, T.C., Easterling, D.R., Karl, T.R., Groisman, P., Nicholls, N., Plummer, N., Torok, S., Auer, I., Boehm, R., Gullett, D., Vincent, L., Heino, R., Tuomenvirta, H., Mestre, O., Szentimrey, T., Salinger, J., Førland, E.J., Hanssen-Bauer, I., Alexandersson, H., Jones, P. & Parker, D. (1998). Homogeneity Adjustments of In Situ Atmospheric Climate Data: A Review. *International Journal of Climatology*, 18(13), 1493-1517.
- Shadmani, M., Marofi, S. & Roknian, M. (2012). *Trend Analysis in Reference Evapotranspiration Using Mann-Kendall and Spearman's Rho Tests in Arid Regions of Iran*. *Water Resources Management*, 26(1), 211-224.
- Suhaila, J., Deni, S.M., Zin, W.Z.W. & Jemain, A.A. (2010). Trends in Peninsular Malaysia Rainfall Data during the Southwest Monsoon and Northeast Monsoon Seasons: 1975-2004. *Sains Malaysiana*, 39(4), 533-542.
- Wijngaard, J.B., Klein Tank, A.M.G. & Können, G.P. (2003). Homogeneity of 20th Century European Daily Temperature and Precipitation Series. *International Journal of Climatology*, 23(6), 679-692.
- Yue, S., Pilon, P. & Cavadias, G. (2002). Power of the Mann-Kendall and Spearman's Rho Tests for Detecting Monotonic Trends in Hydrological Series. *Journal of Hydrology*, 259(1), 254-271.

NUMERICAL SIMULATION OF INUNDATION DUE TO PROBABLE MAXIMUM PRECIPITATION IN HIROSHIMA CITY

NAOKI HAYAMI⁽¹⁾ & YOSHIHISA KAWAHARA⁽²⁾

⁽¹⁾ Graduate School of Engineering, Hiroshima University, Higashi-Hiroshima, Japan,
m155578@hiroshima-u.ac.jp

⁽²⁾ Department of Civil and Environmental Engineering, Hiroshima University, Higashi-Hiroshima, Japan,
kawahr@hiroshima-u.ac.jp

ABSTRACT

With rapid development in urban areas and the increase of extreme climate events due to global climate change, urban areas have become more vulnerable to flooding. Numerical simulations have been done using XPSWMM to clarify the inundation phenomena and associated damage in Hiroshima city when the probable maximum rain attacks the city without levee breach. The validity of the numerical simulation is discussed through comparisons between the numerical results and the actual records of inundated zones and water levels at pump stations. Then, the effects of structural measures such as construction of new drainage pipes and reinforcement of pump capacity on the depth and the duration of inundation were studied. It is found that the installation of new pipes is effective and hence to come before the others while the structural measures have limitation to reduce inundation areas.

Keywords: Inundation; probable maximum precipitation; Hiroshima city; drainage network; XPSWMM.

1 INTRODUCTION

With rapid urbanization and the increase of extreme climate events due to global climate change, urban areas have become more vulnerable to flooding. This trend highlights the importance of effective schemes to mitigate the damage and loss due to inundations. Although it has been recognized that good combination of structural measures and non-structural ones works best to mitigate the flood damage, more emphasis has been placed on non-structural measures than structural ones that take much time and cost (Lee, 2016).

In 2015 after the Great East Japan Earthquake, Flood Fighting Law and Sewerage Law in Japan were amended to provide a possible inundation map when the catchment receives the probable maximum rainfall which has, by far, a long return period. River Bureau of MLIT (Ministry of Land, Infrastructure, Transport and Tourism) of Japan prepared a guideline to estimate the probable maximum rainfall (MLIT, 2015) and has started to announce flood maps resulting from levee breach (MLIT, 2016) with strong impacts to communities and residents because the scale and scope of floods and the damage are sure to greatly exceed assumptions.

Referring to urban pluvial inundation, numerical simulation with an integrated inundation model has been intensively carried out to understand the inundation events over the last two decades. However, integrated analysis of urban inundation against extreme rains has been small (Van Dijk et al., 2014) and those against the probable maximum rain without levee breaches has been very limited. Hence, this study aims to describe the inundation phenomena and associated damage in Hiroshima city when the probable maximum rain causes flooding due to insufficient drainage capacity without levee breaches.

Under the assumption of no levee breach, the magnitude and extent of flooding depends mainly on the total amount of precipitation, carrying capacity of drainage network system including the drainage capacity of pumping system, and micro-topography in Hiroshima city. This study uses XPSWMM to take into full account of real complex urban structures such as street networks, buildings, underground malls, sewer network and river network to discuss the plausible extreme phenomena in Hiroshima city.

2 STUDY AREA AND NUMERICAL MODEL

2.1 Study area

Hiroshima city, having a population of 1.19 million in 2016, is located in the western part of the main island of Japan. The downtown areas of Hiroshima city have expanded over the Ota river delta and reclaimed lands, as shown in Figure 1 (a). Hiroshima city has operated a combined sewer system to drain rainstorm water. Recently, Hiroshima city (2014) has announced an improvement plan to deal with the rainfall of 53 mm/h, corresponding to the return period of 10 years as well as to meet water pollution problems during combined sewer overflow events. The project includes construction of rainwater conduits and a pumping station as inundation prevention measures.

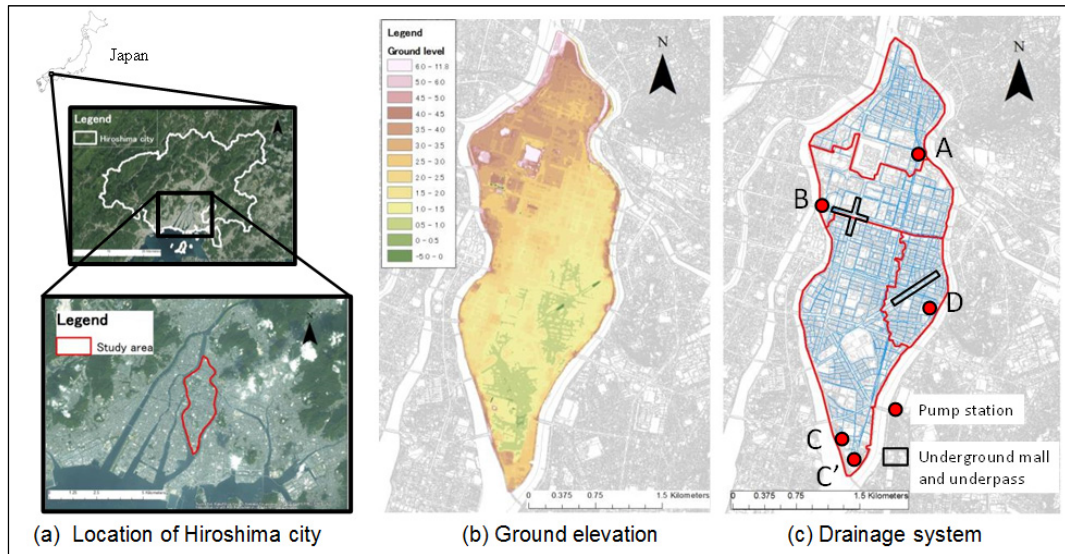


Figure 1. Study area in Hiroshima city.

Figure 1 (b) shows the target area in this study and the ground elevation. The study area is 5.13km² and is surrounded by the tributaries of the Ota River. The land use in the area consists of commercial use (67%) and residential use (31%). The impervious area occupies 74.2% of the total area. The elevation in the area is low and flat with slightly high elevation in the northern part. The green parts in the figure display low-lying areas whose ground elevations are nearly the same as or lower than the mean sea water level.

Figure 1 (c) illustrates the combined sewage network and location of pump stations together with an underground mall and a long underpass. The target area is divided into four drainage districts, and has 5,000 manholes and 5,313 sewer pipes. The average slope of the pipes is 1.1%. 17 discharge pumps are installed with a total discharge capacity of 53 m³/s in the area.

2.2 Outline of numerical model

This study employs XPSWMM, a storm water modeling software for urban drainage with many applications, to numerically simulate flood depth and velocity due to heavy rain with a given hyetograph. The flow in drainage pipes is solved based on the continuity equation and the energy equation (Saint-Venant equation). A Preissmann slot model, a very narrow slot installed at the top of the sewer pipe, provides a conceptual free surface condition of the flow when the water level exceeds the top of a pipe. The basic equations are expressed as follows:

$$\frac{\partial h}{\partial t} + \frac{1}{B} \frac{\partial Q}{\partial x} = 0 \quad [1]$$

$$\frac{\partial Q}{\partial t} + \frac{1}{2} \frac{\partial}{\partial x} \left(\frac{Q^2}{A} \right) + gA \frac{\partial H}{\partial x} + \frac{gQ^2 n^2}{AR^3} = 0 \quad [2]$$

where h is the flow depth, B is the slot width, Q is the discharge, H is the sum of pressure head and elevation head, A is the flow cross-sectional area, R is the hydraulic radius, n is Manning's roughness coefficient, g is the gravitational acceleration, t is the time, x is the distance along the sewer pipe.

We calculate overland flow and return flow to the sewer using the module of XP2D, a computer program for solving depth-averaged, two-dimensional free-surface water flows. The basic equations consist of the continuity equation and shallow water equations:

$$\frac{\partial H}{\partial t} + \frac{\partial M}{\partial x} + \frac{\partial N}{\partial y} = 0 \quad [3]$$

$$\frac{\partial M}{\partial t} + \frac{\partial(MU)}{\partial x} + \frac{\partial(MV)}{\partial y} = -gh \frac{\partial H}{\partial x} - \frac{\tau_{bx}}{\rho} \quad [4]$$

$$\frac{\partial N}{\partial t} + \frac{\partial(NU)}{\partial x} + \frac{\partial(NV)}{\partial y} = -gh \frac{\partial H}{\partial y} - \frac{\tau_{by}}{\rho} \quad [5]$$

where H is the water surface elevation, M and N are the flow rate per unit width in x-direction and y-direction, respectively, τ_{bx}, τ_{by} are the bed shear stress components in x- and y- directions, U and V are the depth-averaged velocity components in x- and y- directions, and ρ is the density of water.

3 MODEL CALIBRATION

3.1 Calibration of model parameters

Prior to numerical simulations of flooding due to the probable maximum rain, model parameters in XPSWMM have to be carefully tuned. The numerical simulations were carried out with the computational grid of 10 m x 10 m and the time step of 1.0 sec.

Figure 2 shows two rainfall events used to tune the model parameters. The calibrations were performed by focusing on the peak water level and the peak time at the pump stations and the flooded areas.

No.	Date	Time	Total rainfall(mm)
I	Jun 22 - 23, 2016	5:20 - 2:20	101
II	Sep 17 - 18, 2016	20:00 - 2:00	100.5

Figure 2. Rainfall events for calibration of model parameters.

The dry weather flow (DWF) is estimated by the following equation to give the initial flow rates in sewer network.

$$DWF = \sum_{i=1}^N S \times A(i) \times P \times D(i) \quad [6]$$

where N is the number of sub-catchments, S is the quotient of plan sewage water divided by population, $A(i)$ is the sub-catchment area, P is the peak coefficient and is a quotient of maximum sewage water divided by time average sewage water, $D(i)$ is the population density.

Figure 3 summarizes the values of nine parameters in XPSWMM, which were identified through the calibrations.

Model	Article		Value	Unit	Note
Rain loss model	Evapotranspiration		2.5	mm/day	default
	Impervious	A	65	%	
		B	56	%	
		C	77	%	
		D	83	%	
	Percentage of direct runoff area		74	%	
	Infiltration loss	Initial infiltration	20	mm/h	
Last infiltration		10	mm/h		
Attenuation coefficient		0.001	—		
Depression storage	Pervious area	6.0	mm		
	Impervious area	2.0	mm		
Surface runoff model	Basin width		—	m	Set each node
	Ground roughness	Pervious area	0.1	—	
		Impervious area	0.08	—	
Pipe hydraulic model	Pipe roughness	Existing pipe	0.013	—	
		Liner pipe	0.010	—	
Inundation analysis model	Ground raghness	Road	0.03	—	
		etcetera	0.06	—	

Figure 3. Parameters for calibration of XPSWMM.

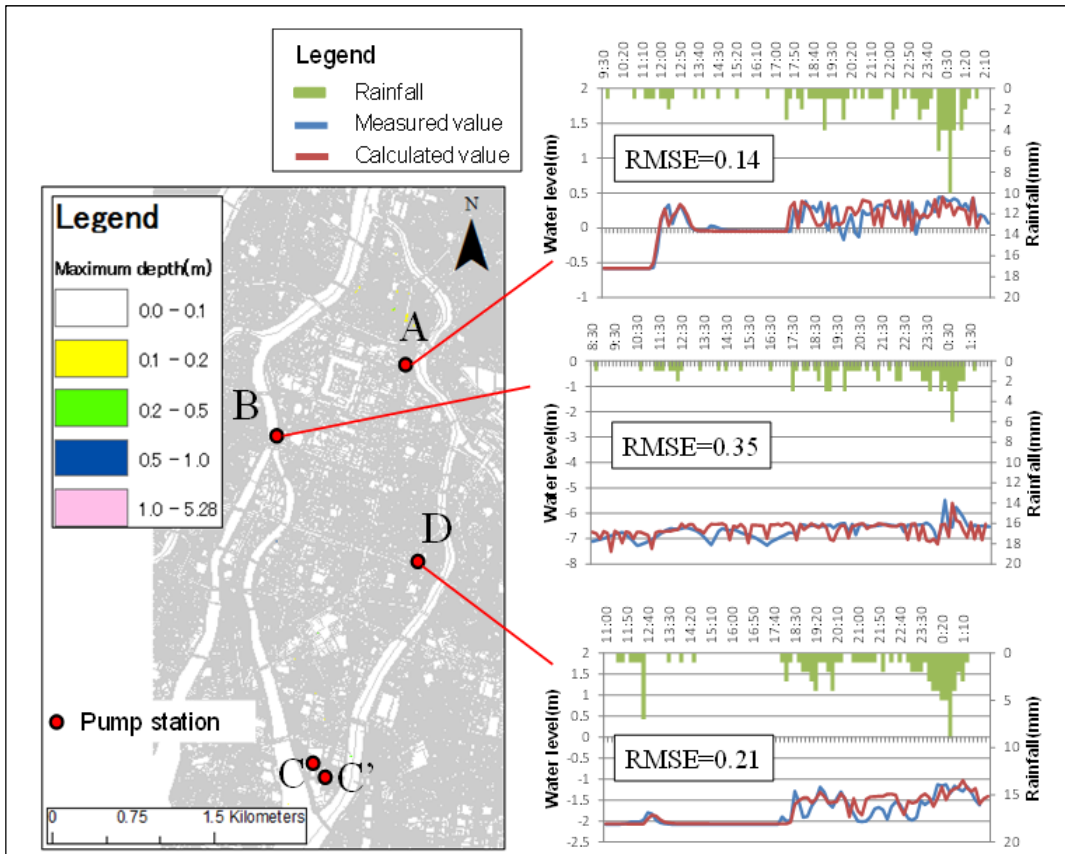


Figure 4. Maximum inundation depth in study area and water levels at pumping stations from 8:30 June 22 to 2:20 June 23 in 2016.

3.3 Results of calibration

Figure 4 shows the calculated inundated water depth during the rainfall event I. There has been no inundation report by the local residents whereas the numerical results showed inundated zones of small water depth near the pumping station A. The right figures in Figure 4 compare the water levels at three pump stations. It can be seen that the numerical simulation well captured the peak and the variation of water level at each pump station including the operation of each pump, which works when the water level exceeds the specified level.

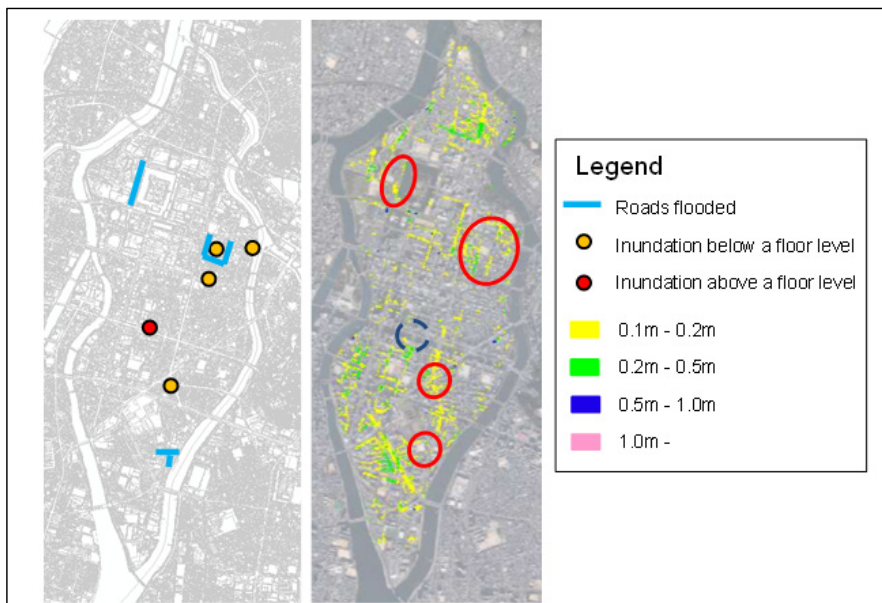


Figure 5. Comparison between recorded inundation area and the calculated maximum inundation depth.

Figure 5 compares the inundation record reported by the residents and the calculated results for the rain event II. The red open circles in the right figure represent the areas where the numerical simulation reproduces the inundation in good agreement with the records. A blue dotted circle, however, displays the area where the numerical simulation fails to predict the flooding. The differences arise from the fact that inundation records depend only on the reports by residents and the insufficient numerical resolution that the micro-topography and mixed land use along the streets are unresolvable.

4 NUMERICAL SIMULATION OF FLOODING DUE TO PROBABLE MAXIMUM PRECIPITATION

4.1 Probable maximum precipitation

The probable maximum rain was prepared by following the manual by MLIT (2015). Figure 6 (a) shows the recorded maximum event in September 17 in 2016. Figure 6 (b) depicts the stretched generated hyetograph from Figure 6 (a). The maximum hourly rainfall is 171 mm and total rainfall is 201mm.

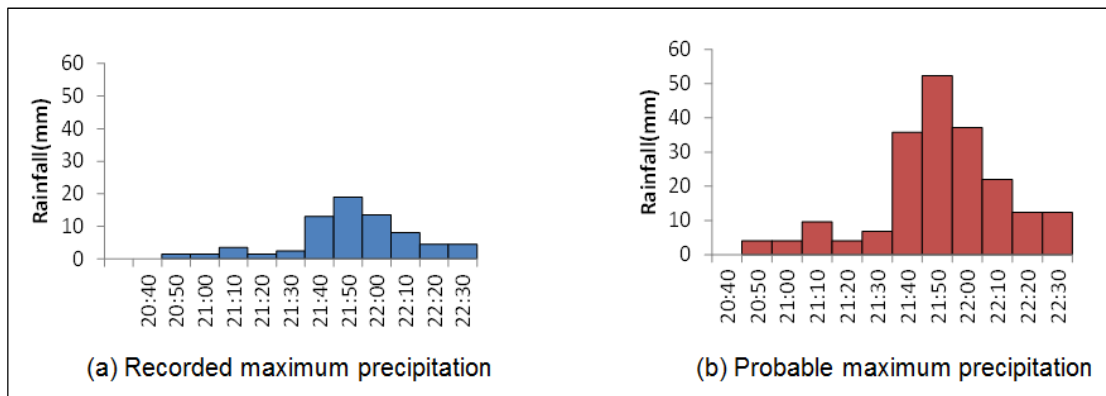


Figure 6. Hyetographs of target precipitations.

4.2 Results

Large scale of flooding is sure to occur in case of the probable maximum rainfall because it greatly overwhelms the design capacity of drainage system. Figure 7 explains the distribution of maximum flooded flow depth in the study area and the inundation process along the drainage pipe shown in red in the left figure. At 20:50, 10 minutes after the beginning of rainfall, the downstream reach is filled with stormwater. At 21:00, the pressurized flow starts to overflow from manholes and then inundation areas expand.

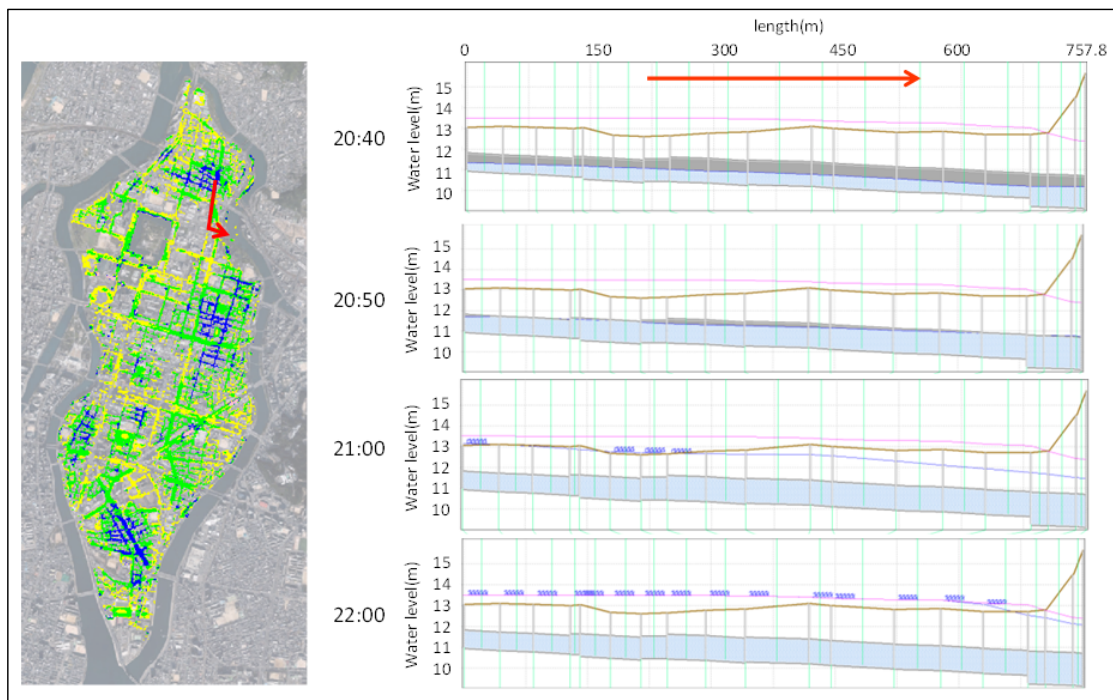


Figure 7. The maximum flooded water depth in study area and temporal change in water level along a sewage pipe in red in the left figure.

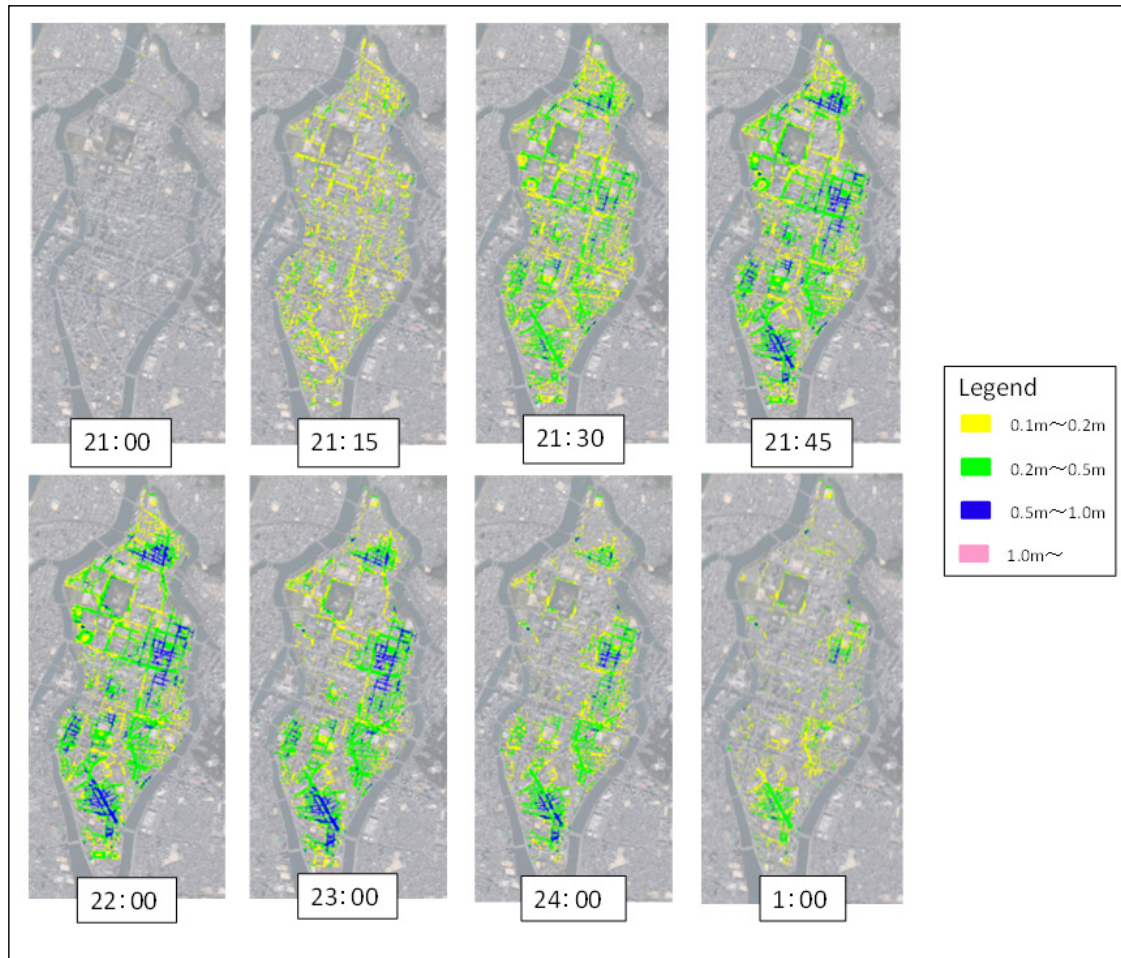


Figure 8. Temporal change of Inundation area and the water depth.

Figure 8 displays the temporal and spatial variation of inundation water depth during the probable maximum precipitation from 21:00 to 1:00. During the first 30 minutes of the simulation, the water depth is shallow. Serious flooding occurs at 21:15 over the study area mostly with water depth deeper than 10 cm. The extent of inundation and inundation water depth show the maximum at around 22:00 just after the peak of precipitation. Thereafter, inundated gradually recedes due to sewer drainage, infiltration and evapotranspiration.

The inundation depth exceeding 50cm means flooding above a floor level. The numerical simulation tells that inundation depth exceeds above a floor level in half an hour or so from the beginning of the rainfall and that flooding above a floor level simultaneously breaks out in various areas. This rapid increase of water depth over the study area highlights the importance of preparedness and the necessity of evacuation toward the upper floor and not to the evacuation center.

5 ASSESSMENT OF EFFECTIVE MEASURES

5.1 Structural measures

Hiroshima city government (2014) has promoted the enhancement of the drainage system to dispose the heavy rain of 53 mm/h. Figure 9 shows the existing and planned sewage pipes in the study area. Red lines indicate the existing pipes and blue lines the planned pipes. A red broad line running from the north to the pump station C' expresses the main line that has a diameter of 4.5 m \Rightarrow 5.85 m and collects rainwater from the pipes as shown in the figure. Figure 10 shows the dimensions of the main pipes. The pump station C' is expected to have a pump whose capacity is increased from 28 m³/s to 53m³/s. This study examined the effects of the following three measures.

- (I) Increase of the pump capacity at pump station C',
- (II) Construction of new pipes, which are shown in blue in Figure 9,
- (III) Combination of the above two measures (I) and (II).

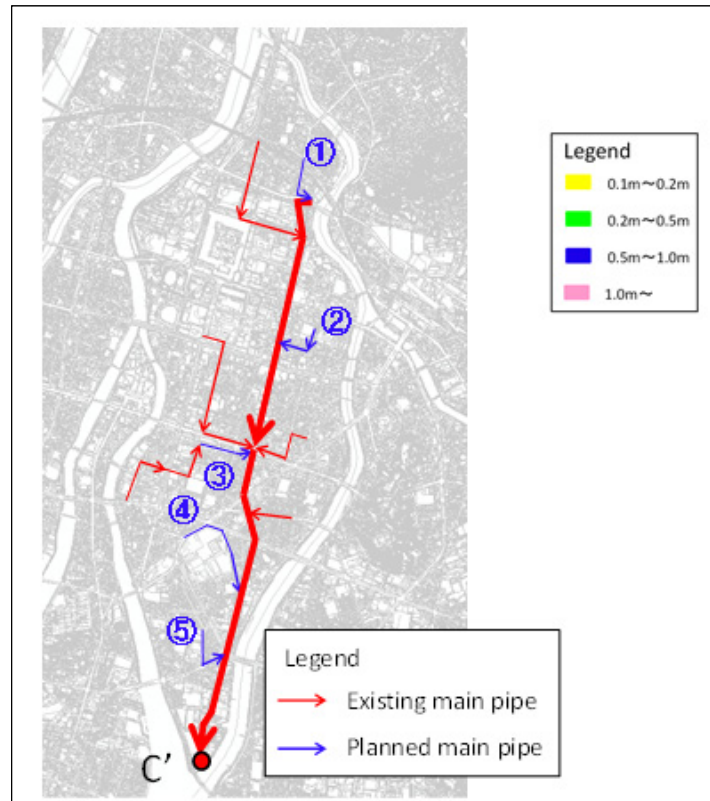


Figure 9. Existing and planned pipes to deal with the rain of 53 mm/h.

Pipe	Diameter(m)	Length(m)
①	3.0	550
②	2.2	141
	2.0	395
③	2.0	463
④	2.2	852
	1.35	8.6
	1.2	44
⑤	3.0	500

Figure 10. Dimensions of sewage pipes.

5.2 Results

Figure 11 compares the effect of each measure on the maximum inundation depth during the probable maximum precipitation. As Figure 11 (b) shows, the measure (I), or, increase of pump capacity, brings little improvement compared with the present situation in Figure 11 (a). This is because the overflow from manholes occurs at the initial stage of heavy rain and hence the inflow into the rainwater main line connected to the pumping station C' is limited. In other words, insufficient amount of rainwater is supplied to the enhanced pump.

The measure (II), or, installation of new pipes, can considerably reduce the inundation area even though some areas still show the inundation depth more than 45 cm. The increased inflow rate into the rainwater main line promotes the drainage in deeply inundated areas. It is also confirmed, although not shown here, that the ponding time can be reduced up to 2.5 hours, and that some areas in the northern part suffer from the increase in inundation time.

The measures (III) that combines the increase of pump capacity and installation of new pipes can significantly decrease the inundation depth, in particular in the southern part of the study area. Comparing the effects by measure (II) and measures (III), we can see that the impact of the measures (III) on inundation depth is more pronounced in the southern area with little improvement in the northern area.

From these results, it can be said that introduction of new pipes in blue in Figure 9 brings the largest improvement in the inundation depth. Thus, the first priority of the measures against the probable maximum rain is to be placed on the construction of new pipes. It is not effective to increase the pump capacity at the initial stage of the plan.

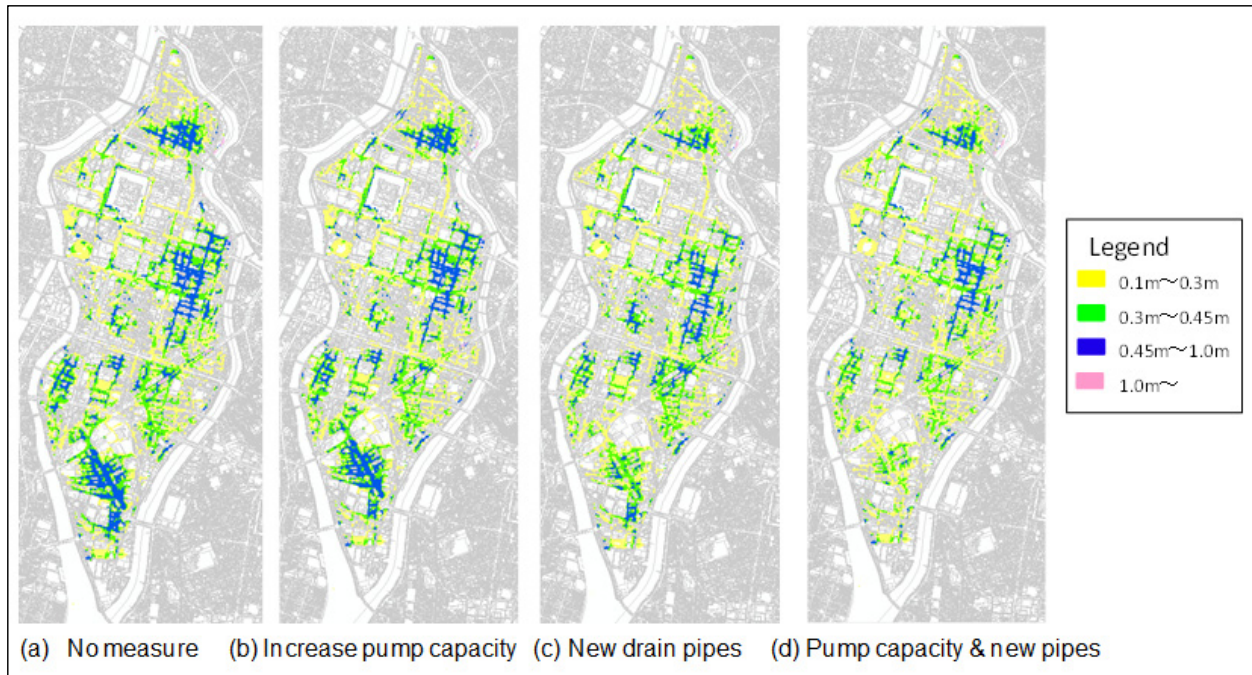


Figure 11. The maximum inundation depth for each measure against the probable maximum rain.

At the same time, it is apparent that the measures (III) planned by Hiroshima city government have limitation against the probable maximum rain. Hence non-structural measures using ICT and IoT technology needs to be developed for residents and visitors to Hiroshima to be aware of the looming danger due to heavy rains.

The numerical simulation suggests that the inrush of rainwater into the underground mall can be avoided by introducing water stops at the entrances since the maximum inundation depth at the entrances just reaches up to 45 cm above the ground.

6 CONCLUSIONS

We have carried out numerical simulations using XPSWMM to understand the possible inundation in the downtown area of Hiroshima city when the city receives the attack of the probable maximum rainfall. The main findings in this study can be summarized as follows.

- 1) The past inundation records have been favorably reproduced by the calibrated XPSWMM;
- 2) The maximum inundation depth and the ponding time for the probable maximum precipitation under the present condition have been estimated. The inundation process has also been analyzed;
- 3) Construction of new pipes has been estimated to be more effective than the reinforcement of pump capacity to reduce the inundation depth. Hence, the new pipes have higher priority;
- 4) In the case of the probable maximum rain, the flooding occurs so immediately that the evacuation time is very short. Hence, weather forecasting can significantly contribute to minimize the flood damage.

ACKNOWLEDGEMENTS

The authors would like to thank Hiroshima sewage work station for providing the data of drainage network system and Forum 8 Co., Ltd for giving technical support of XPSWMM.

REFERENCES

- Lee, E.H., Lee, Y.S., Joo, J.G., Jung, D. & Kim, J.H. (2016). Flood Reduction in Urban Drainage Systems: Cooperative Operation of Centralized and Decentralized Reservoirs. *Water*, 8(10), 469-491.
- Ministry of Land, Infrastructure, Transport and Tourism of Japan (2015). *Estimation Method of The Probable Maximum External Forces to Create Flood Maps*, Ministry of Land, Infrastructure, Transport and Tourism of Japan. pp 45.
- Ministry of Land, Infrastructure, Transport and Tourism of Japan (2016). *Manual for creation of flood map due to heavy rains (in Japanese)*, Ministry of Land, Infrastructure, Transport and Tourism of Japan. pp 60.
- van Dijk, E., van der Meulen, J., Kluck, J. & Straatman, J.H.M. (2014). Comparing Modelling Techniques for Analysing Urban Pluvial Flooding. *Water science and technology*, 69(2), 305-311.
- Hiroshima City Government (2014). *Sewer Vision of Hiroshima City*, Hiroshima City Government .42 p.

COMPARISON OF FLOW HYDRAULICS IN DIFFERENT MANHOLE TYPES

MD NAZMUL AZIM BEG⁽¹⁾, RITA F. CARVALHO⁽²⁾ & JORGE LEANDRO⁽³⁾

^(1,2) MARE - Marine and environmental research center, Department of Civil Engineering, University of Coimbra, Coimbra, Portugal
mnabeg@uc.pt; ritalmfc@dec.uc.pt

⁽³⁾ Chair of Hydrology and River Basin Management, Technical University of Munich, Munich, Germany,
jorge.leandro@tum.de

ABSTRACT

Manhole is a very common and important element in an urban drainage system. The complex flow pattern in a manhole may include the effects of retardation, acceleration and rotation, creating energy losses in the network. Different types of manhole are seen in various countries due to different design criteria. Three different manhole types were modelled in this study to analyze the hydraulic properties of them. Type C has a guided channel at the bottom, while Type A and Type B do not. Type A also has a seal underneath the inflow-outflow pipe; but in Type B, the invert level of the inflow pipe is at the same level of the manhole floor. Analysis were done numerically using volume of fluid (VOF) model with open source CFD modelling tools OpenFOAM®. The numerical results were verified by mesh independency test using Richardson extrapolation method. Results showed that the flow structures and head loss coefficients vary in different manholes. All three manholes showed higher head loss coefficients at low surcharge conditions. Out of the three manhole types, Type A and B showed higher head loss coefficient than Type C. The threshold surcharge levels at Type A and B were found approximately 20% of the manhole diameter. However, for Type C, the surcharge threshold level was found higher. The study may provide essential information to calculate the head losses of these types of manhole in an urban drainage network model.

Keywords: Urban drainage, manholes, CFD, OpenFOAM®, head loss coefficient

1 INTRODUCTION

Manhole is one of the most common features of an urban drainage system. It is usually placed at a drainage network connections where a change in pipe direction, size or gradient is necessary. It also serves as an inspection pit for the pipe network (Butler and Davies, 2011). The flow inside a manhole is normally complex, highly turbulent and possibly multiphase. When the flow enters a manhole, it experiences a sudden expansion and contraction involving energy losses. This loss makes it an important element for storm network modelling consideration. The drainage system is usually designed to operate without surcharging. In normal condition, the water level in the manhole remains below the crown level of the conduit. Thus, the flow is only gravity driven and considered as an open channel flow. During an extreme rainfall event, the water level increases and the system becomes surcharged making a significant contribution to the overall head losses in the network. The head loss calculation in a surcharged manhole is complicated, involving many structural and hydraulic factors, such as the shape of a manhole, inflow rate, surcharge condition, pipe size, angle of connection, pipe to manhole diameter ratios etc. (Marsalek, 1984; Wang et al., 1998; Carvalho and Leandro, 2012; Stovin et al., 2013; Pfister and Gisonni, 2014; Arao et al., 2016). For a large system with several manholes, these head losses become more significant. Thus, it is essential to incorporate the effect of manhole head losses into the design of sewer pipe lines so that the system can store excess flow without flooding and overflows.

Most urban flood routing models are one or two dimensional and therefore cannot represent the complex flow pattern of these structures (Leandro et al., 2009). While modelling a drainage system using a drainage network model, a manhole is considered as a point entity and the complex flow inside it cannot be modelled. The head losses are considered using empirical equations (Leandro and Martins, 2016). Several studies have been done to assess the head loss in a surcharged manhole. Howarth and Saul (1984), Pedersen and Mark (1990), Arao and Kusuda (1999) and Lopes et al. (2014) investigated different types of scaled surcharged manhole using physical models. Pedersen and Mark (1990), Guymer et al. (2005) and Lau (2007) checked the velocity distribution of surcharged manholes and described their results in line with submerged jet theory, originally described by Albertson et al. (1950). Some authors also described numerical modelling of a surcharged manhole using CFD tools. Lau et al. (2007) and Stovin et al. (2013) used rigid lid approximation to numerically model a scaled manhole and described the associated head losses. Beg et al. (2016) used Volume of Fluid (VOF) model and analyzed different flow in a prototype scale manhole. However, different types of manhole have different flow hydraulics, which may contribute to the head loss of a drainage network differently.

This work investigates the flow hydraulics and head losses in three types of prototype scale manhole. The chosen manhole types are commonly found in typical urban drainage networks. Analysis has been done using open source CFD tools OpenFOAM. The work uses VOF model in examining the flow behavior. The aim of the study is to understand the hydraulics in different types of manhole and compare between them.

The work describes the computational domain and numerical model in the 'Methodology' section; followed by mesh independence test at the 'Mesh Analysis' section. In the 'Results and Discussions' section, the comparisons are drawn between hydraulic behaviors of the three manholes. The last section summarizes and concludes the work.

2 METHODOLOGY

2.1 Computational domain

To analyze the hydraulic effects of different manholes, three different inline manholes were chosen. Each manhole has a diameter of 1.0 m, connected with a 300mm inlet-outlet pipe. The geometrical differences in these three manholes are shown in Figure 1. The Type A manhole has a sump bottom relative to the pipes, which has a depth of 0.10 m from the inlet pipe invert level. Type B does not have any sump and its bottom level is merged with the inlet pipe invert. Type C manhole has a more hydraulically shaped bottom. The entrainment is further restricted and has a more complex interior geometric shape with a guided flow channel where the channel is a U-type invert. The inlet-outlet pipe at all the three manholes are horizontal to the ground. The ratio between the manhole diameters to inlet pipe diameters (Φ_m/Φ_p) in all the three cases is 3.33.

The computational meshes were generated using *cfmesh v1.1* (Juretić, 2015). The maximum size of the computational meshes was chosen as 20 mm towards all three Cartesian directions. The boundary meshes were kept as small as 2 mm; keeping three layers at the all close boundaries. The length of the inlet and outlet pipes were kept 4.5 m each, which is 15 times of the pipe diameter. Figure 2 shows the interior parts of the computational meshes of all the three manholes.

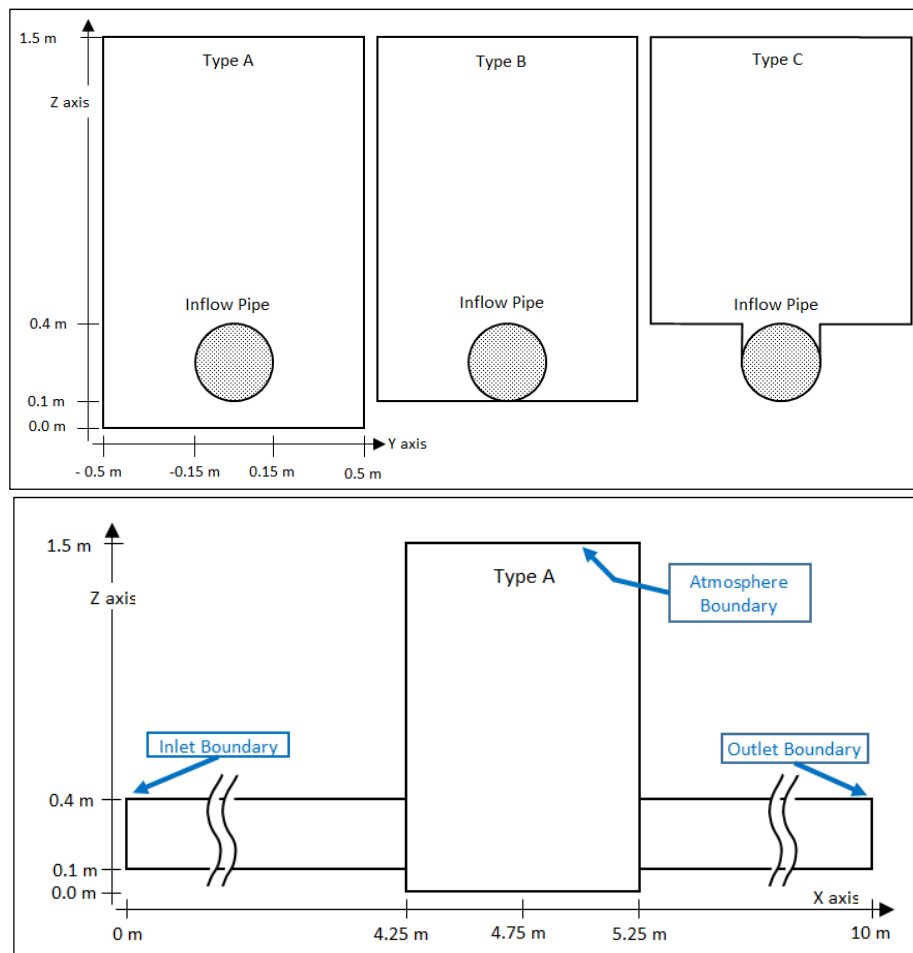


Figure 1. Schematic views of the sides of the three manholes showing sizes and positions of different components.

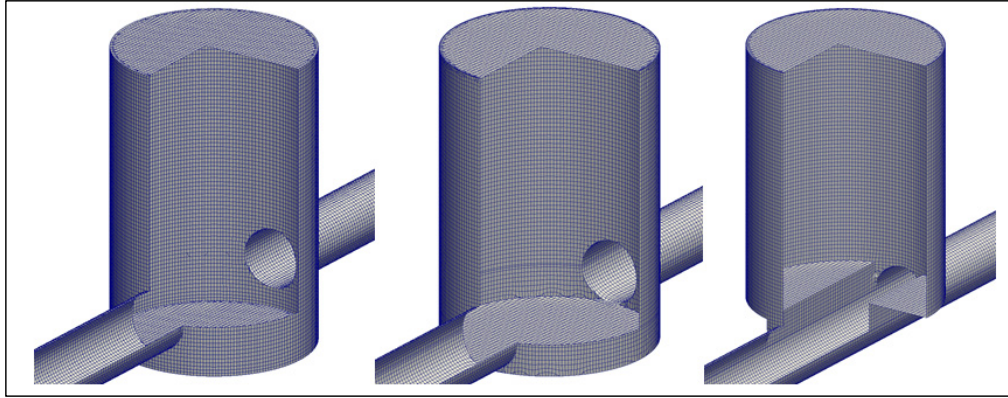


Figure 2. Outline of the computational mesh of each manhole types. Left panel shows Type A, middle panel shows Type B and the right panel shows Type C.

2.2 Numerical model

The numerical modelling part utilizes open source CFD tools OpenFOAM v2.3.0. The solver *interFoam* was used to model the flow phenomena. It considers the fluid system as isothermal, incompressible and immiscible two-phased flow. It uses a single set of Navier-Stokes equations for the both fluids, (here in this case water and air) and additional equations to describe the free-surface (Carvalho et al., 2008). The velocity at free-surface is shared by both phases. The solver deals with Reynolds averaged conservation of mass and momentum for incompressible flow (Jasak, 1996; Rusche, 2002).

$$\nabla \cdot \mathbf{u} = 0 \quad [1]$$

$$\frac{\partial \rho \mathbf{u}}{\partial t} + \nabla \cdot (\rho \mathbf{u} \mathbf{u}) = -\nabla p^* + \nabla \cdot \boldsymbol{\tau} + \mathbf{g} \cdot \mathbf{x} \nabla \rho + \mathbf{f}_\sigma \quad [2]$$

where, \mathbf{u} is the velocity vector towards Cartesian coordinate system, ρ is the density of the fluid, $\boldsymbol{\tau}$ is the shear stress tensor, \mathbf{g} is the acceleration due to gravity and \mathbf{f}_σ is the volumetric surface tension force acting at the interface of the two fluids.

The stress term is defined as:

$$\nabla \cdot \boldsymbol{\tau} = \nabla(\mu(\nabla \mathbf{u})) + (\nabla \mathbf{u}) \cdot \nabla \mu \quad [3]$$

where, μ is the dynamic viscosity of the fluid.

This solver utilizes Volume of Fluid (VOF) method (Hirt and Nichols, 1981) to capture the free surface location. VOF utilizes an additional volume fraction indicator term α to determine the amount of each fluid amount in a computational cell volume.

$$\alpha(x, y, z, t) = \begin{cases} 1 & \text{for a place } (x, y, z, t) \text{ occupied by fluid 1} \\ 0 < \alpha < 1 & \text{for a place } (x, y, z, t) \text{ occupied by interface} \\ 0 & \text{for a place } (x, y, z, t) \text{ occupied by fluid 2} \end{cases} \quad [4]$$

VOF method also utilizes an interfacial compressive term for the interface region to keep it confined at a certain region (Weller, 2002).

$$\frac{\partial \alpha}{\partial t} + \nabla \cdot (\alpha \mathbf{u}) + \nabla \cdot [\mathbf{u}_c \alpha (1 - \alpha)] = 0 \quad [5]$$

where, \mathbf{u}_c is the compressive velocity that acts at a perpendicular direction to the interface. This is calculated as:

$$\mathbf{u}_c = C_\alpha |\mathbf{u}_c| \frac{\nabla \alpha}{|\nabla \alpha|} \quad [6]$$

where, C_α is a Boolean term (value is 0 or 1) which activates ($C_\alpha = 1$) or deactivates ($C_\alpha = 0$) the interface compressive term. The volumetric surface tension \mathbf{f}_σ is calculated by the Continuum Surface Force model (Brackbill et al., 1992).

$$f_{\sigma} \approx \sigma \kappa \nabla \alpha \quad [7]$$

where, κ is the direction of the surface curvature. The last term in Eq. [5] ensures that the compressive force is applied at the interface only.

The turbulence phenomena of this model was calculated using Realizable k - ϵ turbulent modelling approach. This Reynolds Averaged Navier-Stokes equation set predicts the spreading rate of both planar and round jets more accurately. It is also likely to provide superior performance for flows involving rotation, boundary layers under strong adverse pressure gradients, separation and recirculation (ANSYS Ins, 2009; Stovin et al., 2013). In Realizable k - ϵ turbulent modelling, two additional closure equations are solved for k (turbulent kinetic energy) and ϵ (Energy dissipation). In this approach, the dynamic viscosity, μ is calculated as:

$$\mu = \rho(v_t + \nu_0) \quad [8]$$

where, ν_0 and ν_t are molecular viscosity and turbulent viscosity respectively.

2.3 Boundary conditions

The model utilizes three open boundaries; i.e. *inlet*, *outlet* and *atmosphere* (Figure 1). In all cases, the *inlet* boundary conditions were prescribed as fixed velocity/discharge. The *outlet* boundary conditions were prescribed as fixed pressure boundaries corresponding to different water column pressure heads respectively. No inflow was added at the *atmosphere* boundary conditions. The pressure at this boundary was prescribed as equal to atmospheric pressure and *zeroGradient* for velocity to have free air flow if necessary. All the close boundaries were prescribed as *noSlip* conditions (zero velocity at the wall).

Combination of different inlet discharges and outlet pressures was applied in each simulation. All the three manholes were tested using same sets of boundary conditions and corresponding head losses and surcharges at the manhole center were recorded. Table 1 shows all the types of *inlet* and *outlet* boundary conditions used in different simulations.

Table 1. Combinations of numerical simulations.

Manhole Types	Inlet Discharges (l/s)	Outlet pressure heads (m)	Simulations
Type A	30, 60, 90 and 120	0.4, 0.425, 0.45, 0.5, 0.6,	28 simulations
Type B		0.7 and 0.8	28 simulations
Type C			28 simulations
Total: 3 types	4 options	7 options	84 simulations

The inlet turbulent boundary conditions k , ϵ and ν_t were calculated using the equations in FLUENT manual (ANSYS Ins, 2009), considering medium turbulence at the manhole. All the wall turbulent boundary conditions were prescribed as *wallFunction* as this eliminates the necessity of fine layered boundary mesh and hence reduce the computational time (Greenshields, 2015).

The model was ready to be run after the boundary setup. During the simulations, *adjustableRunTime* was used keeping maximum CFL number to 0.8. Cluster computing system at the University of Coimbra was used to run the simulations using MPI mode. Each simulation was run for 65 seconds. The first 60 seconds were required to reach steady state condition and the results of last 5 seconds were saved at an interval of 0.5 seconds as eleven time steps. All the analysis was made using averaged data of the mentioned eleven-time step results.

3 MESH ANALYSIS

A mesh independence test was done for the current work. For this purpose, three different meshes were created for the manhole Type C. The meshes had $dx = 10$ mm (Mesh C1), 14 mm (Mesh C2) and 20 mm (Mesh C3) with total cell counts as 2 137 000, 865 000 and 329 000 respectively. The mesh convergence study was checked using Richardson extrapolation method described by Celik et al. (2008). The refinement ratio between Mesh C2 and C1 as well as Mesh C3 and C2 were more than the recommended value of 1.3.

All the three meshes were simulated with a combination of 120 l/s inlet discharge and 0.8 m of outlet pressure head. The axial velocity profiles were extracted at the manhole center and at the pipe outlet center. A total of 60 point velocities were compared. The comparisons between the three meshes are shown at Figure 3 and Table 2.

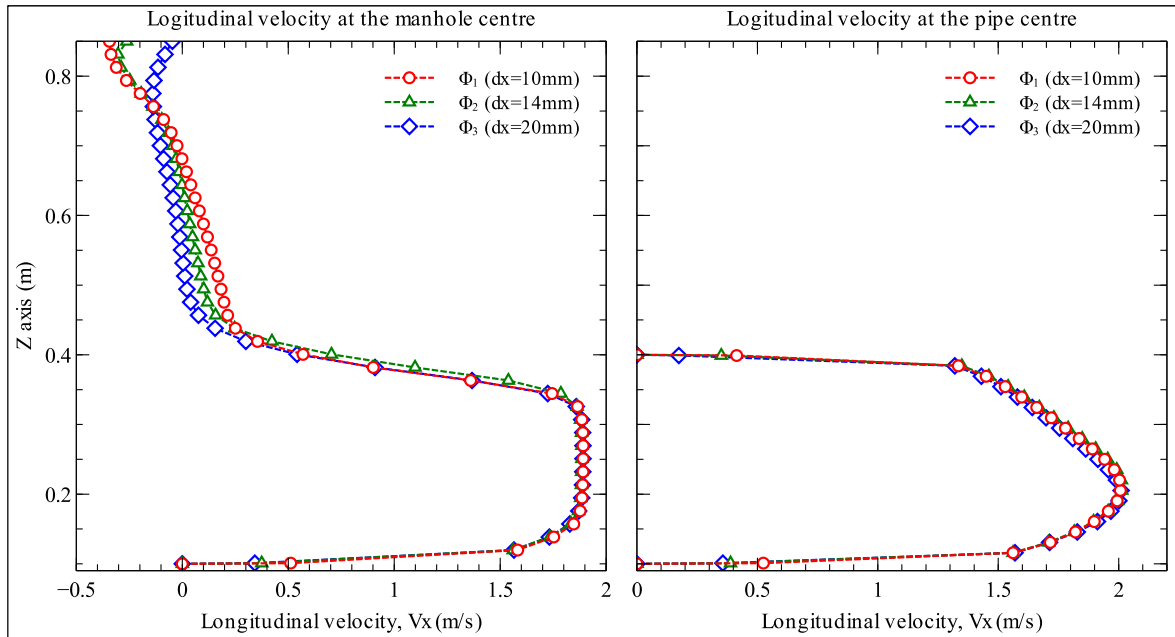


Figure 3. Mesh analysis using three meshes for Manhole Type C. Left panel shows longitudinal velocity profile at the manhole centre and the right panel shows longitudinal velocity profile at the outlet pipe.

Table 2. Comparison between different mesh properties.

Name of mesh	Mesh size, dx (mm)	No. of cells	Grid Convergence Index, GCI	Coefficient of head loss, K
Mesh C1	10	2,137,000	1.38%	0.086
Mesh C2	14	865,000	2.7%	0.086
Mesh C3	20	329,000	---	0.088

In the analysis, 32 points (53%) showed oscillatory convergence. The average uncertainty at the outlet pipe were found to be 4.0% comparing Mesh C3 and C2, and 2.4% comparing Mesh C1 and C2. At the manhole center near the jet stream, the uncertainty was found to be less, average uncertainty was 4.37% comparing Mesh C3 and Mesh C2, and 2.71% comparing Mesh C1 and C2. However, the velocity is very small near the free surface (in the range of 0.1 m/s) and model prediction uncertainty at this zone rises to 32% comparing Mesh C1 and C2, and 54% comparing Mesh C2 and Mesh C3. Large uncertainty close to the free surface was found due to high gradient of velocity. The average grid convergence index (GCI) at the outlet pipe were recorded as 1.38% and 2.7% for Mesh C1 and Mesh C2 respectively, comparing with their immediate coarser meshes.

From Figure 3 (left panel), it can be seen that the coarse mesh of 20 mm (Mesh C3) creates different flow structure close to the water surface. While the other two meshes (14 mm and 10 mm) create similar flow in the manhole. As for this work, focus is given to manhole head loss coefficient $K (=2g\Delta H/v_x^2)$, the value was checked for all the three meshes. The K value in Mesh C1, Mesh C2 and Mesh C3 were found to be 0.086, 0.086 and 0.088 respectively, which are very similar to each other. Therefore, it can be said that although Mesh C3 showed different flow structure in the small scale compared to Mesh C1 and Mesh C2, but when considering the flow at large scale, Mesh C3 gives considerably good results, which justifies the use of similar mesh size for all the simulations.

4 RESULTS AND DISCUSSIONS

4.1 Manhole head loss coefficient and surcharge threshold

The flow through a manhole experiences sudden expansion and compression when entering and exiting a manhole, respectively. These changes involve loss of energy head of the flow. The head loss coefficient, K of the manholes is calculated using the following equation:

$$K = \frac{\Delta H}{v^2/2g} \quad [9]$$

where, ΔH is the change in energy head of the manhole center and v is the averaged flow velocity towards the flow direction at the outlet pipe. Figure 4 explains the change in energy head in a manhole. When determining

the head loss, the energy grade lines from inlet and outlet pipes are extrapolated to the manhole center and the difference between the extrapolated lines at the center gives the measurement of head loss.

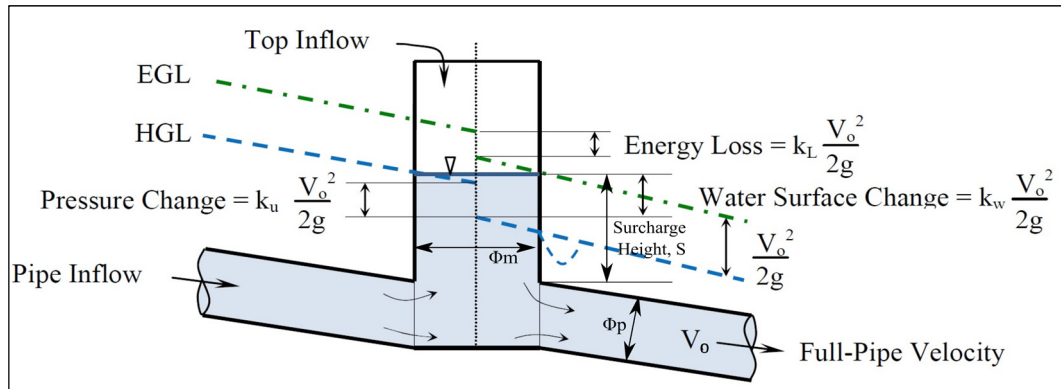


Figure 4. Head loss in a surcharged manhole, adopted from (Pang and O'Loughlin, 2011).

The Head loss coefficients of the manholes were checked at different manhole surcharge levels. The surcharge height (s) for a particular condition was calculated by subtracting the soffit level of inlet-outlet pipes from the water level of the manhole. Surcharge ratio (s/Φ_p) was calculated from each simulation results, as the ratio between surcharge heights (s) and inlet pipe diameter (Φ_p). The plots are shown in Figure 5.

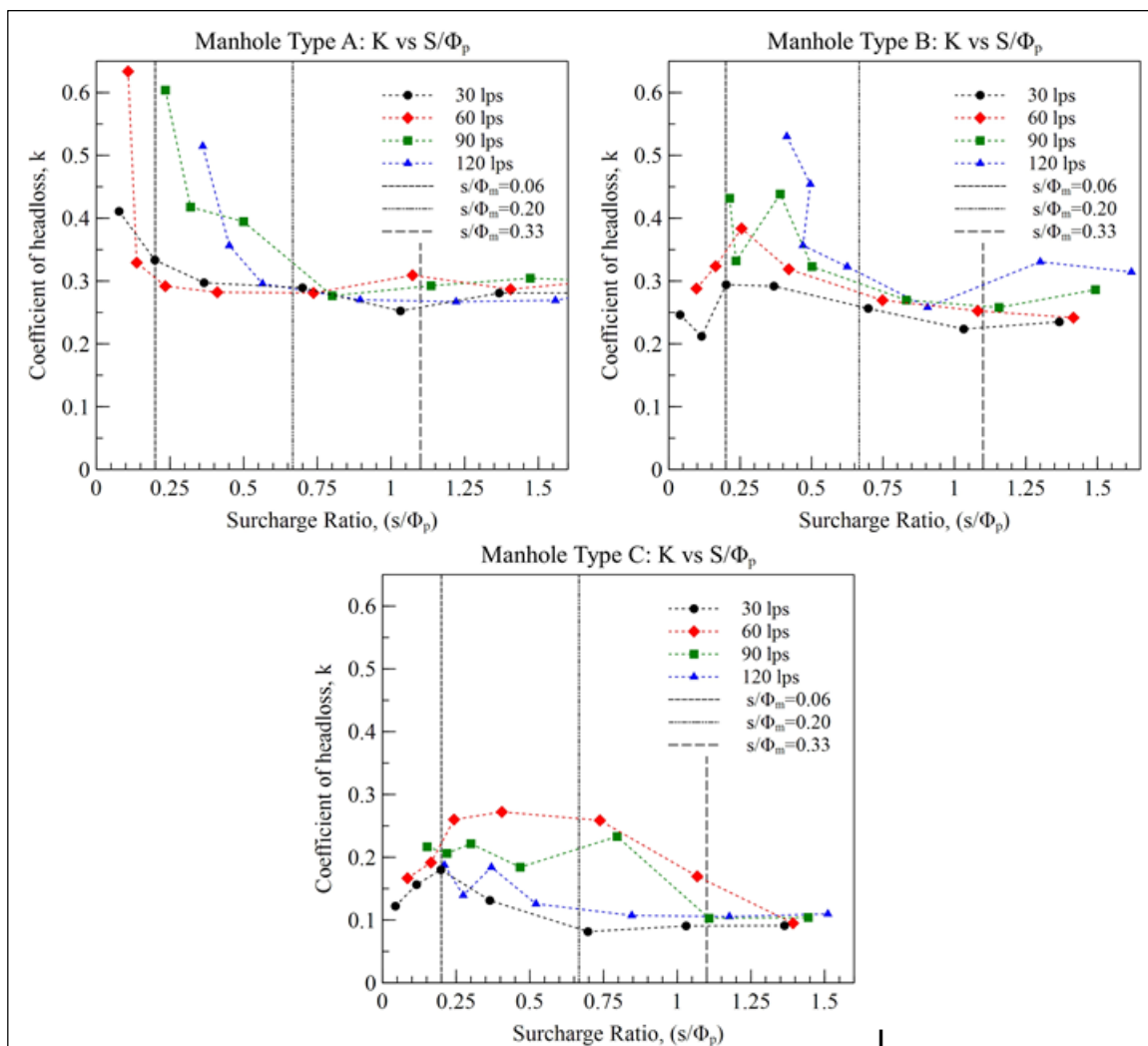


Figure 5. Manhole Head loss coefficient (K) vs Surcharge ratio (s/Φ_p) for manhole types A, B and C.

It can be seen from Figure 5 that out of the three manholes, Type A and Type B have comparably higher head losses in all scenarios than those of manhole Type C. All three manholes show higher head loss coefficients at low surcharge conditions.

For both manhole Type A and Type B, the head loss coefficient stays fairly around 0.3 at higher surcharge conditions (for $s/\Phi_m > 0.20$) with all types of inflow. When the surcharge ratio becomes low (for $s/\Phi_m < 0.20$), the head loss coefficient starts to increase. This can be explained by submerged jet theory. When the inlet flow enters a manhole, the incoming flow acts like a submerged jet and expands as a diffusive zone at a ratio 1:5 with the travelling length inside the manhole (Guymer et al., 2005; Stovin et al., 2013). While travelling through the diameter of the manhole (1 m), the diffusive zone may expand up to 0.20 m. When the surcharge height is below 0.20 m, the diffusive zone interacts with the free surface and creates additional head losses. In Figure 5, the surcharge height of 0.20 m is shown at each graph with a dotted line: $s/\Phi_m = 0.2$; which is also equivalent to the line: $s/\Phi_p = 0.67$ as the $\Phi_m/\Phi_p = 3.33$ for all the three manholes. This surcharge limit is termed as 'Threshold Surcharge' by some authors (Lau et al., 2008; Bennett, 2012; Stovin et al., 2013). The results from Type A and Type B manholes show that at the surcharge ratios (s/Φ_p) below 0.67, the coefficient of head loss becomes very high; which represents that threshold surcharge level is around 20% of the manhole diameter for these two types.

However, for manhole Type C at high surcharge conditions, the coefficient of head loss stays around 0.1 (for $s/\Phi_m > 0.33$). However, the head loss starts to increase at much higher surcharge height when compared to Type A and B manholes. Higher coefficient of head loss can be observed at Type C when $s/\Phi_m < 0.33$; (i.e. $s/\Phi_p < 1.11$). The phenomena can be checked in

Figure 6, which shows the velocity profiles at the center line ($y=0$ m) of the three manholes.

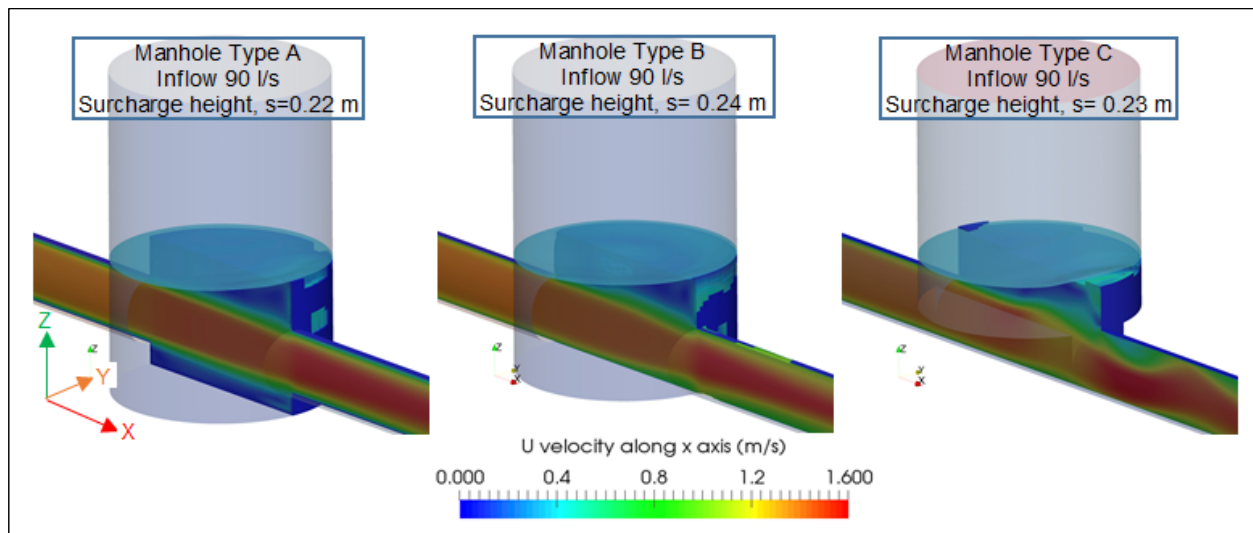


Figure 6. Instantaneous velocity profile at the central axis of the manhole. From left to right: Manhole Type A, Type B and Type C. The flow direction at each manhole is from left to right.

Figure 6 shows the manhole Type A, B and C at surcharge conditions such as $0.20 < s/\Phi_m < 0.33$. Type A and B show steady flow at this surcharge level. However, the jet velocity at Type C manhole expands more towards the vertical and interacts with the free surface creating oscillation inside the manhole and outlet pipe. This indicates that threshold surcharge level is higher than $0.20 \Phi_m$ in Type C manhole.

When the surcharge level is below threshold, the head loss coefficient (K) vs surcharge ratio (s/Φ_p) plot do not follow any particular trend. Perhaps, more simulation results might be required to describe the actual flow behavior at below threshold surcharge zone.

At manhole Type B and C, the head losses become less again at very low surcharge conditions (for $s/\Phi_m < 0.06$); while at Type A, the head loss seems to be the highest at low surcharge.

4.2 Free surface location at the manhole

The free surface position of a manhole varies at different surcharge and inflow conditions. This has been analyzed from the numerical model results. To analyze this, the Hydraulic Grade Lines (HGL) of the manholes with inlet-outlet pipes were checked, where:

$$\text{HGL} = \text{Elevation Head (Z)} + \text{Pressure Head } \left(\frac{P}{\rho g} \right) \quad [10]$$

Figure 7 shows the change of HGL at the manhole and its immediate upstream and downstream pipes from different simulation results. Each subplot represents one particular inflow and downstream pressure condition for all three manholes. It should be noted that the inlet pipe and the outlet pipe is connected to the manhole at $x=4.25$ m and $x=5.25$ m respectively. The value of HGL between $x=4.5$ m and $x=5.25$ m also represents the free surface location inside the manholes.

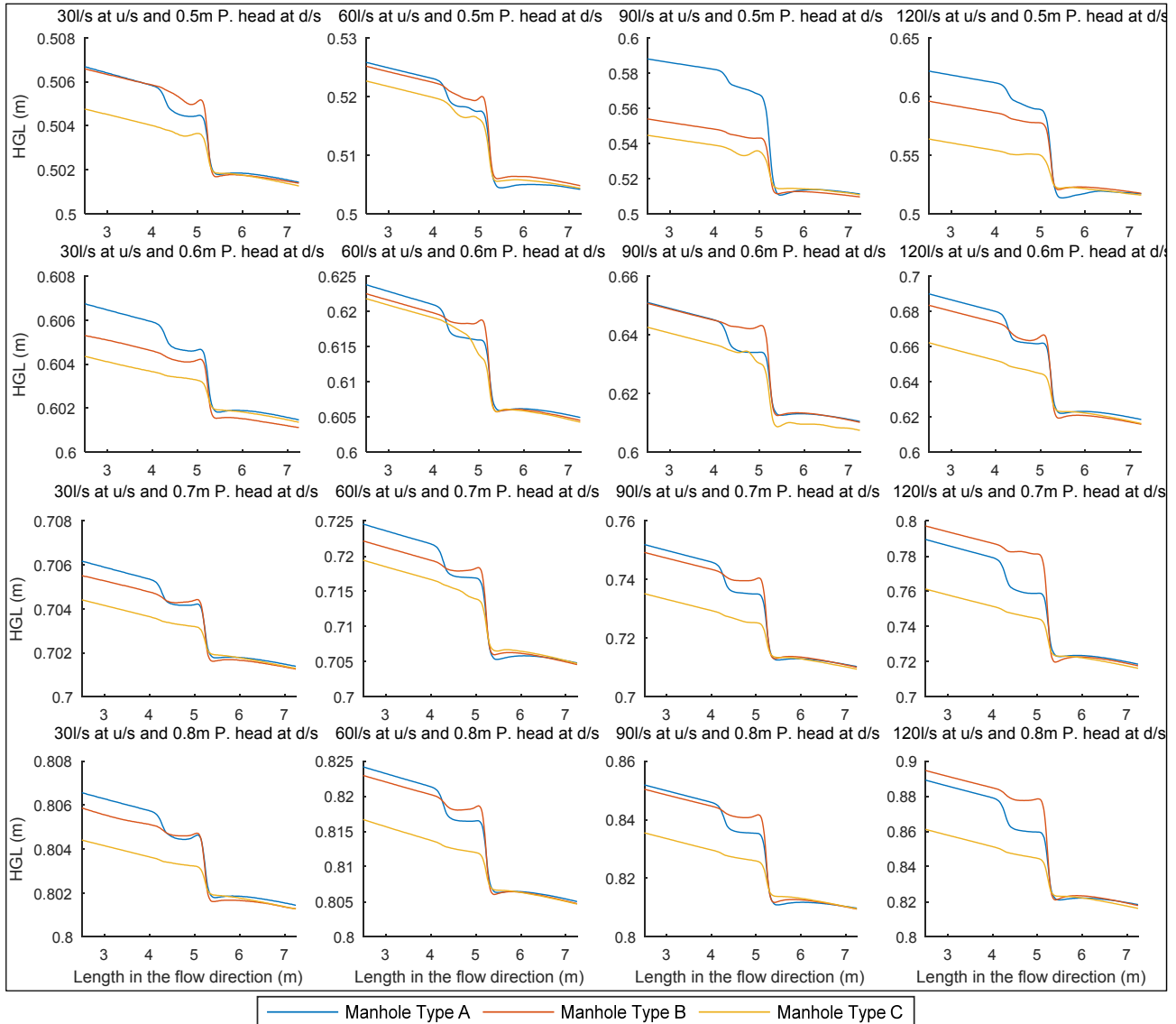


Figure 7. Position of Hydraulic Grade Line (HGL) in three types of manhole at different upstream (u/s) and downstream (d/s) cases. Blue, Red and Yellow lines show the data of Manhole Type A, B and C respectively.

Analyzing Figure 7, it can be seen that all the three manholes experience two different types of loss. The first head loss is seen at the inlet junction (near $x=4.25$ m) due to expansion of flow and the second head loss is observed at the outlet junction (near $x=5.25$ m) due to contraction. It can be seen that head losses at the manhole outlet junctions are more prominent than the losses at inlet junctions at all case scenarios.

Figure 7 also shows that head loss experienced by manhole Type C is significantly less than those of Type A and B. This difference may play a significant role at the time of very high surcharge scenarios. For any particular flood water level at the downstream, there is significantly higher chance of flooding at the upstream when the drainage network is based on Type A or Type B manholes other than Type C.

The total head loss at any manhole is higher at high discharge conditions than those of low discharge conditions. Comparing the simulation results at different inflow conditions with 0.8 m water pressures, it can be seen that the head loss at manhole Type A or B is in the range of 0.03 m per manhole when the inflow is 30 l/s. However, this increases to 0.07 m per manhole when the inflow is as high as 120 l/s. This shows that in higher drainage inflow conditions, it is more likely that the drainage congestion will increase and the chance of

street flooding will be greater. However, for the same surcharge and inflow scenarios, the head loss at Type C manhole is as low as 0.01 m at 30 l/s and 0.03 m at 120 l/s.

5 CONCLUSIONS

The work presented here compares the hydraulics and head loss coefficients of three different types of surcharged manhole. All the three manholes are prototype scales having 1.0 m diameters and connected with 300 mm inlet-outlet pipes. This makes the manhole to pipe diameter ratio equal to 3.33. The three manholes are: Type A, with no guided channel and a 0.10 m sump zone below the inlet outlet pipe invert level; Type B, similar to Type A but without sump at the bottom and Type C, with a U-invert shaped guided channel at the manhole bottom. The manholes were modelled numerically using open source CFD modelling tools OpenFOAM with interFoam solver. Realizable $k-\epsilon$ model was used to replicate the turbulence condition.

The manholes were simulated for different inflow and surcharge combinations. Each manhole showed different head loss coefficients at different surcharge levels. The threshold surcharge levels for Type A and B were found approximately as 20% to that of the manhole diameter; whereas for Type C manhole, it was more than 20%. All the three manholes showed higher head loss coefficients at surcharge conditions lower than threshold surcharge level. For any particular inflow and surcharge condition, manhole Type C was found to be most hydraulically efficient as it showed the lowest head loss coefficients at all inflow and surcharge conditions. The head loss coefficient values at different hydraulic conditions will be useful to provide data in developing an urban drainage model.

The Hydraulic Grade Lines (HGL) for all the manholes at different simulations were compared. Analysis showed that at higher inflow, the head loss becomes higher and makes the pressure or water surface level high at the upstream. This may increase the chance of flooding at the upstream of the drainage network. Analysis also showed that the chance of manhole overflow is higher at Type A and Type B manholes compared to that of Type C manholes.

ACKNOWLEDGEMENTS

The work presented is part of the QUICS (Quantifying Uncertainty in Integrated Catchment Studies) project. This project has received funding from the European Union's Seventh Framework Programme for research, technological development and demonstration under grant agreement No. 607000. The authors would also like to acknowledge the support of FCT (Portuguese Foundation for Science and Technology) through the Project UID/MAR/04292/2013 financed by MEC (Portuguese Ministry of Education and Science) and FSE (European Social Fund), under the program POCH (Human Capital Operational Programme).

REFERENCES

- Albertson, M.L., Dai, Y.B., Jensen, R.A. & Rouse, H. (1950). Diffusion of Submerged Jets. *Transactions of the American Society of Civil Engineers*, 115(1), 639-664.
- ANSYS Ins, (2009). *ANSYS Fluent 12.0 User's Guide*, s.l.: ANSYS Ins.
- Arao, S. & Kusada, T. (1999). Effects of Pipe Bending Angle on Energy Losses at Two-Way Circular Drop Manholes. *Proceeding of Eighth International Conference on Urban Storm Drainage*, 2163-2168.
- Beg, M.N.A., Carvalho, R., Lopes, P., Leandro, J. & Melo, N. (2016). Numerical Investigation of the Flow Field inside a Manhole-Pipe Drainage System.
- Bennett, P. (2012). *Evaluation of the Solute Transport Characteristics of Surcharged Manholes using a RANS Solution*, Sheffield, UK: University of Sheffield.
- Brackbill, J.U., Kothe, D.B. & Zemach, C. (1992). A Continuum Method for Modeling Surface Tension. *Journal of computational physics*, 100(2), 335-354.
- Butler, D. & Davies, J.W. (2011). *Urban Drainage*. London: Taylor & Francis.
- Carvalho, R.F. & Leandro, J. (2012). Hydraulic Characteristics of a Drop Square Manhole with a Downstream Control Gate. *Journal of irrigation and drainage engineering*, 138(6), 569-576.
- Carvalho, R.F., Lemos, C.M. & Ramos, C.M. (2008). Numerical Computation of the Flow in Hydraulic Jump Stilling Basins. *Journal of Hydraulic Research*, 46(6), 739-752.
- Celik, I.B., Ghia, U. & Roache, P.J. (2008). Procedure for Estimation and Reporting of Uncertainty due to Discretization in {CFD} Applications. *Journal of fluids {Engineering-Transactions} of the {ASME}*, 130(7).
- Greenshields, C.J. (2015). Openfoam User Guide. *OpenFOAM Foundation Ltd, version*, 3(1).
- Guymier, I., Dennis, P., O'Brien, R. & Saiyudthong, C. (2005). Diameter and Surcharge Effects on Solute Transport across Surcharged Manholes. *Journal of hydraulic engineering*, 131(4), 312-321.
- Hirt, C.W. & Nichols, B.D. (1981). Volume of Fluid (VOF) Method for the Dynamics of Free Boundaries. *Journal of computational physics*, 39(1), 201-225.
- Howarth, D.A. & Saul, A.J. (1984). Energy Loss Coefficients at Manholes. *Proceeding of 3rd Int. Conf. on Urban Storm Drainage, Chalmers Univ. of Technology, Goteborg, Sweden*, 127-136.
- Jasak, H. (1996). Error Analysis and Estimation for the Finite Volume Method with Applications to Fluid Flows.
- Juretić, F. (2015). *cfMesh User Guide v. 1.1. 1. Zagreb, Croatia: Creative Fields, Ltd.*
- Lau, S.T.D. (2007). *Scaling Dispersion Processes in Surcharged Manholes* (Doctoral dissertation, University of Sheffield).

- Lau, S.D., Stovin, V.R. & Guymer, I. (2007). The Prediction of Solute Transport in Surcharged Manholes using CFD. *Water science and technology*, 55(4), 57-64.
- Lau, S., Stovin, V., & Guymer, I. (2008). Scaling the Solute Transport Characteristics of a Surcharged Manhole. *Urban Water Journal*, 5(1), 33-42.
- Leandro, J., Chen, A.S., Djordjević, S. & Savić, D.A. (2009). Comparison of 1D/1D and 1D/2D Coupled (Sewer/Surface) Hydraulic Models for Urban Flood Simulation. *Journal of hydraulic engineering*, 135(6), 495-504.
- Leandro, J. & Martins, R. (2016). A Methodology for linking 2D Overland Flow Models with the Sewer Network Model SWMM 5.1 based on Dynamic Link Libraries. *Water Science and Technology*, 73(12), 3017-3026.
- Lopes, P. et al. (2014). Velocities Profiles and Air-entrainment Characterisation in a Scaled Circular Manhole. Sarawak, Malaysia, *13th International Conference on Urban Drainage*, pp. 7-12.
- Marsalek, J. (1984). Head Losses at Sewer Junction Manholes. *Journal of hydraulic engineering*, 110(8), 1150-1154.
- Pang, X. & O'Loughlin, G. (2011). Pressure Changes at Stormwater Pits with Part-Full Flows. Porto Alegre, Brazil, s.n., pp. 1-8.
- Pedersen, F.B., & Mark, O. (1990). Head Losses in Storm Sewer Manholes: Submerged Jet Theory. *Journal of Hydraulic Engineering*, 116(11), 1317-1328.
- Pfister, M. & Gisonni, C. (2014). Head Losses in Junction Manholes for Free Surface Flows in Circular Conduits. *Journal of Hydraulic Engineering*, 140(9), 06014015.
- Rusche, H. (2002). *Computational Fluid Dynamics of Dispersed Two-Phase Flows at High Phase Fractions*, London, UK: University of London.
- Shinji, A.R.A.O., Hiratsuka, S. & Kusuda, T. (2016). Formula on Energy Losses at Three-Way Circular Drop Manhole under Surge Flow. *Journal of JSCE*, 4(1), 19-37.
- Stovin, V., Bennett, P. & Guymer, I. (2013). Absence of a Hydraulic Threshold in Small-Diameter Surcharged Manholes. *Journal of Hydraulic Engineering*, 139(9), 984-994.
- Wang, K.H., Cleveland, T.G., Towsley, C. & Umrigar, D. (1998). Head Loss at Manholes in Surcharged Sewer Systems. *JAWRA Journal of the American Water Resources Association*, 34(6), 1391-1400.
- Weller, H.G. (2002). Derivation, Modelling and Solution of the Conditionally Averaged Two-Phase Flow Equations. *Nabla Ltd, No Technical Report TR/HGW/02*.

SUSTAINABLE URBAN STORMWATER MANAGEMENT TOWARDS ACHIEVING THE NEW URBAN AGENDA FOR SUSTAINABLE DEVELOPMENT

MOHD LOTFY MOHD NOH⁽¹⁾, MOHD RADZMAN OTHMAN⁽²⁾, NORLIZA HASHIM⁽³⁾, HASLINA ABU
HASHIM⁽⁴⁾, NOR AZAZI ZAKARIA⁽⁵⁾ & CHUN KIAT CHANG⁽⁶⁾

^(1,2) Kwasa Land Sdn. Bhd., Lot 116, Jalan Hevea, RRIM, Sungai Buloh, Selangor, Malaysia,
lotfy@kwasaland.com.my; radzman@kwasaland.com.my

⁽³⁾ AJM Planning And Urban Design Group, 8 Suria Block A, 33, Jalan PJU 1/42, Petaling Jaya, Selangor, Malaysia,
norliza@apudg.com

⁽⁴⁾ Perunding Hashim & NEH Sdn. Bhd., Level 13A, Block C, Plaza Mont Kiara, Mont Kiara, Kuala Lumpur, Malaysia,
lhashim73@gmail.com

^(5,6) River Engineering and Urban Drainage Research Centre (REDAC), Universiti Sains Malaysia, Nibong Tebal, Penang, Malaysia,
redac01@usm.my; redac10@usm.my

ABSTRACT

The on-going Kwasa Damansara Township development (2332 acres) aspire to be the first township in Malaysia planned and designed as a sustainable green city. The key initiative towards sustainable development goal started from the initial planning of the township. Innovative and creative urban design are provided and green technologies had been applied as an intervention towards a sustainable township where its emphasis is on green connectivity and inclusiveness. In doing so, one of the initiatives was to formulate the long term solution for the flooding, drainage and stormwater related issues by sustainable urban stormwater management. An environmentally-friendly and sustainable urban drainage system (SUDS) which complies with the guidelines of Urban Stormwater Management Manual for Malaysia (MSMA) has been designed and implemented to protect the environment of the surrounding areas. The proposed SUDS is designed for both water quantity and quality controls. This has been embodied in the concept of ecologically sustainable solution to the flooding and pollution problems using the "control at source" and "treatment train" approach, as well as aimed at ensuring that development can occur without long-term degradation of natural resources and the environment. An Urban Design Guidelines Document (UDG) was prepared to guide the future development of the entire township on plot level. These include the on-site and community level stormwater management planning, design and construction. The UDG supports the vision and objectives of the new township development, which carries the promise of a sustainable community township that focuses on three key components: green township, connectivity and inclusivity. They provide recommendations to ensure quality urban design and the establishment of a planning framework that allows for the creation of a successful and sustainable community. SUDS emphasizes the importance of a holistic approach to environmental engineering, landscape architecture and cost effective management, making it unique in the field of stormwater management and innovative urban development.

Keywords: SUDS; green township; urban stormwater management; control at source; treatment train.

1 INTRODUCTION

Stormwater management in Malaysia has traditionally focused on managing flood impacts based on a conveyance-oriented approach. Stormwater systems are designed to collect runoff at some point, and immediately and rapidly convey it to a discharge point, to minimize damage or disruption that could result in its passage to downstream areas. The introduction of Urban Stormwater Management Manual for Malaysia, or MSMA, changed the stormwater management landscape in the country. However, with the increasing need to meet demands for green technologies and arrest climate change, stormwater engineers are facing a stiffer challenge to produce effective and sustainable drainage system. This requires the need to inject new technologies or innovation into the design of drainage facilities. The integrated stormwater management concept will be fully adopted in formulating Stormwater Drainage Master Plan for the township development and compliance with MSMA. This site is planned to become a showpiece of the new concept of drainage system. Emphasis is on the necessity of the use of MSMA in all drainage design and implementation in order to protect the environment of the surrounding areas.

Kwasa Damansara Township aspires to be the first township in Malaysia planned and designed as a sustainable green city. The New Urban Agenda reaffirms the global commitment to sustainable urban development as a critical step for realizing sustainable development in an integrated and coordinated manner at the global, regional, national, subnational and local levels, with the participation of all relevant actors. The implementation of the New Urban Agenda contributes to the implementation and localization of the 2030 Agenda for Sustainable Development in an integrated manner, and to the achievement of the Sustainable Development

Goals and targets, including Goal 11 of making cities and human settlements inclusive, safe, resilient and sustainable (UNDP, 2017). In doing so, the Kwasa Damansara Township aims to be a sustainable green city taking initiatives such as transit oriented development, increasing green densities, promoting sustainable urban stormwater management, managing solid waste, encouraging green buildings and use of alternative energies as part of the city's green features.

2 PROJECT AREA

The proposed Kwasa Damansara new township is a master development project to be carried out on approximately 2332 acres (943 hectares) of land in Petaling District (Figure 1), where the land formerly belongs to Malaysia Rubber Research Institute (LGM), and will be developed under a 15-year construction plan with works that has been commenced in 2013. As a master developer, the objective of developing and delivering a town-city like no other to Malaysians, Kwasa Land Sdn. Bhd. will undertake the development project in collaboration with many notable local developers so as to produce high quality state of the art township.

The proposed development is situated on prime green field site along Jalan Sungai Buloh, amidst mature developments like Kota Damansara, Tropicana, Subang Indah. At the south boundary lies the Subang Terminal 3 Airport, whose flight path dictates height limits of the development. The proposed township lies between two major cities; Petaling Jaya at approximately 10.7km southeast and Shah Alam at about 11.6km southwest. As spanning across the northern zone of Greater Kuala Lumpur/Klang Valley, it also enhance the possibility of escalating land values of the township. The proposed Kwasa Damansara Township is strategically sited with high accessibility to major highways such as the North-South Highway, Damansara-Puchong Highway, Guthrie Highway and North Klang Valley Expressway.

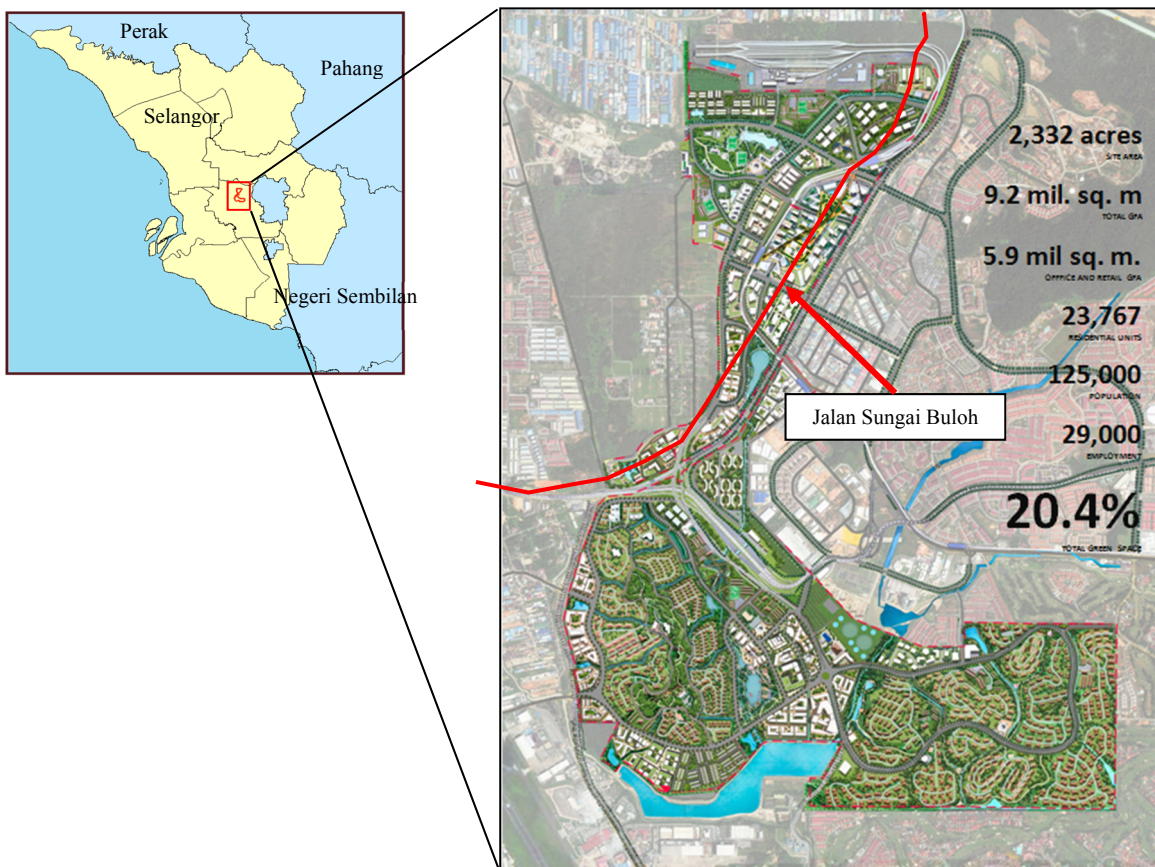


Figure 1. Project area.

3 SUSTAINABLE TOWNSHIP PLANNING

Kwasa Damansara is envisioned to be a green township development to respond to the nation's aspiration for ensuring climate-resilient development for sustainability that tries to reduce the risks of locking in unsustainable infrastructure. Kwasa Damansara Green Township strategy has considered a number of sustainable elements such as landscape and ecology, water, waste, green infrastructure, green buildings, green mobility and green energy. The key design objective for the proposed development is to create a new focal point that reflects the township of a 21st Century; one that is Green, Connected and has a sense of Place Making. In the effort to achieving a sustainable township that is green holistically, it is important to protect the sites' ecology

and develop a sustainable stormwater master plan that shall contribute towards environmental quality, which include protection and conservation of the existing river system.

3.1 Green

A modern green sustainable community township that spearhead's the Nation's commitment towards ecological improvements and efficient energy use which adopts green initiatives that enhance natural environs and ecology whilst creating urban bio-diversity that nurture high quality living environments.

3.2 Inclusive

An inclusive township, offering a built environment that responds to the needs of people from all walks of life including the less privileged within inclusively planned neighbourhood precinct, addresses accessibility aspects of diverse community groups to housing and public amenities, including recreational spaces and barrier free environments.

3.3 Connected

Kwasa Damansara is the first integrated township development complete with public transportation and transit oriented developments based on the principle of creating critical mass surrounding - a transit hub, with mixed use developments capitalizing on urban designs and functional opportunities.

Kwasa Land Sdn. Bhd.'s master developer model is a unique development implementation model that ensures the master developer has a take in the developments of the sub-parcels. The Master Plan indicates the proposed sub-development parcels with their intended land use and development intensity. These sub-parcels are to be jointly developed. One of the special initiatives from Kwasa Damansara is the implementation of Urban Design Guidelines (UDG) document which was prepared to guide the development of the entire township on plot level. The UDG document will also be read together with the local planning authorities' planning guidelines and relevant technical departments' requirements. The Sub-parcel developers are responsible in developing Level 2's infrastructure and public facilities, intended to serve the local community and will be located within the sub-developments' parcels respectively.

4 OVERALL STORMWATER MASTER PLAN CONCEPT

Stormwater management in Malaysia has traditionally been focused on managing flood impacts based on a conveyance-oriented approach. Stormwater systems are designed to collect runoff at some point, and immediately and rapidly convey it to a discharge point, to minimize damage or disruption that could result problems in its passage to downstream areas. In the past, stormwater runoff has been generally regarded as a nuisance that must be disposed off as quickly and efficiently as possible.

The introduction of Urban Stormwater Management Manual for Malaysia, or MSMA (DID, 2000), changed the stormwater management landscape in the country. However, with the increasing need of meeting demands for green technologies and arresting climate change, stormwater engineers are facing a stiffer challenge to produce effective and sustainable drainage system. This requires the need to inject new technologies or innovation into the design of drainage facilities. In 2011, a new-look manual, i.e. the second edition of Urban Stormwater Management Manual for Malaysia (DID, 2011) was released. The second edition, which includes revision of design criterias and improved design calculation methods, would contribute greatly to the continual growth of sustainable urban drainage design in Malaysia. The integrated stormwater management concept will be fully adopted in formulating Stormwater Drainage Master Plan for the township development and compliance to MSMA. This project site is planned to become a showpiece of the new concept of drainage system. Emphasis has been stressed on the necessity of the use of MSMA in all drainage design and implementation in order to protect the environment of the surrounding areas.

4.1 Control at Source

The emphasis on the control at source approach proposed in MSMA could be divided into three main components, which are water quantity control, erosion and sediment control, and water quality control. Water quantity control is a measure to curb post construction flash flood problems while erosion and sediment control are measures to minimize erosion and sedimentation problems during construction stage. The final item, which is the water quality control is intended to reduce post construction non-point source pollution problems. Stormwater quantity control facilities, either detention or retention facilities can reduce the peak and volume of runoff from a given catchment, which then can reduce the frequency and extent of downstream flooding. Detention and retention facilities have been used to reduce the costs of large stormwater drainage systems by reducing the size required for such systems in downstream areas.

4.2 Stormwater treatment train

The stormwater treatment train represents an ecological approach to stormwater management and has proven effective and versatile in its various applications. The stormwater treatment train was designed with sequential components that contribute to the treatment of stormwater before it leaves the site. The components of the stormwater treatment train system were designed to treat stormwater runoff for water quality benefits and

to reduce stormwater runoff peaks and volumes (CIRIA, 2007). This alternative approach to stormwater management not only has the potential to reduce infrastructure costs, but it also reduces maintenance costs. As described above, native plants are adapted to the environment, which will not need extensive watering, chemical treatment, mowing, and replanting that non-native species demand. In addition, there is also a substantial benefit to downstream neighbors. By treating stormwater where it falls on the land, responsible landowners are reducing their contribution to downstream flooding and sedimentation. The treatment train comprise of three stages:

a) Source control

Source controls are needed to reduce runoff from impervious surfaces on development parcels (rooftops, driveways, parking lots) and roads (paved roadway and sidewalks). The source control facilities allow control of runoff at or adjacent to the source (i.e. where rainfall lands on a surface). E.g. permeable or porous surfaces such as permeable paving, infiltration trenches, grassed swales, etc. These source control facilities can be planned for future individual parcel development as part of stormwater quantity and quality requirement.

b) On-site/community control

These local facilities such as community detention pond, on-site detention (OSD) will receive runoff from upstream locations, often with several inlets and only one controlled outlet. According to Selangor State Department of Irrigation and Drainage, the on-site detention (OSD) is required for small scale development, which is defined as a site/project development smaller than 20 acres. Otherwise a community detention pond shall be required.

c) Regional control

These include regional ponds that are larger than OSD. Regional ponds will collect runoff from upstream controls. They should receive less significant pollutants and runoff rates because of the series of stormwater controls by the treatment train upstream. Wherever possible, regional controls should be used as landscape features and provide final 'polishing' of the treatment train prior to discharge. In general, runoff quantity control requirements for any size of catchment in the new township is "Post development peak flow of any ARI at the catchment (regional pond outlet) must be less than or equal to the pre-development peak flow of the corresponding ARI ($Q_{post} \leq Q_{pre}$) before discharge to the receiving water body (river).

The term control facilities is used in this proposed development to describe any combination or arrangement of detention facilities in urban stormwater management systems as shown in Figure 2.

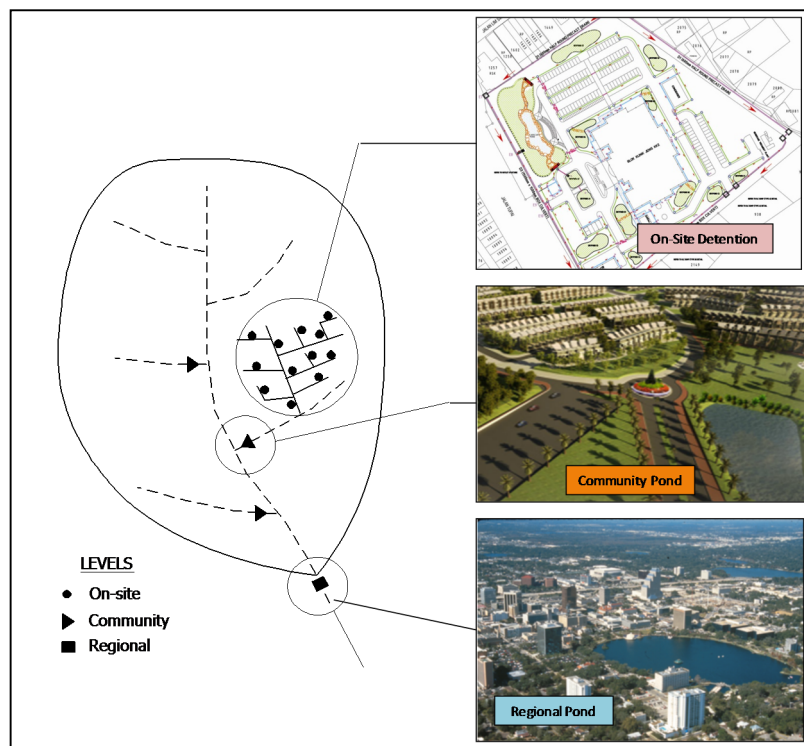


Figure 2. Stormwater quantity and quality control management concept (Control-at source and sotrmwater treatment train approach).

5 FORMULATION OF STORMWATER MASTER PLAN

5.1 Water catchment design

As part of the township's commitment to minimize development impact towards the natural environment, Kwasa Damansara has done a thorough study to ensure the number of pre-development water catchment areas is maintained and further enhanced through design by promote the preservation of pre-development hydrologic conditions. Kwasa Damansara township have a total of 22 water catchment areas, the same number of water catchment as before the development. The proposed Kwasa Damansara new township development is located on a medium hilly to low valley site with the lowest level of natural waterway at 9.00mIL and highest points ranging from around 67m to 119m peak points. With the development area geographically divided into north and south catchments by Jalan Sungai Buloh, the range of existing ground level for northern catchment are between 28m to 54m and between 10m to 119m for southern catchment. The pre-development and post-development catchment for the development area is shown Figure 3. The delineation of the sub-catchment (Figure 3(a)) was based on hydrological analysis using GIS, while post-development catchment Level 1's infrastructure are plan and design based on the stormwater master plan concept.

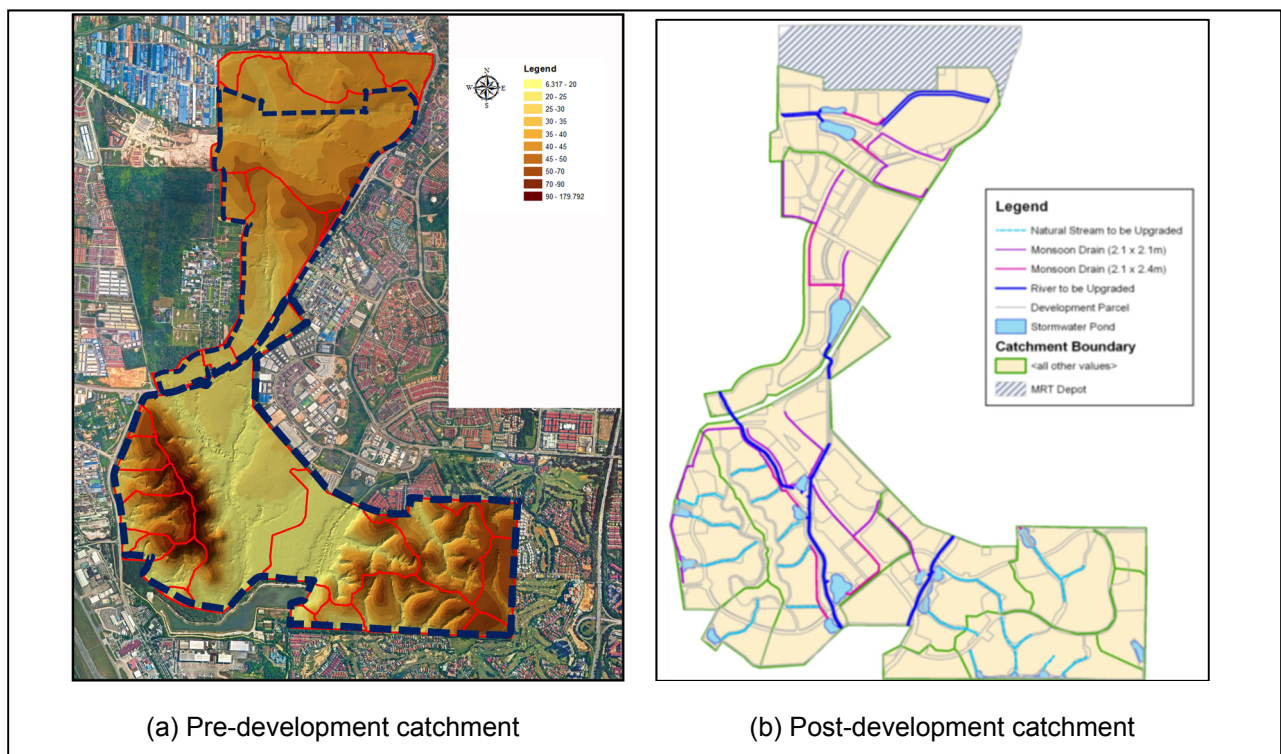


Figure 3. Kwasa Damansara water catchment.

5.2 Stormwater drainage design

Stormwater drainage is the key component in a city's infrastructure to collect and convey stormwater from a catchment to its receiving water by formulating the long term solution for the flooding and providing an appropriate level of flood protection to community expectations. Besides that, it also manages and improves the quality of stormwater runoff from urbanized catchment and its pollution loads in order to minimise the impact and reduce the adverse effects of non-point source contamination of the receiving water environment.

One of the key features of the township will be its sustainable urban water management. Here, the drainage system is designed to provide time for natural processes of sedimentation, filtration and biodegradation to occur, which reduce the pollutant loads in stormwater runoff as much as possible by applying sustainable urban drainage system (SUDS), one of the such system is BIOECODS, developed by River Engineering and Urban Drainage Research Centre (REDAC), Universiti Sains Malaysia (Zakaria et al., 2004). The BIOECODS is a stormwater drainage system designed with the concept of SUDS in mind, and as a result, is in full compliance with the MSMA requirements. BIOECODS is made up of several important components that ultimately form an effective stormwater treatment train that control runoff quantity and preserve runoff quality. The BIOECODS is an ecologically sustainable solution for flash flood, river pollution and water scarcity by providing time for natural processes of sedimentation, filtration and biodegradation to occur, which reduce the pollutant loads in stormwater runoff. In addition, BIOECODS blends easily into its surrounding, adding considerably to the local amenity and/or local biodiversity (Ab Ghani et al., 2004; Ainan et al., 2004; Ayub et al., 2005). Stormwater systems in Kwasa Damansara town development are divided into two categories: minor and major as follows.

5.2.1 Minor system

The minor system is intended to collect, control and convey runoff from buildings, infrastructures and utilities in relatively frequent storm events to minimise inconvenience and nuisance flooding. Components in the minor system are sized to manage runoff generated by the more frequent short duration storm events.

- a. Road side drain - The roadside drain systems shall consist of either concealed concrete lined box culvert with inlets along road kerbs or bio-filtration swale (Figure 4), which is in line with the local council's minimum guidelines. A concealed system was chosen to allow the roadside kerbs to double as pedestrian walkway hence providing connectivity throughout the development.

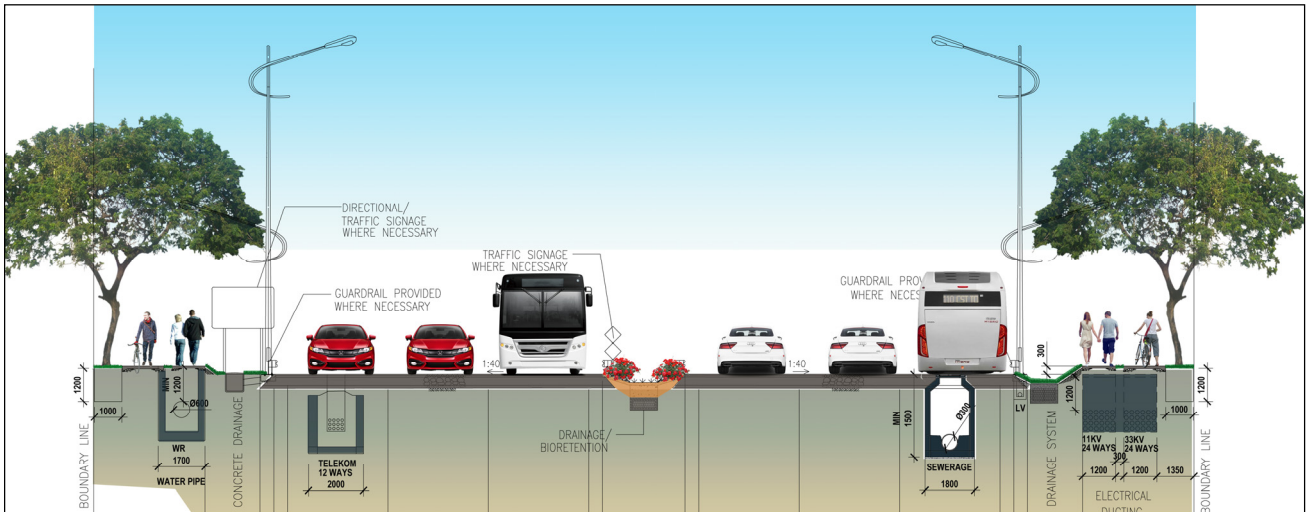


Figure 4. Example of typical road sectional.

- b. Bio-Filtration swale - In order to reduce the drainage footprint of the BIOECODS, as well as to provide additional water treatment, a dual layer conveyance system is introduced (Figure 5). While the surface of the swale is generally not much larger than conventional drain, the total cross section area of the system provides much larger water storage and treatment function than a normal conventional drainage. The surface layer resembles a grassed channel or a swale. Typical swale design of gentle side slope, low gradient and shallow depth is applied to this layer. The underground layer, consist of a geosynthetic module wrapped in nonwoven geotextile and is buried in porous permeable soils. It is connected to the surface layer via a layer of river sand or infiltration media.



Figure 5. Bio-filtration swale.

- c. Bioretention - Bioretention are designed as dual layer conveyance-storage system in road median (Figure 6). Surface runoff is directed into shallow, landscaped depressions that are designed to incorporate many of the pollutant removal mechanisms that operate in forested ecosystems. During storm events, surface runoff remains ponded above the soil/filter media layer. Runoff from larger storms is generally diverted past the facility to the storm drain system. The remaining runoff is filtered through the soil/ filter media later. Typically, the filtered runoff is collected in a perforated underdrain and returned to the storm drain system, or is allowed to percolate further into the ground for groundwater recharge.



Figure 6. Completion of bioretention.

- d. On-site storage - On-site Stormwater Detention (OSD) involves the temporary storage and controlled release of stormwater generated within a site at a predetermined rate. In general, on-site storage are small storages constructed within individual residential, commercial, and industrial lots. Figure 7 shows the example of underground OSD at a 'Park & Ride' sub-parcel. Geosynthetic modules can be arranged to form a rectangular storage system offering virtually limitless storage in a shape that fits any site geometry. The sub-surface storage tank can be achieved with low maintenance, reducing peak flow, frees up space for landscaping and parking lots. The OSD, though is to be dry most of the time, also provides optimal conditions for retaining water during storm event.



Figure 7. Example of underground OSD at 'Park & Ride'.

5.2.2 Major system

The major system is intended to safely convey and control runoff collected by the minor drainage system together with its possible overflow to the larger downstream systems and water bodies. The major system must protect the community from the consequences of large and reasonably rare storm events (up to 100-year ARI), which could cause severe property damage, injury or loss of life.

- a. Main drain - All roadside drains or minor drain from each development shall flow into the downstream main drains where the runoff will be conveyed into a detention system downstream. The proposed main drains shall be covered with box culvert (Figure 8). Primary treatment facilities such as gross pollutant traps (GPTs) required for the main drains will be considered as part of the "treatment train".



Figure 8. Installation of main drain at project site.

- b. Engineered channel - Engineered channel are part of the major drainage system designed to collect and convey flows from the minor drainage system and to provide for the safe passage of larger flows up to the major design storm. The types of engineered channels available for urban drainage systems are almost infinite, depending only upon good hydraulic practices, environmental design, sociological impact, and basic project requirements. However, from a practical standpoint, the basic choice to be made initially is whether the waterway is to be a hard-lined channel or bio-engineered channel for higher velocities, as well as a grassed-lined channel, or existing natural channel to be upgraded.

- c. Community storage - Community storage is a storage facility for sub-parcel developers who are responsible in developing Level 2's infrastructure. In general, facilities such as detention ponds are used for controlling the increase in stormwater quantity resulting from larger urbanization. An overflow spillway set near the top of the embankment is required to safely discharge runoff that exceed the basin's discharge outlet capacity, to the main drain or river.
- d. Regional storage - Large community storage facilities constructed in public open space areas outside of private properties, or in conjunction with public recreation and sporting facilities at the lower end of catchments prior to discharge to receiving waters (river). It is suggested that all the inlets to the ponds shall have pre-treatment pollutant control facilities such as sediment forebay or other type of Gross Pollutant Trap (GPTs'). Generally, detention ponds are the stormwater facilities of the BIOECODS. They are primarily designed for attenuating runoff from developed areas through regulated outlet structures. The facility is typically designed to limit discharge to the pre-development stage, while storing water temporarily. The end product is expected to improve the aesthetic value for surrounding areas with the existence of the "Crystal Clear Blue Water Lake" at the most downstream end of the drainage system before discharging into rivers (Figure 9). The system, combined with landscaping by the planting of aquatic or wetland plants, can help to improve the quality of water naturally and increase infiltration by evapotranspiration process. The wetland plants will promote the increase of biodiversity within the aquatic/semi-aquatic habitat created on site.



Figure 9. Detention pond with sediment forebay.

5.3 River rehabilitation

A river is defined as any natural stream of water that flows in a channel with defined banks. Rivers are valuable natural resources for human, environment and national development. However, during a rain event, domestic waste such as solid waste and garbage will easily be carried by runoff into the open drains and subsequently into rivers. As a consequence, the government will have to allocate huge amount of funds to remove the solid wastes from these polluted rivers. Therefore, it is important that with the implementation of MSMA, which incorporates the latest development in stormwater management, i.e. control-at-source and treatment train concepts, the quantity of the runoff from developed area can be maintained to be the same as predevelopment conditions and thus, also minimise the impact of water quality problems. Besides that, maintenance costs may be minimal where river corridor protection and channel management rights have been secured and less conflict on all or part of the restored channel is anticipated in the future (DID, 2009).

Green infrastructure is strategically planned and managed for river rehabilitation (Figure 10) to ensure that the ecosystem values and function is well preserved and to provide benefits to our daily life and it costs less to be installed compared to traditional infrastructure system. It benefits the environment due to its minimal impact on local ecology and also minimal post-construction maintenance. River rehabilitation for existing rivers in project area is a highly preferred alternative due to the benefits associated with long term economic and ecological sustainability. By restoring vegetation using bio-engineering technique, it can filter pollutant, promotes groundwater recharge, add oxygen into the atmosphere and increase wildlife habitat. Under such implementation, it can be safely expected that such efforts will benefit not only the rich diversity of fishes and other aquatic life but also improve the overall aesthetics of the river and surrounding landscapes, as well as the quality of life for the human communities themselves. With the anticipated clean water quality within the development area, it will not only spur the economic investments by increasing the economic viability, but also the overall townships aspiration to become the top most liveable cities in Malaysia.



Figure 10. On going river rehabilitation work using bio-engineering technique.

5.4 Parks and green spaces

Good quality parks and green spaces contribute to the individual's wellbeing, and through their social, economic and environmental values, contribute to more liveable and attractive towns and cities (CABE Space, 2004; Maas et al., 2006; Hartig, 2007; Bell et al., 2008). Kwasa Damansara masterplan has dedicated 20.4% of overall township area for green and blue corridor, i.e. a combination of stormwater facilities and the green area. This approach is also an opportunity to make full use of the existing water resources, enhancing the aesthetic potential and producing landscape impact while improving the quality of the environment as well as giving added value to the township's development. The concept is the backbone that makes up the character of this development while preserving, protecting and enhancing the ecosystems, flora and fauna and enrich local biodiversity. Parks and their green connectivity also acts as a source of carbon sequestration that is important in the effort to reduce carbon emissions in Kwasa Damansara via its large canopy coverage that can reduce the urban heat island effect.

The Kwasa Damansara masterplan has determined a few types of open spaces to be designated in the township. Different hierarchies of green spaces are allocated to cater various needs of recreation, education, leisure, communal space and nature appreciation. Although the total green areas and open spaces has exceeded the 10% requirement, additional innovative measures are encouraged to green areas, i.e through the usage of elevated parks, green roofs, and terraced garden. As a result, a total of 475.51 acres of green areas or 31.5 sq.m. per person of green spaces (Table 1) will be provided in the township, far exceeding the national standards of 20 sq.m. per person of green spaces as stated in Malaysia Environmental Performance Index (EPI).

Table 1. Green density in Kwasa Damansara.

Landuse	Area (Acres)
Green area	168.6
Graveyard	10.9
Detention ponds	29.55
River reserves	76.53
Road reserves	79.9
Private green from Level 2's sub-parcel infrastructure	110.23
Total Green	475.71
Total Land Area	2332.4
Percentage of green (Public & Communal)	20.40%
Total population (residents from residential and 70% from mixed use)	61,373
Total green (sqm)/ total population	31.3 sqm/ per person

6 CONCLUSIONS

Kwasa Damansara has aspired to become a model township in Malaysia that implements a number of solutions to address the issues of cities today. With having three visions of being green, inclusive and connected, Kwasa Damansara is on its way to achieve the targets set earlier in the design concept stage. The three visions are inline with the sustainable development goals (SDGs) that are part of the 2030 Agenda, i.e. SDG 11, aims at ensuring the development of sustainable cities and communities. Realising this, Kwasa Damansara, as like any other part of the world has embraced sustainability as an important feature for master planning. Kwasa Damansara's sustainable agenda is structured by Malaysia's aspiration towards the objective of sustainable urbanisation.

The primary goal of the stormwater management and drainage master plan development is to minimise the impact of urbanisation of the stormwater environment and to strike a balance between social, economic and environmental concerns to achieve sustainable development. It has been the Malaysian Government's commitment to ensure a balanced approach in its efforts in promoting socio-economic development and the management of natural resources and environmental quality. As the Kwasa Damansara development is planned to become a showpiece of the new management concept using sustainable urban drainage system (SUDS),

the integrated stormwater management and river management approach will be fully adopted in formulating Stormwater Drainage Master Plan for the Kwasa Damansara township development and to meet the technical requirements of the MSMA and DID Manual in all river and drainage design requirements.

REFERENCES

- Ab. Ghani, A., Zakaria, N.A., Abdullah, R., Yusof, M.F., Mohd Sidek, L., Kassim, A.H. & Ainan, A. (2004). BIO-Ecological Drainage System (BIOECODS): Concept, Design and Construction. *The 6th International Conference on Hydroscience and Engineering (ICHE-2004)*, May 30-June 3, Brisbane, Australia.
- Ainan, A., Zakaria, N.A., Ab. Ghani, A., Abdullah, R., Mohd Sidek, L., Yusof, M.F. & Wong, L.P. (2004). Peak Flow Attenuation Using Ecological Swale and Dry Pond. *The 6th International Conference on Hydroscience and Engineering (ICHE-2004)*, May 30-June 3, Brisbane, Australia.
- Ayub, K.R., Mohd Sidek, L., Ainan, A., Zakaria, N.A., Ab. Ghani, A. & Abdullah, R. (2005). Storm Water Treatment Using Bio-Ecological Drainage System. *International Journal River Basin Management, Special Issue Rivers'04*, 3(3), 215-221.
- Bell, S., Hamilton, V., Montarzino, A., Rothnie, H., Travlou, P. & Alves, S. (2008). Greenspace and Quality Of Life: A Critical Literature Review. *Greenspace Scotland, Stirling*.
- CABE Space. (2004). The Value of Public Space: How High Quality Parks and Public Spaces Create Economy, Social and Environmental Value. *CABE, London*.
- Construction Industry Research and Information Association (2007). *The SUDS Manual (C697)*. CIRIA, London, UK.
- Department of Irrigation and Drainage or DID, (2000). *Urban Stormwater Management Manual for Malaysia (MSMA)*. DID, Kuala Lumpur.
- Departments of Irrigation and Drainage or DID (2009). *DID Manual. Vol.2: River Management*. DID, Kuala Lumpur
- Department of Irrigation and Drainage or DID, (2011). *Second Edition of Urban Stormwater Management Manual for Malaysia (MSMA 2nd Edition)*. DID, Kuala Lumpur.
- Hartig, T. (2007). Three Steps to Understanding Restoration Environments As Health Resources. In Ward Thompson, C. and Travlou, P. (Eds.). *Open Space: People Space*. Abingdon, UK. Taylor and Francis, 163-179.
- Maas, J., Verheij, R.A., Groenewegen, P.P., de Vries, S. & Spreeuwenberg, P. (2006). Green Space, Urbanity, and Health: How Strong Is The Relation? *Journal of Epidemiology and Community Health*, 60, 587-592.
- United Nations Development Programme or UNDP. (2017). Sustainable Development Goals, <http://www.undp.org/content/undp/en/home/sustainable-development-goals/goal-11-sustainable-cities-and-communities.html>, [Accessed on Feb. 1, 2017].
- Zakaria, N.A., Ab. Ghani, A., Abdullah, R., Mohd Sidek, L. & Ainan, A. (2004). Bio-Ecological Drainage System (BIOECODS) for Water Quantity and Quality Control. *International Journal River Basin Management*, 1(3), 237-251.

A PRELIMINARY DEVELOPMENT OF A NUMERICAL MODEL FOR SIMULATION OF FLOW IN BINARY MIXTURE

MUHAMMAD FAIZ ABDULLAH⁽¹⁾, HOW TION PUAY⁽²⁾ & NOR AZAZI ZAKARIA⁽³⁾

^(1,2,3) River Engineering and Urban Drainage Research Centre (REDAC), Universiti Sains Malaysia, Engineering Campus, Penang,
m.faiz.abdullah123@gmail.com; redac_puay@usm.my; redac01@usm.my

ABSTRACT

A numerical model based on the Marker and Cell (MAC) method is developed for the simulation of flow in binary mixture. The porous media is represented as obstacles in the numerical model by using the Fractional-Area Volume Obstacle Representation (FAVOR) technique. The numerical model was initially verified against experiment of lateral inflow into single size porous media. For the verification of flow through binary mixture, the vertical infiltration process (column test) was simulated and the hydraulic conductivity was compared against the laboratory experiment result. Good agreement in the saturated hydraulic conductivity obtained from the numerical and experimental work is observed.

Keywords: MAC method; FAVOR; porous media; saturated hydraulic conductivity; binary mixture.

1 INTRODUCTION

With the growing popularity of SuDs in storm water management, the studies of flow in porous media and its application in SuDs facilities deserve attentions. The porosity of the media used is critical in the design of such facilities (Ballard et al., 2007). Although single size porous media is commonly used, a binary-mixture can be an option to overcome material shortage or cost reduction if its hydraulic performance is known. In the case of binary-mixture, the relationship between the mixture porosity and its saturated hydraulic conductivity are of particular interest in the study of hydraulic performance of binary mixture. Mota et al. (2001) investigated the relationship between the hydraulic conductivity and the binary mixture porosity of spherical particles by proposing a porosity model based on linear mixing. Zhang et al. (2011) proposed the mixing coefficient model to determine the porosity of binary mixture and a power-averaging method to determine the effective particle diameter of binary mixture. On the other hand, the characteristic diameter of a mixtures based on moment method by MacDonald et al. (1991) was used by Morad et al. (2009) in the study of transition layer thickness in fluid-porous media of multi-size spherical beads.

The investigation of free surface characteristic through porous media with numerical model can be seen in work of Ghimire et al. (2007) where the Volume of Fluid (VOF) method was used and the volume averaged Navier-Stokes equation with resistance term was solved. In this study, a numerical model based on the MAC method by Welch et al. (1965) was developed to simulate free surface flow in porous media. The MAC method is considered as one of the earlier numerical model for free-surface flow and it is gaining revival in recent years due to the advancement of computational power (McKee et al., 2008). In this study, the porous media is represented in the numerical model as obstacles by using the Fractional-Area Volume Obstacle Representation (FAVOR) technique by Hirt and Sicilian (1985). These obstacles are imaginary and are placed randomly so that in each cell the ratio of obstacle volume to the cell volume is equal to the porosity of the porous media as shown in Figure 1. The ratio of surface opening on the cell boundaries are also set to be equal to the porosity of the media.

In this preliminary study to develop a numerical model for the simulation of flow in binary mixture, the relationship between porosity and hydraulic conductivity is discussed briefly based on the mixing model by Zhang et al. (2011). The porosity and hydraulic conductivity from the laboratory tests are presented and compared with the mixing model theory. The numerical model was used to reproduce the hydraulic conductivity of binary mixtures from the laboratory test. Prior to this, the numerical model was verified against lateral intrusion of flow into single size media.

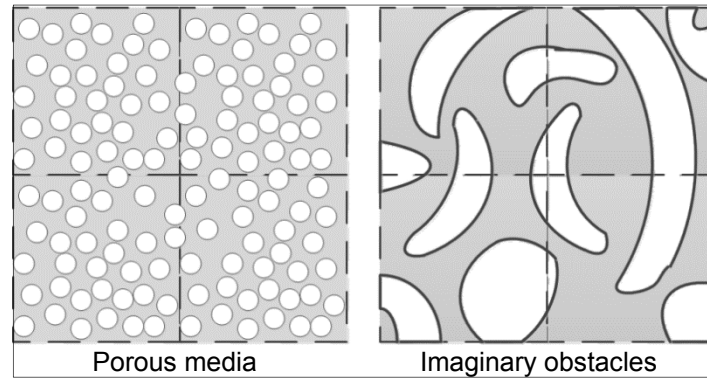


Figure 1. Illustration of FAVOR technique for the representation of porous media with obstacles.

2 MIXING MODEL FOR BINARY MIXTURE

The Kozeny-Carman equation (Bear, 2013) was used to relate the porosity and representative diameter with the saturated hydraulic conductivity as follows,

$$K_{sm} = \left(\frac{\rho g}{\mu} \right) \left[\frac{d_m^2 \phi_m^3}{180(1 - \phi)^2} \right] \quad [1]$$

where

K_{sm}	=	saturated hydraulic conductivity of the mixture
d_m	=	representative particle diameter of the mixture
ϕ_m	=	porosity of the mixture
ρ	=	fluid density
g	=	gravitational acceleration
μ	=	dynamic viscosity

For the case of binary mixture, the mixing model proposed by Zhang et al. (2011) is used where the porosity of the mixture ϕ_m is defined as in Eq. [2].

$$\phi_m = \begin{cases} (b_{vc} - \lambda b_{vc} + \lambda)\phi_c + b_{vf}\phi_f - \lambda b_{vc} & \text{if } b_{vf} < \phi_c \\ (1 - \lambda)b_{vc}\phi_c + b_{vf}\phi_f & \text{if } b_{vf} \geq \phi_c \end{cases} \quad [2]$$

b_{vc} and b_{vf} are defined as the volume fraction of the coarse and fine particles respectively. ϕ_c and ϕ_f are the porosity of the coarse particles and fine particles respectively. The mixing coefficient, λ varies between 0 and 1 depending on the degree of mixing of the mixture and is defined in Eq. [3] with ϕ^{ub} and ϕ^{lb} as the porosity of the upper bound and lower bound and ϕ_m is the porosity based on the degree of mixture or mixing coefficient λ .

$$\lambda = \frac{\phi^{ub} - \phi_m}{\phi^{ub} - \phi^{lb}} \quad [3]$$

We used the power-averaging representative diameter proposed by Zhang et al. (2011) to approximate d_m as follows

$$d_m = (b_{vc}d_c^p + b_{vf}d_f^p)^{\frac{1}{p}}, p = \{1 + \exp[20(1 - \phi_c - b_{vc})]\}^{-1} - 1 \quad [4]$$

In this study, the porosity and K_{sm} of the binary mixture are determined under three conditions, namely: 1) upper bound, assuming the two components are packed without mixing with one another, hence gives the highest value of porosity and K_{sm} of the mixture; 2) lower bound, assuming that to both beads sizes are fully mixed and gives the minimum value of porosity and K_{sm} of the mixture 3) under random mixing condition where both beads sizes are partially mixed.

3 NUMERICAL MODEL

The numerical model solves the following continuity and momentum equations.

Continuity:

$$\frac{\partial c_i^a u_i}{\partial x_i} = 0 \quad [5]$$

Momentum:

$$\frac{\partial u_i}{\partial t} + \frac{c_i^\alpha}{c^v} \frac{\partial u_i u_j}{\partial x_j} = g - \frac{1}{\rho} \frac{\partial p}{\partial x_i} + \nu \frac{\partial^2 u_i}{\partial x_j \partial x_j} - \frac{1}{c^v} \left[\frac{\nu}{K} \phi u_i + F_{ch} \phi^2 |u_i| |u_i| \right] \quad [6]$$

u_i is the velocity vector, also called the pore water velocity in the porous medium, ϕ is the porosity the porous medium, p is the pressure and ν is the kinematic viscosity of the fluid. c_i^α is the ratio of area opened to flow at the cell boundary where u_i is defined. c^v is the ratio of volume opened to flow in that cell based on the definition of FAVOR technique (Hirt and Sicilian, 1985). In this model, the ratios c_i^α and c^v were set to be equal to the porosity of the mixture.

The viscous drag term is introduced at the 4th term at the right-hand side of equation [6] by using Darcy's Law with the K as the permeability of the porous media based on Kozeny equation. The F_{ch} are Forchheimer's inertia factor base on Whitaker (1996) and is introduced at the 5th term of equation [6] to indicate the drag term from porous media into the model as follows,

$$K = \frac{\phi^3 d^2}{b(1-\phi)^2} \quad \text{and} \quad F_{ch} = \frac{1.75(1-\phi)}{d \phi^3} \quad [7]$$

Here, d = representative diameter of particle. The value $b = 180$ is used when the porous medium is made of particle (Nield and Bejan, 1999). A 3rd order Kawamura-Kuwahara scheme (Kawamura et al., 1985) is used to discretize the advection term in Eq. [2]. Mesh cell sizes in x and y directions were set to 5mm.

The numerical model was initially verified by simulating the lateral intrusion of flow into single size porous media under constant head at inlet (0.85m). The result of the numerical model was verified against the experimental work by Ghimire et al. (2007) in terms of the development of free surface. In the next stage, the numerical model was used to reproduce the saturated hydraulic conductivity of flow through binary mixture. The results are compared with the laboratory column tests' results.

4 EXPERIMENTAL SETUP

The saturated hydraulic conductivity of single size media and binary mixture were measured using a constant head method in a column test as shown in Fig. 2. The column has an internal diameter of 0.20m and a height of 1.0m and the sample height, L is 0.30m. Water supply were injected from the bottom of the column from the constant head reservoir. A manometer was connected to column below of the porous media sample for the measurement of water head difference across the porous bed. For measurement of each sample, four to six heads were applied to calculate the K_{sm} of the mixture.

Glass beads with size 30mm and 0.6mm-0.8mm were used to represent the coarse and fine particles. The porosities of single size beads and mixtures based on several coarse ratios (by volume) were measured. The column tests were then carried out based for the single size beads and several binary mixtures.

5 RESULTS AND DISCUSSIONS

5.1 Lateral intrusion into single size porous media

The result for the numerical simulation of lateral intrusion into single size porous media was compared with the experimental data by Ghimire et al. (2007) that using 1mm beads as shown in Fig. 3. In general, the numerical model could reproduce the propagation of flow into porous media. However, the propagation of the flow in the numerical model is slower than the experiment. Besides, although the flow depth at the inlet was set at 0.85m, the experiment showed that the depth in the porous media right after the inlet increases. This phenomenon is due to the capillary effect which could not be reproduced in the numerical model. This explained the lower profile at the beginning of the numerical model if compared with the experimental model. The slower intrusion of flow in the numerical model could be due to the inability of the numerical model to reproduce the capillary effect. Another possible factor to the slower propagation in the numerical model might be due to the inaccuracy in reproducing momentum transfer at the boundaries between porous media and the water at the inlet. Momentum transfer has been discussed by Ochoa-Tapia and Whitaker (1995) and this term has not been included in this numerical model. Future development of this model may consider including this term later.

5.2 Porosity

The porosity of the binary mixtures at different coarse fraction, b_{vc} in the experiment is shown in Fig. 4. The upper bound porosity corresponding to zero-mixing is indicated by the maximum value of the porosity and the lower bound porosity, which corresponds to the ideal packing model, give the minimum value of the porosity of the mixture. These two lines are plotted based on Eq. [4] with $\lambda = 1$ and $\lambda = 0$ for upper and lower bound respectively.

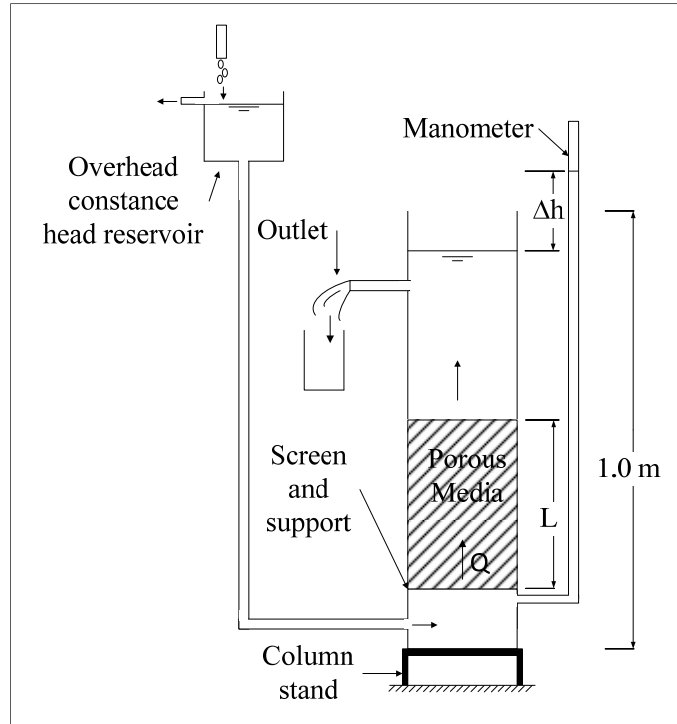


Figure 2. Experimental setup.

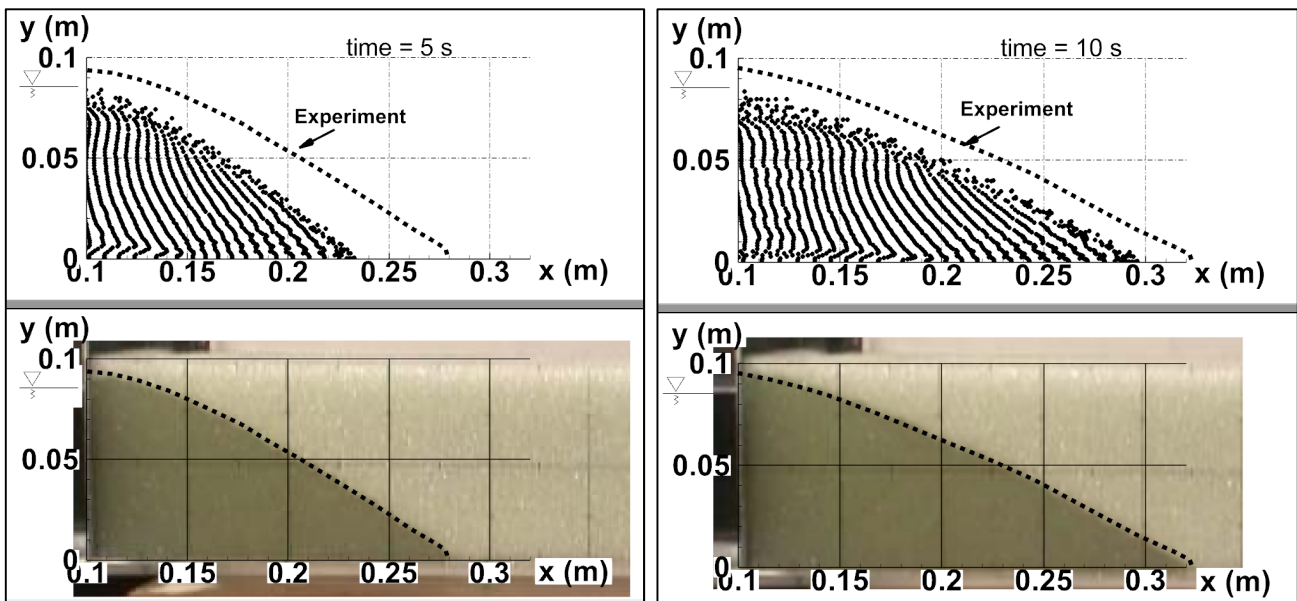


Figure 3. Comparison between numerical model and experiment for lateral intrusion into porous media.

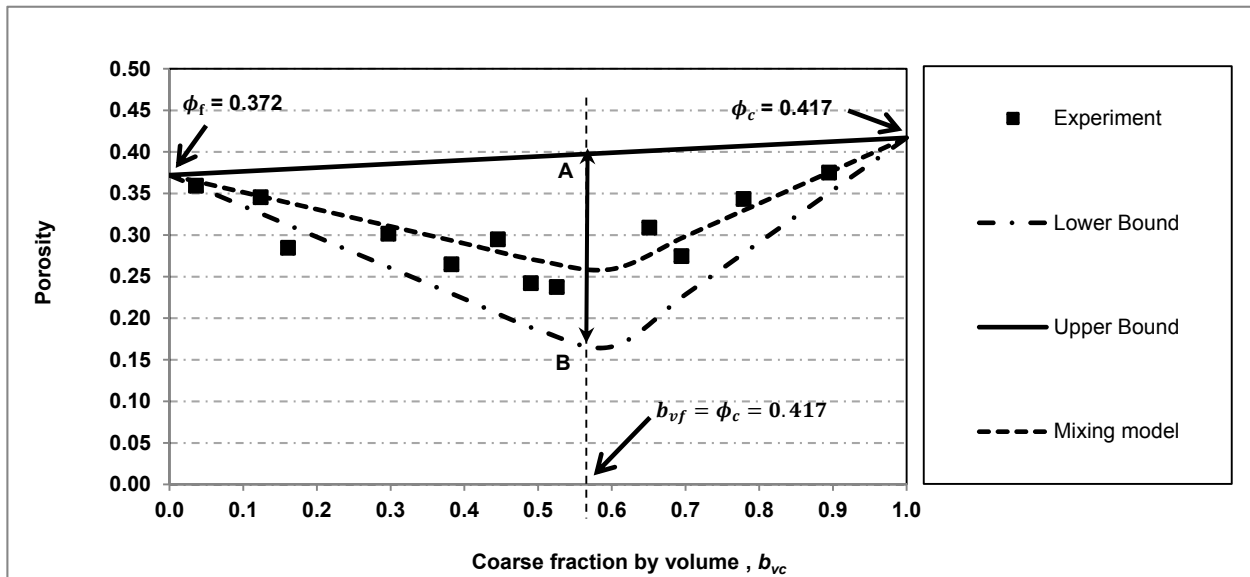


Figure 4. Porosity of binary mixture.

Porosity of the mixture from the experimental result lies in between the upper and lower bounds shows that the result is acceptable. It was found that the porosity of the binary mixture does not increase with the increment of the ratio of coarse to fine beads until the volume fraction of fine particles is equal to the coarse component as shown in the Fig. 4. At this point, the porosity of the binary mixture is most sensitive to the degree of mixing as shown by the huge gap between point A and B in Fig. 3. The mixing model line is plotted by using the value $\lambda = 0.64$ obtained by utilizing Eq. (3) and ϕ_m from the experiment.

5.3 Saturated Hydraulic Conductivity, K_{sm}

Experimental and numerical simulation result of saturated hydraulic conductivity, K_{sm} are shown in Fig. 5. Good agreement between the theoretical and numerical results can be seen in the reproduction of saturated hydraulic conductivities for the upper, lower and mixing model with value of $\lambda = 0.64$. However, the experimental value of K_{sm} is outside the lower bound when the coarse fraction ratio is more than $(1.0 - 0.417 = 0.583)$. Above this ratio, the fine particles volume ratio is less than the void volume ratio in the coarse particles and segregation occurred and the assumption of random packing was not achieved at higher coarse ratio. During the experiment, most of the fine particles tended to sit at the bottom of the column forming a separate layer which lowered the overall K_{sm} value and resulting in out of bound K_{sm} value compared with theoretical value in higher coarse fraction of the mixture.

The pressure distribution for the numerical simulation of column test for binary mixture is shown in Fig. 6.

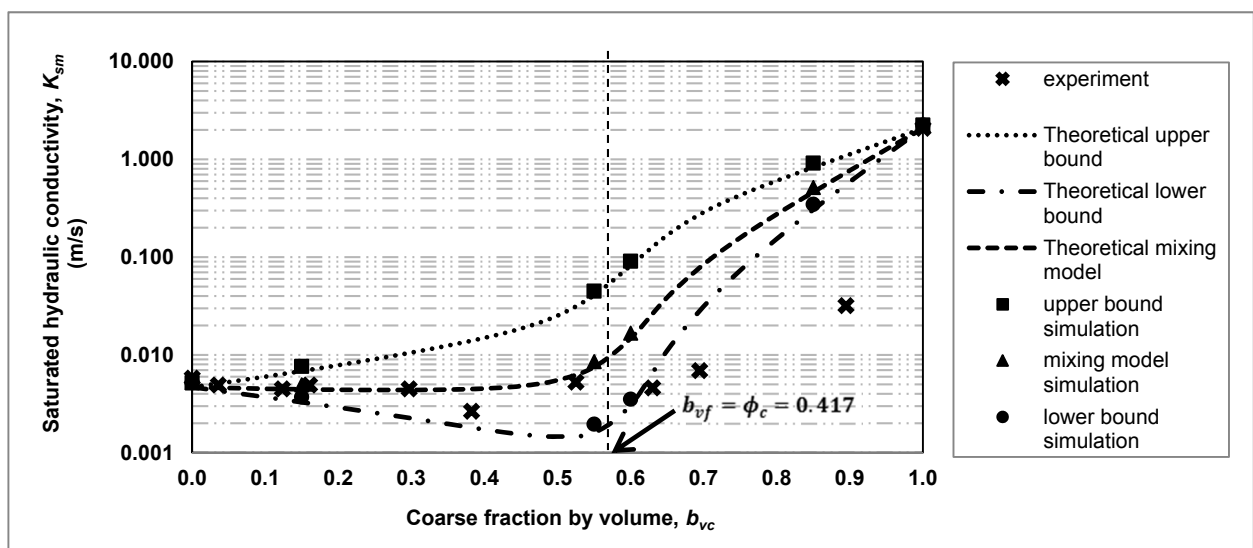


Figure 5. Saturated hydraulic conductivity of binary mixtures.

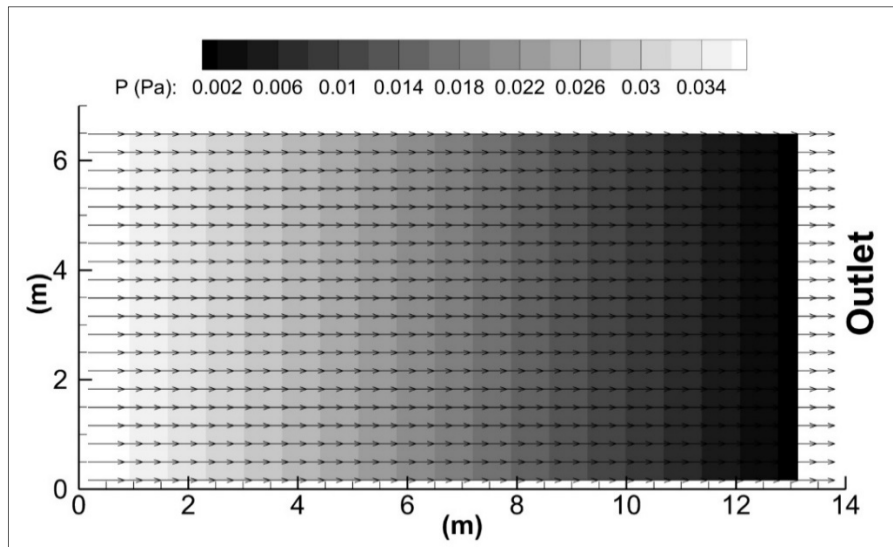


Figure 6. Pressure distribution in column test (numerical simulation).

6 CONCLUSIONS

A numerical model based on the FAVOR method was developed to simulate flow in porous media. The model was verified against lateral intrusion flow into single size porous media. In general, the model could reproduce the flow intrusion. However, the capillary effect and momentum transfer of fine porous media could not be reproduced in the numerical model. On the other hand, the numerical model could satisfactorily reproduce the hydraulic conductivity for the flow in binary mixture. Overall, there are still room for improvements and more simulations are needed for the present numerical model to become a more robust and accurate model to simulate flow in single size and binary mixture porous media.

ACKNOWLEDGEMENTS

This research was supported by the Ministry of Higher Education of Malaysia.

REFERENCES

- Bear, J. (2013). *Dynamics of Fluids in Porous Media*. Courier Corporation.
- Ballard, B.W., Kellagher, R., Martin, P., Jefferies, C., Bray, R. & Shaffer, P. (2007). *The SUDS Manual*. Construction Industry Research & Information Association (CIRIA).
- Ghimire, B., Hosoda, T. & Nakashima, S. (2007). An Investigation on Lateral Intrusion Process of Water into Porous Media under Different Upstream Boundary Conditions. *Journal of Applied Mechanics*, 10, 839-846.
- Hirt, C.W. & Sicilian, J.M. (1985). A Porosity Technique for the Definition of Obstacles in Rectangular Cell Meshes, *International Conference on Numerical Ship Hydrodynamics 4th*, 1-19, Washington DC.
- Kawamura, T., Takami, H. & Kuwahara, K. (1985). New Higher-Order Upwind Scheme for Incompressible Navier-Stokes Equations, *Ninth International Conference on Numerical Methods in Fluid Dynamics*, 291-295, Springer Berlin/Heidelberg.
- McKee, S., Tomé, M.F., Ferreira, V.G., Cuminato, J.A., Castelo, A., Sousa, F.S. & Mangiavacchi, N. (2008). The MAC Method. *Computers & Fluids*, 37(8), 907-930.
- MacDonald, M.J., Chu, C.F., Guilloit, P.P. & Ng, K.M. (1991). A Generalized Blake-Kozeny Equation for Multisized Spherical Particles. *AIChE Journal*, 37(10), 1583-1588.
- Morad, M.R. & Khalili, A. (2009). Transition Layer Thickness in a Fluid-Porous Medium of Multi-Sized Spherical Beads. *Experiments in Fluids*, 46(2), 323.
- Mota, M., Teixeira, J.A., Bowen, W.R. & Yelshin, A. (2001). Binary Spherical Particle Mixed Beds: Porosity and Permeability Relationship Measurement. *Transactions of the Filtration Society*, 1(4), 101-106.
- Nield, D.A. & Bejan, A. (1999). *Convection in Porous Media*. Springer, New York.
- Ochoa-Tapia, J.A. & Whitaker, S. (1995). Momentum Transfer at the Boundary between a Porous Medium and a Homogeneous Fluid - Theoretical Development. *Int. J. Heat Mass Transfer.*, 38(14), 2635-2646.
- Welch, J.E., Harlow, F.H., Shannon, J.P. & Daly, B.J. (1966). The MAC Method - A Computing Technique for Solving Viscous, Incompressible, Transient Fluid-Flow Problem Involving Free Surfaces. *Los Alamos Scientific Lab. Report*, No. 3425, University of California.
- Whitaker, S. (1996). The Forchheimer Equation: A Theoretical Development. *Transp. Porous Med.*, 25(1), 27-61.
- Zhang, Z.F., Ward, A.L. & Keller, J.M. (2011). Determining the Porosity and Saturated Hydraulic Conductivity of Binary Mixtures. *Vadose Zone J.*, 10(1), 313-321.

INTERCEPTOR SYSTEMS FOR IMPROVEMENT OF RIVER WATER QUALITY FOR RIVER OF LIFE (ROL) – DESIGN CRITERIA, ANALYSES AND CHALLENGES

WAI SAM WONG⁽¹⁾, MOHD. AZMI ISMAIL⁽²⁾, PEK SIANG CHENG⁽³⁾ & KOK WAI LOKE⁽⁴⁾

^(1,3,4)Dr. Nik and Associates Sdn. Bhd.
⁽²⁾Department of Irrigation and Drainage Malaysia

ABSTRACT

One of the overall objectives of River of Live (RoL) River Cleaning Task Force leads by Department of Irrigation and Drainage Malaysia (DID) is to improve the river water along the 10.7km of Gombak River and Klang River from the current Class III to IV to Class IIB water quality. Many key initiatives have been identified and among them is to implement Interceptor Systems along the whole 10.7 km stretch. The purpose of the Interceptor Systems is to intercept the polluted sullage drainage discharges along both banks of the 10.7 km rivers so that they can be conveyed to suitably located treatment plants for purification and release back to the rivers subsequently. This paper highlights the criteria and assumptions adopted, the analyses used in designing the systems and the challenges faced during the design stage. Generally, it is important to establish suitable criteria and assumptions to be adopted for a project after the conceptual design is formulated and before the start of any analyses and design work commence. With the criteria and assumptions defined, hydrological and hydraulic analyses are carried out to determine the size, configuration, type, etc. for each of the components that form the integral Interceptor System. This involves using various analytical computer models and spreadsheets to derive all the required parameters. Similarly for the Sullage Water Treatment Plant (SWTP), analytical model is also adopted to estimate the size and dimensions of the holding storage and treatment media required. Implementing a major system in the highly urbanized areas often need to deal with various challenges. These include space constraint, land acquisition, relocation of utilities, traffic and accessibility during construction, river conditions and other on-going works such as the beautification works by Kuala Lumpur City Hall (KLCH).

Keywords: Water quality improvement; wastewater treatment design; pipeline network design.

1 INTRODUCTION

Department of Irrigation and Drainage Malaysia (hereinafter referred to as the DID) intends to implement water quality improvement works along the 10.7km of Gombak River and Klang River from the current Class III to IV to Class IIB water quality and intends to construct water quality purification facilities and other relevant works to form part of overall efforts and key initiatives to achieve the objectives of River of Life (RoL). The works involve implementing interceptor pipelines and sullage water treatment systems to improve the river water quality for the 10.7km of rivers to create a clean and aesthetically pleasing river front for the city centre of Kuala Lumpur.

The stretches of rivers that have been identified for the construction of interceptor systems and water quality improvement facilities are from downstream of Jalan Kampung Bandar Dalam (more specifically from Kampung Puah) to the confluence with Klang River for the Gombak River, and from Jalan Sultan Ismail to Mid-valley City for Klang River (Figure 1). The river corridors of the above stretches of rivers will be beautified under the River of Life (RoL) project. The existing rivers in the RoL area receive both point and non-point source pollutions from their catchments. The prevailing heavy pollution loadings from both sewage and sullage discharges, which enter the rivers have rendered them unable to purify themselves as very limited base flows are available for dilution. The resulting poor river water quality has caused the riverine areas to be unsuitable for leisure and recreational uses. Under the river cleaning initiative in the RoL project, it is the aspiration of the government to improve water quality in these rivers to a clean and aesthetically pleasing state by the year 2020 especially along the 10.7 km of rivers where river beautification works will be undertaken.

Based on the recent study on “Water Quality Improvement and Hydrological Assessment for the Klang River” by DID (2012), the existing river water quality is about Class III and IV (National Water Quality Standards) for most of the rivers in the RoL area except Sungai Gombak at its upstream stretch, which is of Class IIB water quality. The best option for river water improvement is the “Full-fledged Solution” whereby effluents from the two regional Sewerage Treatment Plants (CSTP) will be treated to Class IIB and the rest of the STPs upgraded to a proposed new standard (BOD = 5, COD = 60, TSS = 50 & NH₃N = 2) besides directly connecting all the remaining point sources (e.g. sullage discharges, workshop and industrial effluents, IST, private plants, wet markets, institution treatment units, etc.) to the nearby sewerage systems with pre-treatment to meet the sewer admission limits. Nevertheless, it is foreseen that the connection of point sources to the sewerage systems, except the domestic waste, requires the amendment of certain parts of the current legislation as well as resolving

the tariff issues and thus the target may not be achieved by the year 2020. Furthermore, the relocation of workshops, road side stalls, squatters, etc. by local authorities may require longer time to realize. A more pragmatic approach has been sought to optimize the implementation cost and legislation issues as well as to achieve the river cleaning objectives by the target date. Therefore, it is proposed that part of the “Pragmatic Solution” is to implement the interceptor systems along the 10.7 km stretch of the rivers under the beautification works.

In the prevailing city environment, most domestic and commercial buildings are directly connected to the centralised sewerage system. However, it is still common practice for sullage discharges from the numerous restaurants and food outlets in the city to be directly connected to the drainage systems. Moreover, there are also older institutional premises and private houses equipped with septic tanks, which discharge their effluent to the drains. These polluted discharges will inevitably find their way to the rivers.

Although effort is currently being made under the RoL project to have full sewer systems in the city both for sewage and sullage in the long term. The urgent need to see an improved river water quality to support the new RoL development vis-à-vis the extensive river corridor beautification has brought forth the concept of an interceptor system to improve the river water quality in the interim. The purpose of the interceptor system is therefore to intercept the polluted drainage discharges along both banks of the rivers so that they can be conveyed to suitably located treatment plants for purification and released back to the rivers subsequently.

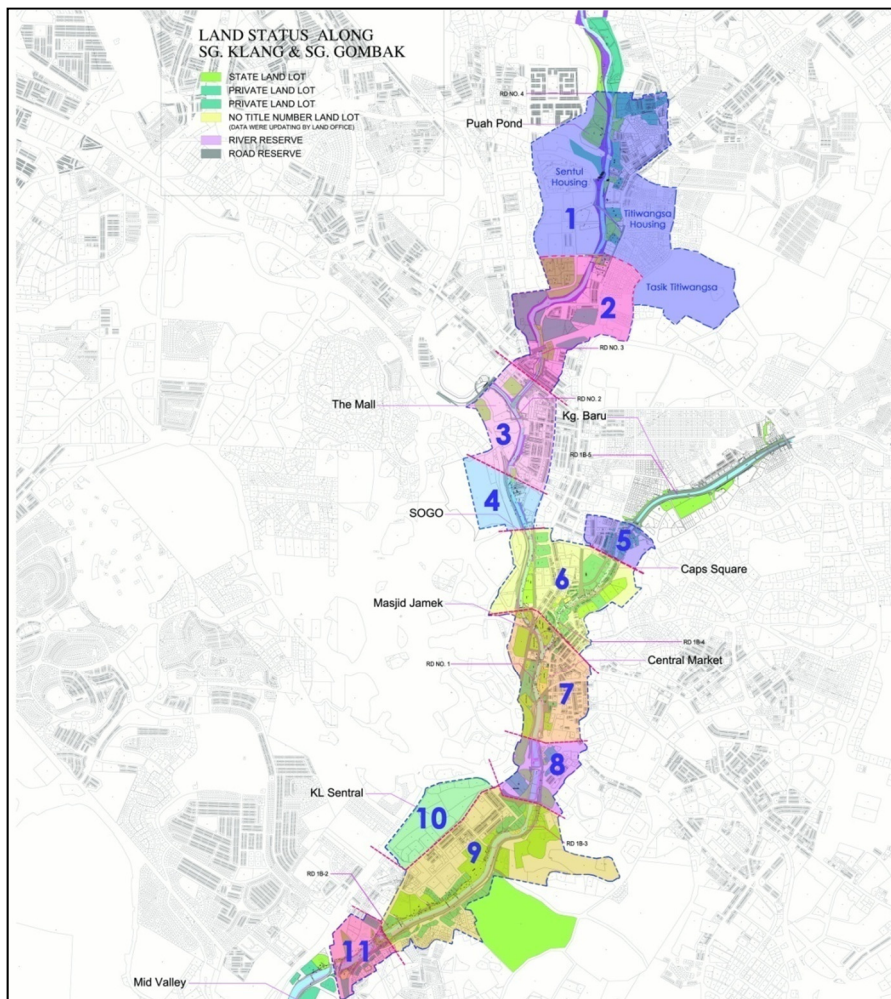


Figure 1. Location Plan of the Project Area

2 DATA COLLECTION

Both secondary and primary data were collected to carry out the planning and detailed design work. All relevant data and information including reports of past studies relevant to the Project were also collected and they include the following:

- Survey plans of existing drainage outlets and cross-sections of tributaries
- Details of existing drainage systems, pump stations and drainage control structures
- As-built drawings of flood mitigation works along the rivers
- Pollution sources and water quality data
- Field sampling of water quality at all drainage outlets to rivers

- Utility maps
- Present and future landuse maps
- Hydro-meteorological data
- Available soil investigation (S.I.) reports (borehole/bore-log data)
- Aerial photographs/Satellite Images
- Reports of relevant projects or studies
- Other related data and information such as proposed beautification and development works to be implemented in the near future.

Figure 2 shows the water quality sampling points at all the drainage outlets along Sg. Gombak at Precinct 3 and Table 1 list out one of the sampling events for the water quality during dry-weather flow at all the drainage outlets for the same stretch.

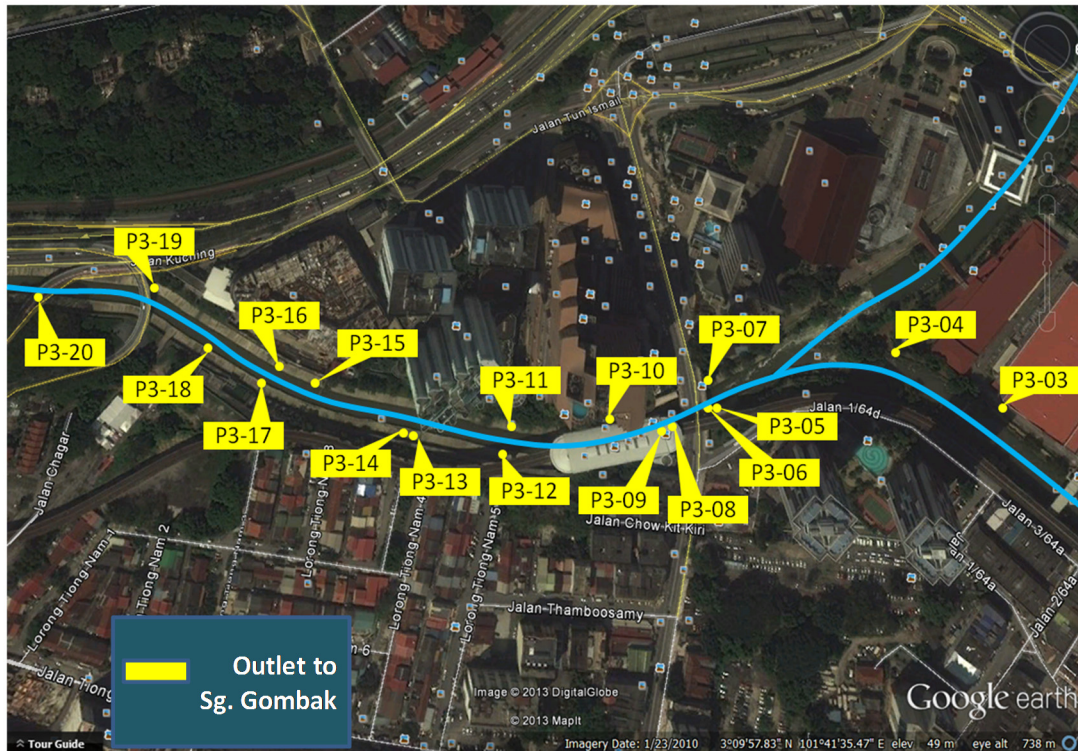


Figure 2. Location of Water Quality Sampling Stations along Sg. Gombak at Precinct 3, PWTC to Jln. Kuching

Table 1. Water Quality and Discharge Results along Sg. Gombak at Precinct 3 on 17th July 2013

Point	pH	DO (mg/L)	Temp (°C)	Flow (m ³ /s)	COD (mg/L)	BOD (mg/L)	TSS (mg/L)	O&G (mg/L)	AN (mg/L)
P3-01	7.9	3.82	27.5	0.00068	10	2	8	ND(<1)	0.6
P3-02	7.65	5.13	27.5	0.0008	77	15	9	ND(<1)	0.07
P3-03	-	-	-	-	-	-	-	-	-
P3-04	7.72	3.54	27.5	0.00144	56	10	17	ND(<1)	0.12
P3-05	-	-	-	-	-	-	-	-	-
P3-06	7.11	2.41	27.7	0.00239	79	14	15	ND(<1)	3.79
P3-07	7.35	3.86	27.9	0.00028	389	72	42	6	0.13
P3-08	-	-	-	-	-	-	-	-	-
P3-09	7.75	3.1	27.8	0.00104	36	7	14	ND(<1)	0.26
P3-10	7.29	5.57	26.7	0.00001	20	4	12	ND(<1)	0.02
P3-11	6.85	3.72	27.9	0.0075	274	52	118	10	0.45
P3-12	7.3	2.39	28	0.00202	294	55	43	5	0.05
P3-13	-	-	-	-	-	-	-	-	-
P3-14	-	-	-	-	-	-	-	-	-
P3-15	-	-	-	-	-	-	-	-	-
P3-16	-	-	-	-	-	-	-	-	-
P3-17	7.71	2.72	28.1	0.02885	122	23	23	ND(<1)	3.45
P3-18	7.56	4.9	28.2	0.00012	20	4	4	ND(<1)	3.09
P3-19	7.68	4.45	27.9	0.00019	26	5	12	ND(<1)	0.43
P3-20	7.35	5.23	28	0.00426	16	3	10	ND(<1)	0.22

No value means no low-flow

3 DESIGN CRITERIA AND ASSUMPTIONS

Generally, in line with the concepts employed in the proposed Interceptor System, the pipeline systems are planned and designed in such a way that:

- a) All drainage outlets with polluted low flows will be intercepted for treatment;
 - b) 5% of the first flush from a 1-month ARI storm event from the sub-catchments will be captured along with the low flows for treatment;
 - c) Interceptor pipeline will be laid within the river banks as far as possible or in some exceptional cases within the river berms where appropriate;
 - d) Open excavation will be employed for laying of shallow pipes including pressured pipelines while pipe-jacking method is used for laying of deep pipes to avoid the numerous utility lines present;
 - e) The polluted low flows (including a fraction of the first flush) are diverted at the drainage outlets by Stormwater Overflows (CSO) to the interceptor pipelines;
 - f) The intercepted flows in the interceptor pipelines will be conveyed to and treated at the Sullage Water Treatment Plants (SWTP) to meet Class IIB standard of National Water Quality Standards (NWQS) before being released back to the rivers; and
 - g) SWTP will be located at appropriate locations along both banks of the rivers where space is available.
- With the above, the specific design criteria for various major components are as follows:

• Sullage Water Treatment Plant

- a) Type of plant: The plant proposed shall be submerged aerated biofilter capable of treating polluted drainage discharges in the pre-existing urban conditions within the project area. The avoidance of clogging of the system shall be effected through periodic back-washing or similar or else the system should be so designed as to require least maintenance. The completed system is able to maintain a horizontal flow mode with low head loss.
- b) Biofilter media: The biofilter media shall be made from inorganic synthetic material that is non-corrodible, resistant to rot or decay and is inert to chemical attack and be able to provide large sustainable contact surfaces for growth of microbes. The media shall have a certified life span of not less than 20 years with proper operation and maintenance as per procedure specified by the manufacturer. The system shall be able to work within the design flow-rates and design pollutant loads required for each site.
- c) Influent: The plant shall be able to treat the influent water quality in accordance to the sampled data and to cater for a flow quantity up to 5% of first flush of 1-month ARI storm event.
- d) Effluent: The effluent water quality shall be in compliance with Class IIB standards of NWQS in particular the following pollutant parameters:
 - BOD: not exceeding 3 mg/l
 - COD not exceeding 25 mg/l
 - Ammoniacal Nitrogen: not exceeding 0.3 mg/l.
 - SS: not exceeding 50 mg/l
- e) Sizing and location of plant: The plant shall have a small footprint and preferably be placed entirely underground within the sites provided except for the control house, entrance to access stairs and electrical supply sub-station in approved locations.
- f) Aesthetics: The space above the underground plant, except that above the pump sumps, blower & control panel chambers as well as the grit & grease and oil-coalescer chambers may be designed with a soil layer of minimum 300 mm and be turfed for green area or otherwise paved for road, if so desired.
- g) Maintenance: The plant shall be designed for ease of maintenance with automatic desludging or back-washing as far as possible unless the minimum amount of sludge formed can be discharged to the river automatically.

• Pipeline System

- a) Design standard and guidelines: In general, the following design standards and guidelines for sewerage pipeline shall be followed in the design of the interceptor pipeline systems.
 - Malaysia Standard MS 1228: 1991 Code of Practice for Design and Installation of Sewerage System and Industrial Research Institute of Malaysia.
 - Guidelines for developers: Malaysian Sewerage Industry Guidelines – MSIG by Suruhanjaya Perkhidmatan Air Negara (SPAN).
- b) Pipe sizes: Reinforced concrete pipes (RCP) or HDPE pipes of minimum 600 mm diameter shall be used for the interceptor pipeline with gravity flows. Ductile Iron pipes (DI) or HDPE pipes of suitable grade for force main shall be sized according to required flows under the design pressure heads and normally shall have sizes ranging from 75 mm to 250 mm diameter for D.I. pipes and to as large as 450 mm diameter for HDPE pipes. On the other hand, Vitrified Clay Pipe (VCP) of 225mm diameter

will generally be employed for connecting outflows from Combined Stormwater Overflows (CSO) to manholes in a gravity flow pipeline.

- c) Flow capacity: Pipe flow capacity shall be sufficient to meet part of first flush requirement, which is equal to 5% of 1-month ARI storm discharges accruing from the contributing sub-catchments.
 - d) Flow velocities:
 - Flow velocities in interceptor pipelines in gravity flows shall be not less than 0.8 m/s to reduce siltation (under maximum design flow of the pipes).
 - ii) Flow velocities in force main pipelines shall not exceed 2 m/s to reduce any surge effect (preferably not exceeding 1.5 m/s) but not less than 0.8 m/s to reduce siltation (under maximum design flow of the pipes).
 - e) Friction losses: Friction head losses shall be no less than those computed by either the Hazen-Williams equation, using a roughness coefficient 'C' equal to 150 for HDPE pipes and 110 for D.I. pipes or Colebrook-white of equivalent roughness coefficient.
 - f) Pipeline alignments: The proposed interceptor pipelines shall be laid either through pipe-jacking (micro-tunneling) for deep pipelines, by open cut for shallow pipelines or bracketed to sides of bridges for D.I. pipelines in river crossings. The depth of jacked pipeline is generally about 5-6m below ground so as to avoid the pre-existing shallower utility lines. For the open cut installation, the depth may not exceed 3 m. In any case, distance from existing pipelines shall be preferably kept no less than 5 m.
 - g) Depth of pipeline and cover: Interceptor pipes shall be installed at sufficient depth below ground surface or river berms at a level equal to or lower than the invert levels of drainage outlets to enable the polluted drainage discharges to be collected by gravity flows unless pumps are used to lift the flows. The minimum depth of cover for the shallower pipes laid by cut and cover method shall be 1,200 mm as normally employed in pressured pipes.
 - h) Pipe materials: Materials used for the interceptor pipelines may include Reinforced Concrete Pipe Class Z Jacking Pipe with M.S. Sleeves (RCP), Vitrified Clay Pipe (VCP), HDPE pipe, Ductile Iron (D.I.) pipe or other suitable pipe materials. In the case of force main, Ductile Iron pipe (Class K9 or Class 40 PN16) or HDPE (PE 80 PN12.5) pipes are normally used unless circumstances dictate otherwise. Ductile iron pipes shall be lined with cement mortar internally and zinc coated and then covered by bitumen coating externally.
 - i) Joints and connections: All joints and connections shall be designed to withstand the design maximum working pressure of the pipeline without leakage and leave the inside of the pipe free of obstruction that may tend to reduce its capacity.
 - j) Fittings and Couplers: All fittings and couplers shall meet or exceed the same strength requirements as those of the pipes and shall be of material that is recommended for use with the pipes. Fittings made of steel or other metal shall be protected from corrosion by a protective coating such as plastic tape wrap, coal tar-epoxy or other corrosion resistant coatings.
 - k) Manholes: Standard manholes to be used shall have minimum diameter of 1200 mm for depths not exceeding 5 m. For deeper manholes, internal diameter of 1500-1800 mm may be required. The distances between manholes shall be kept to within 175 m for the deep pipelines laid through pipe-jacking. Shorter distances may be employed for shallow pipelines laid with open cut and cover method or as the site conditions dictate.
 - l) Pumps: Pumps, which are generally of small capacities, shall be submersible pumps installed within the underground pump sumps. Two or more pumps, one or more duty and one standby, will be installed and operated in rotation in bigger pump stations while a single pump may be used for smaller station to save cost. The control panel in weather-protected housing, however, will be placed underground in most cases except in locations where above ground housing is permissible.
- Combined Stormwater Overflows (CSO)
 - a) Purpose: The main purpose of the CSO is to divert the polluted low flows from the drainage outlets to the interceptor pipeline so that they can be conveyed to the SWTP for purification before being released back to the river.
 - b) Flow capacity: The CSO shall be able to pass a discharge up to the capacity of the existing drainage outlet during high flows and to divert to the interceptor pipeline a flow equal to 5% of the 1-month ARI storm discharges from the sub-catchment during initial storm discharges.
 - c) Facilities: The CSO shall be a two-chamber in-line structure located slightly upstream of the drainage outlet. The main chamber receives the inflow from the upstream and the low weir located on the chamber floor will divert the low flow and initial storm discharge to the adjacent chamber, the Gross Pollutant Trap (GPT). During high flows, most of the storm discharges in the main chamber will overflow the low weir and pass straight on to the outlet and into the river. The GPT shall be designed with a lowered chamber where a semi-circular mesh is installed with enough capacity to trap coarse debris as well as to settle out sediment within it before they enter the interceptor pipeline. Non-return Check Valves shall, wherever required, be installed at downstream end of the Combined Stormwater

Overflow (CSO) or at the outlet pipe itself to minimize backflow of river water into the interceptor pipelines.

4 INTERCEPTOR SYSTEM LAYOUT DESIGN

The layout of the Interceptor Systems for the 10.7 km along the Sg. Gombak and Sg. Klang is designed and Figure 3 shows the portion at the city centre. They consist of a collector system, which can be in the form of gravity-flow pipelines, force mains, and covered drains/conduits depending on site conditions. Deep pipelines will be laid within the river banks with pipe-jacking (micro-tunneling) method for gravity-flow interceptor pipeline while cut and cover method may be employed more economically for shallow interceptor pipelines. To circumvent constricted site conditions due to the existing structures, the collected sullage water may need to be pumped from one side of the river to the other side for treatment or from one discharge point to the next before reaching a treatment plant. In such situation, pump stations and force mains become necessary. In other circumstances, surface drains may be diverted or their low flows intercepted with the use of covered drains or conduits, the flows of which will be channeled to a manhole and into the receiving interceptor pipeline subsequently.

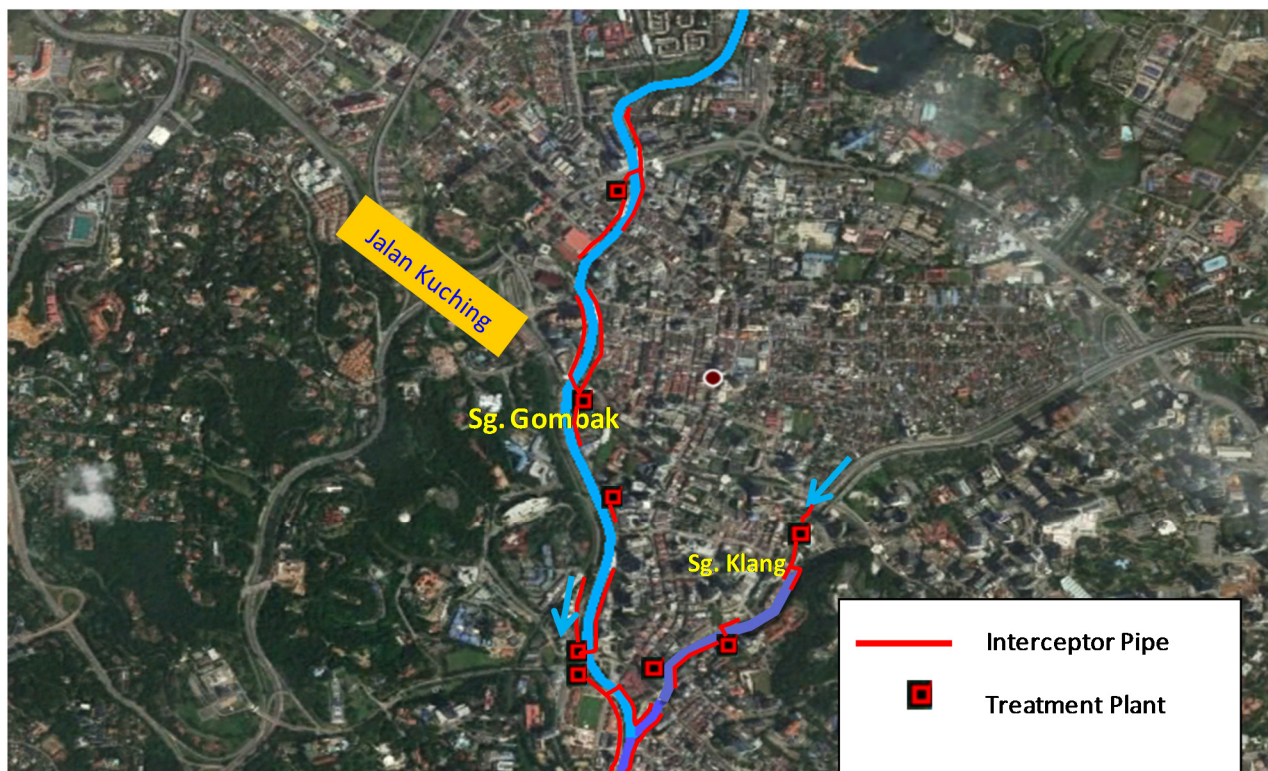


Figure 3. Layout Plan of Interceptor Systems at City Centre

As only the low flows and a fraction (5%) of the first flush of a 1-month ARI storm will be intercepted for treatment, there is a need to have a flow separation structure installed at the drainage outlets. Such a structure is termed Combined Stormwater Overflow (CSO). It is an on-line structure with two chambers. The main chamber will receive the incoming flows from the drain upstream and a low weir situated on its chamber floor will divert the low flows into the second chamber while allowing high flows to pass over the low weir and discharge downstream to the river. The second and deeper chamber, equipped with trash screen or basket, acts as a Gross Pollutant Trap (GPT) as it will trap debris and settle out sediment from the flow before it enters the interceptor pipeline. Debris and sediment deposited in the chamber can then be removed from time to time by the use of suction hose from mobile tanker. A typical general plan of the proposed CSO is as showed in Figure 4. Check valves also need to be installed at the outlets to river to avoid backflow of flood water from the river into the Interceptor system during high flood levels that may affect the SWTP.

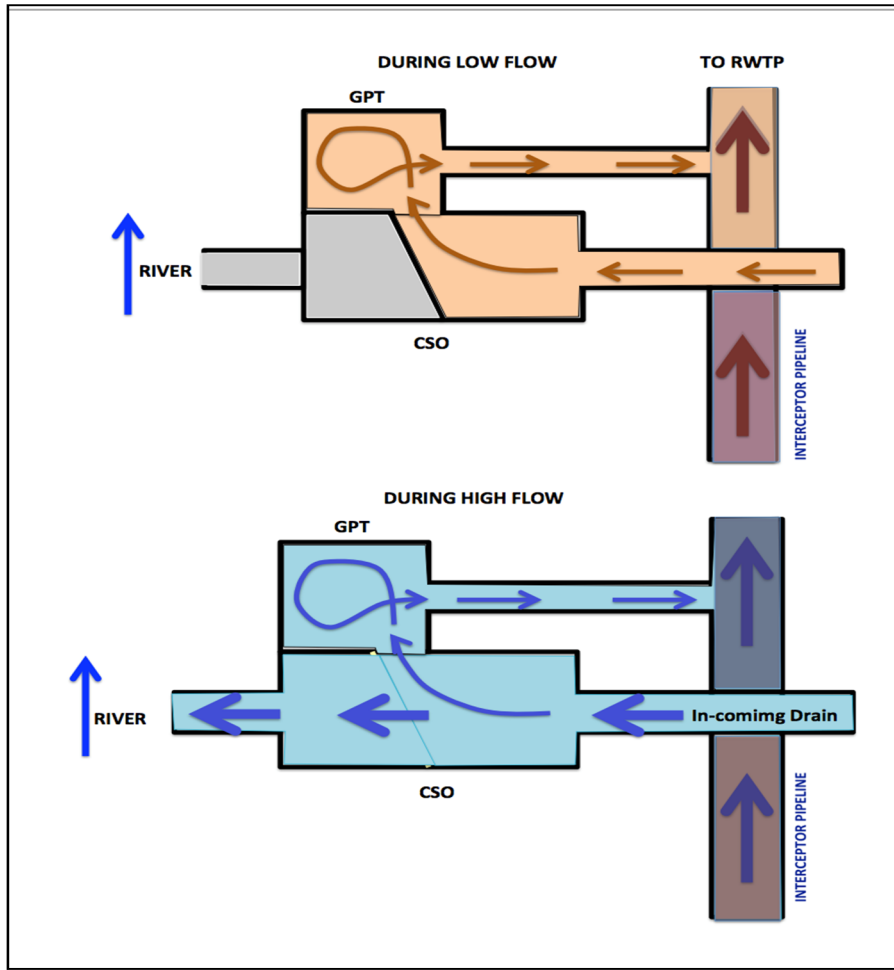


Figure 4. Operation of CSO during Low Flow and High Flow

At suitable intervals or where space permits, sullage water treatment plants (SWTP) will be constructed to receive and treat the collected polluted flows. These SWTP will have the capacity to treat the design quantity and quality of polluted flows to Class IIB water quality standard in compliance with the National Water Quality Standard (NWQS) by the Department of Environment (DOE). The water quality parameters of particular importance are the Biochemical Oxygen Demand (BOD), Chemical Oxygen Demand (COD), Ammoniacal Nitrogen (NH₃N) and Suspended Solid (SS). The mechanism to be adopted in the SWTP will follow that of the natural eco-cycle in purifying the river water. In a natural waterway, organic and oxidizable non-organic pollutants are oxidized and consumed by aerobic organism or bacteria that are present naturally in the waterway. The flow diagram of the main components of the plant is as shown in Figure 5.

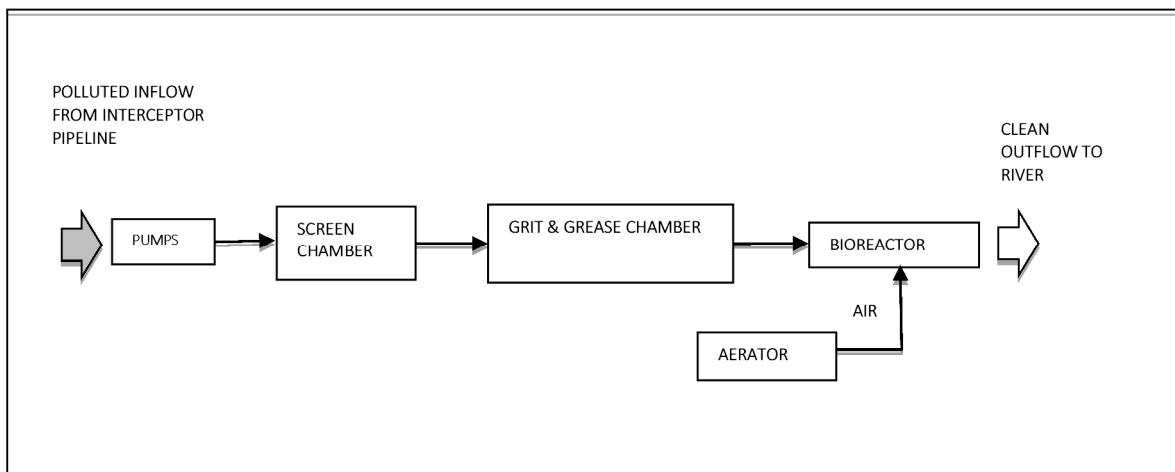


Figure 5. Flow Diagram of Main Submerged Bio-filter Components

5 DATA ANALYSIS AND FIRST FLUSH DISCHARGE ESTIMATION

Based on the sampling collected, water quality analysis was carried out for all the outlet points and Table 2 shows the analysed results for the outlets at Precinct 3.

Table 2. Water Quality Analysis for Precinct 3

Point	Morning			Point	Afternoon		
	WQI	CLASS	WQ STATUS		WQI	CLASS	WQ STATUS
P3-01	76	II	SP	P3-01	57	III	P
P3-02	69	III	SP	P3-02	61	III	SP
P3-03	-	-	-	P3-03	-	-	-
P3-04	67	III	SP	P3-04	55	III	P
P3-05	-	-	-	P3-05	-	-	-
P3-06	45	IV	P	P3-06	46	IV	P
P3-07	44	IV	P	P3-07	41	IV	P
P3-08	-	-	-	P3-08	-	-	-
P3-09	67	III	SP	P3-09	53	III	P
P3-10	86	II	C	P3-10	68	III	SP
P3-11	41	IV	P	P3-11	34	IV	P
P3-12	42	IV	P	P3-12	30	IV	P
P3-13	-	-	-	P3-13	-	-	-
P3-14	-	-	-	P3-14	-	-	-
P3-15	-	-	-	P3-15	-	-	-
P3-16	-	-	-	P3-16	-	-	-
P3-17	39	IV	P	P3-17	34	IV	P
P3-18	71	III	SP	P3-18	82	II	C
P3-19	75	III	SP	P3-19	74	III	SP
P3-20	83	II	C	P3-20	74	III	SP

Note: C=clean, SP=slightly polluted, & P = polluted; No value means no low-flow

Based on the criteria given to estimate the first flush discharges, the flows were computed for all the outlets within the Project areas by demarcation of their respective sub-catchments, which are contributing to polluted flows. Table 3 lists out the first flush discharges at some of the outlets.

Table 3. First Flush Discharge Estimation

River	Outlet No.	SWTP Location	Catchment Area (km ²)	Design Q-1mth ARI (m ³ /s)	Design Q (5% of Tc) (m ³ /s)
	P3-06		3.7	0.63	0.012
	P3-09		0.5	0.11	0.002
	P3-12		7.5	1.16	0.023
	P3-17		5.1	0.90	0.017
	P3-18	SWTP at	1.9	0.38	0.007
Gombak River	P3-20	Jln Kuching to	4.3	0.71	0.014
	P3-07	Jln Sultan Ismail	5.2	0.86	0.017
	P3-10	Flyover	2.0	0.39	0.008
	P3-11		3.8	0.67	0.013
	P3-19		1.6	0.34	0.007
	P4-01		6.9	1.07	0.021
	P4-03		0.6	0.13	0.003
	P4-04		1.5	0.32	0.006
	Total		44.6	7.67	0.149

6 HYDRAULIC MODELLING

SWMM has been adopted to perform the hydrodynamic modeling of the pipeline systems. With the computed first flush discharges, the flows for the pipeline systems that lead to the nearby SWTP were modeled to check for the hydraulic behavior of the flows as well as the pipeline dimensions and pump sizing requirements so that they meet the required design criteria. Figure 6 shows the typical model setup of the pipeline system and Figure 7 shows the results of the SWMM simulation.

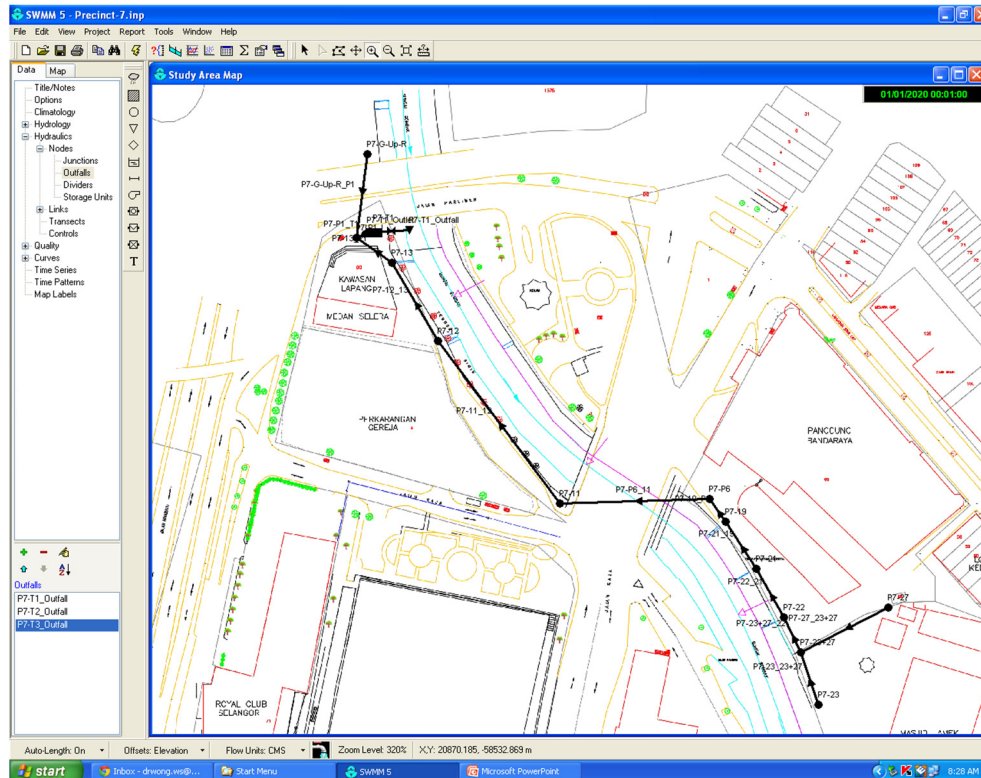


Figure 6. SWMM Model Setup for Interceptor System at Precinct 7

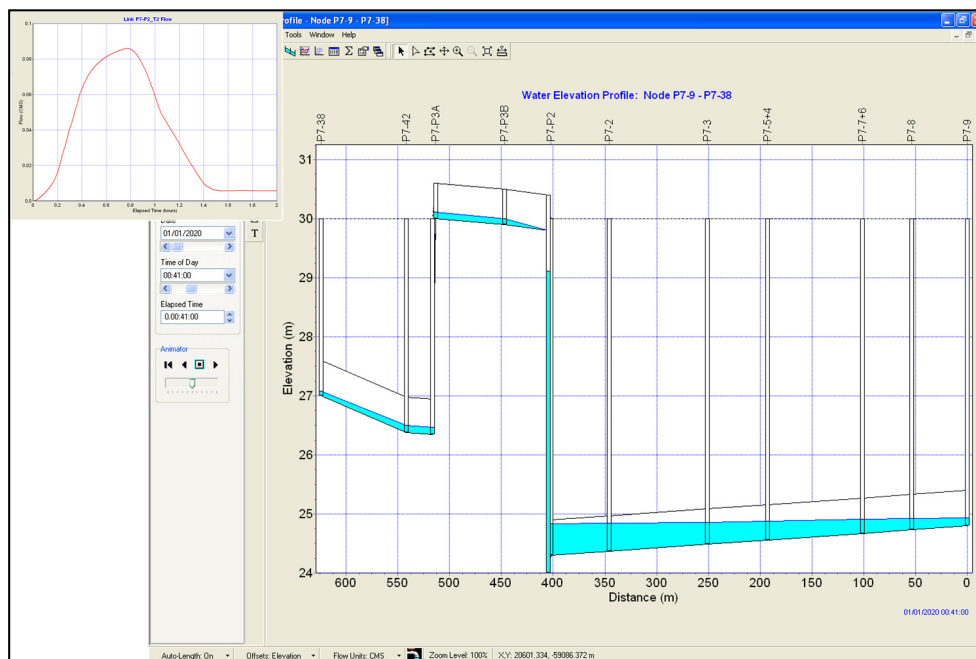


Figure 7. Longitudinal Profile and Flow Rate for the Interceptor System at Precinct 7

7 DESIGN OF SULLAGE WATER TREATMENT PLANT

Generally, the main components of the plant comprises the pump chamber, the grit & grease chamber, the blowers, the bio-filter media and where required other components such as the clarifier, the sludge thickener, and the sludge holding tank may be included. The Bio-filter media is to be fixed type and made of polypropylene material with maximum surface for attached growth of microbes yet would not be easily clogged up. The volume of the bio-filter chamber is determined by the organic loading rate of the media which should be as high as possible to reduce the size of the plant, the optimum rate being 0.6 kg/m³/day of BOD. Aeration is to be provided to the bio-filter media to ensure efficient pollutant removal by the bacteria. The whole plant is to be constructed underground as far as possible except the M&E room and electrical supply sub-station where permitted. The proposed Bio-filter System includes:

- a) Pumps sumps with pumps to lift the inflows from the interceptor pipeline to the Screen Chamber.

- b) Screen Chamber with trash screen to prevent any debris from entering the Bio-filter Chamber.
- c) Grit & Grease Chamber to intercept silt, sand and grease. A baffle wall with oil coalescer is provided to prevent oil & grease from entering the bio-reactor.
- d) The Bio-filter Chamber is packed with modules of synthetic inorganic media to house the bacteria. Adequate numbers of aerators are provided to supply oxygen to the bacteria for the decomposition of pollutants, which are the nutrient for the bacteria to multiply.
- e) The sludge form is minimum and normally can be discharged with the effluent to the river without degrading its water quality.

The bio-filtration system is generally a proprietary product and the final design and sizing of the plants will be determined by the supplier during project implementation to meet the performance specifications which includes the design criteria and assumptions highlighted earlier.

8 CHALLENGES AND CONCLUSIONS

Implementing infrastructure projects such as the Interceptor System in the highly urbanized area are always fought with numerous challenges as listed below:

- Since the project does not allow for any land acquisition, to search for the space to locate various facilities especially the SWTP is very difficult if not impossible;
- Many underground utilities running along the riverbanks as well as underneath the roads;
- Proper traffic management plan is required during construction period;
- Accessibility to adjacent premises during and after the project implementation;
- Most of the drainage outlets have low invert levels and thus, the interceptor pipelines need to be laid quite deep to collect the flows. Open cut will be difficult and pipe jacking and micro-tunneling will be required for gravity flow systems;
- High flood levels in the river will cause backflow into the Interceptor Systems and also pose a challenge during construction and maintenance times;
- With shallow karstic limestone ground conditions, laying deep pipelines especially pipe jacking will be difficult;
- Since space is a constraint, close coordination with the beautification works is required to avoid conflict during implementation times.

With proper planning and design of the Interceptor System, it will definitely contribute significantly towards meeting one of the RoL objectives of improving the river water quality. It also will minimize many site issues during constructions as well as shorten the construction period.

ACKNOWLEDGEMENTS

The authors would like to thank Department of Irrigation and Drainage Malaysia, under the “Detailed Design of Interceptor Systems and Related Works for Improvement of River Water Quality along 10.7 km of Gombak River and Klang River for River of Life (ROL)” for the contribution and allowing this paper to be presented. The authors would also like to express their gratitude to all the team members from Dr. Nik & Associates Sdn. Bhd. who were involved in the study.

REFERENCES

- AECOM, Kuala Lumpur City Hall (2013). River of Life (RoL) Master Plan – Beautification.
- AECOM, Kuala Lumpur City Hall (2013). River of Life (RoL) Master Plan – Hydraulic Report.
- Caboolture Shire Council, Queensland, Australia (2005). Environmental Management Plan & Trade Waste Policy.
- Department of Environment, Malaysia, (2012). Malaysia Environmental Quality Report.
- Dr. Nik & Associates Sdn. Bhd. in association with DHI and SMEC, Department of Irrigation and Drainage, Malaysia, (2002). Klang River Basin Environmental Improvement and Flood Mitigation Project.
- Dr. Nik & Associates Sdn. Bhd., Department of Irrigation and Drainage, Malaysia (2012). Study on Water Quality Improvement and Hydrological Assessment for the Klang River.
- Dr. Nik & Associates Sdn. Bhd., Department of Irrigation and Drainage, Malaysia (2015). Detailed Design of Interceptor Systems and Related Works for Improvement of River Water Quality along 10.7 Km of Sungai Gombak and Sungai Klang for River of Life (ROL).
- Environmental Protection Agency, Ireland (1997). Wastewater Treatment Manual – Primary, Secondary and Tertiary Treatment.
- Perunding W Mokhtar, (2004). Study and Preparation of Drainage and Stormwater Management Master Plan for Wilayah Persekutuan Kuala Lumpur.

OBTAINING REDUCTION FACTORS BY AREA FOR THE STATE OF SONORA IN NORTHERN MEXICO

SINUHÉ ALEJANDRO SÁNCHEZ MARTÍNEZ ⁽¹⁾, RAMÓN DOMÍNGUEZ MORA ⁽²⁾, MARITZA LILIANA &
ARGANIZ JUÁREZ ⁽³⁾

^(1,2,3) Institute of Engineering, National Autonomous University of Mexico, Mexico City, Mexico.
ssanchezm@iingen.unam.mx; rdominguezm@iingen.unam.mx; marganisj@iingen.unam.mx.

ABSTRACT

The lack of reliable meteorological data is a frequent issue for further engineering projects in Mexico. Due to this, it is necessary to optimize the available measured historic data within a Hydrologic Region in order to guarantee a reliable database. This requires using extrapolations of the phenomenon to characterize them. One of the most usual methods to get a design rainfall within large areas is the calculation of the Areal Reduction Factors (ARFs) in bounded zones; those factors consider the ratio of the simultaneous annual maximum rainfalls, and the annual maximum ones for punctual measurements of precipitation. In this paper, the Areal Reduction Factors for the state of Sonora in northern Mexico were obtained. The main reason for choosing this state, as well as in both north and south Baja California, is because there are extreme winter events, that is, rainfall events during the months of December, January and / or February, which differs from other regions of the country in which the highest rainfall events occur from June to October. Thus, the previously obtained factors in Sonora will be representative of the northwestern region of Mexico. The used method in this paper for the determination of the Areal Reduction Factors is an empirical method that relates annual maximum rainfalls with the simultaneous annual maximum rainfalls occurred within climatological stations with no less than 15 years data commonly to each other. Finally, an adjustment to a probability distribution was carried out to get the factors for different return periods.

Keywords: Reduction Factor by Area; Extreme Winter Events; Climatological Stations; Probability Distributions; Return Periods.

1 INTRODUCTION

In a certain area, the maximum rainfall generally does not occur in different points at the same time, it occurs simultaneously. Simultaneity is defined as the correct measurement of a maximum hydrological event at the same time but in different places (Torres, 2013). This is more characteristic within larger areas.

The traditional hydrological models consider maximum annual punctual rainfalls, which leads to an over-calculation of the rainfall itself. The Reduction Factors by Area are coefficients that help us to convert punctual rainfalls with their respective duration and a return period (T) to areal rainfalls of the duration itself and the return period of a region.

This factor defines the height of rainfalls magnitude as a function of the area where it happens, and it is used when the average rainfall of the studied area is desired (Mena, 2004). Thus, rainfall calculation is obtained as follows:

$$P_a = ARF \times P_{av} \quad (1)$$

P_a is areal rainfall in (mm) within the zone for the studied duration.

ARF is Areal Reduction Factors depending in function of the rainfall duration, the studied area and the return period

P_{av} is average precipitation in (mm) of the punctual measurements for the studied area and duration.

The Institute of Engineering of the National Autonomous University of Mexico has carried out several regionalization studies of annual maximum rainfall within Mexico. The results allow a very reliable estimation of punctual rainfalls for any basin in Mexico. Complementary studies have also been carried out by several authors, in which they have previously calculated the RFAs in different areas of the Mexican republic. This makes it possible to shift from a punctual rainfall intensity pattern (punctual rainfall hyetograph) to an average rainfall intensity pattern (average rainfall hyetograph) of each basin, to obtain the associated rainfall values with any return period for one-day durations for any site in the Mexican territory (Carrizosa, 2016).

ARF has been determined for representative zones in several regions within the Mexican territory: the states of Sinaloa (Mena, 2004) and Guerrero (Canavese, 2015) for the Pacific zone; the Panuco basin (Acuña, 2015; González, 2012) and the Valley of Mexico basin (Franco, 1998) for the central plateau area; the Grijalva Basin (Sánchez, 2015; Guichard, 1998) for the southeast zone; the hydrological region Soto la Marina (Acuña,

2015) and the state of Tamaulipas (Severiano, 2014) for the Gulf area, as well as the state of Durango (Severiano,2014) for the “Lagunera” region. The main purpose of this paper is to show the results of the calculated ARFs for the state of Sonora as a representative state of the northwest zone, which is characterized by the presence of extreme winter events, that is, maximum rainfall during the months of December, January and February.

2 BACKGROUND

The concept of ARF was originated in the United States, specifically in the US Weather Bureau, in 1962, by David M. Hershfield, who determined two empirical methods of RFAs: the storm center method and the fixed geographical area method (Sevensson and Jones, 2010).

In addition, in further researches to David M. Hershfield's study (Guichard, et al., 2004), to get reduction factors by area, they proposed several methods which could be divided into three groups.

Empirical: they relate the areal rainfalls with punctual rainfalls, but they have a lack of theoretical foundations.

Theorists: they do have theoretical foundations, and the generally follow a law of probability.

Theoretical-practical: they are a combination of the empirical and the theoretical methods.

3 METHODOLOGY

3.1 Empirical method

The empirical method of frequency analysis consists of determining the simultaneous maximum and annual maximum events. Circles that cover at least three climatic stations with 15 years of common data determine these areas.

In order to cover the entire state of Sonora, the state was divided into three zones in which three circles, (North, Central and South) were drawn on each of those zones, with the condition that they would be very close to climatic stations so that the circles of smaller area could have the necessary condition for this study, that is the coverage of minimum of three stations with 15 years of common data. In each zone, three circles were drawn resulting a total of nine smaller zones throughout the state.

Once the small area circles zones were defined, three bigger circles zones were then defined, by including the small ones within the new drawn zones. This resulted that the stations contained in the small circles will also be contained in the bigger circles, enlarging from the minimum of three stations to more than twenty stations with a minimum of 15 years of data.

3.2 Process

The developed process consists of the following steps:

1. Circles were drawn to enclose at least three climatological stations that have at least 15 years of simultaneous data at different points in the state of Sonora (Figure 1)
2. The average of the daily maximum rainfalls of each climatic stations and the average of the daily simultaneous maximum rainfalls were obtained.
3. For each year of simultaneous data or recording, RFAs were obtained with the ratio of the average of the daily maximum rainfall of the three climatic stations and the average of the daily simultaneous rainfalls. Sometimes, these two values are the same, which indicates that the maximum rainfall of each climatic station occurred on the same day.

$$RFAs = \frac{\text{Average of the daily simultaneous maximums}}{\text{Average of the daily maximums}} \quad (2)$$

where

ARFs is Areal Reduction Factors for each year of common data.

Average of the daily simultaneous maximums is obtained by averaging the daily simultaneous maximum rainfall for each year of common data

Average of the daily maximums is obtained by averaging the daily maximum rainfalls for each year of common data.

4. The ARF was obtained as the average of the ARF '.

where

$$RFAs = \frac{\sum_i^n ARF'}{n} \quad (3)$$

ARFs is the Areal Reduction Factors of the studied circled area.

ARF's is the Areal Reduction Factors for each yearly common data.

n is the number of years of records in common (fifteen years as the minimum value)

5. A probability distribution was applied to the maximum precipitation values and to the simultaneous maximum values, by doing this, the ARFs were obtained for different return periods for the studied circled area.
6. Circles were drawn with larger areas containing the circles mentioned in step 1. These circles would contain more than three stations (figure 2). In the same way as in step 1, those circles must have at least 15 years of simultaneous data.
7. Steps 2, 3, 4 and 5 were repeated for each circle in step 6.
8. Once several ARFs were obtained for each different region and different zones, a linear correlation was carried out with which the representative ARFs could be obtained for different return periods of the state of Sonora and the northeastern region of the Mexican Republic.

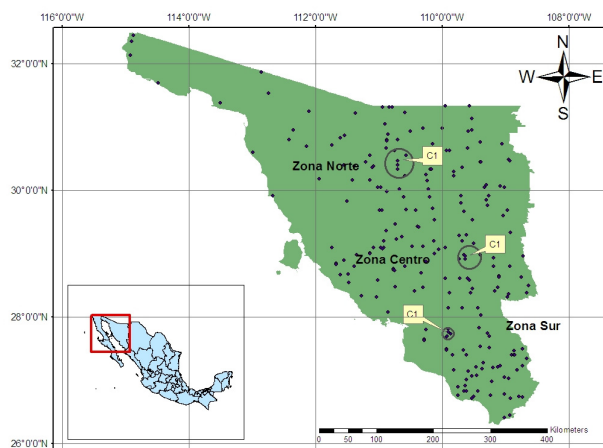


Figure 1. Circles of small areas in each of the three zones of the state

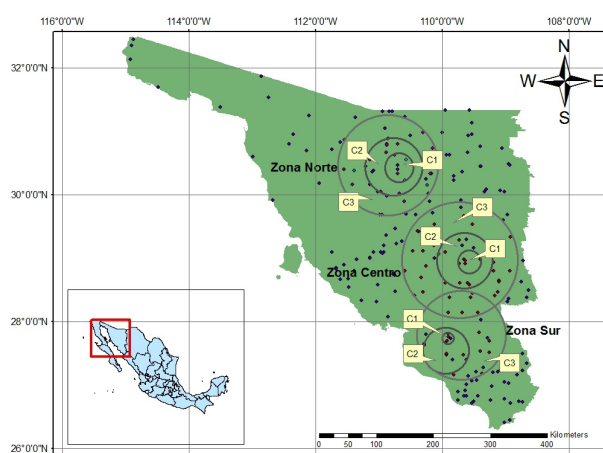


Figure 2. Circles of different areas in the three zones of the state

4 OUTPUT RESULTS

4.1 Obtaining the representative ARF

With the purpose of getting the representative ARF of the northwest zone of the Mexican Republic, the state of Sonora was divided into three zones: north, center and south. In each of them three circles were drawn with different areas containing at least three stations with 15 years of common data to each other. For each of the circles, an ARF was obtained with the methodology described above. Tables 1 to 9 are presented as the average ARF for each year of common data (ARFs) as well as a extrapolation for 2, 5, 10, 20, 50, 100, 500, 1000, 2000, 5000 and 10000 years of return period for each circle and for each of the zones.

4.2 Area-ARF-Tr graphs

Once the ARFs were obtained for the nine circles, an Area-ARF graph was drawn in order to get an equation that relates the ARF with the area. In Table 10, average ARF for each circle are shown.

North Zone (NZ)

Table 1. Results of the ARF for circle 1, north zone.

NZC1	Average		0.6156
T	Mixed distribution Gumbel		ARF
	Simultaneous	Maximum	
10000	164.59	252.79	0.7039
5000	155.21	235.63	0.7064
2000	141.76	212.57	0.7121
1000	131.67	195.41	0.7158
500	121.58	177.98	0.7208
200	108.17	154.95	0.7281
100	97.93	137.36	0.7358
50	87.49	119.43	0.7463
20	72.99	94.72	0.7691
10	60.73	75.46	0.7957
5	46.7	60.14	0.7742
2	31.3	46.65	0.6776

Table 2. Results of the ARF for circle 2, north zone.

NZC2	Average		0.6156
T	Mixed distribution Gumbel		ARF
	Simultaneous	Maximum	
10000	378.31	377.93	1.0010
5000	350.76	349.83	1.0027
2000	310.81	312.93	0.9932
1000	280.96	284.39	0.9879
500	251.11	255.95	0.9811
200	211.5	218.07	0.9699
100	181.22	189.06	0.9585
50	150.22	159.3	0.9430
20	106.67	117.14	0.9106
10	67.66	81.71	0.8281
5	38.53	62.29	0.6186
2	28.29	49.48	0.5717

Table 3. Results of the ARF for circle 3, northern zone.

NZC3	Average		0.5360
T	Mixed distribution Gumbel		ARF
	Simultaneous	Maximum	
10000	253.56	252.23	1.0053
5000	234.3	234.84	0.9977
2000	208.41	212.01	0.9830
1000	188.69	194.34	0.9709
500	169.13	176.81	0.9566
200	143.09	153.34	0.9332
100	123.18	135.37	0.9100
50	102.76	117.01	0.8782
20	73.78	91.42	0.8070
10	47.93	72.05	0.6652
5	31.55	58.19	0.5422
2	22.58	45.7	0.4941

Center Zone (CZ)

Table 4. Results of the ARF for circle 1, center zone.

CZC1	Average		0.7794
T	Mixed distribution Gumbel		ARF
	Simultaneous	Maximum	
10000	290.44	274.13	1.0595
5000	270.94	256.57	1.0560
2000	244.43	235.15	1.0395
1000	224.77	218.5	1.0287
500	205.04	201.86	1.0158
200	178.83	179.69	0.9952
100	158.79	162.74	0.9757
50	138.32	145.35	0.9516
20	109.53	120.73	0.9072
10	83.79	98.33	0.8521
5	55.72	72.76	0.7658
2	42.8	57.01	0.7507

Table 5. Results of the ARF for circle 2, center zone.

CZC2	Average		0.6180
T	Mixed distribution Gumbel		ARF
	Simultaneous	Maximum	
10000	108.28	171.58	0.6311
5000	102.58	162.67	0.6306
2000	94.95	151.32	0.6275
1000	89.25	142.81	0.6250
500	83.59	134.27	0.6226
200	76.05	122.88	0.6189
100	70.35	114.21	0.6160
50	64.62	105.39	0.6132
20	56.97	93.24	0.6110
10	51.04	83.26	0.6130
5	44.83	72.79	0.6159
2	35.25	62.42	0.5647

Table 6. Results of the ARF for circle 3, center zone.

CZC3	Average		0.4359
T	Mixed distribution Gumbel		ARF
	Simultaneous	Maximum	
10000	104.07	120.01	0.8672
5000	98.28	115.25	0.8528
2000	89.96	109.45	0.8219
1000	83.68	104.93	0.7975
500	77.44	100.45	0.7709
200	69.14	94.49	0.7317
100	62.83	89.98	0.6983
50	56.44	85.43	0.6607
20	47.73	79.35	0.6015
10	40.77	74.6	0.5465
5	33.48	69.55	0.4814
2	25.09	61.03	0.4111

South Zone (SZ)

Table 7. Results of the ARF for circle 1, southern zone.

SZC1	Average		0.8374
T	Mixed distribution Gumbel		ARF
	Simultaneous	Maximum	
10000	201.71	209.06	0.9648
5000	190.31	197.99	0.9612
2000	175.24	183.35	0.9558
1000	163.85	172.28	0.9511
500	152.44	161.2	0.9457
200	137.35	146.55	0.9372
100	125.92	135.44	0.9297
50	114.44	124.29	0.9207
20	99.12	109.41	0.9060
10	87.29	97.91	0.8915
5	74.95	85.93	0.8722
2	56.32	67.83	0.8303

Table 8. Results of the ARF for circle 2, south zone.

SZC2	Average		0.7149
T	Mixed distribution Gumbel		ARF
	Simultaneous	Maximum	
10000	240.82	258.25	0.9325
5000	227.57	244.04	0.9325
2000	209.75	224.94	0.9325
1000	196.29	210.62	0.9320
500	182.98	196.3	0.9321
200	165.24	177.34	0.9318
100	151.68	162.81	0.9316
50	137.83	147.93	0.9317
20	118.42	126.91	0.9331
10	101.25	108.05	0.9371
5	72.77	83.86	0.8678
2	43.99	65.02	0.6766

Table 9. Results of the ARF for circle 3, southern zone.

SZC3	Average		0.6282
T	Mixed distribution Gumbel		ARF
	Simultaneous	Maximum	
10000	256.08	267.33	0.9579
5000	239.26	251.46	0.9515
2000	216.83	229.99	0.9428
1000	200.13	214	0.9352
500	183.37	198.01	0.9261
200	161.14	176.77	0.9116
100	144.24	160.56	0.8984
50	127.17	144.13	0.8823
20	104.1	121.69	0.8555
10	85.87	103.85	0.8269
5	66.88	86.41	0.7740
2	42.82	68.08	0.6290

Table 10. Grouped areas and averages values.

		Area km ²	Average
North Zone	C1	1994.16	0.6877
	C2	8069.46	0.6156
	C3	24417.13	0.5360
Center Zone	C1	1247.00	0.7794
	C2	7405.82	0.6180
	C3	32627.79	0.4359
South Zone	C1	322.34	0.8374
	C2	5075.82	0.7149
	C3	19052.15	0.6282

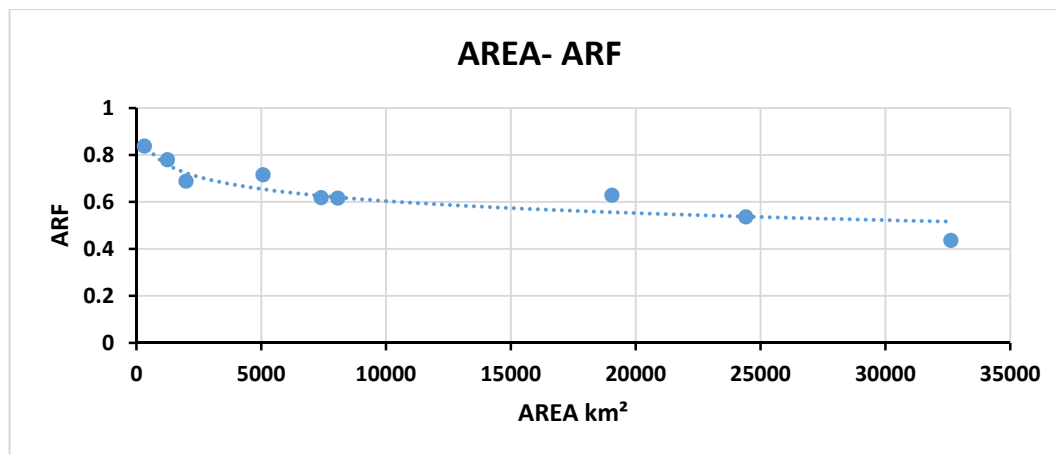


Figure 3. Area-ARF graph obtained for each circle

The adjustment equation that correlates the ARF with the area in the study area is

$$y = -0.044 \ln(x) + 1.0282 \tag{4}$$

In the same way, the extrapolated RFA values were grouped to their different return periods, the corresponding results for 2, 10, 50, and 100 years are presented in table 11 to table 14. In addition, we present the adjustment equations that correlate the RFA with the area for the same return periods.

Table 11. Areas and ARF for a return period of 2 years.

		Area km ²	T=2 years
North Zone	C1	1994.16	0.6776
	C2	8069.46	0.5717
	C3	24417.13	0.4941
Center Zone	C1	1247.00	0.7507
	C2	7405.82	0.5647
	C3	32627.79	0.4111
South Zone	C1	322.34	0.8303
	C2	5075.82	0.6766
	C3	19052.15	0.6290

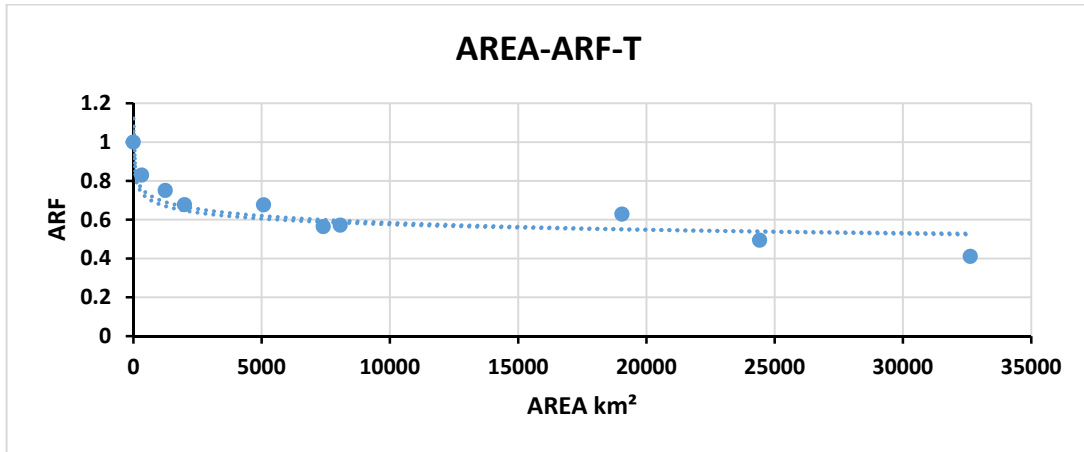


Figure 4. Area- ARF -T of 2 years obtained for each circles

Table 12. Areas and ARF for a return period of 10 years.

		Area km ²	T=10 years
North Zone	C1	1994.16	0.7957
	C2	8069.46	0.8281
	C3	24417.13	0.6652
Center Zone	C1	1247.00	0.8521
	C2	7405.82	0.6130
	C3	32627.79	0.5465
South Zone	C1	322.34	0.8915
	C2	5075.82	0.9371
	C3	19052.15	0.8269

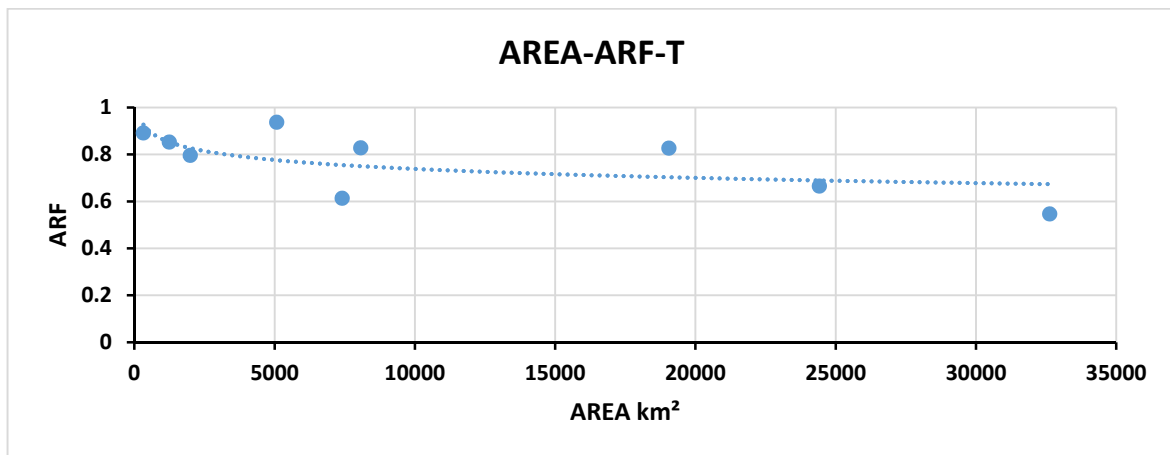


Figure 5. Area- ARF -T of 10 years obtained for each circles

Table 13. Areas and ARF for a 50-year return period.

		Area km ²	T=50 years
North Zone	C1	1994.16	0.7463
	C2	8069.46	0.9430
	C3	24417.13	0.8782
Center Zone	C1	1247.00	0.9516
	C2	7405.82	0.6132
	C3	32627.79	0.6607
South Zone	C1	322.34	0.9207
	C2	5075.82	0.9317
	C3	19052.15	0.8823

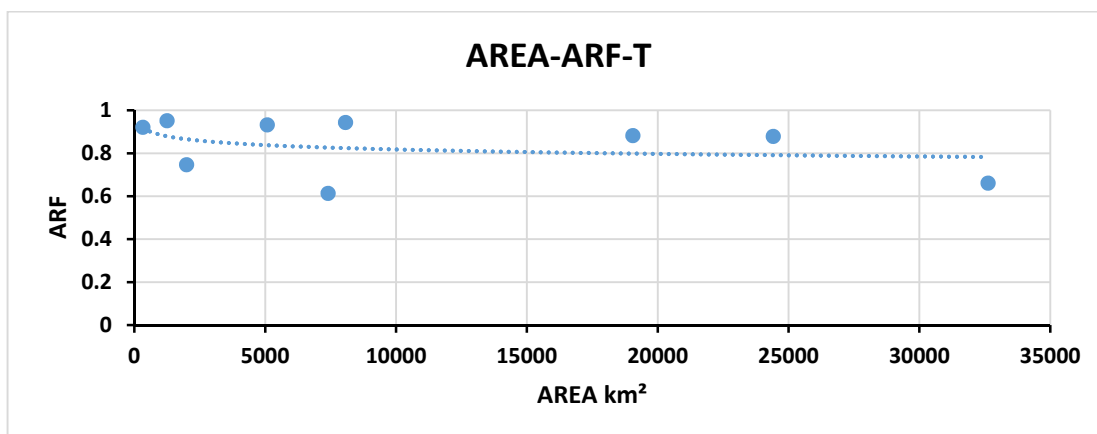


Figure 6. Area- RFA -T of 50 years obtained for each circles

Table 14. Areas and ARF for a return period of 100.

		Area	T=100
		km ²	years
North Zone	C1	1994.16	0.7358
	C2	8069.46	0.9585
	C3	24417.13	0.9100
Center Zone	C1	1247.00	0.9757
	C2	7405.82	0.6160
	C3	32627.79	0.6983
South Zone	C1	322.34	0.9297
	C2	5075.82	0.9316
	C3	19052.15	0.8984

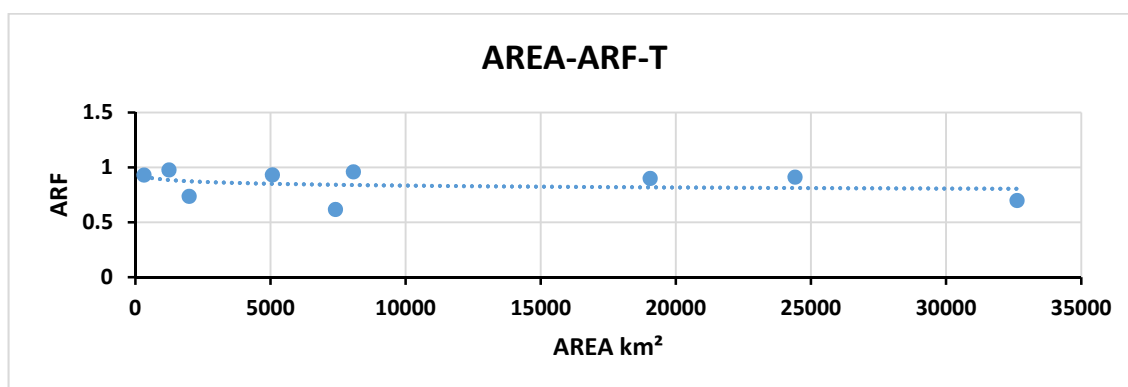


Figure 7. Area- ARF -T of 100 years obtained for each circles

The adjustment equations that correlate the ARF with the area and return period in the studied area are

For T = 2 years

$$y = -0,046 \ln(x) + 1.0171 \quad (5)$$

For T = 10 years

$$y = -0.036 \ln(x) + 1.766 \quad (6)$$

For T = 50 years

$$y = -0.036 \ln(x) + 1.145 \quad (7)$$

For T = 100 years

$$y = -0.029 \ln(x) + 1.0971 \quad (8)$$

5 CONCLUSIONS

The calculated ARFs decrease as the area increases. This variation is not proportional due to the studied area orography. The ARF also increases as the return period increases.

With the obtained results, it is possible to get the representative ARF for any area and return period of the entire Mexican Northeast area (Sonora, Baja California Norte and Sur). With it, a design rainfall can be estimated anywhere within this region.

ACKNOWLEDGEMENTS

We would like to thank the civil engineer Eliseo Carrizosa for providing the data of the climatological stations used in this paper.

REFERENCES

- Acuña, G. (2015). *Factor de Reducción por Area Regiones Hidrológicas: 25.- San Fernando-Soto la Marina, 26.- Río Pánuco*. Proyecto de Investigación, Posgrado de Ingeniería, UNAM, México.
- Canavese, N. (2015). Estimación de Factores de Reducción por Área (FRA) en Región Hidrológica 19 (RH19). *Proyecto de Investigación, Posgrado de Ingeniería*, UNAM, México.
- Carrizosa, E. y Domínguez, R. (2016). Análisis Regional Para la Estimación de Precipitaciones de Diseño en la República Mexicana, *CDMX, MÉXICO*
- Franco, C. (1998). Análisis Regional de Lluvias Convectivas. Aplicación al Valle de México, *Tesis de maestría*. Posgrado de Ingeniería, UNAM, México
- González, S. (2012). Estimación de Factores de Reducción por Área. Aplicación a la cuenca del río Pánuco, *Tesis de Maestría*, Posgrado de Ingeniería, UNAM, México.
- Guichard, E. y Domínguez, R. (1998). Regionalización de Lluvias en la Cuenca del Alto Río Grijalva, *Quehacer científico en Chiapas*, vol. 1 No.2
- Guichard, D., Domínguez, R. y García, R. (2004) Factores de Reducción Areal: Revisión Histórica, Aplicación a Cuencas de la Zona Mediterránea de España, *Memorias del XXI Congreso Latinoamericano de Hidráulica*.
- Mena S, (2004). Factores de Reducción por Área Para el Cálculo de Lluvias de Diseño. Aplicación al estado de Sinaloa. *Tesis de maestría*, Proyecto de Investigación, Posgrado de Ingeniería, UNAM, México.
- Sánchez, S. (2015). Aplicación de Métodos Para la Determinación del Factor de Reducción por Area (FRA), *Región hidrológica 30*. Proyecto de Investigación, Posgrado de Ingeniería, UNAM, México.
- Severiano, M. (2014). Estimación de Factores de Reducción Areal. Aplicación a los Estados de Durango y Tamaulipas. *Tesis de maestría*. Posgrado de Ingeniería, UNAM, México.
- Svensson, C. & Jones, D.A. (2010). Review of Methods for Deriving Areal Reduction Factors. *Journal of Flood Risk Management*.
- Torres, N. y Domínguez, R. (2013). Obtención de Factores de Reducción por Area Usando el Método de regionalización. Aplicación a la cuenca del río Sonora. *Tesis de maestría*. Posgrado de Ingeniería, UNAM, México.

LONG-TERM PERFORMANCE OF ENHANCED BIORETENTION MEDIA UNDER NUTRIENT RICH RUNOFF IN TROPICAL CLIMATE

HUI WENG GOH⁽¹⁾, CHEE HUI LAI⁽²⁾ & NOR AZAZI ZAKARIA⁽³⁾

^(1,2,3) River Engineering and Urban Drainage Research Centre (REDAC), Universiti Sains Malaysia, Engineering Campus, Penang, Malaysia
redac_gohhuiweng@usm.my

ABSTRACT

Treating nutrient from stormwater runoff is necessary to enhance public health and to protect the quality of environment. In recent years, bioretention system has become one of the most common green infrastructures as Best Management Practices (BMPs) for stormwater management in the Asian-Pacific Region. This study investigates the performance of different types bioretention media in treating nutrient-rich runoff over a long period of time. Of five types of enhanced bioretention media tested (coconut husks, tyre crumbs, shredded printed papers, crushed cockle shells, and shredded newspapers), vegetated mesocosm studies on crushed cockle shells (CS) and shredded newspapers (NP) were chosen to be extended to 49 weeks to compare with the standard bioretention media (STD) on their long-term performance in hydraulic conductivity, total nitrogen (TN), total suspended solid (TSS), and total phosphorus (TP) removals, and N retention ability within soil and plant. The hydraulic conductivity for all three types of media changes over time, which increases significantly to an average range of 170 to 178 mm/hour at week 15, and the hydraulic conductivity declines gradually to an average range of 112 to 134 mm/hour towards the end of the study. The long-term monitoring study indicated that NP's result in TSS and TN is the most significant among all types of bioretention media, followed by CS for TP removal, CS performed the best, followed by NP for vegetated mesocosm. The results show that both enhanced bioretention media have better performance in nutrient removal over a long-time period.

Keywords: Best Management Practices (BMPs); Bioretention System; Hydraulic Conductivity; Long-Term Performance; Nutrient Removal

1 INTRODUCTION

In the era of sustainable development, sustainable management of stormwater is necessary to ensure public health and to protect the quality of environment (Barbosa et al., 2012). In urban area, increase of nutrient concentration in stormwater runoff has been a worrying issue as excessive amount of nutrient could deteriorate water quality and cause negative impacts on the aquatic life and environment (Liu & Davis, 2014). Fertilizer used on residential lawns, parks and landscapes contributed a significant amount of nutrients in urban runoff when fertilizer is improperly applied or when soil is over-fertilized. According to Duncan (1999), urban runoff can be further subdivided into residential, industrial, commercial and other urban subgroups. In developing countries such as Malaysia, urbanization and industrialization which were taking place rapidly in recent decades, has led to significant change in quality of surface runoff (Goh, 2016).

Among the various treatment technologies available for stormwater management, bioretention has gained considerable attention in the past decade, and has become one of the most popular BMPs. Research has shown that bioretention has been an effective method in removing nutrient from stormwater runoff (Bratieres et al., 2008). In previous laboratory studies and site monitoring, the results have demonstrated that the effectiveness of bioretention systems in removing nutrients from stormwater, especially TSS and TP, which achieved over 90% removal for TSS and over 80% removal for TP (Barrett et al., 2013; Bratieres et al., 2008; Carpenter et al., 2010; Lucas et al., 2010). However, TN removal performance remain a variable, ranging from removal of 59% to leaching of 75% (Davis, 2006; Brown and Hunt, 2011) due to its complexity in chemistry associated with the removal mechanisms of nutrients (Davis et al., 2009). Besides the inconsistency in nitrogen removal, it was reported in the study of Paus et al. (2014) that there are three factors that affected the useful lifespan of bioretention media, which are pollutant breakthrough, pollutant accumulation exceeding the soil reference values, and media clogging that caused hydraulic failure.

Table shows a comparison of nutrient removal requirements stated in selected BMP Manuals (DID, 2011; PUB, 2011; WaterbyDesign, 2012; NJDEP, 2009; DEP, 2006). Among various manuals from different countries, New Jersey Stormwater BMP Manual (USA) has the highest requirement for TSS removal (90%), MSMA has the highest requirement for TN removal (50%) and Pennsylvania Stormwater BMP Manual (USA) has the highest requirement for TP removal (85%). In this study, the performance of bioretention will be assessed using MSMA requirement and compared with the highest requirement set by other BMP manual.

Table 1. Nutrient removal requirements in selected BMP Manuals (Goh et al, 2015)

BMP Manual	Nutrient removal requirement		
	TSS	TN	TP
MSMA, Malaysia	80%	50%*	50%
ABC Waters Design, Singapore	80% removal or less than 10mg/L (90% of all storm events)	45% removal or less than 1.2mg/L (90% of all storm events)	45% removal or less than 0.08mg/L (90% of all storm events)
WSUD, Australia	80%	45%	60%
New Jersey Stormwater BMP Manual, USA	90%*	30%	60%
Pennsylvania Stormwater BMP Manual, USA	85%	30%	85%*

Note: * indicate highest removal requirement

In previous study, Goh et al. (2015) has proven that under an exaggerated nutrient input, the nutrient concentration in the effluent of urban runoff from enhanced vegetated bioretention system still fell within the discharge requirements in various guidelines: Pennsylvania BMP Manual, Urban Stormwater Management Manual for Malaysia (MSMA), New Jersey (United States) BMP Guidelines, Singapore Engineering Procedures for ABC Waters Design Features, and Bioretention Technical Design Guidelines for Brisbane, Australia (DEP, 2006; DID, 2012; NJDEP, 2009; PUB, 2011; Water by Design, 2012). Therefore, it is important to find out whether the enhanced bioretention media is able to sustain the nutrient removal ability and at the same time maintain the hydraulic performance of the media. The objectives of the study were to identify the performance of hydraulic conductivity and nutrient removal of enhanced bioretention system under nutrient-rich runoff using the shortlisted bioretention media over a long-term period.

2 MATERIAL AND METHODS

In this study, the enhanced bioretention media was used to compare its performance with standard bioretention media mixture (STD) in hydraulic conductivity (k_s) and removals of total nitrogen (TN), total suspended solid (TSS), and total phosphorus (TP). The standard bioretention media (STD) was composed by referring to the Urban Stormwater Management Manual for Malaysia (MSMA), which contains 60% medium sand, 20% top soil, and 20% leave compost (DID, 2012). For the enhanced bioretention media, 10% additives (shredded printed paper, coconut husk, cockle shell and shredded newspaper) by volume were used to replace the leave compost in the STD. These bioretention media were inserted into 300 mm diameter polyvinyl chloride (PVC). The main structure of PVC pipe consists of 600 mm depth to hold bioretention media, 150 mm free board for extended detention of water and 50 mm gravel drainage layer. Red Hot Chinese Hibiscus (*Hibiscus rosa-sinensis*) was selected for this study as it is an easy-growing plant in the tropical region. Stormwater runoff collected from municipal and agriculture drainage were used as the sample for this study.

Natural runoff was used in all experiments to simulate the actual condition on site. The criterion for runoff outlet to be selected are: the main drain should have minimum depth of 1m and received runoff from mixed development area; there is access available for four wheel drive (to transfer the runoff); minimum fluctuation of TSS, TN and TP concentration in the runoff. After 3 months of on-site water sample monitoring, one of the main drain nearby University Sains Malaysia Engineering Campus was selected (Figure 1). The range of TSS, TN and TP concentration ranged between 658 to 1156 mg/L, 8.9 to 13.2 mg/L and 3.88 to 5.98 mg/L respectively, which is much higher than typical range of urban runoff (2.1mg/L for TN concentration and 0.2mg/L for TP concentration) (Duncan, 1999).

Prior to the long term performance study, a 16-week study was conducted to compare the nutrient removal performance of five types of enhanced bioretention media with STD. During the dosing week, the runoff from the selected main drain was collected and transferred to a 500 L tank equipped with auto-mixer. To ensure the even distribution of influent applied to each mesocosm, the runoff was divided into five passes of 3.5 L using jugs, passing through a plastic plate with 2 mm holes to promote even distribution of flow. After 16 weeks of weekly monitoring, the study for two vegetated mesocosm each for STD and the best enhanced bioretention media, which are the media with shredded newspapers (NP) and crushed cockle shells (CS) were then extended to 49 weeks to further monitor the hydraulic conductivity, TSS, TN, and TP removals. After 16 weeks of weekly study, the test for nutrient removal was conducted on week 21, 26, 30, 36, and 49 for long-term monitoring.

Saturated hydraulic conductivity (k_s) of the mesocosm was measured using single ring infiltration test method, as adopted from Le Coustumer et al. (2008) on week 1, 8, 16, 31, and 49. As for TSS, TN and TP removals, the following computations were made (Davis et al., 2003):

The mean influent concentrations of the tested parameters ($\overline{C_{inf}}$):

$$\overline{C_{inf}} = \frac{C_{inf1} + C_{inf2} + \dots + C_{inf_n}}{n} \quad [1]$$

where C_{inf} is the influent concentration (mg/L) and n is the total number of samples.

The mean effluent concentrations ($\overline{C_{eff}}$):

$$\overline{C_{eff}} = \frac{C_{eff1} + C_{eff2} + \dots + C_{eff_n}}{n} \quad [2]$$

where C_{eff} is the effluent concentration (mg/L) and n is the total number of samples.

The percentage concentration reductions (C_R):

$$C_R = \frac{\overline{C_{inf}} - \overline{C_{eff}}}{\overline{C_{inf}}} \times 100\% \quad [3]$$



Figure 1. Targeted natural runoff collection point

3 RESULTS AND DISCUSSIONS

As runoff storage and holdup ability is a key performance metric in bioretention system (Davis, 2008), hydraulic conductivity (k_s) has become one of the key parameters to determine the success of the system. Lower k_s provides longer hydraulic retention time, improves nutrient removal but it reduces runoff capture and increases bypass flow due to reduced infiltration rate (Liu et al., 2014). Higher k_s increases runoff capture but resulted in lower nutrient removal as there might be insufficient hydraulic retention time (HRT) for microbial activities and adsorption mechanism to take place, and lower ability to retain moisture for plant growth. In this study, k_s within 100 to 200 mm/hour was selected as the recommended range, based on the comparison of hydraulic conductivity requirements in selected BMP manuals from different countries under tropical or temperate climates (DEP, 2006; DID, 2012; NJDEP, 2009; PUB, 2011; Water by Design, 2012).

Figure 2 presents the performance of different bioretention media in hydraulic conductivity. It shows that the hydraulic conductivity of all three types of media changes over time. Over 49 weeks of experimental period, the hydraulic conductivity of all three types of media meet the recommended range. During the initial stage, STD ($k_s = 85 \pm 7$ mm/hour) does not meet the recommended range between 100 to 200 mm/hour, as the root development of the tropical shrub has not reach its matured state. Over the time, the hydraulic conductivity for all three types of bioretention media has changed, which increases significantly (paired t-test $p < 0.05$ in all three cases) to an average range of 170 to 178 mm/hour at week 15 (due to root development of plant), and the hydraulic conductivity declines gradually to an average range of 112 to 134 mm/hour towards the end of the study (due to combination of hydraulic loading compaction and sediment deposition at the surface of the media (Le Coustumer et al., 2012)). In a 72-week large scale column study conducted by Le Coustumer (2012) on

hydraulic conductivity in bioretention system, it was found that although k_s decreases substantially over time, the rate of reduction also decreases, reaching an asymptote value after 60 weeks. Therefore, it was predicted that k_s for all three types of media will still meet the requirement of MSMA design guideline, which recommends the k_s between 13 to 200 mm/hour (DID, 2012).

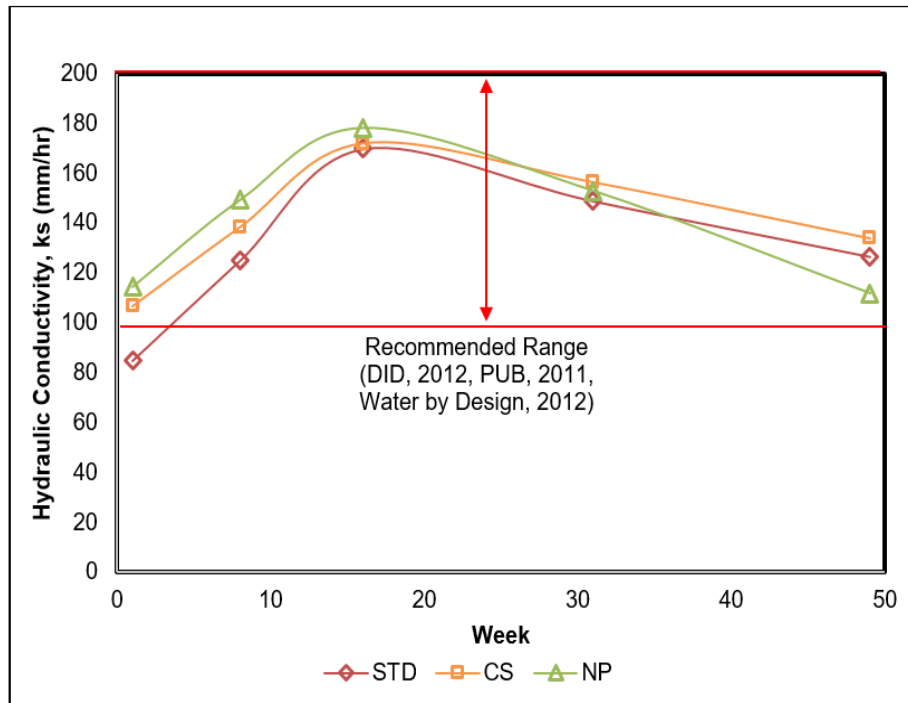
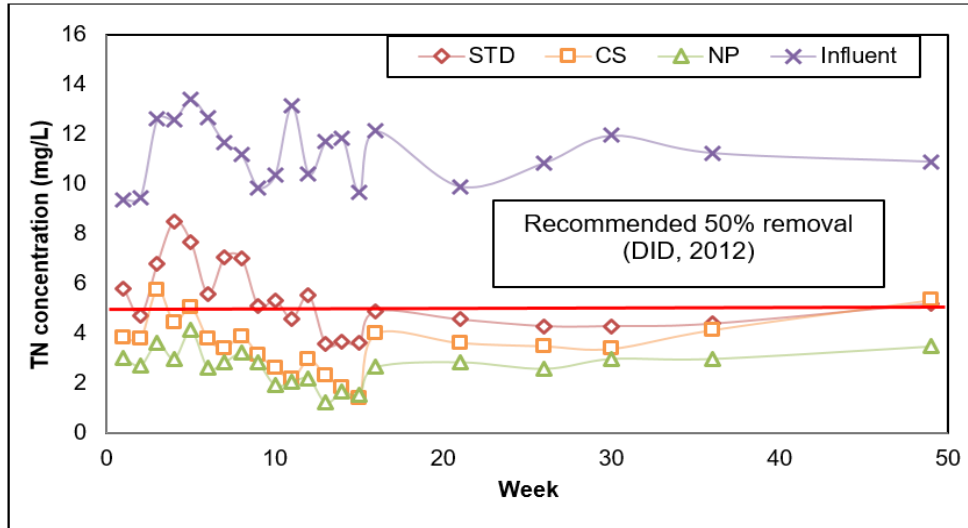


Figure 2. Saturated hydraulic conductivity of STD, CS and NP bioretention media after 49 weeks of study.

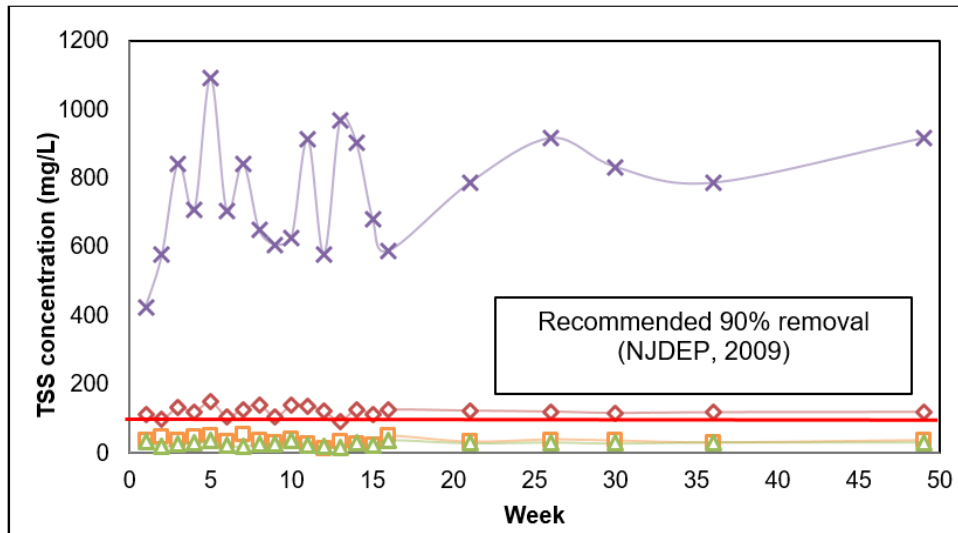
Figure 3 compares the performance of different bioretention media in removing nutrient over 49 weeks. For nutrient removal, the BMP manual that has the highest requirement among manuals from different countries was used as the reference, which is MSMA for TN (50% removal), New Jersey stormwater removal criteria for TSS (90% removal), and Pennsylvania BMP Manual for TP removal (85% removal).

Referring to Figure 3, the performances of NP and CS in removing TN, TSS, and TP were better than STD. Apart from TN, both NP and CS succeeded in removing nutrient under the recommended range over the experimental period. This has proven that the potential of the selected media to treat nutrient-rich runoff under a long-term period. Figure 2(a) shows that after week 3, the TN removal performance has gradually improved and achieved the optimum removal rate at week 13 to 15. The increase in TN retention may be due to the trend of considerable plant growth (Carpenter and Hallam, 2009), indicating that longer period is needed to achieve the optimum performance of mesocosm in TN removal to treat nutrient-rich runoff. After week 16, the performance has slightly reduced and achieved an almost consistent effluent concentration. Towards the end of the study (after week 35), STD and CS performances have gradually decreased but NP remains over 50% of TN removal.

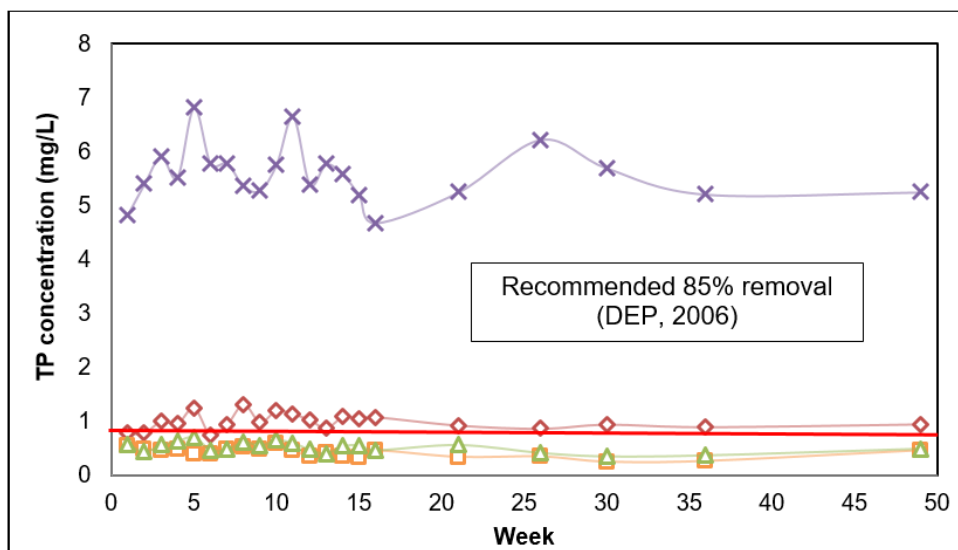
Over 49 weeks of studies, the data indicated that CS and NP performed significantly better than STD in TSS and TP, which remained within the recommended 90% and 85% removals, respectively (Figure 3(b) & (c)). All types of media seem to reach an asymptote value after week 13. Statistical analysis shows that NP's result in TSS and TN is the most significant among all types of bioretention media, followed by CS. As for TP removal, CS performed the best, followed by NP for vegetated mesocosm. This has proven that the potential of the selected additives for onsite application to treat higher nutrient loading as the system remains consistent under long-term monitoring.



(a)



(b)



(c)

Figure 3. Long-term nutrient removal performance of STD, CS, NP bioretention media in comparison of influent and effluent for: (a) TN, (b) TSS, and (c) TP.

4 CONCLUSIONS

This study investigates the performance of different types bioretention media in removing nutrient from stormwater runoff over a long-time period. Both enhanced bioretention media (NP and CS) have minimal effect on hydraulic conductivity as compared to STD. For nutrient removal, both NP and CS did better in removing TP, TSS, and TN as compared to STD. NP had the best performance in removing NP over a long-time period, whereas CS did better in removing TSS and TP. It is concluded that these enhanced bioretention media have better performance in nutrient removal over a long-time period as compared to standard bioretention media.

ACKNOWLEDGEMENTS

This work was supported by the Ministry of Higher Education Malaysia under the grant title of “Urban Water Cycle Processes, Management and Societal Interactions: Crossing from Crisis to Sustainability” with grant number as: 203/PKT/6720004.

REFERENCES

- Department of Irrigation and Drainage Malaysia. (2011). *Urban Stormwater Management Manual for Malaysia*. Kuala Lumpur.
- Barbosa, A. E., Fernandes, J. N. & David, L. M. (2012). Key issues for sustainable urban stormwater management. *Water Research*, 46(20), 6787-6798.
- Barrett, M. E., Limouzin, M. & Lawler, D. F. (2013). Effects of media and plant selection on biofiltration performance. *Journal of Environmental Engineering (United States)*, 139(4), 462-470.
- Bratieres, K., Fletcher, T. D., Deletic, A. & Zinger, Y. (2008). Nutrient and sediment removal by stormwater biofilters: A large-scale design optimisation study. *Water Research*, 42(14), 3930-3940.
- Brown, R. A. & Hunt, W. F. (2011). Underdrain configuration to enhance bioretention exfiltration to reduce pollutant loads. *Journal of Environmental Engineering*, 137(11), 1082-1091.
- Carpenter, D. D. & Hallam, L. (2009). Influence of planting soil mix characteristics on bioretention cell design and performance. *Journal of Hydrologic Engineering*, 15(6), 404-416.
- Davis, A. P., Shokouhian, M., Sharma, H. & Minami, C. (2006). Water quality improvement through bioretention media: Nitrogen and phosphorus removal. *Water Environment Research*, 78(3), 284-293.
- Davis, A. P., Shokouhian, M., Sharma, H., Minami, C. & Winogradoff, D. (2003). Water quality improvement through bioretention: Lead, copper, and zinc removal. *Water Environment Research*, 75(1), 73-82.
- Davis, A. P., Hunt, W. F., Traver, R. G. & Clar, M. (2009). Bioretention technology: Overview of current practice and future needs. *Journal of Environmental Engineering*, 135(3), 109-117.
- DEP, P. (2006). *The Pennsylvania Stormwater Best Management Practices Manual*. Bureau of Watershed Management: Department of Environmental Protection (DEP).
- DID (2012). *Urban Stormwater Management Manual for Malaysia (2nd Edition)*. Kuala Lumpur, Malaysia: Department of Irrigation and Drainage Malaysia (DID).
- Duncan, H. 1999. *Urban Stormwater Quality: A Statistical Overview*. Report 99/3. Cooperative Research Center for Catchment Hydrology, Melbourne, Australia.
- Goh, H. W., Lau, T. L., Foo, K. Y., Chang, C. K. Leow, C. S. & Azazi, N. A. (2015). Mesocosm study of enhanced bioretention media in treating nutrient rich stormwater for mixed development area. *Urban Water Journal*, In-press.
- Goh, H. W. (2016). Influence of enhanced bioretention media and tropical shrub on nutrient removal for urban runoff in mixed development area. *PhD Thesis*. Universiti Sains Malaysia.
- Le Coustumer, S., Fletcher, T. D., Deletic, A., Barraud, S. & Poelsma, P. (2012). The influence of design parameters on clogging of stormwater biofilters: A large-scale column study. *Water Research*, 46(20), 6743-6752.
- Liu, J. & Davis, A. P. (2014). Phosphorus Speciation and Treatment Using Enhanced Phosphorus Removal Bioretention. *Environmental Science & Technology*, 48(1), 607-614.
- Lucas, W. C. & Greenway, M. (2010). Phosphorus retention by bioretention mesocosms using media formulated for phosphorus sorption: response to accelerated loads. *Journal of Irrigation and Drainage Engineering*, 137(3), 144-153.
- NJDEP (2009). *New Jersey Stormwater Best Management Practices Manual. Chapter Four: Stormwater Pollutant Removal Criteria*. State of New Jersey, United States: Department of Environmental Protection, Division of Watershed Management.
- Paus, K., Morgan, J., Gulliver, J. & Hozalski, R. (2014). Effects of bioretention media compost volume fraction on toxic metals removal, hydraulic conductivity, and phosphorous release. *Journal of Environmental Engineering*, 140(10), 04014033.
- PUB 2011. *Engineering Procedures for ABC Waters Design Features*. Singapore: Public Utilities Board (PUB).
- Water by Design (2012). *Bioretention Technical Design Guidelines (Version 1)*. Brisbane, Australia: Health Waterways Ltd.

IMPACT OF SUBMERGED ZONE DEPTH ON STORMWATER POLLUTANTS REMOVAL IN TROPICAL BIOFILTRATION SYSTEMS

ANDREAS ADITYA HERMAWAN⁽¹⁾, MUHAMMAD IRFAN RAHMAN⁽²⁾, AMIN TALEI⁽³⁾ & FANG YENN TEO⁽⁴⁾

^(1,2,3) School of Engineering, Monash University Malaysia, Subang Jaya, Selangor, Malaysia,
andreas.aditya@monash.edu; mirah4@student.monash.edu; amin.talei@monash.edu

⁽⁴⁾ Department of Irrigation and Drainage Malaysia, Kuala Lumpur, Malaysia,
teofy@water.gov.my

ABSTRACT

Stormwater quantity and quality management is one of the major concerns in fast developing countries significant growth in urbanization. Urbanization has caused deterioration in stormwater quality and has increased floods' peak, volume, and frequency. One of the components of Best Management Practice (BMP) to address such issue is biofiltration system which consists of a layered soil system covered with plants on the top. Plants play a major role of removing nutrients and maintaining the hydraulic conductivity of the system. To assure plants survival during dry period, submerged zone can be provided by raising the outlet level. This will provide internal water storage for plants to survive. Although biofiltration systems are well studied in many countries including US and Australia, very limited studies are conducted for tropical conditions. In the present study, a water sensitive plant was selected from 10 local plants candidates through a monitoring process. Then, an experimental setup consisting of soil columns with three different levels of submerged zone were provided and tested for watering gap from 0 up to 10 days. The performance of the system in removing heavy metals, Total Nitrogen (TN), and Total Phosphorus (TP) was measured. Results showed that submerged zone even with lowest level can still support plants survival during dry period. Columns with high level of submerged zone were found to be more successful in removing TN and TP. For heavy metals, however, all three levels of submerged zones produce almost same results in heavy metal removal showing that heavy metal removal is independent of submerged zone level. It was also concluded that removing Fe can be affected by a prolonged dry period. This was attributed to the potential cracks in soil during dry period which can reduce surface contact between Fe ions and filter media particles.

Keywords: Tropical biofiltration system; stormwater treatment; nutrient removal; submerged zone.

1 INTRODUCTION

Stormwater management has been a major concern in urban areas as rapid growth of urbanization has increased the percentage of impervious surfaces which in turn has contributed in deteriorating stormwater quality and increasing the peak, volume, and frequency of the flash floods. This situation could be even worse in fast developing countries such as Malaysia which are located in tropical region with high rainfall intensity. Stormwater contamination mainly includes sediments, heavy metals, nutrients (such as nitrogen and phosphorus), oil and grease, and pathogens. The source of heavy metals are automobiles fluid leaks and tires, paints and metal components of buildings as well as atmospheric deposition (Davis et al., 2003). Moreover, excess nutrient and pathogens in stormwater have caused harmful environment for aquatic organisms (Hunt et al., 2006). Nutrients are mainly consisted of phosphorus and nitrogen which can be found in fertilizers and concentrated sewage while pathogens are usually found in the form of E. coli and fecal coliform.

To date, several solutions have been practiced to treat stormwater pollution including wetland, green roof, and biofiltration (Blecken et al., 2009). Biofiltration system is one of the Best Management Practice (BMP) that consists of layers of engineered soil media with different particle sizes covered with vegetation on the top and is used for both stormwater quantity and quality management (Sun and Davis, 2007). Biofiltration systems have reasonably large volumetric capacity which is useful in flood mitigation and are able to reduce pollutants concentration by retaining them in the system (Dietz, 2007). Studies have shown that relatively high percentage of concentration of heavy metals and suspended solids can be reduced by soil media alone (Reddy et al., 2014; Hatt et al., 2008; Pitcher et al., 2004). In contrast to heavy metals, studies have revealed that soil media alone is not able to remove nutrients effectively and the presence of vegetation is necessary. Henderson et al. (2007) found that the vegetated soil column biofilters are more effective in nitrogen and phosphorus removal while the non-vegetated ones suffer from nitrogen leaching. Nitrogen leaching was also reported in some other lab studies including Hatt et al. (2007) and Fletcher et al. (2007). Read et al. (2008) studied the influence of using different types of vegetation in biofiltration systems. Authors concluded that the plant size and root structure have key roles in pollutant removal. Vegetation was found to be effective for phosphorus and nitrogen removal. Moreover, studies have shown that plants in biofiltration systems play an

important role in maintaining the hydraulic conductivity of the system high due to the penetration of plants root into the soil media (Emerson and Traver, 2008). However, in order to support the plants survivability especially in dry periods, sufficient water supply is required. Therefore, submerged zone was introduced to the biofiltration system design which is a saturated zone resulted by an increased outlet level (Zhang et al., 2011). Submerged zone somehow emulate ground water level for plants from which they can absorb water. The presence of this zone in biofiltration system is quite vital especially during establishment period where the roots have not penetrated deep enough. It has been also reported in literature that the presence of submerged zone could improve the denitrification process in the system which in turn can improve removal efficiency for nitrogen-based pollutants.

Despite several successful applications of biofiltration systems especially in US and Australia, they are still not so prominent in Malaysia. To date, very few profound studies have been carried out on the hydrological and pollutant removal performance of biofiltration systems under tropical conditions and there are still lots of unaddressed issues in designing and maintaining of such systems. One of the unaddressed issues in design requirement of tropical biofiltration system is the optimal depth of submerged zone. Since in tropical region, the dry period is not long, there is a need to study the functionality of submerged zone and its impact on system performance in pollutants removal. It is necessary to find the most suitable depth for submerged zone to help the survivability of sensitive plants during dry periods. The presented work is an experimental study on soil column biofilters under tropical conditions which aims to assess the functionality of submerged zone and identify its optimal depth to support the survivability of sensitive plants to dry period.

2 LITERATURE REVIEW

The performance of a biofiltration system is normally measured by two criteria: (1) hydraulic conductivity of the system which helps in stormwater quantity management; and (2) pollutant removal efficiency which supports stormwater quality management. Unlike other climate conditions, in tropical regions, the first criteria becomes very significant as rainfall intensity is so high. If the hydraulic conductivity is too slow, the surface runoff rate would be greater than the infiltration rate which can cause the system get overflowed quickly (Pitt et al., 2008). Therefore, it is necessary to choose the filter media, plants, and the depth of the submerged zone in a way that hydraulic conductivity can be maintained in an acceptable range. Soil media in biofiltration system can absorb heavy metals and suspended solids while plants can uptake nutrients as it is one of the growth requirement beside their need to water and sunlight. Plants root penetrate into the soil to reach water and this assist the soil microorganism to cultivate bacteria which acts as a catalyst to start the purification reaction of breaking down nutrients such as nitrogen and phosphorus (Bais et al., 2006). Moreover, it is believed that not only plants can assist in filtering out the nutrients but also they can improve infiltration rate by creating channels in soil (Read et al., 2008). Despite the significance role of plants in reducing the nutrients content from infiltrated stormwater, there are still cases with unacceptable amount of nitrogen leached from the system. Therefore, to further improve the nitrogen removal, researchers proposed usage of submerged zone (Zhang et al., 2011).

Submerged zone is known to be able to provide an anaerobic condition in the soil (Zhang et al., 2011). An anaerobic condition would cause a depletion in oxygen which in turn can deplete oxygen-dependent denitrification enzymes (Smith and Tiedje, 1979). The disappearance of enzyme would lead to new denitrification enzyme which is independent of oxygen. This enzyme will start cultivating nitrate in the soil. It can convert the nitrate to nitrogen gas which will be released to the atmosphere (Von Rheinaben and Trolldenier, 1983). Therefore, nitrogen removal can be improved by having a combination of plants and submerged zone. It is worth mentioning that plants root assist in denitrification process by excreting sugar and protein which provides nutrients for microorganism in the soil (Woldendorp, 1963). The cultivation of rhizosphere organism would lead to an increase in rate of oxygen depletion as more organism consume more oxygen (Woldendorp, 1962). This will lead to a faster transition to the denitrification process and speed up the process of nitrogen removal in the system. Despite the successful application of submerged zone in biofiltration systems in different countries such as US and Australia, there is no in-depth study to evaluate their functionality under tropical condition. One of the key design parameters in biofiltration systems is the depth of it as it helps plants survivability during dry period. This becomes important as different plants have different level of sensitivity to dry period and their root structure and growth rate are also different. Therefore, there is a need to study submerged zone and optimize its design criteria for tropical biofiltration systems.

3 METHODOLOGY

3.1 Plants selection

Following FAWB (2009), several criteria were adopted for plant selection including low maintenance, good root penetration, ability to absorb pollutant loads, and the ability to survive in highly variable soil moisture and ponding conditions. Considering the above-mentioned criteria and the availability in Malaysia, total ten different types of plants were chosen as candidates and kept in a greenhouse in Monash University Malaysia which included *Bambusoideae*, *Cordyline fruticosa*, *Cymbopogon nardus*, *Cyperus alternifolius*, *Heliconia*

psittacorum, *Hibiscus rosa-sinensis*, *Hymenocallis speciosa*, *Iris pseudacorus*, and *Pedilanthus tithymaloides*. Eight replicates of each plant were provided for consistency check of the observations. In monitoring stage, plants were kept in pots with nutrient-rich soil. Due to the environment difference (especially soil moisture) between pot and natural soil, plants were initially watered twice a day by tap water while after 2 weeks, daily watering practice was adopted. After establishment stage, dry periods of 1 to 7 days were made to monitor the plants sensitivity to dry period. Then, the most sensitive plant was chosen to be used in experimental study on submerged zones.

3.2 Soil media

A biofiltration system has three soil media layers including: (1) filter media which is normally a sand-based filter and sits on top of the other layers and accommodate plants in itself; (2) drainage layer which contains coarse gravels and sits at the bottom of the system to drain the filtered water from the system; and (3) transition layer which is mainly made of coarse sands and sits between filter and drainage layers. Transition layer should be designed to avoid filter media particles being washed out to the drainage layer. To date, several soil media have been suggested in literature for being used in biofiltration systems. Filter media selection is normally linked to the soil properties, catchment characteristics, rainfall patterns, land use, and availability of material in the local market. FAWB (2009) gave a detailed guideline on filter media selection for Australian biofiltration systems. It has been found that using a small portion (2-3%) of fine particles (such as fly ash, etc.) enhance the pollutants (especially heavy metals) removal (Zhang, 2006; Hsieh and Davis, 2005). However, to maintain a reasonably good infiltration rate, using high percentage of fine material is not recommended. Perhaps for tropical regions with intense rainfall events, sand-based filters would be good enough to provide both high infiltration rate and pollutant removal. Therefore, in this study, no fine materials used as additives to the filter media. Table 1 shows the particle size distribution in the soil column setup of this study.

Table 1. Weight distribution of different particle size in different layers of soil column setup.

	Particle size (mm)	Drainage layer (%)	Transition layer (%)	Filter media (%)
Fine sand	0.15-0.30	0	0	15
Medium sand	0.30-0.60	0	5	55
Coarse sand	0.60-1.18	0	10	20
Very coarse sand	1.18-2.36	5	60	10
Fine gravel	2.36-3.35	10	25	0
Coarse gravel	3.35-4.75	55	0	0
Very coarse gravel	> 4.75	30	0	0

3.3 Experimental setup

The 200mm diameter PVC pipes with a height of 1000mm were provided as experimental setup of this study. The freeboard was considered in a way that it doesn't block the sunlight for plants. Moreover, the solid media was consisted of filter layer, transition layer, and drainage layer with 400, 100, and 335mm thickness, respectively. The column outlet was located at 135mm from the bottom. However, the desired depth of submerged zone was provided by raising the outlet. In this study, three different depths were considered for submerged zone including 150, 250, and 350mm above the outlet level which are denoted as small (S), medium (M), and high (H) columns in this study, respectively. Figure 1 schematically shows the column setup of this study. For each column type, four replicates were provided to ensure the reliability of the findings. Therefore, a total of 12 columns were considered for the testing phase.

Prior to filling, all columns were washed off from any dust or dirt and the internal wall were then sand-papered to prevent any preferential flow. A perforated pipe was installed horizontally at the outlet inside the drainage layer to prevent the outlet from clogging. After filling the columns, 3 rounds of flushing with tap water was made to wash off the dust and very fine material as they were not desired in the system. Then the selected plants were transferred to the columns. Care was made to ensure removing most of the organic soil attached to the roots. After transferring the plants, an adaptation period of 2 weeks was given to plants to adjust themselves to the new environment. During this period, a daily watering practice was considered to help the plants adapt.

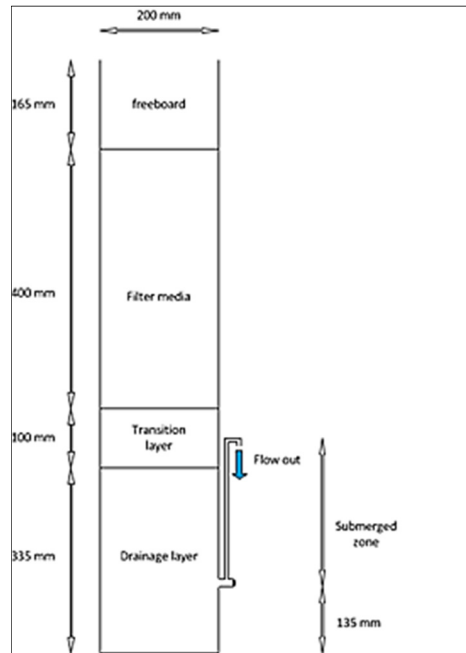


Figure 1. Schematic setup of the soil columns of this study.

3.4 Synthesized stormwater

In this study, synthesized stormwater was used for experiments to maintain and control the physical and chemical characteristics of stormwater (FAWB, 2009). The pollutants were artificially provided in this synthesized stormwater including Total Nitrogen (TN), Total Phosphorus (TP), and heavy metals such as Zn, Cu, Pb, Ni, Fe, Mn. Reviewing the reported pollutants concentration in Malaysia (Yusop et al., 2005) and other countries in the world (Duncan, 1999), the maximum pollutants concentration were adopted to assume a worst case scenario. A summary of pollutants concentration in synthesized stormwater is shown in Table 2.

Table 2. Concentration of different pollutants in synthesized stormwater of this study.

Pollutant	Concentration (mg/L)
TN	4.315
TP	1.118
Zn	0.250
Cu	0.150
Pb	0.140
Ni	0.030
Fe	0.860
Mn	0.230

3.5 Stormwater volume dosage

To determine the stormwater dosage for watering the columns, the method proposed by Urban Stormwater Management Manual for Malaysia (Manual Saliran Mesra Alam Malaysia, MSMA) (MSMA, 2012) was adopted. A 3-months Annual Recurrence Interval (ARI) was considered to calculate the design rainfall for this study. The infiltration rate of 100mm/hr was assumed as the operating value for the designed biofiltration system. It is worth mentioning that, the adopted infiltration rate was intentionally underestimated compared to the measured values. This more conservative value accounts for the potential clogging that may happen after some time of operation. Considering the above-mentioned assumptions, the required size of a biofiltration basin to capture the 3-months ARI event was calculated. Then, the captured volume of water was translated to the lab scale soil column using the area ratio of $A_{\text{column}} / A_{\text{basin}}$. Results of this method showed that a total dosage of 13lit per event can be considered for the experiments of this study.

3.6 Sampling and testing

Sampling of the stormwater was done based on the volume of infiltrated water. Timely based sampling was avoided due to the fact that different columns have different hydraulic conductivities. Infiltrated water samples obtained from each column were then tested with Perkin Elmer Optima-8000, ICP-OES to find the concentration of heavy metals. The results were then compared with the initial concentration of pollutants in

synthesized stormwater. However, for nutrients reading, the Hach method 10071 and Hach method 8190 were used to measure TN and TP, respectively. The detection limit for Hach method was 0.01ppm.

4 RESULTS AND DISCUSSIONS

4.1 Plant selection

The monitoring stage of this study showed that out of the 10 selected candidates, *Bambusoideae* is the most sensitive plant to dry period as a dry period of one week was able to turn all its leaves to yellow or red and the plant showed serious stress toward such change. Therefore, the study of submerged zone depth was carried out on this individual plant as the most sensitive one. In order to study the functionality of different depths of submerged zone, total 7 experiments with 0, 1, 2, 3, 5, 7, and 10 days' gap in watering was considered.

4.2 Hydraulic conductivity

Hydraulic conductivity of the columns was measured using constant head method for each round of experiments (i.e. 0, 1, 2, 3, 5, 7, and 10-days gap) and the results are presented in Figure 2. As it was expected, infiltration rate in columns S was the highest followed by columns M and H due to the fact that water head on the column is decreasing from column S to M and from M to H. However, having dry day gaps didn't have much impact on the values in each column type as the hydraulic conductivity remained almost constant for 0 to 10 days gap in watering. It was concluded that, the presence of submerged zone and the plants maintain the hydraulic conductivity of the system during wet and dry periods.

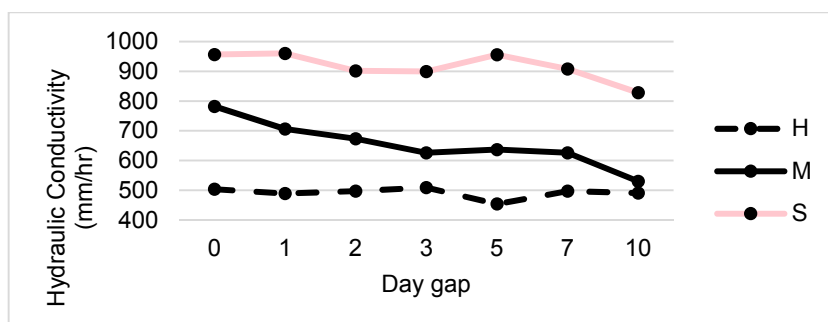


Figure 2. Hydraulic conductivity values measured in columns S, M, and H for different gaps in watering.

4.3 Heavy metals removal

Table 3 presents the percentage removal for different heavy metals of this study for the zero and 10 days gap. As can be seen, except for Mn and Fe, the depth of submerged zone and the length of dry period didn't have significant impact on percentage removal. For Fe, having a long dry period resulted in a lower removal in columns S, M, and H consistently. This was attributed to the fact that during dry period soil may have cracks that work as tiny pipes in the system which may reduce the contact between metal particles and filter particles. For Mn, however, the result was opposite. In early stage of the experiment, the removal was poor and it gradually improved and reached quite high percentages of 94.89, 94.89 and 92.07 for columns S, M, and H, respectively. In order to investigate on the reason, samples were taken from the sands used in this study which are outsourced from a local river bank. Results showed that the sand was rich of Mn and after several rounds of washing it, the concentration of Mn reduced to a very low level. This was also evident in presented experiments (See Figure 3) as a gradual improvement in Mn removal can be seen. Therefore, system can only perform well in removing Mn when all initial Mn particles are washed out from the system.

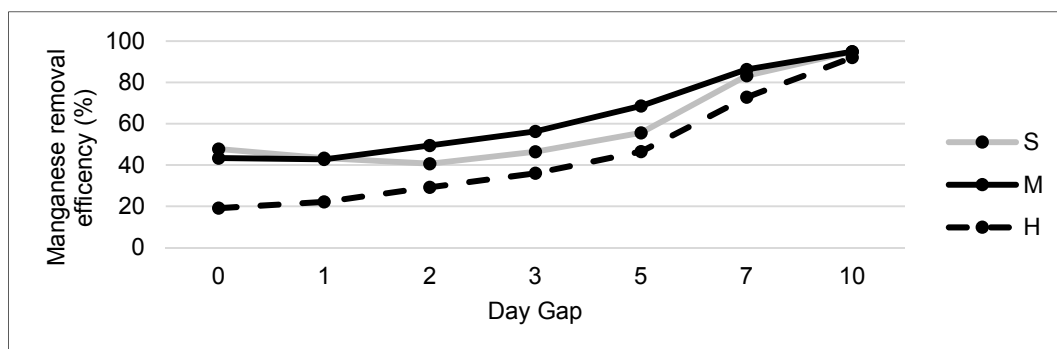


Figure 3. Gradual improvement in Mn removal from 0-gap to 10-days gap.

Table 3. Heavy metal removal performance in different column types of the study.

Heavy Metal	Column	Percentage Removal (%)	
		0-day gap	10-days gap
Zn	S	98.40	98.20
	M	98.90	98.70
	H	97.60	98.60
Pb	S	96.25	94.29
	M	95.89	95.18
	H	96.79	96.07
Ni	S	87.50	89.17
	M	90.00	90.00
	H	88.33	89.17
Fe	S	83.81	28.92
	M	87.01	57.35
	H	88.40	69.24
Mn	S	47.72	94.89
	M	43.37	94.89
	H	19.13	92.07
Cu	S	98.50	97.67
	M	98.00	97.33
	H	98.00	97.00

4.4 Nitrogen removal

Nitrogen removal is dictated by the denitrification process (Zhang et al., 2011) which is assisted by the bacteria content in the system. Moreover, submerged zone would promote constant production of nutrients by plants which in turn would lead to an increase in bacteria growth. Therefore, a high submerged zone will increase the survivability of the plants and would also increase the bacteria content in the columns. However, a change in watering pattern may cause fluctuations in bacteria number and in turn affects the Nitrogen removal. The results of Nitrogen removal for different dry periods are shown in Figure 4. As can be seen, there is no stable trend in Nitrogen removal as it is reported by several researchers (Hatt et al., 2008; Hsieh and Davis, 2005). The highest Nitrogen removal were achieved at 10-days gap in Columns M and H. It was concluded that a long stagnation period for water in submerged zone can promote bacteria growth and cause better nitrogen removal.

4.5 Phosphorus removal

Performance of the system in removing Phosphorus is illustrated in Figure 5. Phosphorus removal at 0-day gap is relatively high with a percentage of 89.04%, 87.70%, and 88.37% for columns S, M, and H, respectively. As can be seen, the removal efficiency in all 3 column types of this study decreases over time. The decrease in phosphorus removal was attributed to denitrification process. In order to filter out the nitrogen, system undergoes a denitrification process which is in anaerobic condition. Although the denitrification process contributes in nitrogen removal, it will produce phosphorus as one of its by-products (Falkentoft et al., 2000). This is evident in Figure 5 where removal percentage keeps decreasing consistently in time. At the 5-days gap where there is a sudden drop of bacteria (as it was evident in Nitrogen removal as well), small increase in phosphorus removal was observed. The submerge zone plays an important role in phosphorus removal as oxygen depletion is needed to create an environment for denitrification to happen. The rate of which a column needs to reach a denitrification stage plays an important role in the removal efficiency of phosphorus. The longer it takes to reach a denitrification stage, the less phosphorus is produced in the system. In H columns, the rate of reaching to denitrification stage is the slowest as the oxygen content in the column is small. For S column, however, a lower submerge zone provides more oxygen content in the soil voids which in turn leads to a longer time for the system to reach denitrification stage.

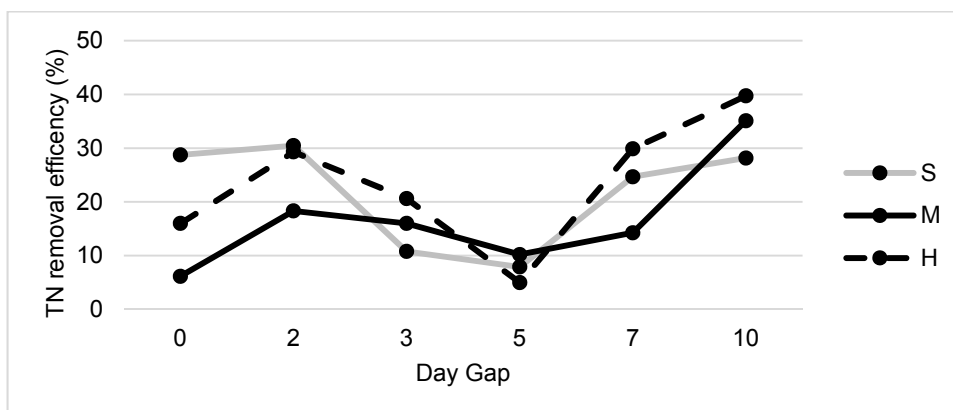


Figure 4. Nitrogen removal efficiency in columns S, M, and H for 0 to 10-days gap.

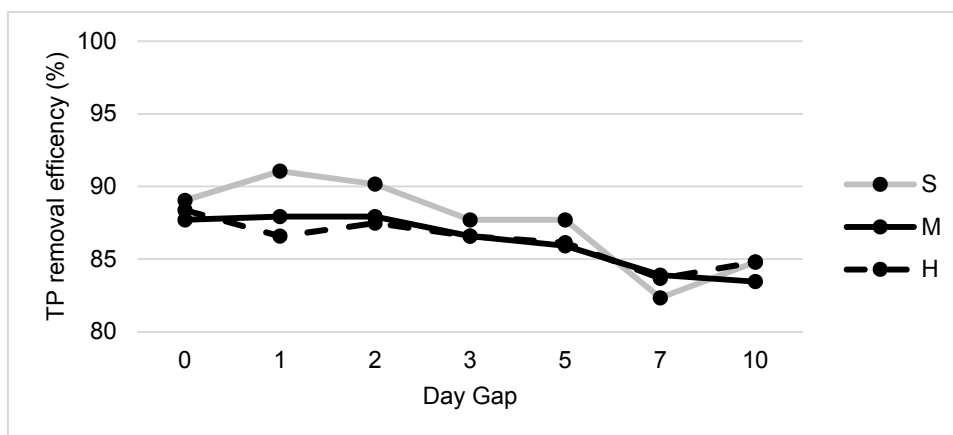


Figure 5. Phosphorus removal efficiency in columns S, M, and H for 0 to 10-days gap.

4.6 Plants survivability

During the 7 rounds of the experiment, the survivability of the plants were closely monitored to see if any plant in any of the columns shows any stress or symptom. This monitoring showed that plants in all three types of columns have survived well. It was evident that even the S columns with deeper submerged level can still support the plants survivability and provide required water in dry period. Therefore, it was concluded that regarding the survivability point of view, all three depths of submerged zone can be applied in tropical biofiltration system.

5 CONCLUSIONS

The conclusions of this study can be summarized as the following:

- (i) The selected sensitive plant of this study, *Bambusoideae*, can survive in biofiltration columns with small, medium, and high submerged zones;
- (ii) Heavy metals can be successfully removed by all three types of columns except for Mn and Fe. Percentage removal for Mn could be still as good as other heavy metals if the biofiltration systems go through several rounds of flushing to remove all Mn particles which naturally exist in sand. For Fe, however, a prolonged dry period can deteriorate its removal efficiency due to the cracks in soil. There were no significant differences between columns S, M, and H for heavy metal removals;
- (iii) A higher submerged zone level (Columns H) can improve TN and TP removal. However, columns M were also reasonably good. It was concluded that bacteria content and the related denitrification process can improve TN removal; however, it will deteriorate TP removal as phosphorus is a by-product of the process. It was also concluded that TP removal gradually deteriorate by prolonging the dry period.

ACKNOWLEDGEMENTS

The research reported herein was financially supported by ScienceFund provided by Ministry of Science, Technology, and Innovation (MOSTI) of Malaysia with eScience grant number of 06-02-10-SF0279. Authors would like to thank Monash University Malaysia for providing the required green house, testing equipment, and admin support.

REFERENCES

- Bais, H.P., Weir, T.L., Perry, L.G., Gilroy, S. & Vivanco, J.M. (2006). The Role of Root Exudates in Rhizosphere Interactions with Plants and Other Organisms. *Annu. Rev. Plant Biol.*, 57, 233-266.
- Blecken, G.-T., Zinger, Y., Deletić, A., Fletcher, T.D. & Viklander, M. (2009). Impact of a Submerged Zone and a Carbon Source on Heavy Metal Removal in Stormwater Biofilters. *Ecological Engineering*, 35(5), 769-778.
- Davis, A.P., Shokouhian, M., Sharma, H., Minami, C. & Winogradoff, D. (2003). Water Quality Improvement through Bioretention: Lead, Copper, and Zinc Removal. *Water Environment Research*, 75(1), 73-82.
- Dietz, M.E. (2007). Low Impact Development Practices: A Review of Current Research and Recommendations for Future Directions. *Water, Air, and Soil Pollution*, 186(1-4), 351-363.
- Duncan, H. (1999). Urban Stormwater Quality: A Statistical Overview. *CRC for Catchment Hydrology*.
- Emerson, C.H. & Traver, R.G. (2008). Multiyear and Seasonal Variation of Infiltration from Storm-Water Best Management Practices. *Journal of Irrigation and Drainage Engineering*, 134(5), 598-605.
- Falkentoft, C.M., Harremoes, P., Mosbæk, H. & Wilderer, P. (2000). Combined Denitrification and Phosphorus Removal in a Biofilter. *Water Science and Technology*, 41(4-5), 493-501.
- Facility for Advancing Water Biofiltration (FAWB). (2009). Adoption Guidelines for Stormwater Biofiltration Systems, Facility for Advancing Water Biofiltration, Monash University.
- Fletcher, T., Zinger, Y., Deletic, A. & Bratières, K. (2007). Treatment Efficiency of Biofilters; Results of a Large-Scale Column Study. *Rainwater and Urban Design 2007*, 266.
- Hatt, B.E., Fletcher, T.D. & Deletic, A. (2007). Hydraulic and Pollutant Removal Performance of Stormwater Filters under Variable Wetting and Drying Regimes. *Water Science & Technology*, 56(12), 11-19.
- Hatt, B.E., Fletcher, T.D. & Deletic, A. (2008). Hydraulic and Pollutant Removal Performance of Fine Media Stormwater Filtration Systems. *Environmental Science & Technology*, 42(7), 2535-2541.
- Henderson, C., Greenway, M. & Phillips, I. (2007). Removal of Dissolved Nitrogen, Phosphorus and Carbon from Stormwater by Biofiltration Mesocosms. *Water Science & Technology*, 55(4), 183-191.
- Hsieh, C.-H. & Davis, A.P. (2005). Multiple-Event Study of Bioretention for Treatment of Urban Storm Water Runoff. *Water Science & Technology*, 51(3), 177-181.
- Hunt, W., Jarrett, A., Smith, J. & Sharkey, L. (2006). Evaluating Bioretention Hydrology and Nutrient Removal at Three Field Sites in North Carolina. *Journal of Irrigation and Drainage Engineering*, 132(6), 600-608.
- Department of Irrigation and Drainage (DID). (2012). *Manual Saliran Mesra Alam*, Kuala Lumpur, Malaysia.
- Pitcher, S., Slade, R. & Ward, N. (2004). Heavy Metal Removal from Motorway Stormwater using Zeolites. *Science of the Total Environment*, 334, 161-166.
- Pitt, R., Chen, S.-E., Clark, S.E., Swenson, J. & Ong, C.K. (2008). Compaction's Impacts on Urban Storm-Water Infiltration. *Journal of Irrigation and Drainage Engineering*, 134(5), 652-658.
- Read, J., Wevill, T., Fletcher, T. & Deletic, A. (2008). Variation among Plant Species in Pollutant Removal from Stormwater in Biofiltration Systems. *Water Research*, 42(4), 893-902.
- Reddy, K.R., Xie, T. & Dastgheibi, S. (2014). Removal of Heavy Metals from Urban Stormwater Runoff using Different Filter Materials. *Journal of Environmental Chemical Engineering*, 2(1), 282-292.
- Smith, M.S. & Tiedje, J.M. (1979). Phases of Denitrification Following Oxygen Depletion in Soil. *Soil Biology and Biochemistry*, 11(3), 261-267.
- Sun, X. & Davis, A.P. (2007). Heavy Metal Fates in Laboratory Bioretention Systems. *Chemosphere*, 66(9), 1601-1609.
- Von Rheinhaben, W. & Trolldenier, G. (1983). Influence of Mineral Nutrition on Denitrification on Plants in Nutrient Solution Culture. *Journal of Plant Nutrition and Soil Science*, 146(2), 180-187.
- Woldendorp, J.W. (1962). The Quantitative Influence of the Rhizosphere on Denitrification. *Plant and Soil*, 17(2), 267-270.
- Woldendorp, J.W. (1963). The Influence of Living Plants on Denitrification, *PhD Thesis*. Veenman.
- Yusop, Z., Tan, L., Ujang, Z., Mohamed, M. & Nasir, K. (2005). Runoff Quality and Pollution Loadings from a Tropical Urban Catchment. *Water Science & Technology*, 52(9), 125-132.
- Zhang, W. (2006). Improvement of Phosphorus and Heavy Metals Retention in Stormwater Treatment, *PhD Thesis*. Oklahoma State University.
- Zhang, Z., Rengel, Z., Liaghati, T., Antoniette, T. & Meney, K. (2011). Influence of Plant Species and Submerged Zone with Carbon Addition on Nutrient Removal in Stormwater Biofilter. *Ecological Engineering*, 37(11), 1833-1841.

